VIBRATION-BASED FAULT IDENTIFICATION FOR ROTOR AND BALL BEARING IN ROTATING MACHINES

A thesis submitted to the **University of Manchester** for the degree of

Doctor of Philosophy (PhD)

in the Faculty of Science and Engineering, School of Engineering

2022

Kenisuomo C. Luwei

Department of Mechanical, Aerospace and Civil Engineering

TABLE OF CONTENT

Word Count: 70,925

List of Figures

List of Tables

Nomenclature

A	acceleration (m/s^2)
AC	Alternating Current (Hz)
A(k)	Fourier Transform of acceleration signal
$\bar{a}$	mean value of data set
a(n)	acceleration discrete FFT
a(t)	acceleration signal
a_{peak}	amplitude of peak value
a_{rms}	amplitude of rms value
$a^2(t_k)$	waveform function a(t) when squared
$aT_{rms_{D_m}}$	Root Mean Square of acceleration-based time domain data
$a\ T_{CF_{D_m}}$	Crest Factor of acceleration-based time domain data
$aT_{Ku_{D_m}}$	Kurtosis of acceleration-based time domain data
B Img	Bispectrum Imaginary components matrix
B R	Bispectrum real components matrix
$B_{C_k S_p}$	Data matrix of bispectrum components for machine conditions observed at all running speed
B_{pq}	Bispectrum components
C_k	Machine conditions
cX	mean of conditions at PC1
cY	mean of conditions at PC2
cZ	mean of conditions at PC3
D	Original value in normalisation
Df	Frequency resolution (Hz)
D_m	Number of data set recorded for each condition during machine operation
dt	change in time of measuring acceleration signal (s)

$\boldsymbol{E_a[t]}$	Envelope of a filtered signal
$\boldsymbol{ES_a}$	Envelope spectrum
$F_{C_k S_p}$	Data matrix of fused acceleration-based time and velocity-based frequency domain for machine conditions observed at all running speed
F_s	Sampling frequency (Hz)
$\frac{f_s}{2}$	$f_{Nyquist}$ (Hz)
$\frac{1}{f_s}$	Sampling time (s)
f_d	lower cut of frequency range
f_u	upper cut of frequency range
H(k)	frequency characteristics of the band pass filter
J	imaginary unit
$K_{C_k S_p}$	Data matrix for rotor related faults conditions observed at all running speeds
rpm	revolution per minute
M_2, M_4	Second and fourth order moment
N	number of data point
nc	number of datasets for quantification
n_s	number of equal segments used for Fourier Transform computation
S_p	Machine running speed
$S^r_{X_1 \gamma^2_{12} X_2}(f_k)$	coherent cross-power spectrum between bearing 1 & 2,
$S^r_{X_2 \gamma^2_{23} X_3}(f_k)$	coherent cross-power spectrum between bearing 2 & 3,
$S^r_{X_{(b-1)} \gamma^2_{(b-1)b} X_b}(f_k)$	coherent cross-power spectrum between bearing (b-1) & b,
T	Period (second/cycle)
V	Velocity (mm/s)
V(k)	Fourier Transform of velocity signal

$\overline{\boldsymbol{v}}(\boldsymbol{t})$	dynamic velocity component after integration
$\boldsymbol{v_0}$	Static velocity component after integration
$vF_{SE_{D_m}}$	Spectrum energy features of velocity-based frequency domain data
$vF_{1x_{D_m}}$	1x component of velocity-based frequency domain data
$vF_{2x_{D_m}}$	2x component of velocity-based frequency domain data
$vF_{3x_{D_m}}$	3x component of velocity-based frequency domain data
$vF_{4x_{D_m}}$	4x component of velocity-based frequency domain data
$vF_{5x_{D_m}}$	5x component of velocity-based frequency domain data
v(n)	Velocity discrete FFT
$X_{CCS}^{r}(f_k)$	Coherent Composite Fourier Transform
$X_{CCS}^{r*}(f_k)$	Complex conjugate of Coherent Composite Fourier Transform
Xi	sum of X dataset in quantification
X_{pCCS}^{r}	poly-coherent composite Fourier Transform
Yi	sum of Y dataset in quantification
Zi	sum of X dataset in quantification
∞	Infinite data
μ	mean data in normalisation
σ	Standard Deviation
Δt	Time step (s)
γ_{12}^{2}	coherence between bearing 1 & 2
γ_{23}^{2}	coherence between bearing 2 & 3
$\gamma_{(b-1)b}^{2}$	coherence between bearing (b - 1) & b
$2\pi k\Delta f$	Omega arithmetic

Abbreviations

ANN	Artificial Neural Network
AT-pCCB	Acceleration-based Time domain and poly-Coherent Composite Bispectrum
AT-ApCCB	Acceleration-based Time-domain with amplitude of poly-Coherent Composite Bispectrum
AT-RIpCCB	Acceleration-based Time-domain with real and imaginary poly Coherent Composite Bispectrum
Bg1	Bearing 1
Bg2	Bearing 2
Bg3	Bearing 3
Bg4	Bearing 4
CBg	Crack close to bearing location
CF	Crest Factor
CS	Composite Spectrum
CSD	Cross-power Spectrum Density
CCS	Coherent Composite Spectrum
CM	Condition Monitoring
D	Balance Disc
DAQ	Data Acquisition Card
DFT	Discrete Fourier Transform
DWT	Discrete Wavelet Transform
dFAVF	Data Fusion of Acceleration and Velocity Features
EDM	Electric Discharge Machining
EEMD	Ensemble Empirical Mode Decomposition
EMD	Empirical Mode Decomposition
FD	Fault diagnosis
FEA	Finite Element Analysis
FFTR	Flange-based flexible test rig
FFT	Fast Fourier Transform

HHT	Hilbert-Huang Transform
HOS	Higher Order Spectra
pCCSHOS	Poly-Coherent Composite Spectrum Higher Order
ISO	International Standard Organization
IFFT	Inverse Fast Fourier Transform
IMFs	Intrinsic Mode Functions
Ku	Kurtosis
LCT	Linear Carnonical Transform
M	Misalignment
M-Loose	Mechanical looseness
PC	Personal Computer
PCs	Principal Components
PCA	Principal Component Analysis
pCCB	Poly-Coherent Composite Bispectrum
PSD	Power Spectrum Density
RMRU	Residual Misalignment Residual Unbalance
RMS	Root Mean Square
RubD	Rub close to balance disc location
S-Bow	Shaft Bow
SE	Spectrum Energy
SFTR	Spring-based flexible test rig
STFT	Short Time Fourier Transform
TG	Turbogenerator
Unb	Unbalance
VCM	Vibration-based Condition Monitoring
VFI	Vibration-based Fault Identification
WVD	Wigner-Ville Distribution
WT	Wavelet Transform

List of Publications

Conference Publications

1. Luwei, K. C., and Yunusa-Kaltungo, A. (2020) Data combination for a consolidated diagnosis of rotor and bearing faults. 12th International Conference Vibration in Rotating Machinery (VIRM-12) online. Institution of Mechanical Engineers, ISBN 978-0-367-67742-8. p. 1 -12

2. Luwei, K. C., Sinha J. K. and Yunusa-Kaltungo, A. (2020) Comparison of Amplitude to Real and Imaginary Features of the poly-Coherent Composite Bispectrum (pCCB) Components in Machine Diagnosis. Advances in Asset Management and Condition Monitoring: COMADEM 2019. 1 ed Springer Nature, Vol. 166. p. 1-8

3. Luwei, K. C., Sinha J. K., Yunusa-Kaltungo, A. and Elbhbah, K. (2018) Data fusion of acceleration and velocity features (dFAVF) approach for fault diagnosis in rotating machines. 14th International Conference on Vibration Engineering and Technology of Machinery (VETOMAC XIV), Lisbon, Portugal. MATEC web of conference, Vol 211. p6

4. Luwei, K. C., Sinha J. K. and Yunusa-Kaltungo, A. (2018) Poly-Coherent Composite Bispectrum Analysis for Fault Diagnosis in Rotating Machines. Proceedings of 3rd International Conference on Maintenance Engineering (InCoME-III) Coimbra, Portugal. Journal of Maintenance Engineering, 3rd Edition, Aylesbury, Buckinghamshire: Shieldcrest Publishing Vol. 2. pp 74-85 12p
5. Luwei, K. C., Sinha J. K. and Yunusa-Kaltungo, A. (2018) Improvement of pCCB Components for Identification of Rotor Faults. Proceedings of 4th International Conference on Maintenance Engineering (InCoME-IV) Dubai, UAE. (Abstract)

6. Luwei, K. C., Sinha J. K. and Yunusa-Kaltungo, A. (2017) Optimizationop of different vibration acceleration and velocity features for faults diagnosis in rotating machines. Proceedings of 2nd International Conference on Maintenance Engineering (InCoME-11) Manchester, UK. Journal of Maintenance Engineering, 2nd Edition, Aylesbury, Buckinghamshire: Shieldcrest Publishing Vol. 2. pp 74-85 12p

7. Luwei, K. C., Yunusa-Kaltungo, A. and Sinha J. K. (2016) A simplified rotor-related faults detection approach based on a combination of time and frequency domain features. Proceedings of the International Conference on Maintenance Engineering (InCoME-1) Manchester, UK. Journal of Maintenance Engineering, 1st Edition, Aylesbury, Buckinghamshire: Shieldcrest Publishing Vol. 1. P.138-147 10p

Journal Publication

8. Luwei, K. C., Yunusa-Kaltungo, A. Sha'aban, Y. A. (2018) Integrated Fault Detection Framework for Classifying Rotating Machine Faults Using Frequency Domain Data Fusion and Artificial Neural Networks. Machines 6, no. 4: 59

Abstract

Vibration-Based Fault Identification for Rotor and Ball Bearing in Rotating Machines
Kenisuomo Churchill Luwei – PhD in Mechanical Engineering
The University of Manchester – August 2022

The study uses an experimental approach in contributing to advance vibration-based fault identification (VFI) techniques for rotor and ball bearing in rotating machines using data fusion of time and frequency domain features. Consequently, it proposes novel VFI approaches which can effectively detect a wide range of rotor and bearing faults in a single analysis.
Vibration signals are collected from three test rigs; the flanged-based flexible test rig (FFTR) designed in earlier research, and the spring-based flexible test rig 1 and 2 (SFTR-1 & 2) are improved versions of FFTR. Dynamic characterisation provided the first few natural frequencies of the rigs, which helped in the selection of machines running speed. The FFTR ran below its first critical speed, while the STFR ran below and above its first critical speed. Simulated rotor-related faults included unbalance, misalignment, crack shaft, looseness, and shaft rub, while the simulated bearing fault were cage defects.
The preliminary investigation considered only rotor-related faults using acceleration features from vibration signals from FFTR, a build-up from an earlier unified multispeed approach (UMA). Data trending was carried out using selected acceleration features from the time domain; root mean square (RMS), crest factor (CF) and kurtosis (Ku), and frequency domain; 1x – 5x and spectrum energy (SE), and the classification result reaffirms the UMA. Furthermore, acceleration was converted to velocity and similar features were obtained for improved classification. Afterwards, acceleration-based time and velocity-based frequency domain features were fused for improved classification.
A proposed novel data fusion of acceleration and velocity features (dFAVF) model helped strengthen the improved approach using signals from STFR-1 with rotor and bearing faults classified in a single analysis. Although spectrum analysis amplitude is helpful in the proposed method, a drawback is the loss of phase during computation due to its complex conjugate. However, the poly-Coherent Composite Bispectrum (pCCB) for rotor fault diagnosis proposed in an earlier study combined different frequency components, which retained their phase during analysis. It also combined multiple sensor data. Therefore, rotor conditions from the SFTR-1 were analysed, and the faults were classified using the first few pCCB components extracted. Additional pCCB components and complex number representations of the components were classified separately and compared.
Another proposed novel approach is the fused acceleration-based time domain features with poly-coherent composite bispectrum components (AT-pCCB) model. The valuable result from the pCCB classification of rotor faults led to incorporating bearing features. Thus, developing the AT-pCCB showed improved classification for rotor and bearing faults in a single analysis.
Observation of more rotor and bearing conditions and comparing similar machines with varying foundation flexibility, i.e., the SFTR-1 and SFTR-2, using the proposed dFAVF and AT-pCCB models, proved the insensitivity of the proposed model in fault identification in such a scenario. Comparing faulty to baseline conditions for all scenarios showed the quantified classification for effective diagnosis. The distinct separation between the rotor and bearing faults could be from their low and high-frequency ranges. Consequently, these fault identification models have viable prospects for industrial application.

Copyright statement

Acknowledgements

My sincere gratitude goes to Prof. Jyoti K. Sinha my supervisor for his invaluable support and leadership in the timely and successful completion of this thesis. He applied his wealth of experience in giving constructive criticism and fatherly encouragement and has been of immeasurable benefit to me. He also challenged me to build confidence and meet targets during this research. I also sincerely appreciate Dr Akilu Yunusa-Kaltungo for his role as part of my supervisory team and his passion in this research.

My appreciation goes to Dr Adrian Nembhard and Dr Akilu Yunusa-Kaltungo whose works helped form the basis for the research.

I also appreciate Mr Bill storey and Ross Holmes in the Dynamics Laboratory of the University of Manchester, for their support during the design setup and simulations of my experimental rig. I also acknowledge Dr Keri Elbhbah for his suggestions at the initial stage of this research.

My sincere appreciation goes to every teacher and lecturer that have contributed to my academic and social development from kindergarten to graduate studies. I appreciate Mrs Betty Ofotokun, late Mrs Victoria Iduh, Mr Charles Alimasunya and so on. I want to specially acknowledge Dr Engr. Patrick Aguh my undergraduate project supervisor for his role and support in my academic pursuit.

I will always remember to appreciate my parents Mr Matthew and Mrs Helen Luwei for their prayers and support. Even though my dad passed away a few months before my thesis submission and my brother over a year to this submission, they both mean a lot to me. I also appreciate all my siblings especially Mr Doubra Luwei, Mrs Diepreye Ogionwo, Mrs Tare Nwaeze, Mrs Funebi Ekos, and Mrs Ebiye Agbai, Mrs Ebiki Akpowowo, Miss Addy Luwei, Mr Keme Luwei, Mr Gesiye Luwei my warmest greetings to you all.

Special thanks to Dr. (Engr) Edward Agbai for his tireless mentorship, encouragement, and motivation. I also appreciate Pastor Abimbola and Pastor (Mrs) Bisi Komolafe for their prayers and covering. I also appreciate a great mentor Mr Abraham Ayo Oni and Funmi Oni for their prayers, encouragement, and support both spiritually and financially.

I appreciate Dr Abimbola Aminu for her encouragement towards the end of writing this thesis. My love for her knows no bound. I love you dear.

Special appreciation to my friends, collaegues, and those that supported and encouraged me during this project in the likes of Itohan Inomwan, Joel Uwabor, Edet Afangide, Lilian Iheukwumere-Esotu, Lois Komolafe, Bukola Odedere, Lucky Awarionta, Shirley Esiegbe and all that has inspired me especially JCM RCCG.

Dedication

This thesis is dedicated to my dearest Daddy **Mr Matthew Camble Luwei** I miss you greatly.
Also, to my beloved mother **Mrs Helen Luwei.**

CHAPTER 1

INTRODUCTION

In this chapter, an overview of the thesis is presented. The rationale for the research, aim and objectives, and outline of report is presented.

1.1 Overview

The most used classes of mechanical equipment are rotary in their operation and have vital industrial applications [1] some of which are electrical and mechanical power conversion, fluid pumping, ventilation and cooling, and propulsion [2]. They are referred to as rotating machinery and cover various industrial mechanisms such as turbogenerator (TG) sets, centrifugal pumps, aircraft engines, reciprocating gasoline, diesel engines, compressors, gases, and steam turbines [2,3]. Rotating machines are vital equipment in the production processes of major industries such as oil and gas, power generation, aerospace, chemical and mining. Failure, especially of non-redundant components, negatively impact industries in terms of production and cost-effectiveness [4]. However, vibration-based condition monitoring (VCM) approaches help to provide early detection of faults where maintenance is carried out to prevent such failures. Thus, Industries look for machines with high durability and reliability that can effectively undergo production long enough [5].

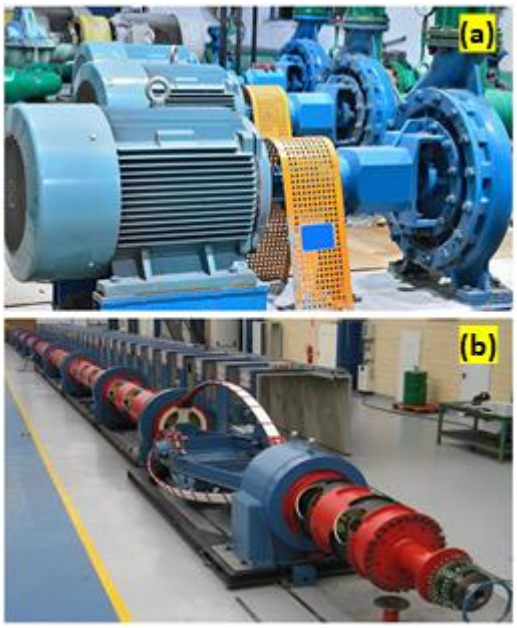

Figure 1. 1 Photograph of rotating machineries (a) with a motor connected to a pump accessed from [6] (b) with multiple shafts accessed from [7]

Rotating machines have three major components, i.e., the rotor, Bearing and foundation [3]. Rotating machines are structured so that the rotor is the heart and connects to the foundation by the Bearing [8,9]. The rotor is an essential part of a

rotating machine which rotates around a central point. The Bearing is another essential element that restraints the relative movement of the rotor to the desired motion and reduces friction between moving parts. Bearings support rotors and transfer axial and radial load from the source to the foundation. However, the machine foundation is the installation platform provided below the superstructure. Its primary function is to provide support for the rotating machine.

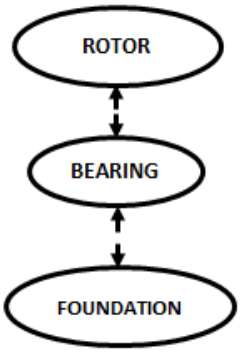

Figure 1. 2 Abstract representation of rotating machinery with its critical parts.

Rotor and bearing systems are crucial in rotating equipment and directly influence a machine's operation and condition [10]. Understanding the behaviour of the rotor and Bearing of a system is very useful in rotor dynamics as it helps to determine its operational requirements and health status [10].

Most machine faults are either rotor-related or bearing defects. The rotor faults show up as unbalance, misalignment, looseness, shaft bow, and shaft crack [11], while bearing defects can be detected from the fundamental frequencies based on their geometry. The fundamental frequency of the Bearing includes ball pass frequency inner race (BPFI), ball pass frequency outer race (BPFO), fundamental train frequency (FTF) and ball spin frequency (BSF) [12].

According to Nakhaeinejad and Ganeriwala [13], 70% of machine faults are rotor-related. In contrast, bearings' design retains a lengthy and useful life during operation [14], based on assumptions of adequately handling and usage. However, most Bearings undergo premature failure for different reasons [14], as up to 80% of bearing

failure stems from improper lubrication. Other sources that affect bearing durability include improper installation, contaminations, production errors during manufacturing of connecting parts, and bearings handled by unskilled personnel [14].

1.2 Rationale' for the research

Vibration-based condition monitoring (VCM) techniques investigate the state of a machine, detect faults, and predict their severity [15, 16]. However, operation in the industry is currently more complex, and this development is due to improvements in automation and the mechanization of machines. Therefore, continuous improvement to achieve a simplified and robust method is the pursuit of researchers and sometimes in conjunction with the industries for decades [16-18]. To effectively carry out VCM, popular non-destructive techniques are used in collecting vibration measurements with transducers such as displacement probes, velocity pickups and accelerometers. An extensive range of machine conditions can be diagnosed efficiently from the signals obtained, including misalignment, shaft bow, looseness, shaft rub, bearing defect, and structural resonance [18]. Thus, getting factual information about a machine's condition helps detect faults early and gives adequate time for maintenance planning to prevent fatal breakdown [5,9,18-19].

Earlier studies on rotor-related faults inspired this research and incorporated bearing fault diagnosis [20-25]. Given continuous improvement for developing improved fault diagnosis techniques, an earlier study [20] proposed using the unified multispeed approach (UMA) for classifying machine conditions. The UMA considered time and frequency domain parameters from the conventional fault identification techniques. However, only acceleration signals were used in all classifications, and vibration data was obtained only below the machine's critical speed. Further studies [23] developed the individual speed individual foundation (ISIF) and multispeed individual foundation (MSIF) fault diagnosis methods, all of which uses a single vibration sensor per Bearing. However, the fast Fourier transformation approach used in these studies does not retain the signal's phase information, which has its uniqueness in fault diagnosis.

As faults develop in a system, the frequency structure of a vibration signal is altered by either change in magnitude or phase of its periodic components. The power spectrum density (PSD) helps to determine these harmonic components of a signal.

The PSD is computed as an average of the magnitude of a signal's discrete Fourier transform (DFT). However, there are some limitations to the PSD. Firstly, peaks at a particular harmonic frequency occur because of random excitation of a component which resonates at or close to the particular frequency. Secondly, phase information is not detected due to its combination with the conjugate of the Fourier transform. Thus, PSD limitation can be mitigated by the higher order spectrum (HOS) analysis which incorporates both the amplitude and phase. Using the higher order spectrum (HOS) fault diagnosis techniques, earlier studies [21] developed the poly-Coherent Composite Higher Order Spectrum (*pCCHOS*), which is an improvement of a previously developed composite spectrum (CS) [24]. This earlier CS, like the PSD, lacks the phase information considered in the improved *pCCHOS.* The *pCCHOS* is made up of the poly-Coherent Composite Bispectrum *(pCCB*) and poly-Coherent Composite Trispectrum *(pCCT*). In this study, fault diagnosis and machine condition classification were carried out using data collected with the machine operating below its first critical speed.

Further studies addressed the issue of using similar rotating machines for transferability of developed fault identification methods and for similar machines installed in different locations, thus having different foundation flexibilities. In this study, Nembhard et al. [23] developed methods on another test rig to check for transferability and developed a new multispeed and multi-foundation (MSMF) method. Yunusa-Kaltungo et al. [25] also developed a sensitive fault identification method using the *pCCHOS* techniques. The current research is a follow-up to these earlier studies [20-25,28,29]. Investigation in this research work will be to

1. Observe parameters from both time domain and simple spectrum that will be useful for identifying rotor and bearing faults, especially if there is a consolidation of all the sensitive features.
2. Observe vibration signals obtained with the machine operating below and above its first critical speed. This observation helps with machines that operate at multiple speeds and even run over their critical speed during operation.

3. Observe both rotor and bearing faults in a single analysis. This observation helps to simplify diagnosis by providing both rotor and bearing fault identification at an instance.
4. Try out the higher order spectrum (HOS) for fault identification due to its advantage of retaining both amplitude and phase information.
5. Understand fault identification using a similar machine with different foundation flexibilities. This investigation builds from an earlier study which helps to indicate the indifference in fault identification for a similar machine. Since the machine can run over its critical speed, an approach for fault identification around the critical speed is tested, notwithstanding the foundation's flexibility.

1.3 Aim of research

This research aims to develop a vibration-based fault identification (VFI) approach capable of diagnosing an extensive range of 'rotating machine critical parts faults' in a single analysis.

1.4 Objectives of research

Below are the research objectives;

Objective 1: To carry out data trending of time and frequency (spectrum) domain parameters using existing data from an earlier built flange-based flexible test rig (FFTR) which ran only below its first critical speed. The data trending will help to determine parameter sensitivity for fault identification.

Objective 2: To improve an earlier unified multispeed analysis (UMA) fault identification method developed using acceleration data to an approach that considered acceleration and velocity features in its analysis. The data is from a flange-based flexible test rig (FFTR) which ran below its first critical speed.

Objective 3: To improve the existing FFTR to a spring-based flexible test rig (SFTR) to operate below and above its first critical speed. Afterwards, both rotor and bearing faults will be simulated on the SFTR.

Objective 4: To develop a novel fault identification approach for diagnosing a rotating machine consolidated critical parts (i.e., rotor and bearing) faults in a single analysis.

Objective 5: To improve an existing method, "the poly-coherent composite bispectrum (pCCB)," for rotor-related fault identification by updating the number of pCCB in the model. Furthermore, to analyse the complex number of the pCCB components, which combines the real and imaginary parts of the pCCB components for fault identification.

Objective 6: To develop a novel fault identification approach using a blend of time domain and pCCB components for a single analysis of an extensive range of rotating machine critical part faults.

Objective 7: To understand fault identification and dynamic behaviour of similar rotating machines having different foundation flexibility using the proposed method. So, vibration signals from more than one test rig are investigated and analysis observed while combining data from these rigs.

1.6 Outline of the report

The focus of this research is to provide a single analysis for an extensive range of rotating machine faults while understanding their dynamic behaviour exhibited with changes in speed during machine operation. The research is structured thus.

Chapter 1 presents an introduction, rationale for this research and the research aim and objectives.

Chapter 2 gives a literature review of relevant peer-reviewed articles, journals and published works that help to create a background for this research.

Chapter 3 describes the existing flange-based flexible test rig (FFTR) and the improved spring-based flexible test rig (SFTR). Also discussed are instrumentation and modal analysis. Simulated rotor-related and bearing faults with the data acquisition for this research purpose are also covered here.

Chapter 4 covers the methodology of the research. It discussed the selected methods and theories guiding them.

Chapter 5 looks at the improved acceleration and velocity features analysis using existing vibration data with rotor-related fault only from the flanged-based flexible test rig (FFTR), which operated only below the machine's first critical speed.

Chapter 6 covers the proposed data fusion of acceleration and velocity features (dFAVF) approach for the consolidated rotor and bearing faults identification. This

analysis uses the improved spring-based flexible test rig 1 (SFTR-1), which can be operated below and above the machines' first critical speed.

Chapter 7 looks at poly-coherent composite bispectrum (pCCB) for identifying and classifying rotor-related faults. The pCCB is a subset of higher order spectrum (HOS) analysis, a growing area of research for fault diagnosis in rotating machines.

Chapter 8 proposes a feature reduction approach for fault identification in the consolidated rotor and bearing analysis in rotating machines. The feature reduction approach involves acceleration-based time domain (AT) and poly-coherent composite bispectrum components (pCCB) parameters.

Chapter 9 looks at understanding the dynamic behaviour for effective fault identification of similar rotating machines operating under different foundation flexibility. This study is built up from earlier studies where some machines may not have baseline data for comparison and where the machine's installation may vary due to locations and foundation type. Here the improved spring-based flexible test rig 1 (SFTR1) and spring-based test rig 2 (SFTR2) are considered.

Chapter 10 is devoted to the conclusion of this research, contribution to knowledge and future work. It discusses the main outputs of the study, and additions to the relevant body of knowledge and shows how successfully the objectives of this research have been achieved. Recommendations to be considered for further research work were made.

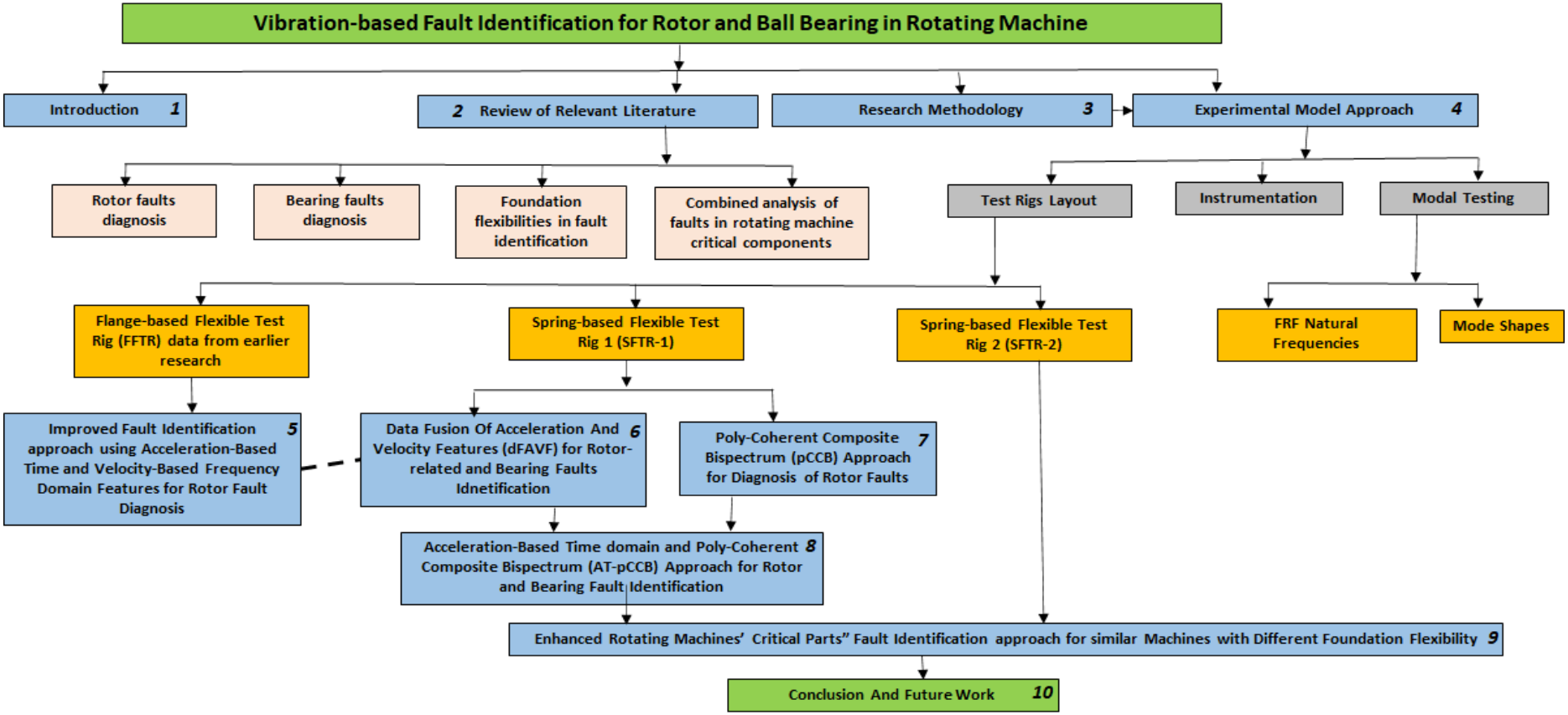

Figure 1. 3 Structural outline showing the progression in chapters for the thesis.

CHAPTER 2

REVIEW OF RELEVANT LITERATURE

This chapter covers a literature review of relevant peer reviewed articles, journals and published works that helps to create a background for this research. The aim of this review is to understand some basic approaches in vibration-based condition monitoring and discuss relevant methods proposed in various research and critically assess the current state of various techniques. The review builds from data management approach for VCM and focuses on techniques such as time and frequency domain analysis, envelope analysis, bispectrum analysis, modal testing, data fusion, clustering, and pattern recognition. It covers an extensive review of existing rotor and bearing fault identification approaches and critical pointing out gaps in fault identification especially in relation to industrial expectations.

2.1 Overview

Many studies have developed vibration-based fault identification (VFI) methods. However, more demand for improved and robust VFI methods is being made. The improvement is due to industry 4.0 (internet of things), computerisation and mechanisation of production processes [28]. On the other hand, the desire for increased output to meet customers' requests may stretch production processes. Thus, the machine needs to have high availability and reliability so that VFI methods that can detect faults efficiently and promptly are helpful in industrial applications [29].

This chapter presented background literature and research papers relevant to the review of VFI methods. This review helps to explore some existing VFI methods, their robustness, and their limitations. It provided abstraction for considerations of developments of new methods and potential future research work. However, the focus was on critical areas, including time domain and spectrum analysis, bispectrum analysis, envelope analysis, modal analysis, data fusion, pattern recognition, clustering, and classification of machine faults, as seen in Figure 2.1.

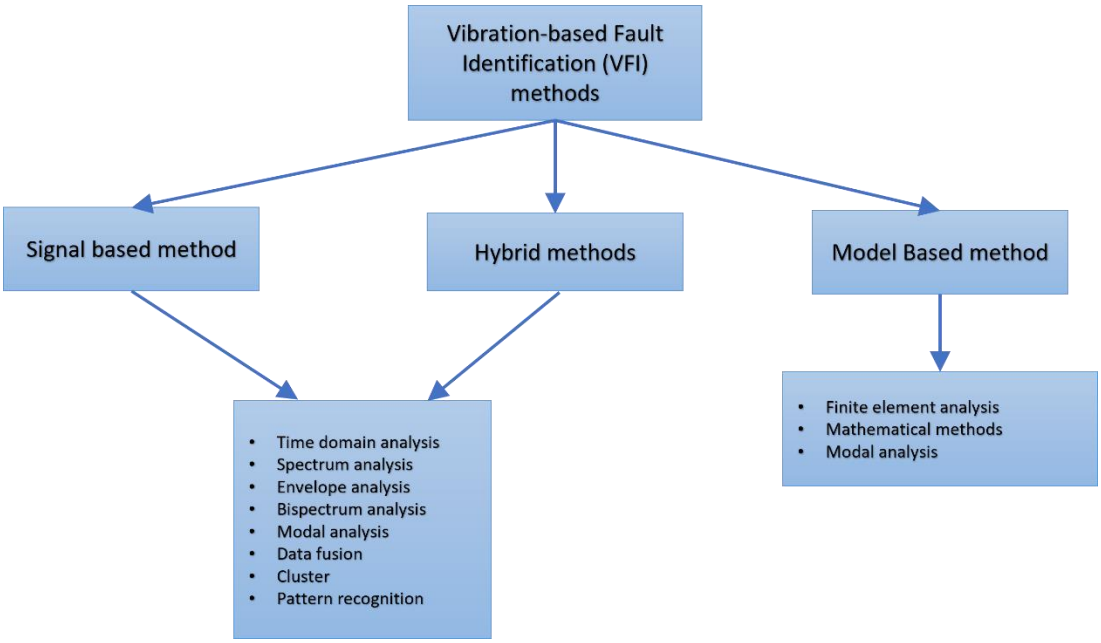

Figure2. 1 Vibration-based fault identification recent methods.

The model-based method used in fault diagnosis shows the possibilities provided by modern computers and software developments [30]. It can be broken down into mathematical modelling and finite element analysis (FEA) [31]. The mathematical model often provides a theoretical basis upon which data-driven FEA studies can be built and validated [31]. Even though the mathematical methods are traditional in rotordynamic problems, they are still being used to tackle advanced problems.

The FEA approach gives a continuously expanding simulation area to explore systems behaviour. Many studies have shown the power of FEA techniques with highly accurate simulations performed [32-35]. However, there are limitations to computer power. Applying FEA methods to a complete machine model could be too expensive computationally. As a result, alternative approaches such as model reduction and system level modelling are employed in an industrial scenario [34]. Notwithstanding accurate validation of experimental approaches using FEA, a complete understanding of the vibrational phenomena of rotating machines is not viable [27].

There are various fault identification methods, as can be seen from Figure 2.1 above. These methods have proven successful in the diagnosis of faults in rotating machines. Each of these methods showcases its uniqueness. However, this study has only selected several of these approaches to form a unique hybrid fault identification approach. This study's analytical review of vibration-based fault identification approaches on critical machine parts emphasises the demand for simplified, innovative and potent fault identification methods.

2.2 Vibration-based condition monitoring

Vibration-based condition monitoring (VCM) of the industrial system is vital for the early detection of faults or failures that may show up during machine operation. In this overview, VCM is classified into data management and fault diagnosis approach. These two concepts are discussed briefly in sections 2.3 and 2.4, respectively.

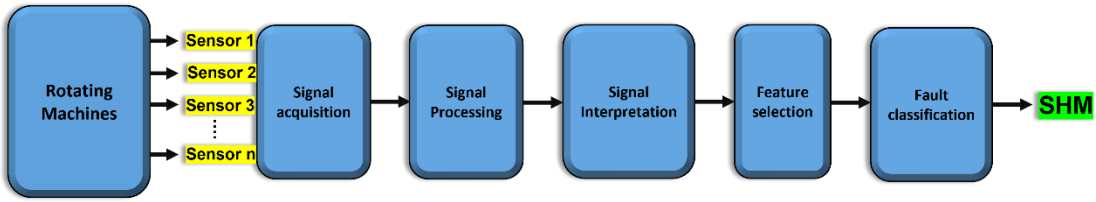

Figure2. 2 Vibration-based condition monitoring process for rotating machines.

Over the past decades, the increased interest and demand for a reliable machine cannot be overemphasised. Extensive research using vibration-based condition monitoring (VCM) techniques for diagnosing a wide range of machine failures has been on for decades [35]. The vibration-based condition monitoring (VCM) techniques are a popular tool that helps obtain machine conditions. As defined by Barron [36], "it is the ability to record and identify vibration signatures". These VCM approaches investigate faults that can be identified and various methods for their identification and detection.

Much information is present in measured vibration signals about the machine's condition. Therefore, advanced signal processing techniques are employed to investigate vibration signals to obtain fault peculiarity. This strategy is presented as the vibration-based condition monitoring (VCM) analysis [37]. It is presented in the time and frequency domain form [36]. VCM examines the interaction of distinct signatures with a particular fault in detail.

Recently, signal processing techniques have been applied in research work in the form of Fast Fourier Transform (FFT), Wavelet Transform (WT), Hilbert-Huang Transform (HHT) and Wigner-Ville Distribution (WVD) [38] and Higher Order Spectra (HOS)[39]. This help identifies and quantify faults, express their severity, and predict machine conditions [40].

Sinusoidal waves represent vibration signals, and it helps describe how vibration measurement can be obtained, i.e., the amplitudes of acceleration, velocity, or displacement. These have a mathematical relationship by a function of frequency and

time. In this light, variables describing vibrational behaviours have less focus, and however much is from a scale of time and phase [41].

Most fault diagnostic considers the traditional approach, i.e., power spectrum density (PSD) represented in time, frequency and time-frequency. They have been helpful in signal analysis for understanding machines' behaviour as regards early fault detection. However, challenges from industrialisation, computerisation, intelligent production processes and remotely-controlled factories have led many researchers to develop methods that accurately and reliably predict machines' dynamic behaviour. Some of these research works look at developing and improving various models and techniques for diagnosing and understanding the characteristic behaviour of different faults that may show up during the active life of rotating machinery.

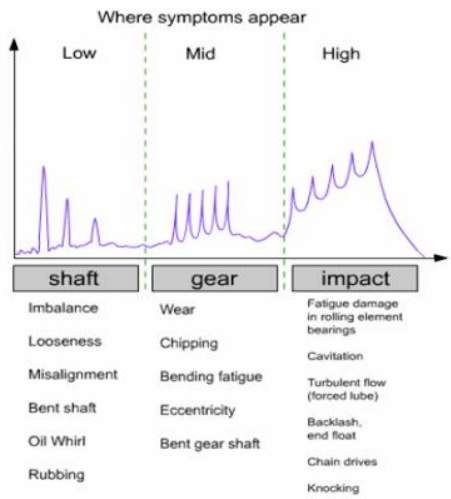

Figure2. 3 Frequency values range with the associated likely faults [46].

The recent industry 4.0 bring to the fore the consideration of intelligent models for machine faults diagnosis and prognosis using the condition monitoring (CM) approach [37,38]. Also, faults that show up in rotating machines are extensive, which may include rotor-related faults [35], bearing faults [44] and foundation-related issues [45]. Observation of these faults from vibration signals may appear around the low or high-frequency faults ranges. The low-frequency faults are rotor-related (unbalance,

misalignment, crack, and their likes.), while the high-frequency faults may appear as bearing or gear related (pitting in inner-race, cage, or gear tooth).

This chapter explains the characteristics of these 'low-frequency' (rotor-related) and 'high-frequency' (Bearing-related) frequency machine faults in rotating machines. It also considers appropriate diagnostic methods for identifying and classifying these rotating machine faults.

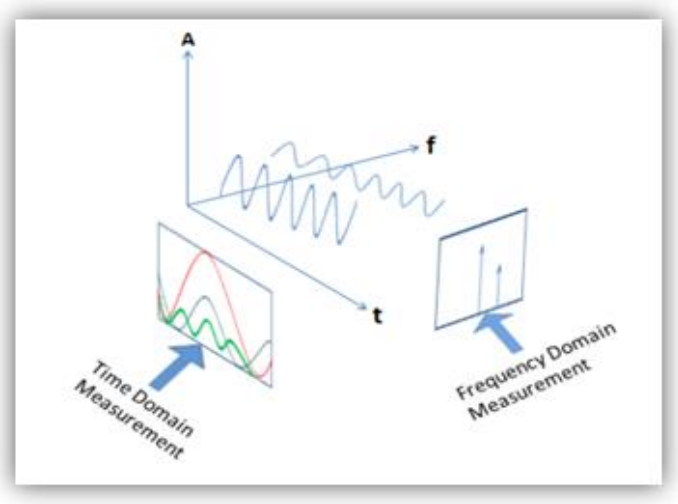

Figure2. 4 Transformation from time to frequency domain [47].

Features for VCM analysis are extracted when vibration data are obtained at a certain speed. Comparison is then made with a healthy reference state generated at the same speed. Machines have dynamic behaviours, so the features tend to be sensitive to changes such as speed [21]. This reference healthy helps to determine the presence of a fault or speed variation, thus acting as a check. However, in complex machines where there is always a change in machine speed, executing VCM poses some challenges.

Tumer and Bajwa [48] noted that the VCM diagnosis tool for such machines is presently lacking, with examples in aircraft, helicopters and their likes. In addressing this challenge, Huo et al. [49] developed a multi-speed fault diagnosis approach in which wavelet components were extracted from the vibration signal. The result was helpful as it identified four rolling bearing conditions. This work only dealt with bearing failure.

In the same vein, these researchers [20-25] developed classification approaches for effective VCM, which address the dynamics in machine behaviour relating to speed. A unified multi-speed tool [20] was proposed using acceleration features extracted from time and frequency domain parameters. The tool gave a helpful diagnosis of faults. Even though these studies cover some rotor-related and bearing faults, there is no consolidated fault identification tool for rotor and bearing in a single analysis. Overall, continuous improvement is crucial in achieving the demand for preferred VCM techniques in identifying machine faults [49] especially with industrial machines' recent complexities and intelligent behaviour.

2.3 Vibration data management

The VCM process is a data management approach which involves handling the data to get valuable information for assessing the machine behaviours and detecting faults or failures. The first step in VCM is data collection, which depends on the measurement location and type of transducers [45]. Data collection also depends on the type of signal to be measured (displacement, velocity, and acceleration). In the signal input, the transducers may be displacement, velocity pick-ups or accelerometer sensors.

The next stage is the data acquisition of vibration signals from the sensor. The recorded data may be analogue; thus, converted to digital. The data analysed is in terms of signal processing, development of algorithms for analyses and extractions of sensitive features.

The health assessment is the final stage of VCM. This assessment covers the estimation of the machine's current health grade, diagnosis and classification of machine condition, identification of faults and recommendations on the way forward for improved and efficient machine operation. Some signal processing and health assessment approaches are discussed in section 2.4. The selected assessment approaches for discussion are used in this research work.

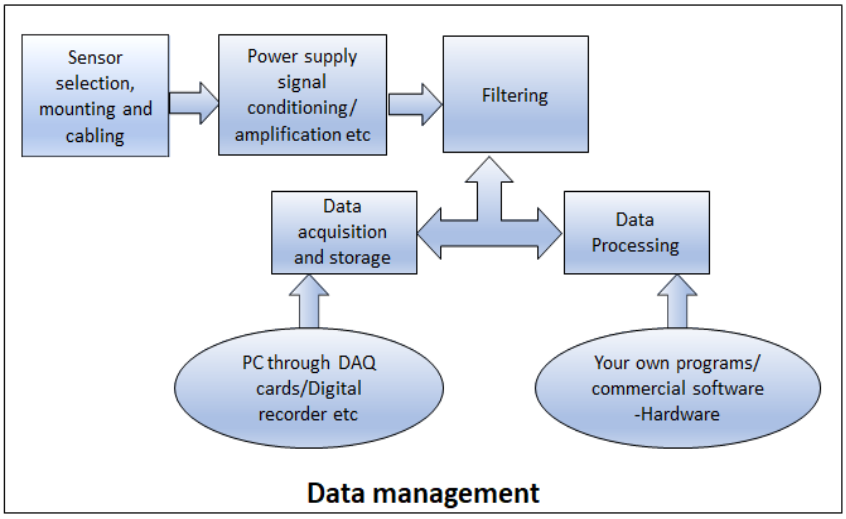

Figure2. 5 Data management for vibration signal.

2.4 Vibration-based fault identification techniques

2.4.1 Time domain analysis

Time domain analysis is a waveform representation of the measured vibration data [46]. Observation of the waveform, if not clear sinusoidal, may be challenging to carry out any proper analysis. Thus, some parameters help understand analysis in its representation, such as root mean square (RMS), crest factor (C.F.) and kurtosis (Ku).

A waveform's root mean square (RMS) measures energy [26-41]. It can be described as the square root of the mean value of squared values collected over an interval. It is simply obtained by squaring the waveform value. The result is averaged, and the square root is obtained. The crest factor (C.F.) is the ratio of the peak value to the RMS value of a waveform. It is a non-dimensional value. Kurtosis (Ku) measures the extent of peaks or flats a waveform has in relation to normal distribution. The higher the kurtosis, the more prominent peaks around the mean with a heavy base, while the low kurtosis gives a flat top around the mean. Kurtosis is a non-dimensional value, and it is defined as 'the normalised fourth order moment of a time domain signal [11,41].

Nembhard et al. [21,26,45] used these time domain parameters as part of features for fault classification in their studies. Time domain analysis has been useful, especially in electronics, vibration analysis, acoustics, communication, and construction. However, the main drawback in time domain analysis is that noise and disturbance

characteristics are less understood in the time domain than in frequency domain analysis. Time domain may not be a robust approach in VFI as computation is laborious and time-demanding when it involves a lengthy signal. Another cumbersome experience using time domain analysis is when the order of a system becomes large enough. However, the benefit of time domain analysis is its good indication of transient response.

2.4.2 Spectrum density analysis

Spectrum density analysis is a frequency domain signal representation [45]. This analysis is achieved by converting time domain signals to frequency to determine the different harmonic components contents found in the signal for a better understanding of the dynamic behaviour of the machine. This conversion is achieved using the fast Fourier transformation (FFT) and is represented in the amplitude and frequency plot. The spectra density is a build-up from the FFT where an issue may arise from a random start-up point for a segment, assumptions of selected segment size where time-period may be wrong. These may lead to amplitude and phase variation from segment to segment [45]. Also, some spurious peaks at the frequency may show up with the original peaks. So, large averaging numbers are recommended to reduce these random peaks in the signal. Spectrum density is an approach used when averaging is considered during FFT [45].

Harmonic components from the spectral density can be used to identify some faults that may show up in the rotating machines. These components are the 1x and its harmonics which help to show the appearance of faults such as unbalance, misalignments, shaft rub, bent shaft, etc. In various studies, Nembhard et al. [21,26,45] employed simple spectrum fault identification in a laboratory-size experimental rig. The study focused mainly on rotor-related faults diagnosis. You et al. [52] conducted an experimental diagnosis of typical rotating machine faults. The proposed fault diagnosis approach used spectrum analysis of vibration acceleration and velocity signal to determine fault severity and frequency division amplitude. Leob [53] presented an overview study of spectrum analysis with rotor and bearing fault diagnosis. The study covered basic information to carry out successful spectrum analysis, such as

components identification, machine running speed, the operational environment, and the measurement type.

In frequency domain analysis, several signal characteristics become visible, which were not easily seen when viewed in the time domain. For instance, frequency domain analysis is observed when considering the cyclic behaviour of a signal. In frequency domain analysis, signals are not changing over time, so transient information is lost. However, this factor can be addressed in several ways, but it depends on the time/frequency approach. Noise and disturbances are best understood using various parameters such as response peak, resonant frequency, gain and phase across frequency etc. The Bode plot and Nyquist plot are some established useful frequency domain analysis tools; however, interpretation may be indirect. Even though analysis can be robust in the frequency domain, it gives less accurate mathematical models than in the time domain.

2.4.3 Envelope analysis

Envelope analysis has been a helpful technique in studying amplitude modulation of machine vibration signals. The tool is powerful as it helps signals stand out from the noise. Regularly spaced signal components can be observed, such as defects found in the raceway or cage. Envelope analysis is an established method of determining faults in rolling element bearings. [54]. According to Leob [53], envelope in bearing fault diagnosis considers the frequency range at which the bearing defects impact occurs repetitively. Enveloping can also be referred to as "Envelope Detection" or "Amplitude Demodulation"[55], and it is a technique used in extracting modulated signals. The extractions can be investigated in both time and frequency analysis.

Envelope analysis represents the fast Fourier transform (FFT) frequency spectrum of the modulated signal [55]. Analysis of envelope (demodulated) signal brings out the modulated frequencies, which are the bearing fundamental defect frequencies [45][56]. Group [57] compared signal analysis techniques and observed envelope analysis were best in detecting machine conditions which generate shock pulse. The work successfully diagnosed anti-friction bearing running with low speed using

envelop analysis. The study considered various rotating machines with valid envelope analysis diagnoses, i.e., diesel engine and gearbox diagnoses.

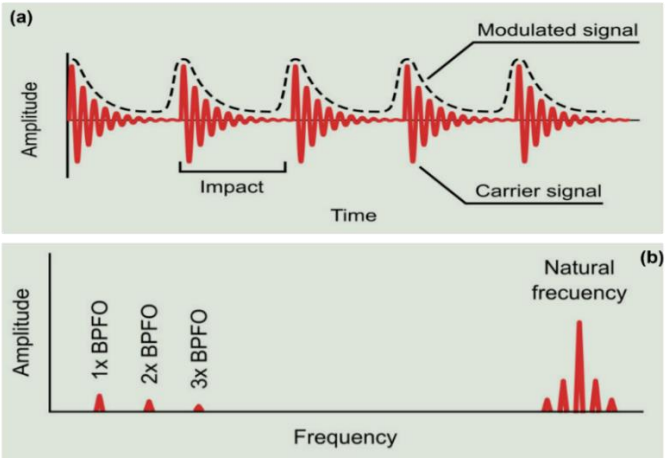

Figure2. 6 Envelope analysis (a) Time domain (b) Frequency domain accessed from [58].

In envelope analysis, both input and output signals are analysed simultaneously, which is relatively effective. However, the effect of exogenous variables on the operations is ignored. In signal envelope analysis, the stress comes with choosing the central frequency filter in which experience is needed. Also, the spectral line of fundamental frequencies may be difficult to locate in the envelope spectrum.

2.4.4 Bispectrum analysis

Wang, Wu and Chen [62] classified rotating machine faults with the combination of correlation dimension and bispectral analysis. Sinha and Elbhbah [15] proposed reducing the number of transducers at bearing pedestal measurement locations using a composite spectrum and bispectrum to understand the signals from a rotor-related fault on a rigid test rig. Elbhbah et al. in various studies, [15,60 - 68] employed bispectrum in rotor-related fault identification. Yunusa-Kaltungo et al. also in various studies [22,24,25], used composite coherent bispectrum in rotor-related fault diagnosis. The study improved [21] the composite coherent spectrum analysis and later proposed the poly-coherent composite bispectrum (pCCB) [70] analysis.

The bispectrum analysis has shown usefulness in many fields such as seismology, signal analysis, music, wave pattern and earth tides. However, its usefulness in fault identification in rotating machines is still expanding. Most studies have used bispectrum diagnosing rotor-related faults only as few have applied it for bearing fault diagnosis, however, in combination

with other approaches. Since it helps investigate non-linear signals, much functional analysis is expected in further research using bispectrum analysis in bearing and gear fault diagnosis and further improvements in rotor diagnosis.

2.5 Modal analysis approach

The idea behind modal testing is to create the resonate conditions at the natural frequencies of a machine by applying external force so that the resonance peaks can be acquired by the accelerometer response [40, 66]. According to Sinha [45], "In experimental modal analysis, an external dynamic force (excitation) to the structure is applied in a controlled frequency band, and simultaneously the vibration response at several locations were picked up and then the collected vibration data are analysed to extract the modal parameters, namely, natural frequencies, mode shape and modal damping". The step-by-step procedure for modal analysis is detailed in Sinha's book [45].

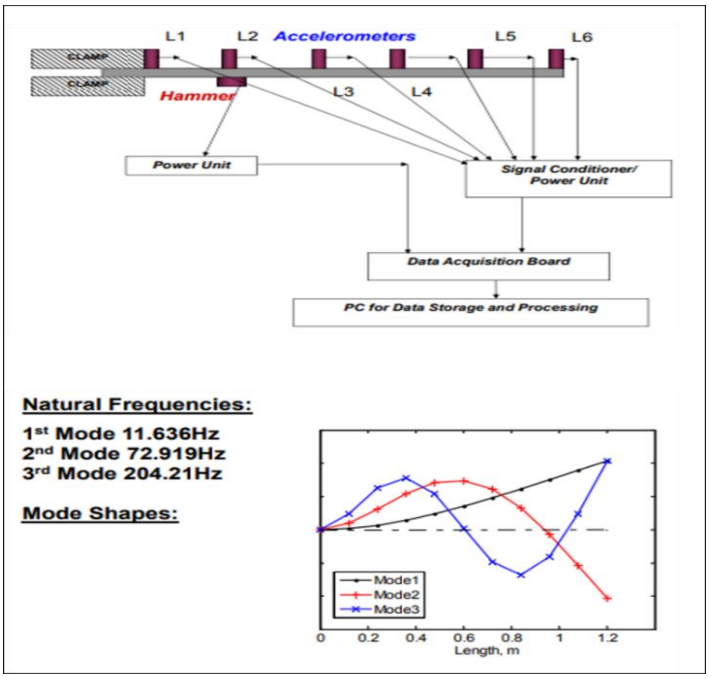

Figure2. 7 Modal testing for a cantilever beam, its natural frequencies and mode shape accessed from [56].

Figure 2.7 shows typical modal testing on a cantilever beam, the natural frequencies and mode shape. These studies identified critical speed in rotating machines using

modal analysis [72] [79-66,80]. The use of modal analysis for fault identification can be found in this literature [67-68,78,81].

A significant benefit of modal analysis is the identification of natural frequencies, i.e., the frequencies at which the system vibrates freely and mode shapes, i.e., the deformation of the structure. The analysis helps to keep the system safe as the excitation frequency is set so that it is different from the natural frequency to avoid resonance.

Many studies have used experimental and modelling approaches in developing modal analysis, especially for rotating systems; however, the industries still have not considered fault identification approaches using modal analysis. Most industrial operations only look at the nameplate to get the value of the natural frequency. However, the natural frequency may shift with constant operations and fault development. If care is not taken, it may coincide with the excitation frequency causing much vibration, which can lead to severe bearing faults, unbalance, and misalignment around the coupling, and if not checked in time, the machine breaks down. Industries should be encouraged to perform modal testing before other forms of maintenance are done.

2.6 Data fusion approach

Data fusion involves integrating, combining, and consolidating various data sources to achieve clear, useful, and correct information. The information provided by data fusion is more robust than any of the individual sources [82-83]. The data sources may vary in size, events, sources, and components. However, once they are in a data block set, they complement each other [79].

Some selected literature that achieved distinct machine fault identification through data fusion was included [84-87]. Yunusa-Kultango et al. [21] used data fusion of composite spectrum and poly-coherent composite spectrum to diagnose rotor-related faults in a rotating machine. The approach gave outstanding fault identification. In various studies [28,45,88], Nembhard applied data fusion of time and frequency analysis and temperature parameters to identify machine faults. Further

considerations included data fusion of multiple speeds and multiple foundation parameters [20,28,88]. Most of the studies by Yunusa-Kaltungo and Nembhard fused data from multiple sensors and bearings. Jiang et al. [83] performed fault diagnosis in a rotating machine based on multi-sensor data fusion using support vector machine (SVM) and Time-Domain Features. In these studies, the fusion of sound signals [5], and dual sensor fusion [84], helped diagnose the fault in a rotating machine.

Recent studies in VFI that considered multiple fault investigation tends to fuse data from multiple sensors. The data fusion can give an overall behaviour of the machine's condition in one analysis. Also, using various sensitive parameters can show an indication of a particular fault and another for a different fault, but overall fault identification is achieved. However, too much data could make diagnosis cumbersome, so parameter reduction is helpful to filter out some non-essential features that may not contribute so much to fault identification.

2.7 Clustering approach

Clustering analysis is a statistical approach to grouping related data into a given set. In clustering analysis, algorithms are written to discover patterns and group datasets for investigative purposes [85]. Groupings of various data are achieved in such a way that similar data form clusters. Similarity measures used in clustering analysis include Euclidean, probabilistic, cosine distance and correlation. Many of the unsupervised learning approaches are, one way or the other, a form of clustering analysis.

A clustering algorithm is broadly classified into two main groups, i.e., hard and soft clustering [85]. Hard clustering is such that in a particular data, each data point belongs to just one cluster, like in the k-means approach, while in soft clustering, each data point can belong to more than one cluster, like in Gaussian mixture models. The use of cluster analysis covers exploratory data analysis, fault detection, segmentation and pre-processing in supervised learning. It also helps in discovering groups in dimensionality reduction and feature ranking.

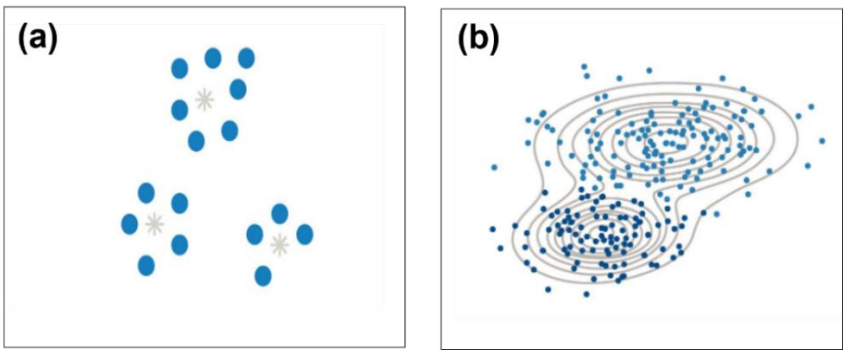

Figure2. 8 Clustering analysis (a) k-means clustering (b) Gaussian mixture model which assign cluster membership probabilities both accessed from [85].

As helpful as cluster analysis may be, its application has some limitations. Amongst which are the availability of enough relevant data, so that in fault identification, the first few data from a machine may not provide sufficient diagnosis using the clustering approach, but as machine data increases, then there is an improvement in diagnosis [86]. Note that the analysis is a simple statistical tool with no prior evaluation of the trends existing in similar datasets. Using clustering analysis is less skilful but interpreting the results obtained to understand machine behaviour and using it to determine the trend for determining machine health is of much higher skill.

2.8 Pattern recognition and classification approach

Pattern recognition is a data analysis method that uses a programmed approach to recognise patterns with regularities in data. Familiar patterns can be recognised promptly and accurately. It is applied in data analysis, image analysis, computer graphics, and machine learning. It is a vast technology behind data analytics, and pattern recognition has recently helped investigate big data.

Principal component analysis (PCA) is a pattern recognition method used to visualise patterns and understand potential relationships in systems. PCA is possibly one of the best-known and simple classification techniques [93-94]. It is a widely used technique. Some recent works with good diagnosing results in VCM using PCA can be found in [24-26,95-101]. Figure 2.9 show a PCA pattern recognition where the original data space undergoes dimensionality reduction and is represented in the component space.

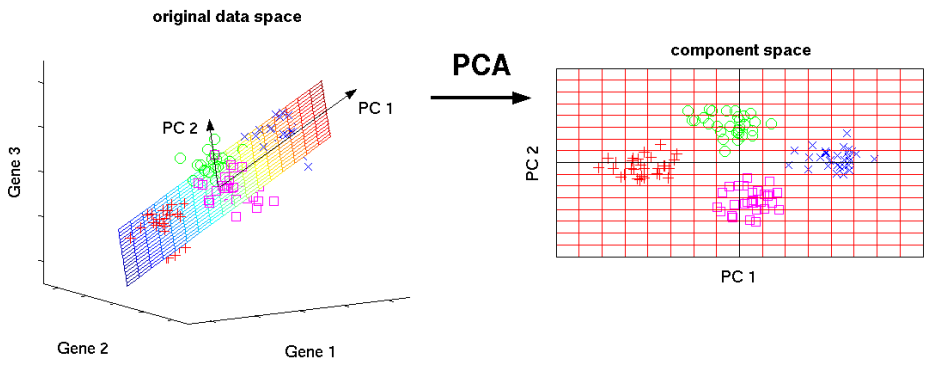

Figure2. 9 PCA pattern recognition from original data space to component space [91].

In most practice, extensive data sets are obtained for VCM analysis where a considerable part contains unnecessary data. These parts of the data may hinder effective condition monitoring and fault diagnosis. A solution is for such machine data to undergo dimensionality reduction where helpful information can be collected from the data for analysis [92]. Thus, a dimensionality reduction technique for fault diagnosis is proposed by Haung et al. [92]. PCA was a vital tool in the development where the result tends to be better than existing methods.

Song et al. [8] employed PCA in both simulated and experimentally extracted residual fault shaft bow features on a rotor longitudinal response. The result from both analyses consistently proved helpful. Sun et al. [93] investigated data mining technology and applied PCA for fault diagnosis. The aim was to validate a proposed method with six rotor conditions simulated on a Bently Rotor kit R.K. 4. Results showed higher accuracy with data needing less training. Serviere and Fabry [94] tried to address data collection from rotating machines with highly corrupted signals. PCA was used as a first step filter for noise and whitening of the observation. The result showed the efficiency of PCA.

Features that make up machine conditions are very sensitive as they change under different conditions. Hence the demand for a good feature selection tool cannot be compromised. Malhi and Gao [95] presented a feature selection scheme based on PCA tool analysis. Supervised and unsupervised fault classification approaches were employed experimentally on data from a bearing test rig. An important aspect is the detection of fault severity with no prior knowledge of machine conditions. Analysis

proved accurate classification concluding the proposed tool is helpful in machine health monitoring.

Widodo et al. [96] investigated low-speed bearing fault diagnosis using relevance vector machine (RVM) and support vector machine (SVM). Different bearing faults classification were conducted using PCA. The result showed RVM as a promising tool. Nembhard et al. [97] express the need for an experienced condition monitoring analyst to diagnose faults using conventional diagnostics methods efficiently. However, developing a simplified technique where analysis is done using a single vibration and temperature sensor on each bearing of a rotating machine was the focus of their work [97]. Measured vibration data from a laboratory scale experimental rig was obtained. PCA is then employed to classify machine conditions, firstly without temperature and then with a combination of vibration and temperature. In dealing with the dynamic behaviour of a machine where a change in speed during operation is the norm, such as the aircraft, Nembhard and Sinha [22] developed the unified multi-speed diagnostic approach. PCA was employed under four scenarios 'single speed at single bearing, integrated feature from multiple speed at single bearing, single speed for integrated features from multiple bearings and the proposed unified multi-speed analysis' [22].

2.9 Machine critical components' faults identification techniques

Failure is the inability of a system or component to function according to specified standards of operation [28,106-107]. Various faults may appear or continue during the rotating machines' operation [11]. Investigation of faults in rotating machinery has a broad scope [35] as an extensive range of faults may show up during the operation of the machine over time. These investigations focus on parts such as rotating shafts, bearings, gears, and pumps, [100] which may be seen as the machine's critical parts. The works of Sinha [45], Bently [101], Muszynska [102] and Walker et al. [35] discussed basic details of rotor-related faults while [39-40, 111-114] focused on bearing failure.

However, to achieve a definite outcome in this research, some popular machine critical parts faults (rotor-related or bearing faults) are considered, including unbalance, misalignment, shaft bow, mechanical looseness, shaft rub, crack shaft and bearing cage defects. These faults' occurrences vary; some are more prevalent than others

[35]. Also, some of these faults do not exist separately; for instance, the presence of misalignment may lead to other faults [11]. Some studies in fault differentiation with helpful diagnosis also have limitations, such as the faults may be more complex in real life than in the lab. The systems for research in fault differentiation are simple and cannot be exactly compared to a more complex real-life machine. Descriptions of their occurrence and identification are discussed to create the basis for understanding the faults considered in this research.

2.9.1 Condition monitoring tools for fault identification

Fault identification in a rotating machine can mainly be achieved through condition monitoring (CM) which is a tool relevant to the improvement of condition-based maintenance (CBM) [45]. CBM is carried out in the plant to reduce maintenance costs while improving plant availability to avert failure [46].

Some CBM approaches for effective fault identification are acoustics, lubricant analysis, infrared thermography, oil condition sensors and most importantly, vibration analysis.

Acoustics is a non-invasive, non-intrusive CBM tool. It is used in complex machines where temperature or humidity is involved. It mainly covers the use of recorded sound emissions in diagnosing machine conditions. It should be noted that installation should be in proximity to the section of the machine to be monitored as this will provide valid data, not corrupted by external noise [100, 115].

Lubricant/oil analysis is a routine test to observe and determine the oil contamination and wear from machines. It deals with tracking the health of a machine over the years to establish trends, identify machine faults and detect failure parts. Lubricants help to reduce maintenance costs [41, 116].

Infrared thermography analysis is a non-contact and non-destructive approach to measuring the radiation from the surface of heated rotating machine parts [41, 117]. Thermal images from infrared have been helpful in condition monitoring to detect causes of heat, friction, and excess vibration on a machine. Thermal signatures

obtained from rotating machines have provided information for fault identification and diagnosis [105, 117].

Notwithstanding the usefulness of these CBM techniques, vibration-based condition monitoring (VCM) is the basis of any condition monitoring strategy. Page [109] quoted Art Crawford (founder of IRD) to say, "No single measurement can provide as much information about a machine as the vibration signature." Thus, it is the most accepted and preferred approach in CBM for fault identification in the industry and for many research purposes. [41-50].

In vibration analysis, signals are recorded, and analysis is carried out either in the time or frequency domain. Parameters from time domain analysis give useful fault identification information for rotor-related and bearing faults. Such as information obtained from peak-to-peak and root mean square (RMS) parameters for rotor diagnosis and the crest factor (C.F.) and kurtosis (Ku) parameter due to their impulsiveness for bearing fault diagnosis [40-41]. The frequency domain analysis, however, uses harmonic components of the machine running speed to provide diagnostic information, especially for rotor-related faults.

However, bearing diagnosis depends on its defect frequency calculated based on the configuration of the bearing [40-41,50]. Also, time and frequency analysis features can be used to develop data fusion and classification tools for a better understanding of machine dynamics and fault identification [25-26,119]. Some vibration-based fault identification (VFI) approach relevant to this study is discussed briefly in the subsections below.

2.9.2 Rotor-related faults identification

The rotor is one of the three critical components of a rotating machine. Fault identification methods that may appear in the rotor during machine operation are discussed here.

2.9.2.1 Unbalance

Unbalance is one of the most common rotodynamic faults [101]. There is an inherent degree of unbalance in every rotating machine. A machine's imbalance occurs when

the centre of mass of a rotating disc does not coincide with its centre of rotation [30]. The shaft of a rotating machine is not perfectly balanced in practical terms, which may be due to errors from manufacturing and loss or gain of material during operation [11]. Unbalance leads to a high amplitude of vibration in a shaft because of the centrifugal force generated by the rotating shaft. An indicator of unbalance is the overwhelming presence of 1x component of the shaft speed. Figure 2.10 shows a representation of and dynamic unbalance.

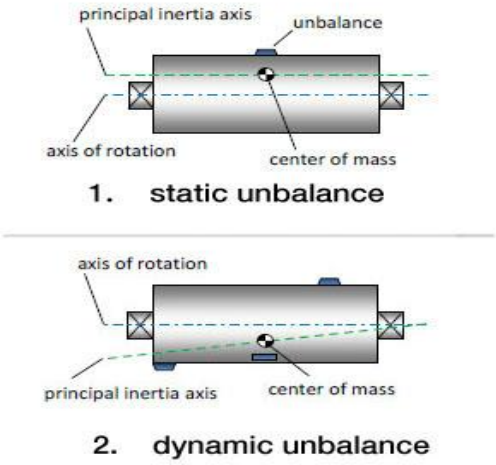

Figure2. 10 Diagram showing the static and dynamic unbalance [111].

Extensive studies [112] on unbalancing in rotating machines have been done and are ongoing using various approaches. Some of which may include, but are not limited to, unbalance as a result of misalignment and other faults [123-124], diagnostic identification of unbalance [125-126], and prediction of unbalance fault using simulation techniques [126-127]. Also, experimental-based investigation from labs [128-130]and artificial intelligence (A.I.) and artificial neural network (ANN) [120,131-136] approaches.

He et al. [122] proposed the novel tensor classifier method called the "dynamic penalty factor support tensor machines" (DC-STM) for the diagnosis of rotating machinery with unbalanced data. This model can diagnose machine conditions using tensor data instead of traditional vector data. So that the relevance of the study is seen as the DC-STM carries out diagnoses in tensor space.

Morais et al. [123] developed a new approach for identifying rotating machinery and the unbalance distribution in linear and non-linear conditions using pseudorandom improvement methods and a finite element approach for modelling the system. Experimental validation was achieved using a test rig. Xu et al. [120] proposed a renewable fusion fault diagnosis network (RFFDN) for variable speed conditions monitoring using an unbalanced sample. This approach is a branch of the convolution neural network (CNN). Results show high diagnostic accuracy and useful invariant feature at variable speed under unbalance samples with the accurate classification of new faults.

Zhao et al. [124] observed that the deep learning (DL) diagnostic approach suffers some adverse effects with unbalance data, thus giving limited accuracy improvement. In order to improve diagnosis, the variational auto-encoder (VAE) is introduced to enhance data amplification; after that, an improved fault detection technique which combines convolution neural network (CNN) is introduced.

Yan, Hu and Guo, [28] proposed a rotor unbalance fault diagnosis method using a deep belief network (DBN) to learn the representative features automatically and accurately identify faults. The study used multi-source heterogeneous information made up of vibration signals and shaft orbits plots generated by displacement signals from multi-sensor. With the aid of a multi-DBM model, information fusion was achieved, which adaptively learns useful features through multiple non-linear transformations, which was better than the traditional approaches where feature extraction was time-consuming and labour-intensive. Rotor unbalanced faults were accurately classified.

Moravian et al. [125] aimed to develop a proper intelligent technique for detecting an unbalanced fault in rotating machines using KNN and SVM classifiers in this study. Vibration data was obtained from an experimental approach with three machine conditions, i.e., no load, balanced load, and unbalanced load. A transformation of the vibration signals from the time to frequency domain was achieved using the FFT method. Some feature parameters were extracted from the FFT amplitude. After that, SVM and KNN were used in classifying the three conditions. KNN had a quicker training

test time. However, the performance of SVM was better than KNN in fault identification and classification.

2.9.2.2 Misalignment

Misalignment is a prevalent fault that exposes rotating machines to increased potential failure [35]. It is one of the most frequently occurring faults in rotating systems after unbalance [126]. Misalignment shows up when the shaft of the driving and driven machines are eccentric because of improper assembly [30]. Diagnosis of misalignment faults can be achieved by having a good knowledge of dynamics [127]. Excessive vibration is generated from misalignment, making the fault diagnosis difficult. Machine misalignment increases due to temperature increase, uneven load, and inappropriate foundation set-up [127]. Misalignment occurs as either parallel or angular as seen in figure 2.11.

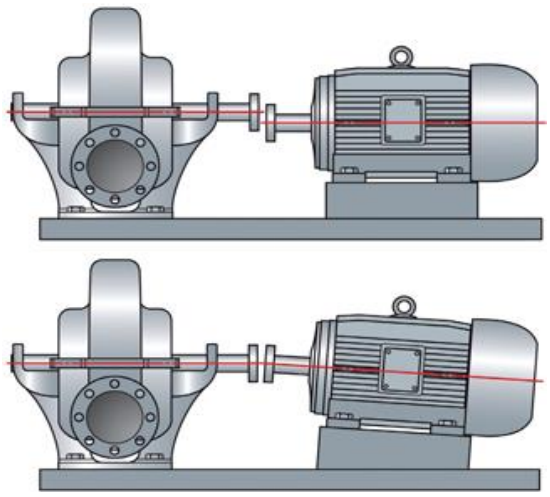

Figure2. 11 Showing the representation of angular and parallel misalignment [128].

A theoretical model that can detect the vibratory response of misalignment in a shaft with flexible coupling was developed in [129]. The work presented a new finite stiffness matrix tested on coupling stiffness. Using finite element analysis (FEA), an investigation of a mechanical signal obtained by a mixture of angular and parallel misalignment features with residual unbalance was presented. The result showed that the vibration produced depends on the difference in coupling stiffness in the rotation. It was also observed that the amplitude of the measured vibratory component directly

depends on the frequency response function related to coupling and measured point. Experimental validation of the developed model was done using the response from a test rig [130]. Waveform, frequency spectrum and phase shift were observed from various magnitudes of misalignment and coupling types. Investigation showed successful validation of the proposed theoretical model. However, further work considering the dynamics of the machine experiencing a change in speed during operation would be helpful.

Also, angular and parallel misalignment dynamics in rotating machines were investigated [102]. Spectra Quest Machinery Fault simulator (MFS) generated data for the experiment. The result showed that misalignment leads to Bearing fault and excessive vibration. However, more work on a giant rotating machine, especially with changing speed during operation, would enhance this work.

According to Ahmed [131], misalignment is a prevalent fault in rotating machines. However, no comprehensive research has been performed to resolve this failure. Few pieces of research have some impact in this area. Most research in the lab makes use of single coupling while investigating misalignment faults. However, real machines have multiple couplings, thus many locations of misalignment.

2.9.2.3 Shaft bow

This fault is a primary source of unwanted vibrations in rotating machinery. A significant cause of shaft bow is thermal deformation in a running system [35]. It also shows up when a machine is stationary over a long period [98], as the weight of the rotor makes the shaft deflect and is set permanently in a bow shape. A picture representing the shaft bow is shown in figure 2.12.

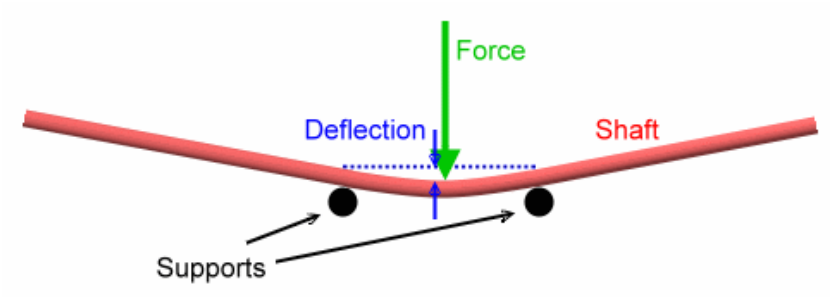

Figure2. 12 Shaft Bow Sourced from [75].

Meagher et al. [132] developed a mathematical modelling technique to diagnose residual shaft bows differentiated from other faults. The model was developed based on established techniques and showed a distinctive approach as responses were extracted at the Bearing point. This application would favour industrial analysis due to easy access to the bearing point. In addressing the inconsistencies and variations that occur in the life of a machine over a period, Gaka and Tabaszewski [133] used statistical symptoms on established data in the diagnosis and prognosis of various faults with a focus on shaft bow and unbalanced.

Also, the modelling of shaft bow systems having a permanent bow with a view of understanding the impact of dependent faults like rub was investigated by Shen et al. [134]. An essential aspect of this work is the combination of faults to provide a functional classification approach for fault differentiation. However, this work did not consider fault severity and the process vibration as faults are developed [35].

Song et al. [34] use simulation and experiment to investigate the impact of residual shaft bow on the rotor longitudinal responses. Different simulated cases were considered, with the result showing the severe effect on rotor vibration with the presence of residual shaft bow. Wavelet and non-linear learning methods were used to extract features from the experimental signal. Using PCA, faults were identified whilst obtaining the residual shaft bow faults. The simulation and experiment presented valuable results. However, further work on diagnosing shaft rub and other faults can be considered on a machine having to change speed during operation.

2.9.2.5 Mechanical looseness

Mechanical looseness is one of the common rotor faults that a rotating machine encounters during its life cycle [135]. It leads to other faults, such as rub, eventually leading to machine breakdown. The cause of mechanical looseness is an outcome of improper fitting of components, which is observed in the internal assembly, based and the structure of the machinery. Early detection of looseness saves maintenance costs, keeps operators safe and makes the machine last longer [135]. Figure 2.13 shows mechanical looseness at an assembly point.

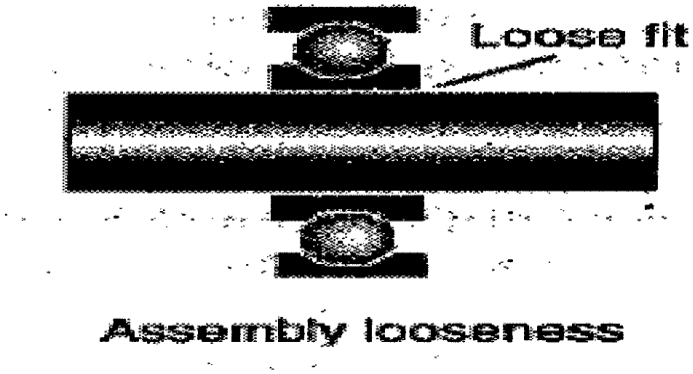

Figure2. 13 Showing looseness fault in a component.[136].

In the work of Ngolah et al. [137], a three-layer artificial neural network (ANN) was employed in monitoring and diagnosing some machine faults in which looseness was included. A few key performance indicators were determined and adopted for training. Investigation showed it to help study looseness and rub fault [35]. This work was on a laboratory scale; however, the industrial application is suggested.

In developing a model to identify looseness fault that shows up in various components of rotating machines, Wu et al. [135] used the post-processing Ensemble Empirical Mode Decomposition (EEMD) and Autoregressive (A.R.) model. This work was validated on a test rig, and the results showed the detection of looseness faults on various mechanical components. Nonetheless, a combination of faults in dynamic systems should also be considered.

2.9.2.6 Shaft rub

Shaft rub is always observed as a dependent fault, i.e., it occurs due to other faults such as looseness [35], which leads to wear and fatigue. Rub fault frequently happens in areas with little clearance in the rotating machine. This fault tends to become severe as it worsens, leading to failure during production and economic loss [138]. Rub leads to a system rise in temperature as well as metallic particles drops in oil. Figure 2.14 shows a picture of a turbine with blade rub leading to bending.

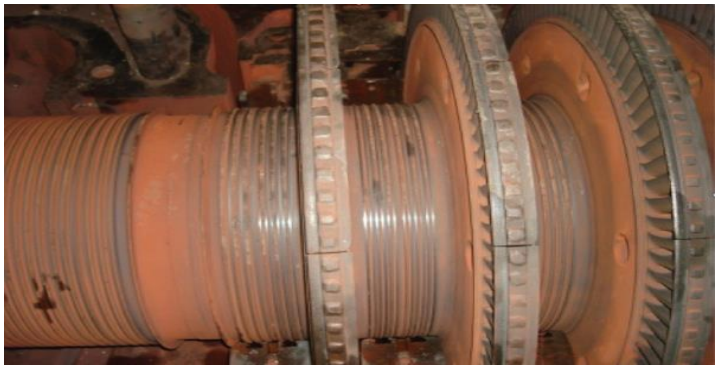

Figure2. 14 Blade rub fault [139].

Limin et al. [2] observed that pedestal looseness leads to shaft rub fault. Once this occurs, the system becomes non-linear and unstable. The analysis focused on presenting a turbulent system that could operate normally adaptively, notwithstanding agitation from external systems. The numerical analysis gave valuable results. However, further investigations can precisely manage the rotor-bearing system.

In the work of Peng et al. [140], detail of shaft rub fault was examined with a focus on causes and severity. Investigation into effective monitoring of rub-caused impact was carried out by comparing conventional scalogram and reassigned scalogram methods. Analysis shows a beneficial result for determining rub fault and its severity. The signal for analysis was obtained from a test rig. The reassigned scalogram was seen as more effective in figuring out rub-caused impact as it also helps recognise the exact time and frequency of impact. Whilst this study achieved success, the reality of most machines is that the faults exist together. Therefore, a combined analysis of faults would present a better application for industrial purposes.

A study by [137] ANN method was used to diagnose rub and looseness faults. Notwithstanding the developed approach's usefulness, the research used apparent features of each fault, which are much easier to identify in a lab environment than in a noisy industrial application.

2.9.2.7 Crack shaft

A crack shaft is a potentially severe fault in rotating machines, so early detection of such a fault is critical. A crack shaft causes the shaft stiffness to change from high to low to high in a complete revolution caused by breathing (opening and closing) of the crack [11]; this is due to the self-weight of the rotor. A 2x component observed in the shaft results from the open and close movement; however, the amplitude and phase of 1x and 2x components change with time [11]. Figure 2.15 is a pictorial representation of a crack on a shaft. The simulation of the crack shaft can have a great advantage over data-driven methods.

Figure2. 15 Crack Fault [80].

Stoisser and Audebert [141] broadly discussed the theoretical, numerical and experimental method for crack identification in a rotating machine in a power plant. The study used the approaches adopted by EDF for crack detection. The theoretical beam model developed by S. Andrieux and C. Vare and their associates were employed in the numerical and experimental approaches for crack detection. The theoretical aspect of the study considered a deviation of lumped cracked beam model of a three-dimensional formulation with general issues of elasticity and unilateral contact condition on the crack lips. Experimental validation was performed using various

cracked samples from static and dynamic configurations. Observation of torsional behaviour using the cracked beam model was proposed to obtain a more accurate estimation of when external forces act on the shaft.

Ren et al. [142] combined the 3-D waterfall and the reassigned wavelet scalogram approach to analyse a crack fault's temporal frequency characteristics. Experimentally simulated crack faults at three different crack depths, and analysis showed effective results using the proposed approach. This observation showed especially the twofold frequency component with the measurement at half the critical speed.

Oppenheimer and Loparo [143] presented a physics-based fault identification approach using integrated observers and life models. The observers used are filters on physical models of a combination of machine faults and measured signals in the identification and characterisation of the machine's health, while the life model is based on the "Forman crack growth law of linear elastic fracture mechanics" to ascertain the useful remaining life before machine breakdown. The study observed shaft crack and imbalance.

Other studies on crack fault identification approaches included a diagnosis of shaft crack in gearbox [144], novel transverse crack detection on rotation shaft [145], and active magnetic bearing actuators for shaft crack identification [146]. Also, were detection and diagnosis of the crack shaft [147], a survey on crack rotor dynamics state of the art [148], detection and monitoring of crack using Hilbert-Huang transform [149], diagnostics of transverse open crack on a stationary shaft [150], review of modelling and analysis of crack rotor [33], review on dynamics of the crack rotor [151], higher-order spectra for crack identification [39].

2.9.3 Bearing defect identification

In rotating machines, the bearings are part of the most critical components with demand on their carrying capacity and reliability [152]. Thus, much research has been done over the years on rolling elements bearing, with many benefits. One is the calculation of its life with reasonable accuracy [153]. However, in real life, a bearing may not operate up to its calculated life rating, which may be due to handling

carelessly, heavy loading, and inadequate lubrication. Each of the factors causes peculiar damage to the bearing [153]. Figure 2.16 shows micropitting and flaking in the ball and cage of a rolling element bearing.

In diagnosing the rolling element bearings defects, some frequencies are generated based on the bearing geometry and the relative speed between the inner and outer race [12]. The frequencies result from local faults in the rolling element bearing, giving a sequence of repeated periodic impacts [54]. These repetition rates are called the fundamental fault frequencies. Knowledge of the bearing geometry helps to determine the fundamental fault frequencies, which are ball pass frequency inner race (BPFI), ball pass frequency outer race (BPFO), fundamental train frequency (FTF) and ball spin frequency (BSF) [12].

McFaddam and Smith [154] noted several VCM techniques for bearing fault diagnosis, including crest factor analysis, shock pulse monitoring, kurtosis, spectrum analysis and demodulated resonance analysis or envelope power spectral density analysis.

Figure2. 16 Micropitting and flaking in ball and cage defect of a rolling element bearing accessed from [155].

Zhang and Randall [103] expressed that the envelope analysis (resonant demodulation technique) is widely accepted for bearing fault diagnosis. However, the sensitivity of the diagnosis parameters using envelop analysis for different working conditions, such as changes in speed, may not reflect reality, especially for a wide frequency range with weak strength. Nevertheless, the kurtosis of the vibration signals of a bearing is

different from average to bad conditions, with a robust sensitivity in varying conditions. The study considered the fast kurtogram and genetic algorithms diagnostics approach. Therefore, it proposed a model and algorithm design for improving resonance demodulation by combining a fast kurtogram and a genetic algorithm. Experimental studies were used to check for the feasibility and effectiveness of the proposed method. A better result was achieved compared to the traditional method.

Randall, Antoni, and Chobsaard [39, 112] carried out studies on comparing cyclostationary and envelope analysis in the diagnostics of rolling element bearings [44] and other cyclostationary signals [156]. In the studies, it was observed that some machines' signals might not be precisely periodic and so not phase-locked to shaft speed. The occurrence may be in impulsive signals from faulty rolling element bearing, and the slip makes them cyclostationary of second order. Observation of spectral correlation diagram shows discrete cyclic frequencies. Thus, integrating the spectral correlation diagram along the frequency axis produces a discrete frequency spectrum [39, 112]. The process may be complex, as expressed in the study [156]. However, the studies used the Fourier transform of the average squared envelope of a signal and compared it with spectral correlation [39, 112]. Although both have similar results, the Fourier transform of the average squared envelope is much easier to obtain directly.

The study [44] compares optimum results from the squared envelope signal over the spectral correlation. However, the wide acceptance and usage of envelope analysis in the diagnostics of rolling element bearing can be used in the spectral correlation. They may give some benefit in diagnosing the modulation effect in gear rotation and bearing inner race [156].

Attoui et al. [157] proposed a bearing fault diagnosis approach based on predictive features using wrapper model analysis on vibration signals. The study considered the Most Impulsive Frequency Bands (MIFBs), where several features parameter were selected. Afterwards, the wrapper model is applied while the features are reduced until the set with the most efficient diagnostic sensitivity is obtained. Experimental results using the proposed wrapper model gave a 99.83% accuracy.

Misra et al. [104] considered bearing fault detection of induction motors using vibration-based analysis. The study focused on diagnosing inner-race and outer-race faults, and the vibration-based analysis was used due to its simplicity and early detection of any fault that may appear in the bearing. The study proposed mathematical formulae that could determine the fundamental frequencies of the inner and outer races even without prior knowledge of the manufacturer's bearing geometry and technical specifications. Validation was obtained using the proposed formulae and experiments from an industry with helpful diagnosis.

Morhain and Mba [106] used non-destructive testing (NDT) acoustic emission (AE) in the diagnosis of bearing defects. In the study, an extensive review of current AE methods used in bearing diagnosis. The acoustic emission (AE) is seen to provide better early fault detection than vibration analysis. However, bearing monitoring using AE techniques has drawbacks due to difficulty in processing, interpreting, and classifying collected data. In order to show proper diagnosis, the study focused on an experimental test rig with a radially loaded bearing having defects in the inner and outer race. Results showed the validation of the use of r.m.s., amplitude, energy, and AE count values as a robust approach for detecting damaged bearing.

Some studies that addressed various approaches to identifying and diagnosing bearing defects are considered. Bearing defect diagnoses a comparative study between Empirical Wavelet Transform and Empirical Decomposition method [158], multi-scale enveloping spectrogram (MuSEnS) for bearing defect diagnosis [159], and envelope analysis based on resonance mode of the mechanical system for bearing defect diagnosis [160]. Others are bearing defect identification and estimation of defect size using acoustic emission and vibration analysis in a comparative study [161] which proposed vibration signal demodulation in bearing defect diagnosis using a complex filter for Hilbert transform [175-176]. A review of rolling element bearing fault detection analysis [177- 179], time encoded signal processing and pattern recognition approach for detection and diagnosis of bearing defect [166],. Experimental evaluation for bearing defect feature extracted with unified time-scale-frequency techniques [167], wavelet transform based on deep convolution neural network (DCNN) for

bearing defect size assessment [168], spectral kurtosis for vibratory surveillance and diagnosis of rotating machines [169], and combination of minimum entropy deconvolution and spectral kurtosis for enhancement of fault detection and diagnosis in rolling element bearing [184-185].

All types of bearing used in rotating machines are the subject of ongoing research, all of which have the potential to produce relevant research papers. Many studies have calculated and observed bearing failure frequencies from a lab-based analysis. However, detecting which bearing is failing across a complex system has received fewer research activities.

2.9.4 Foundation for machine fault identification

The foundation is also a critical part of rotating machines, and understanding its dynamics and how it helps in fault identification, which may appear in the rotor and bearing, is also essential [3,9].

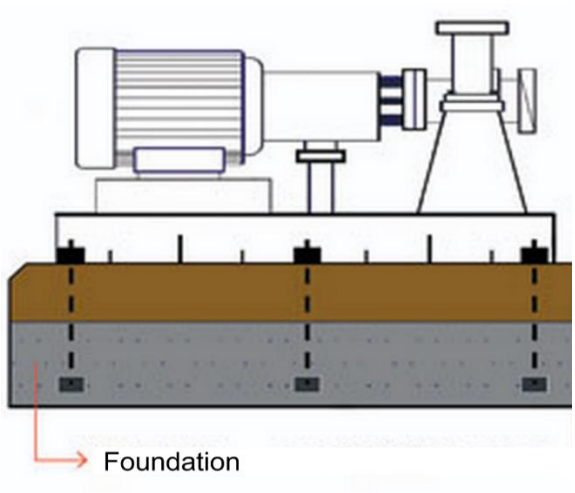

Figure2. 17 Structure of a rotating machine with installed foundation [172].

Also, due to standardisation which helps to provide cost-effective spares, most machines are built to have similar configurations and components which are installed at different industrial plants. Although these machines may have identical set up, their dynamic behaviour may differ due to the foundation flexibility [25].

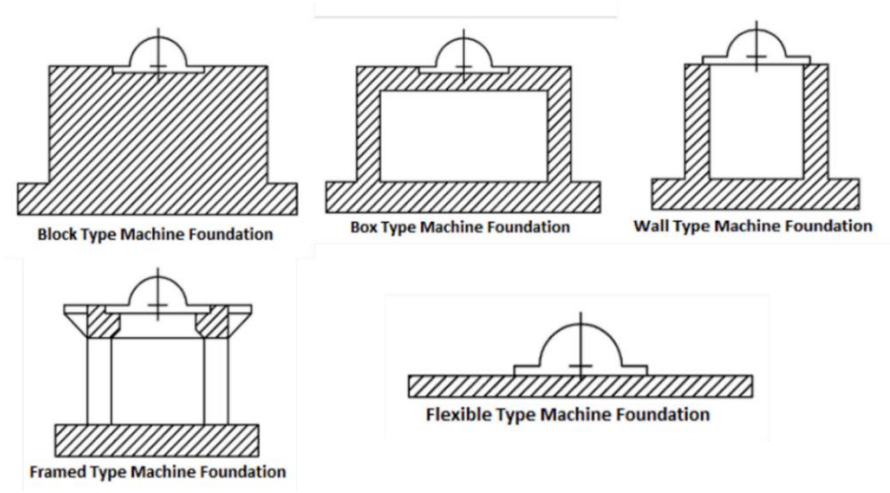

Figure2. 18 Diagram of various types of foundation for installation of rotating machines accessed from [173].

The difference may arise from the foundation type and installation location [24-45]. Also, some machines may not have baseline data for comparing their vibration response during CBM. Similar machines may provide this data if VFI methods can show indifference in their diagnosis approach when combining data from newly installed with existing ones, even though there are differences in their foundation flexibilities [45,188].

Sinha et al. [9] study gave an abstract representation of a turbogenerator set with connections between the rotor and flexible foundation through oil-film journal bearing using the equation of motion of a system. Foundation model estimation was used to obtain the foundation parameters using the linear least-square and non-linear estimations [9]. Models for linear and non-linear improvement were applied to the simulation of a flexible rotor fluid bearing-foundation model to fit a sample machine in the laboratory. The setup, which had four bearings, also included various unbalance configurations on the rotor. Foundation model identification was carried out using different regularisation methods. Iterations based on linear and non-linear estimations and fault prediction proved useful in foundation model estimation [9].

Less and Friswell [175] also considered the estimation method for developing foundation models that will accurately represent machines that will effectively identify

faults. Various fault models were considered, and the integrity of the models was discussed based on the outcome of the investigation.

Yunusa-Kaltungo, Sinha and Nembhard [25] developed a novel fault diagnosis approach considering rotating machines having different foundation flexibilities. The study presented the demands of fault diagnosis of a single machine with varying operation conditions, such as operating speeds. It considered the usefulness of having a diagnostic approach that provides value for early fault detection, notwithstanding the foundation flexibilities and operating speeds. The study is based on earlier work [69], where rotor faults were identified using a novel poly-coherent composite higher-order spectrum (pCCHOS) with a subset of bispectrum and trispectrum. The approach considered the combination of pCCB and pCCT to classify rotor faults. However, in the study [25], a data set from two flexible flange-built experimental rigs was observed, and combined pCCB and PCCT were classified. This investigation was done to observe the dynamics of the rotor faults in the two machines with different foundation flexibilities. Results showed good classification of rotor faults, hence useful fault detection method.

In a similar approach, Nembhard, Sinha and Yunusa-Kaltungo [51] and Nembhard and Sinha [174] tried to transfer a novel unified multispeed approach (UMA) [22] where valuable results were obtained from the classification of selected rotor faults from multiple speed, single foundation [22], to multiple speed multiple foundation analysis [45,188]. Results showed better classification of rotor faults.

Lee [176] carried out a survey study where smart mechatronic devices have been used in addressing rigid and flexible foundations of rotating machines and understanding vibration measurement. The study was done with the prospect of opening up more research on mechatronics as it relates to rotodynamic.

The area of foundation flexibility has received research attention but with less outcome concerning vibration-based fault identification methods. Studies on foundations are popular in model-based approaches, but little is seen in experimental approaches. Most industrial fault identification approaches suffered set back until

attention was moved to their foundations. The focus is either in terms of re-examining its natural frequency (as a machine may have over time adjusted this close to the excitation frequency) or in terms of its set up for production (which, if not aligned correctly, can lead to unbalance, misalignment, rub and bearing failure). Moreover, if not correctly fitted can lead to looseness, fault and its likes.

2.10 Critical assessment of vibration-based fault identification methods

A critical assessment of VFI methods based on various studies from this review is presented in this section. The assessment presents discussions on related VFI approaches showing their limitations and, in some cases, proposing how they can be addressed. The review considered three broad VFI methods: signal-based, hybrid, and model-based. The signal and hybrid methods share similar features. This study focuses on these methods, and a critical assessment is presented. The model-based method is a theoretical or mathematical approach. A unique approach in the model-based method is the finite element analysis (FEA) which has helped to advance VFI in rotating machines. However, applying FEA may be too expensive computationally. A model reduction approach helps to mitigate this limitation. However, understanding vibration phenomena in rotating machines is not viable in this situation. A critical review of the signal and hybrid method used in this thesis is addressed.

Time and spectrum analysis: In time domain and spectrum analysis, the features helpful in detecting faults are well established; however, most of these features are present in more than one fault so an expert view may be helpful in this investigation. Time domain analysis is laborious and demanding, especially when the signal is lengthy. Time domain analysis is sometimes cumbersome when there is an extensive system order. This drawback does not take away its benefit, where it indicates a transient response significantly. On the other hand, the frequency domain has shown robust analysis in signal processing. Noise and disturbances in the signal are best understood in the frequency domain. However, its mathematical models may be less accurate when compared to the time domain.

Envelope analysis: This helps to distinguish signal from sound during analysis efficiently. It helps observe regularly spaced signals. It is an established method in rolling element-bearing fault identification. However, the demand in selecting a central frequency filter comes with experience. Also, spectral lines of the fundamental frequencies may not be easy to identify in the envelope spectrum.

Bispectrum analysis: This is a developing area in rotating machine fault identification. It combines various frequency components from a signal and produces a unique feature for fault identification. Most studies of bispectrum cover rotor-related fault diagnosis, and just a few have covered bearing fault diagnosis but with a combination of other methods. Its usefulness in investigating non-linear signals should encourage more research on bearing and gear faults and improvements in rotor faults.

Modal analysis: This helps to identify the natural frequencies of a machine by creating resonant conditions. With the natural frequency of a machine identified, its excitation frequency can be set to support safe operation. Constant operation of the machine can shift the natural frequency due to 'reduced mass or increased stiffness. Thus, it is advisable to carry out a regular modal test.

Data fusion: Data fusion combines, integrates, and consolidates different data sources for a valuable interpretation of machine information. Lots of researchers have achieved sound output in their studies using data fusion. However, too much data makes fault diagnosis inconvenient; thus, parameter reduction approach would be helpful to take out non-essential parameters.

Clustering: Clustering analysis aims to detect patterns and groupings in data for effective diagnosis. Some drawbacks in cluster analysis are the unavailability of enough data, especially for newly installed machines, and the skills required in clustering analysis may be basic. However, interpretation and trending to determine machine health demands a good understanding of machine behaviour.

Pattern recognition: This may be similar to clustering; however, in pattern recognition, a programmed approach helps to recognise patterns with regularities in data (i.e. familiar patterns can be identified correctly). Principal component analysis (PCA) is one

of the best-known and simple pattern recognition classification tools. It has been widely used in VFI analysis.

Rotor-related and bearing faults: Rotor and bearing faults have received very high volumes of investigations, research, and publications. These faults show up mostly during machine operation; some occur because of improper installation, while a few are because of production errors of machine parts. In earlier sections, details have been given on the rotor and bearing faults, which are the focus of the research. Various works of literature critically reviewed considered VFI methods in identifying rotor and bearing faults. However, the author cannot cover a detailed critical assessment of each article due to the extensive studies on rotor-related and bearing faults. It is worth noting that there is a constant demand for improved methods for identifying rotor and bearing faults using a simple, robust, and timely approach.

Foundation flexibility: Understanding the dynamic behaviour of the machine foundation helps determine the dynamics of the rotor and bearing faults in that machine. Also, standardisation makes similar machine configurations available but with different foundation flexibility. However, most research in VFI relates to the foundation of a machine being model-based, while little has been achieved in the experimental approach. Industrial plants sometimes underperform due to constant failures until focus is placed on the foundation to determine its natural frequency, which may have adjusted close to the excitation frequency. Also, improper set-up may lead to the rotor and bearing faults.

Several industrial plants run through multiple natural frequencies (critical speeds) during their operation, especially during run-up operations. The effect of resonance may affect this operation. Thus, observing such machines would help plant operators understand their dynamics, which contributes to VFI approaches.

Other critical assessment of vibration-based fault identification includes the following.

Maintenance time reduction: There is much demand for increased vibration-based fault identification (VFI) methods in the quickest possible time, especially in the airline industry [35]. A review by Anderson [184] summarises the maintenance time

breakdown for several military aircraft. The outcome shows as much as 44% of an aircraft maintenance time (this takes over 90% of total maintenance operations) is consumed with inspection alone. Maintenance could be more informed and targeted, with inventory available when needed, reducing maintenance time.

Broad subject area: The subject area of rotodynamic faults identification is an extensive research area. It is challenging to quantify faults with regard to the rate of occurrence as there is a lack of commercially available data. Also, rotating machines are the most important and most applicable classes of industrial machinery, so for decades, a considerable body of information has been published around it, ranging from articles, books, patents, reports, and various texts. Invariably, gathering every significant contribution in the field would be much more demanding. So, a general description of various outputs and contributions made by research is presented in the review.

Occurrences of faults: Fault occurrences are not mutually exclusive, notwithstanding individual investigation, as dependencies exist between many faults. Fault chains could become very complex; for example, misalignment can lead to unbalance, which can cause rub. Most research contains single fault analysis, and a few focus on two or more faults. Such fault dependencies are limiting factors when moving VFI from the lab to the industry. A case scenario is when a method can effectively diagnose an unbalanced fault without consideration for misalignment, which can be a root cause that would render such a method ineffective when applied in real-life cases.

Acceptance of new diagnosis methods in the industry: The research into the diagnosis and prognosis of machine critical parts faults in rotating machines is a developing area. The use of new methods in industries has not yet reached a level where standard solutions or procedures to follow are generally accepted.

Research output variation: Due to variation in research output on proposed VFI models, separating which research has the potential for moving beyond the lab environment into the industry can be challenging to identify from initial observation.

The complexity of research work: Many studies look at single or dual rotor systems where fault identification is less complex. In an industrial setting, complex systems comprise several rotors with compressor and turbine stages, which significantly complicate diagnoses of such faults.

Effect of noise on data – lab/industrial perspective: Vibration signals from the lab may not have as much noise as in the industry, which may prove difficult to apply these labs-based developed VFI techniques in industrial situations.

Scaling up Model-based methods: Most useful finite element analysis models' fault identification techniques are challenging to scale up to complete industrial-size applications.

Diagnosis output based on heavy instrumentation in the lab: Many data-driven techniques for diagnosis and prognosis claim good results by heavily instrumenting specific test system components. Heavy instrumentation is not possible, practical, or cost-effective in many industrial cases. For instance, a key phasor transducer can be particularly useful in diagnosing faults such as rotor bow; however, this equipment requires the ability to cut a keyway for measurement to be performed.

Less corresponding research into localised faults: With continuously developed for new fault identification, diagnosis and prognosis methods in rotating machines, there is a lack of corresponding studies into the localisation of these faults, which is a limitation in promoting most research into live industrial application.

More diagnosis and less prognosis for combined faults: Several studies have carried out a combination of faults for diagnosis. However, only a few have a combination of faults for prognosis. Nevertheless, according to Jaw and Meril [185], prognosis and diagnosis techniques can be combined into a sound CBM system.

2.11 Research gap in consolidated rotor and bearing fault diagnosis

Most of the literature covered in these studies have either used one or more methods to identify rotor-related and bearing faults. Some focused on just one fault either rotor-related [122,145,154,155,191] or bearing faults [39,111,112,115,173,192] as it may seem important to the study. Many researchers have moved from studying individual faults to a combination of faults, i.e., multiple rotor faults [20,22,45,65, 180] or multiple bearing faults [194-196]. Some considered rotor and bearing faults [5,30,197], but each is investigated independently, and maybe comparisons are made. However, most faults that appear as rotor-related or bearing defects may appear around the same period and are interdependent. There is a lack of research that develops a VFI approach where the diagnosis of a consolidated rotor and bearing faults is achieved in a single analysis. This study area is complex, as seen from various reports. In the industry, simple rectifying an unbalance fault does not provide a satisfactory solution if the root cause is misalignment. This subject is complex as several faults exhibit similar vibration characteristics rendering the traditional fault identification methods inaccurate in some scenarios.

A vibration-based fault diagnosis approach that can identify rotor and bearing faults in a single investigation would help to reduce not just maintenance costs but helps maintenance planning and plant availability. Such a single diagnosis approach would also provide an overall understanding of the machine's behaviour concerning identifying a consolidated rotor and bearing fault in a rotating machine [81].

2.12 Summary of literature review

Investigation into these critical parts of a rotating machine, i.e., rotor and bearing, to understand their dynamic behaviour and the faults that appear in them is essential in improving VFI methods. This thesis has critically reviewed some relevant literature on VFI techniques that have been developed for improved fault diagnosis. Various studies have attempted to improve VFI methods using the traditional approach; however, interpreting its results is often ambiguous. The signal-based method takes its root from the traditional approach and has been improved by combining various techniques, which gives credence to the hybrid methods. The model-based methods are primarily

theoretical but have contributed immensely to advancing VFI. This review considered various VFI approaches relevant to this study, including time and frequency domain analysis, spectrum analysis, envelope analysis, bispectrum analysis, modal analysis, data fusion, clustering, and pattern recognition approaches. Various studies explained and showed the application of these techniques in fault analysis and diagnosis. However, there may be drawbacks to some of these methods, especially where the aim is to develop a simple and robust approach. Some significant limitations as observed and would be addressed in this study are presented below.

1. The review has presented gaps and limitations in many VFI techniques for rotor and bearing fault diagnosis. This thesis discussed these gaps; a significant gap is the consolidated diagnosis of the rotor and bearing faults in a single analysis. One which this research address with valuable outcome.

2. Most machines operate above their natural frequencies. However, an earlier study focused on signals below the machine's first natural frequency. Understanding the dynamic behaviour when a machine operates below and above the natural frequency helps investigate the dynamics of the faults that show up for easy identification. This study improved the existing test rig to operate below and above its first critical speed.

3. Earlier studies focused on time domain and spectrum analysis as their parameters help detect most faults. However, they are laborious, and analysis sometimes shows similar features for different faults making diagnosis cumbersome. Thus, data trending would help determine the effectiveness of features selected for diagnosis, especially for rotor faults.

4. Earlier studies used acceleration features in their investigation and focused only on rotor faults. However, acceleration and velocity signals have shown usefulness in diagnosing bearing and rotor faults, respectively. Although most studies focus on acceleration signals, it is easy to obtain using accelerometers. This study converts acceleration to velocity and combines features in its investigation into the rotor and bearing faults in a single analysis.

5. In spectrum analysis, the amplitude is used in fault diagnosis. However, the phase information is lost due to the complex conjugates of the Fourier transformation. The earlier study proposed a pCCB, an improved bispectrum where both amplitude and phase are retained in the computation. This research builds on the results from pCCB and then uses its complex number of components to investigate rotor faults. Bearing features are incorporated and observed in a single analysis.

6. The necessity of diagnosing similar machines with different foundation flexibility is now widespread as standardization of machine parts. Diagnosing similar machines demands a VFI approach that allows data sharing between several identical rotating machines. This approach takes out the storage of individual machine data history.

Further research in rotordynamics would provide valuable outcomes that bridges the gap between these research studies and real-life systems by combining simulations with data-driven techniques and validating experimental data. Although quantifying the overall success of the research studied is laborious; however, it is possible to define the critical areas in which a technique must excel to be considered viable; the research outcome provided such as presented in the methodology chapter.

CHAPTER 3

RESEARCH METHODOLOGY

This chapter covers the entire methodology for this research work. It presents the framework of the research, the methods used and their theoretical representation. Also, the benefits and limitations of some of the methods used in this study is discussed.

3.1 Overview

The demand for continuous improvement of vibration-based fault identification (VFI) in a rotating machine is a drive for this study. The experiment-based research aims to develop a fault identification approach that diagnoses a wide range of the machine's critical components (rotor and bearing) faults in a single analysis.

This study looks at conducting a preliminary investigation using existing data from a flange-based flexible test rig (FFTR) developed by two former PhD students, Dr Akilu Yunusa-Kaltungo and Dr Adrian Nembhard, during their research studies. This FFTR data is acceleration-based and was collected when the test rig operated below its first critical speed because it is above the nameplate rpm of the motor. The current study modified the FFTR to a spring-based flexible test rig (SFTR). This rig was to create an industry base scenario where machines can run over critical speeds, such as in aircraft and other complex turbines. The modification of the SFTR was achieved by using spring connectors in place of the flange connectors at the bearing pedestal, which reduced the stiffness, thus a reduction of the natural frequency. This adjustment made the test rig operate below the nameplate rpm of the motor. Therefore, it could run below and above the first critical speed.

An earlier study [20] proposed a unified multispeed analysis (UMA) for diagnosing an extensive range of rotor faults using acceleration-based vibration data obtained from the FFTR when the machine ran below its first critical speed. Building from this earlier study, the current study intends to use similar rotor faults acceleration signals from the FFTR in a preliminary investigation. Signal processing and data trending of selected features from the acceleration data led to a classification approach, which further validates the UMA.

The further investigation involves velocity data converted from the acceleration signals. A diagnosis was improved by combining features of acceleration and velocity data.

On the SFTR, modal analysis is carried out to present the natural frequencies of the rig. The collected data from SFTR were investigated in the study, and novel data fusion

approaches were proposed. Considering an earlier proposed poly-coherent composite bispectrum (pCCB) on the SFTR and further investigation of its components, including the complex number representation for analysis, helped improve diagnosis. A combination of acceleration features and pCCB components proposed a novel fault identification approach. Figure 3.1 shows the flow diagram of the research methodology. Section 4.2 gives a brief of the experimental approach; other sections discuss methods applied in this research and, where necessary, the theoretical approach in detail.

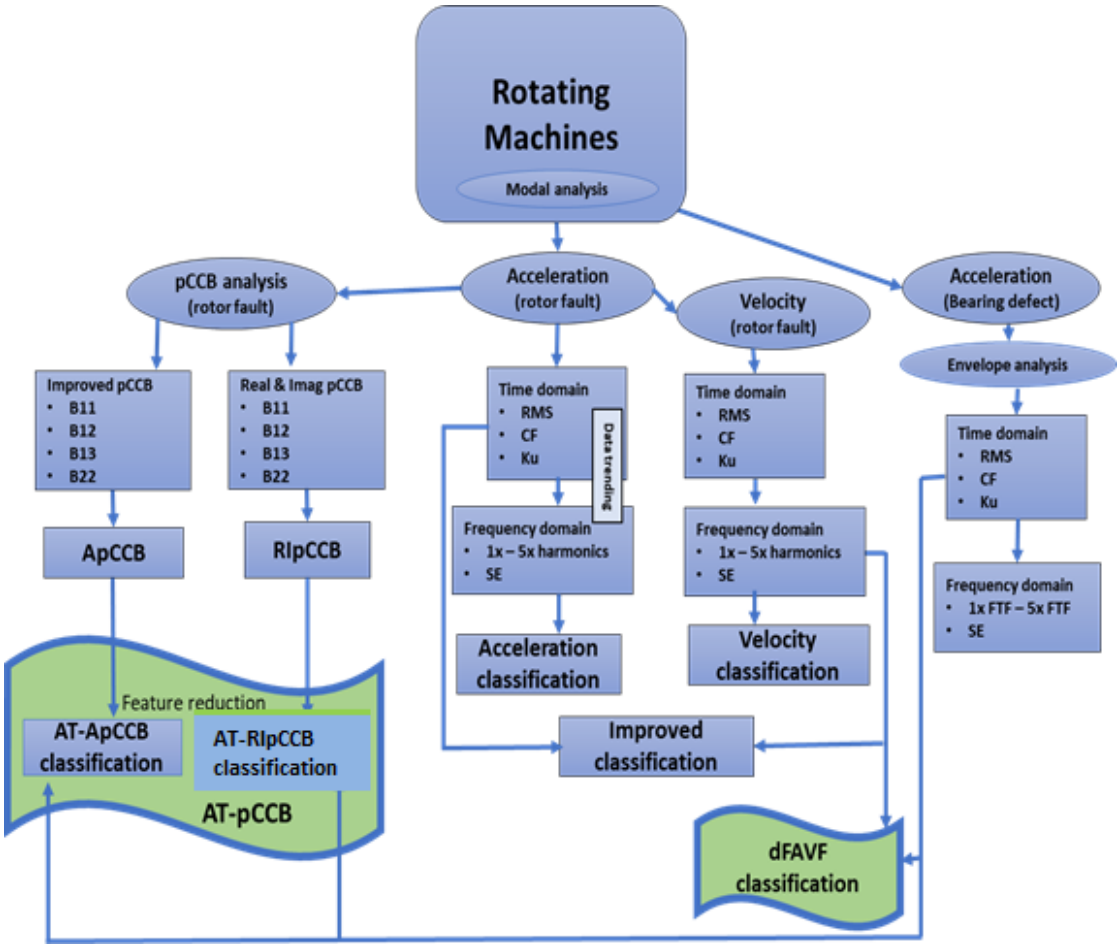

Figure 3. 1 Methodology for the research study.

3.2 Test rigs and experiments and analysis

This section covers the description of the test rigs used in the analysis. It presents the data collected, obtained, and conducted experiments, showing the various machine conditions simulated on the test rigs. It also discusses the analysis of the data obtained

from the test rigs. It should be noted that more details on selected features and the build-up of the data matrix are found in [20], as this study was developed from them.

3.2.1 Test rigs

This study proposed the usage of data from three test rigs. Data from the flange-based flexible test rig (FFTR) was built in earlier research, as described in section 3.1. The researcher carried out the modal analysis, and the natural frequencies obtained were 56.76 Hz (1st mode), 59.20 Hz (2nd mode) and 127 Hz (3rd mode). This informed the decision to obtain vibration data below the machines' first critical speed (1st mode) as the nameplate speed is below the first natural frequency. On the other hand, the spring-based flexible test rig one and two (SFTR-1 & 2) modified to fit the current research is also described in section 3.1. The framework for the FFTR showing its data and modal analysis is in Figure 3.2.

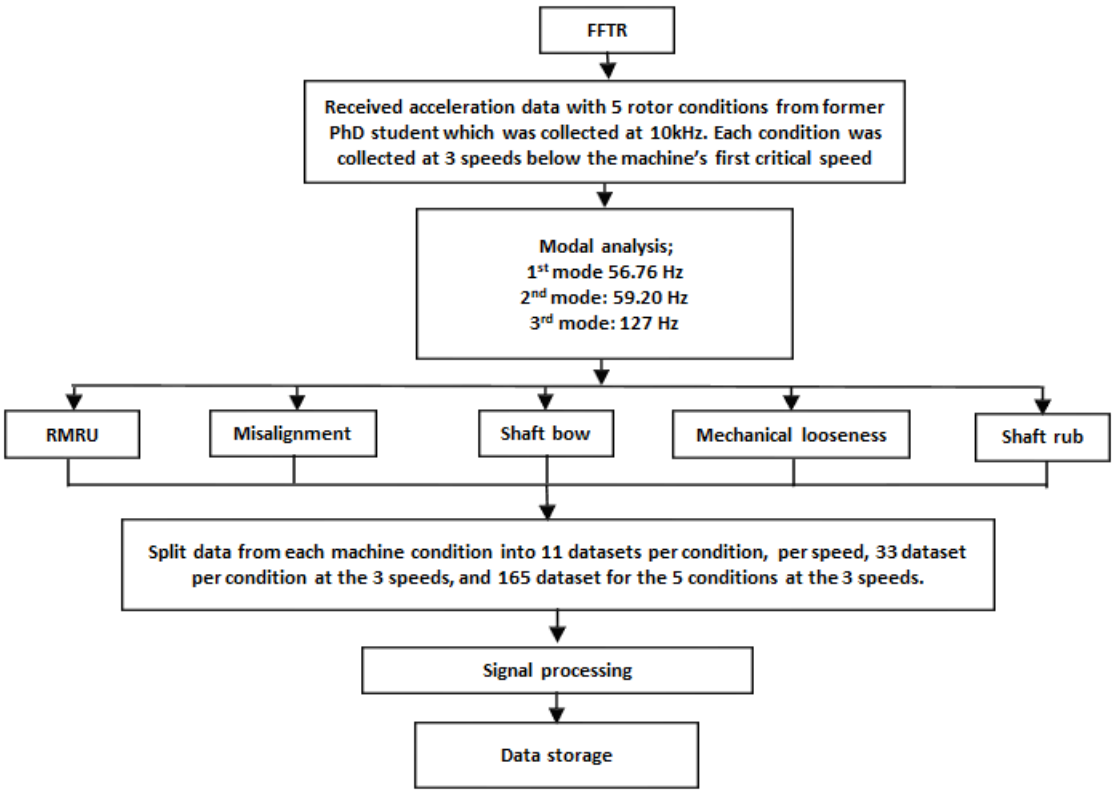

Figure 3. 2 Framework for the FFTR with modal analysis simulated machine conditions.

The SFTR-1 was built using a spring with stiffness of 4.69N/mm per spring. The spring connects the bearings to the pedestal at the four-bearing location. This connection helps adjust the system's entire stiffness, thus reducing the natural frequency. This reduction of the natural frequency creates a machine that operates over its critical speeds, a representation of real-life machines such as turbogenerators and aircraft, which operate with changing speeds across their critical speeds. Afterwards, the modal analysis showed the first few natural frequencies of the SFTR, which included 11.52 Hz, 18.62 Hz, 30.73 Hz, 49.13 Hz and 85.83 Hz. These modes were below the nameplate rpm of the motor that will operate the test rig, which is 3000 rpm (50 Hz). Thus, three-speed were selected, which are 450 rpm (7.5 Hz) below the first critical speed (11.52 Hz), 900 rpm (15 Hz) below the first critical speed and 1350 rpm (22.5 Hz) above the first critical speed.

The SFTR-2 was adjusted using a spring with higher stiffness, i.e., 14.4N/mm. A higher stiffness increases the natural frequency of a system. The reason for increasing the natural frequency is to observe a similar machine with different foundation flexibility, compare analysis and investigate the transference of diagnostic approaches between similar machines. Modal testing on SFTR-2 showed the first few natural frequencies, including 17.78 Hz, 23.88 Hz, 32.65 Hz, 51.19 Hz and 86.36 Hz. The three speeds selected for running SFTR-2 are also 450 rpm (7.5 Hz) below the first critical speed (17.78 Hz), 900 rpm (15 Hz) and 1350 rpm (22.5 Hz) above the first critical speed. Observation of data at 1350rpm would help to understand machine operation close to a critical speed. Figure 3.3 shows the framework for the SFTR, modal analysis and simulated conditions.

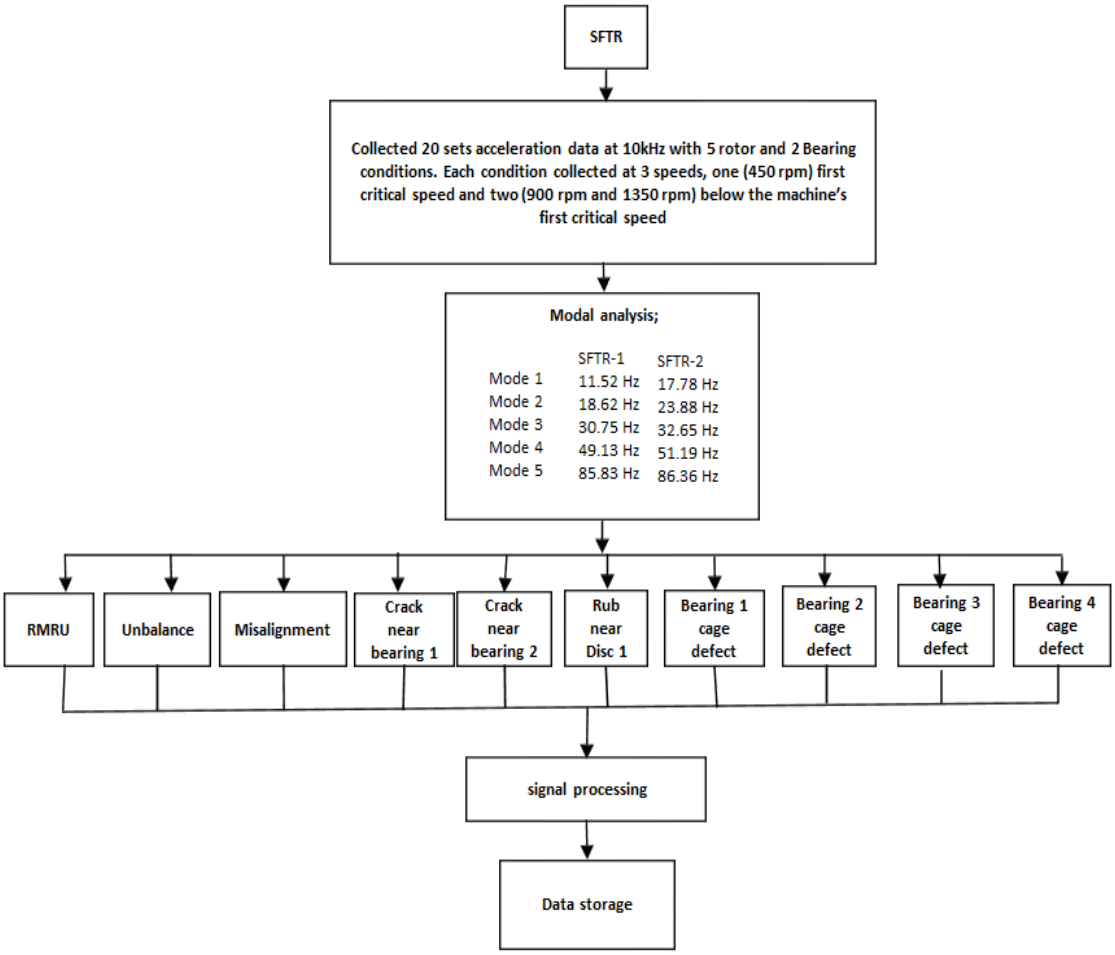

Figure 3. 3 Framework for the SFTR with modal analysis simulated machine conditions.

3.2.2 Experiments conducted

For preliminary investigation, data from the FFTR was used for data trending for selected acceleration-based time domain and frequency domain parameter features. These selections were based on results from an earlier study [20]. As seen in Figure 3.2, the signal for this investigation included baseline residual misalignment and residual unbalance (RMRU), Misalignment (M), shaft bow (S-Bow), mechanical looseness at bearing three (M-LooseBg3), and shaft rub near disc two (RubD2), all of which are rotor related conditions.

Acceleration-based vibration data was collected at 10kHz using accelerometers placed on the four-bearing location at an angle of 450. This placement takes responsibility for the vertical and horizontal effect of the vibration in the signals [20]. As shown in Figure 3.3, eleven simulated machine conditions simulated in SFTR include rotor-related

RMRU, M, Unbalance (Unb), Crack near bearings one and two (CBg1 and CBg2), rub near disc (RubD1) and bearing-related bearing cage defect at bearing one to four (Bg1Cg – Bg4Cg). The simulated conditions are the same for SFTR-1 and 2. Whereas bearing defect and Bearing locations 3 and 4 were excluded from the initial analysis with SFTR-1, it was included in the final analyses for comparison with SFTR-2.

3.2.3 Data analysis

Figure 3.4 shows the framework in the data analysis for developing the proposed approaches using the data from the different test rigs. A description of what the entire analysis entails is presented in this subsection. Data analysis from FFTR, SFTR-1 and SFTR-2, a comparison between SFTR-1 and SFTR-2 and the combination of parameters for diagnosis using the proposed approaches were discussed. After that, a comparison of the results from the proposed approaches was presented.

FFTR data analysis

Data from the FFTR was split into 11 samples in order to achieve an average analysis for understanding the dynamic behaviour of the signals. Time and frequency domain analysis for each machine condition (RMRU, M, S-Bow, M-LooseBg3 and RubD2) at the three machine speeds, i.e., 1200 rpm (20 Hz), 1800 rpm (30 Hz and 2400 rpm (40 Hz). Time and frequency domain parameters were extracted for data trending. The parameters are time domain RMS, CF and Ku and frequency domain 1x -5x harmonic components and SE. This data trend was done to reaffirm the sensitivity of features selected in an earlier study [20] in a proposed UMA approach. The outcome showed the sensitivity of the individual parameters; however, there was no consistency in the result for a comprehensive diagnosis for the entire system.

Thus, data fusion and PCA-based classification of the acceleration features for the rotor conditions reaffirm earlier UMA [20]. However, an extensive range of rotating machine faults could be diagnosed effectively if the approach is improved. Thus, velocity analysis was considered. The acceleration data was converted into velocity using the integration method. Velocity-based time and frequency analysis gave a good diagnosis. Similar time and frequency domain parameters were extracted and classified using PCA-based pattern recognition. The outcome showed improved

diagnosis compared to acceleration feature classification. However, acceleration signals cover a high range frequency useful for bearing fault diagnosis, while velocity covers a lower frequency range valuable for rotor fault diagnosis.

Since the aim is to diagnose an extensive range of rotating machines' critical parts faults, including rotor and bearings, in a single analysis, a combination of features that are sensitive to the behaviour of these faults would be helpful. Also, since bearing faults are mostly impulsive, time domain features like kurtosis would be helpful, while the frequency domain is great in projecting rotor faults mainly due to the harmonic components. Thus, a combination of acceleration-based time and velocity-based frequency domain features would help diagnose a wide range of machine faults. The selected acceleration-based time domain features (RMS, CF and Ku) and velocity-based frequency features (1x – 5x harmonic components and SE) were combined to build a data matrix and input into the PCA-based pattern recognition model. The outcome showed a much more improved diagnosis compared to only acceleration or velocity classification.

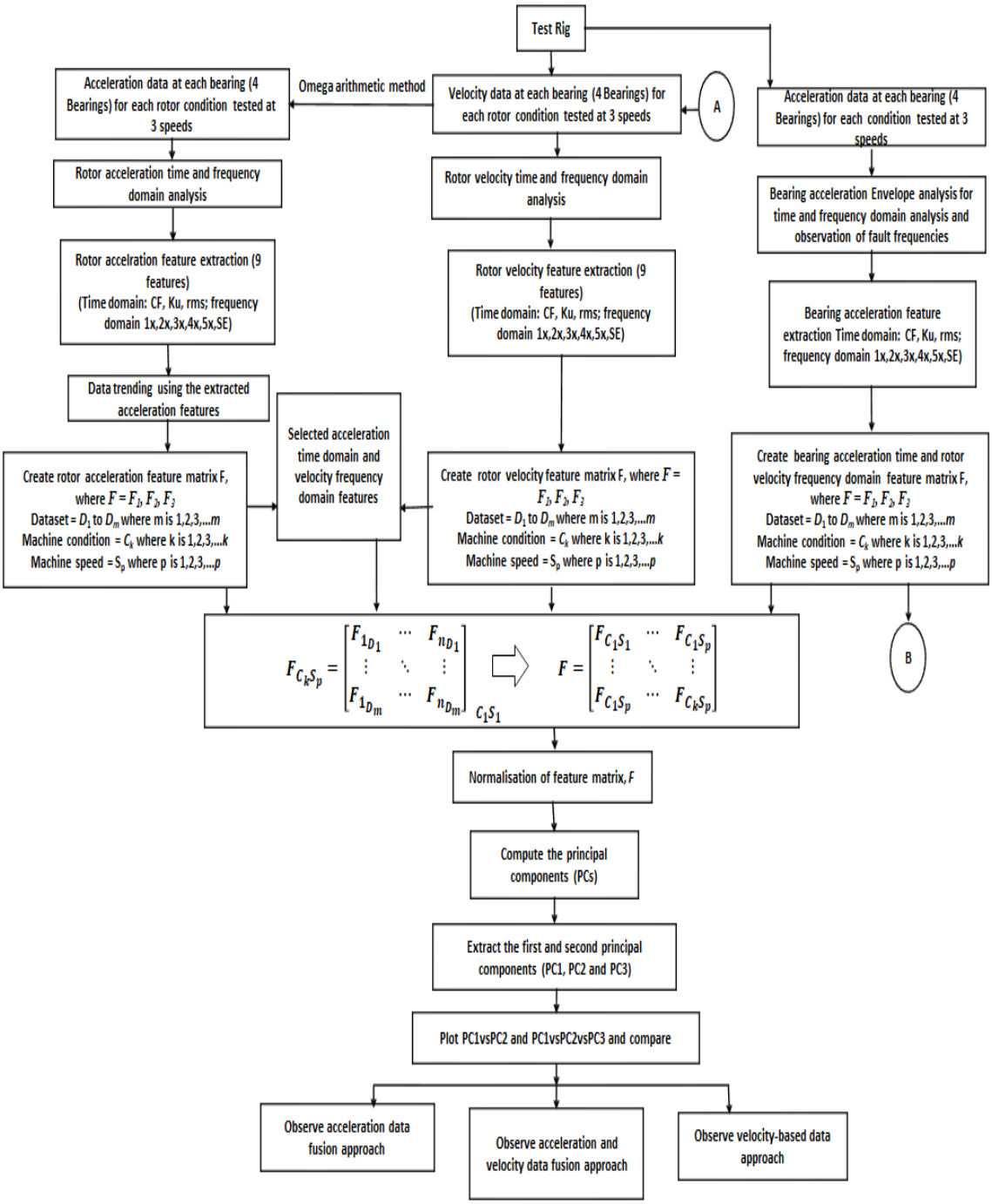
Test Rig
Acceleration data at each bearing (4 Bearings) for each rotor condition tested at 3 speeds
Omega arithmetic method
Velocity data at each bearing (4 Bearings) for each rotor condition tested at 3 speeds
A
Acceleration data at each bearing (4 Bearings) for each condition tested at 3 speeds
Rotor acceleration time and frequency domain analysis
Rotor velocity time and frequency domain analysis
Bearing acceleration Envelope analysis for time and frequency domain analysis and observation of fault frequencies
Rotor acceleration feature extraction (9 features) (Time domain: CF, Ku, rms; frequency domain 1x,2x,3x,4x,5x,SE)
Rotor velocity feature extraction (9 features) (Time domain: CF, Ku, rms; frequency domain 1x,2x,3x,4x,5x,SE)
Bearing acceleration feature extraction Time domain: CF, Ku, rms; frequency domain 1x,2x,3x,4x,5x,SE)
Data trending using the extracted acceleration features
Selected acceleration time domain and velocity frequency domain features
Create rotor acceleration feature matrix F, where $F = F_1, F_2, F_3$ Dataset = D_1 to D_m where m is 1,2,3,...m Machine condition = C_k where k is 1,2,3,...k Machine speed = S_p where p is 1,2,3,...p
Create rotor velocity feature matrix F, where $F = F_1, F_2, F_3$ Dataset = D_1 to D_m where m is 1,2,3,...m Machine condition = C_k where k is 1,2,3,...k Machine speed = S_p where p is 1,2,3,...p
Create bearing acceleration time and rotor velocity frequency domain feature matrix F, where $F = F_1, F_2, F_3$ Dataset = D_1 to D_m where m is 1,2,3,...m Machine condition = C_k where k is 1,2,3,...k Machine speed = S_p where p is 1,2,3,...p
$F_{C_kS_p} = \begin{bmatrix} F_{1_{D_1}} & \cdots & F_{n_{D_1}} \\ \vdots & \ddots & \vdots \\ F_{1_{D_m}} & \cdots & F_{n_{D_m}} \end{bmatrix}_{C_1S_1} \Rightarrow F = \begin{bmatrix} F_{C_1S_1} & \cdots & F_{C_1S_p} \\ \vdots & \ddots & \vdots \\ F_{C_1S_p} & \cdots & F_{C_kS_p} \end{bmatrix}$
B
Normalisation of feature matrix, F
Compute the principal components (PCs)
Extract the first and second principal components (PC1, PC2 and PC3)
Plot PC1vsPC2 and PC1vsPC2vsPC3 and compare
Observe acceleration data fusion approach
Observe acceleration and velocity data fusion approach
Observe velocity-based data approach

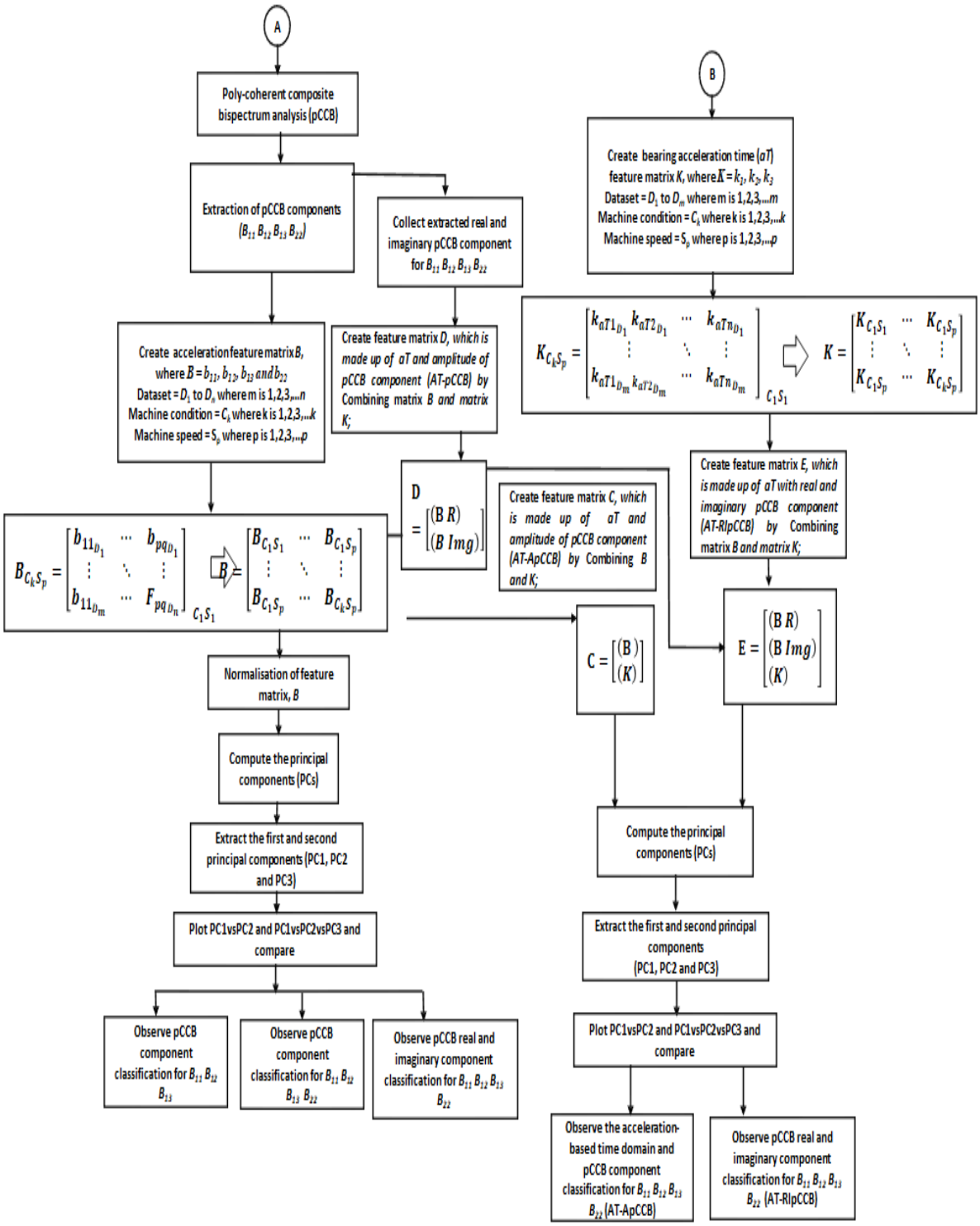

Figure 3. 4 Framework for the analysis in developing the fault classification approaches.

SFTR-1 data analysis

The further investigation considered signals from the SFTR-1. 20 sets of data were collected for all machine conditions. The machine conditions simulated are the rotor and bearing faults, as stated in section 3.2.2 and Figure 3.3. The data were recorded

at three running machine speeds, i.e., 450 rpm (7.5 Hz), 900 rpm (15 Hz) below the machine's first critical speed and 1350crpm (22.5 Hz) above the machine's critical speed.

Time and frequency domain analysis was repeated for the rotor conditions and feature extraction as in the FFTR diagnosis. The acceleration-based PCA classification also reaffirms the UMA. However, since the velocity-based time domain feature was not considered in the improved diagnosis for FFTR, the same is considered here. So, the omega arithmetic approach converted acceleration-based frequency domain spectra to velocity-based frequency domain spectra. Thereafter, data fusion of the acceleration-based time domain and velocity-based frequency domain were classified using the PCA-based pattern recognition model. The outcome reaffirmed the improved approach and showed outstanding clustering and classification of the rotor conditions.

Furthermore, the signals from bearing defects obtained from bearing pedestals one and two were analysed. The signal was filtered at 500 Hz to remove rotor-related features, and envelope analysis of the time and frequency domain was done. The spectra indicated the presence of bearing cage defect at the three speeds. However, data fusion of bearing acceleration-based time domain features and rotor velocity-based frequency domain features (dFAVF) were computed into a data matrix and input into the PCA-based pattern recognition for clustering and classification. The outcome showed good clustering of each rotor and bearing conditions. However, it was observed that the rotor conditions were positioned at a section of the plot while bearing conditions were further away. This could indicate the faults show clustering close to their frequency range of occurrence.

However, the PCA-based classification was done using the first two principal components (PCs). This approach was done because research has shown that the first few PCs carry the essential variance information of the data. However, other PCs apart from the first two may also have important diagnostics information. Thus, an investigation using more PCs was done. Here, additional PC3 was input in the

classification model, and the result showed improved classification compared to analysis using the first two PCs.

Also, to validate the result from the PCA classification plots, data quantification was carried out. The data quantification calculated the mean of each condition and did a separation between the baseline RMRU and all faulty conditions. The value showed good classification for the dFAVF model compared to acceleration alone. Also, in the comparison between the PC1vsPC2 and PC1vsPC2vsPC3, the latter showed values of increased separation, which could indicate better classification.

Since the earlier UMA has been improved and bearing defect features has also been incorporated for extensive faults diagnosis, further investigation to achieve a single analysis could provide a more robust approach. Thus, consideration was given to an earlier proposed poly-coherent composite bispectrum (pCCB) analysis [27]. The pCCB analysis provides a robust diagnosis as its analysis contains both amplitude and phase information from the signal, which is lost in the traditional spectrum analysis used in earlier dFAVF studies. It also fuses the signals from all four bearings in its analysis. This fusion provides reduced but robust data.

In this study, 10 sets of vibration data for rotor faults considered from SFTR-1 were RMRU, CBg1, CBg2 and RubD1. Signals were analysed and observed in the pCCB plots with components of pCCB, such as B11, B12, and B13, up to B33. In the earlier study [27], the components B11, B12 and B13 were extracted and input into the PCA-based data matrix with good clustering and classification. Thus, this study repeated a similar investigation using data from a different test rig and achieved good classification. However, the presence of some components in the spectrum analysis provides useful analysis in the form of a combination in pCCB analysis, such as crack and rub faults that hows the 2x and 4x components in spectrum analysis which could be observed in B22 components. Thus, further investigation considered analysis of the various pCCB components to check for their sensitivity in diagnosing machine conditions. The outcome showed that B22 carried sensitive information to diagnose crack and rub conditions. So, it is included for an improved diagnosis where PCA-based classification was achieved. Also, the complex number of

pCCB component was observed as it may also carry some sensitive information in fault diagnosis. A PCA-based classification was achieved using features from the real and imaginary pCCB components.

Comparison of the initial, improved, and real and imaginary pCCB components showed better classification for the real and imaginary pCCB components. On the other hand, observation of the comparison between PC1vsPC2 and PC1vsPC2vsPC3 showed very little difference in the analysis. Thus, additional PCs may not contribute much to pCCB analysis for fault diagnosis. Similarly, the data quantification approach presented the real and imaginary pCCB classification showing better separation than the initial and improved classification.

Since good classification was achieved using the pCCB components, acceleration-based features from bearing defects were incorporated into the data matrix with pCCB components. PCA-based pattern recognition and comparison of AT-ApCCB and AT-RIpCCB were done. The result showed good clustering for individual conditions. However, there was a separation between the rotor and bearing conditions, indicating their frequency ranges of occurrence. On the other hand, the classification at AT-RIpCCB showed better separation than that of AT-ApCCB. Observation of PC1vsPC2 and PC1vsPC2vsPC3 also indicated better separation in the bearing cases than the rotor ones. Data quantification comparing the plots for the two scenarios proved that the separation was more evident in the bearing cases than in the rotor.

SFTR-2 data analysis and comparison with SFTR-1

The setup of SFTR-2 was to create a similar machine with different foundation flexibility. Rotor and bearing conditions were simulated on SFTR-2. Twenty datasets were collected at similar speeds as in SFTR-1. As seen in Figure 3.4, time and frequency domain analysis for rotor and bearing defects was carried out for each set of data, and extracted features were populated into the data matrix with a PCA-based pattern recognition model used in clustering and classification for the dFAVF approach.

A similar classification was carried out using the AT-pCCB (AT-ApCCB and AT-RIpCCB) approach. Comparison of diagnosis between SFTR-1 and SFTR-2 helped to understand the dynamic behaviour of similar rotating machines with different foundation

flexibility. The outcome showed a similar trend in diagnosis. After that, a combination of features from SFTR-1 and 2 helped to understand the transference of diagnostic features. This approach also compared the analysis outcome using dFAVF and AT-pCCB approaches in fault identification. The outcome provided insensitive features for fault identification in similar machines with different foundation flexibilities. It also showed that the AT-pCCB gave better rotor fault diagnosis than dFAVF because of the vital information from both amplitude and phase presence. Overall, rotor conditions appeared separate from bearing conditions in. a single analysis, indicating their frequencies of occurrence where rotor faults occur around low frequencies and bearing at high frequencies.

Note: Since the research is experimentally based, chapter four is dedicated to an in-depth discussion of the test rigs and experiments. It covered a description of the test rigs, instrumentation, modal testing, simulated faults and data acquisition and storage. In order to provide an understanding of the analysis, relevant methods mentioned as applied in the investigation are discussed in subsequent sections.

3.3 Time domain analysis

Time domain analysis is a general method is investigating vibration signals. Its parameters are sensitive in showing the behaviour of a system. This study's selected time domain parameters include root mean square (RMS), crest factor (C.F.) and Kurtosis. The theoretical expressions of these parameters are described as follows:

Time domain analysis is a waveform representation of the measured vibration data [11]. Observation of the waveform, if not clear sinusoidal, may be challenging to carry out any proper analysis. Thus, some parameters help understand analysis in its representation, such as root mean square (RMS), crest factor (C.F.) and Kurtosis (Ku). The theoretical expressions of these parameters are described as follows:

3.3.1 Root mean square

Root mean square (RMS) of a waveform is the measure of the energy contained in it [45]. It can be described as the square root of the mean value of squared values collected over an interval. It is simply obtained by squaring the waveform value. The

result is averaged, and the square root is obtained. Sinha [11] computed the RMS value as in equation (3.1);

$$a_{\text{rms}} = \sqrt{\frac{\int_0^T a^2(t)dt}{T}} \tag{3.1}$$

where *T* is the time period of the signal *a(t)*. Thus, for a small segment of the time domain signal, *a(t)*, we can assume that the selected segment contains *p* data points, which is represented as $a_k(t_k)$ at time t_k where $t_k = (k-1)dt$, and *k* = 1, 2, …, *p.* So that the a_{rms} was represented in equation (3.2) as;

$$a_{rms} = \sqrt{\frac{\sum_{k=1}^{p} a_k^2}{p}} \tag{3.2}$$

3.3.2 Crest Factor

Crest factor (CF) is the ratio of the peak value to the rms value of a waveform. It is a non-dimensional value. Mathematically, it is represented in equation (3.3) as;

$$CF = \frac{|a_{peak}|}{a_{rms}} \tag{3.3}$$

where a_{peak}= Amplitude of peak value and a_{rms} = the amplitude of rms value. The crest factor helps to give a quick idea of the amount of impact occurring in a waveform and is closely associated with roller bearing, etc.

3.3.3 Kurtosis

Kurtosis (Ku) is a measure of the extent of peaks or flats a waveform has in relation to normal distribution. The higher the kurtosis the clearer peaks around the mean with heavy base while the low kurtosis gives flat top around the mean. Kurtosis is a non-dimensional value and it is defined as '*the normalised fourth order moment of a time domain signal* [45]. In defining the *kth* order central moment for any acceleration data for instance *a(t),* it is represented in equation (3.4) as;

$$M_k = \frac{1}{p}\sum_{k=1}^{p}(a_i - \overline{a})^k \tag{3.4}$$

where $a_i = a(t_i)$, $\bar{a}$ is the mean value of the data set, *a(t)*, and *i* = 1, 2, 3, …, *p*.

The normalized fourth order moment, i. e. kurtosis Ku, is calculated using

$$Ku = \frac{M_4}{(M_2)^2} \tag{3.5}$$

Having M_4 as the fourth order moment and M_2 the second order of moment

3.4 Frequency domain analysis

The Fast Fourier Transform is a principle employed to convert the time domain waveform to the frequency domain. Also, the spectrum energy (SE) gives the energy content of the spectrum amplitude. These are essential parameters in carrying out spectrum analysis. In this section theoretical representation of the FFT and SE is done.

3.4.1 Fast Fourier Transform

Spectrum analysis is a frequency domain representation of measured vibration data. Once data is collected and expressed in the time domain, it must be converted to the frequency domain for further analysis. Fast Fourier Transform (FFT) is applied in this conversion. A mathematical representation, as stated by Sinha [11], is represented in equation 3.6;

$$X(f)=\int_{-\infty}^{\infty} x(t)e^{-j2\pi ft}dt \tag{3.6}$$

Applying (3.6) on the vibration acceleration signal a(t), it is

$$X(f)= \int_{-\infty}^{\infty} a(t)e^{-j2\pi ft}\, dt \tag{3.7}$$

For computational analysis using discrete data according to Sinha [11] , it is represented in equation (3.8)

$$X(kdf) = \frac{2}{N}\sum_{n=0}^{n=1} a(t_p)e^{-j\frac{2\pi(p-1)k}{N}} \tag{3.8}$$

Where;

N=0,1,2,…N-1, k=0,1,2…N/2 -1 and p = 1,2, …, N; Time step=dt *and T* is the pseudo time period selected for the signal for FT = Ndt; *Sampling frequency,* $fs=\frac{1}{\Delta t}$; *Frequency Resoution,* $df = \frac{1}{T} = \frac{1}{Ndt} = \frac{fs}{N}$; *Frequency, f =* Kdf *; fmax =* $f_{Nyquist} = \frac{fs}{2}$

a(t) is the accelerometer signal inputed into the analyser which gives the spectra coefficient of these signals [187].

3.4.2 Spectrum Energy

Spectrum energy (SE) gives the energy content of signals in a spectrum with respect to its amplitude. It is a globally accepted indicator that covers all forms of spectrum dynamics. It is obtained from the computation FFT when the selected frequency range within the number of data points is considered. The work of Nembhard and Sinha [22] gave a mathematical representation so that the SE between two frequencies, say *f1* to *fn*, is given as in equation (3.9);

$$SEa(t) = \sum_{k=f1}^{fn} A(f_k) * df \tag{3.9}$$

where $A(f_k)$ *is the FFT* of the signal *a(t)* at f_k *and* $f_k = (\left(\frac{N}{2}\right) - 1)$,*N* is the number of data points for computing FFT, and, *df* is the frequency resolution.

3.5 Data trending

Data was trended on the acceleration-based vibration signals based on time and frequency parameters. The data trend showed how various parameters could contribute to indicating the presence of different faults in a signal. This work and previous studies [16, 19] carried out similar data trending, which showed that individual parameters provide a sensitive indication of a particular fault based on benchmarks and standards but may not give an exact indication of faults, as different faults could show similar indications. In data trending for this research, the time (**RMS**, **CF** and **Ku**) and frequency domain (**1x** – **5x** and **SE**) features discussed in sections 3. 3 and 3.4 were extracted from the acceleration signal. The data trending is represented on bar charts.

3.6 Envelope analysis

Envelope detection is widely accepted in the diagnosis of bearing faults. It is also called amplitude demodulation, where the modulated signal is extracted from an amplitude-modulated signal; this gives the time history of the modulating signal. Parameters of this signal in the time domain can be investigated and subsequently transformed to the frequency domain for further analysis. Envelope analysis can be used in diagnosing machine faults with amplitude-modulating effects on the characteristic frequency of the machine. The representation of envelope detection is such that a given filtered

signal is transformed through the Hilbert transform and obtained the envelope by equation 3.10 [18]

$$E_a[t] = \left|a_f[t] + j \cdot Hilbert\{a_f[t]\}\right|^2 \tag{3.10}$$

Where a_f is the filtered signal and *j* the imaginary unit. The envelope spectrum ES_a is obtained as the squared absolute value of the discrete Fourier transform (DFT) of the envelope as in equation (3.11) [188].

$$ES_a[t] = |DFT\{E_a[t]\}|^2 \tag{3.11}$$

This study employs envelope analysis in both time and frequency domain analysis. The envelope spectrum is used to observe the fault's presence, whereas the envelope analysis's time domain features were extracted for fault classification.

3.7 Conversion of vibration acceleration to velocity signal

Vibration data can be measured either as acceleration, velocity, or displacement. These signals can be measured using an accelerometer, velocity sensor or proximity probes. However, since this study does not cover displacement signals, the proximity probes will not be discussed.

Accelerometers are the most popular and commonly used transducers and are seen to be the best for vibration measurements covering a wide range of frequencies between 3 Hz to 20 kHz. The accelerometers are small and firmly constructed to withstand harsh environments.

A benefit of the measured acceleration signal is that the integrated approach can easily obtain both velocity and displacement signals from them. It also has an extensive dynamic range which can be used to obtain significant resonance of the systems being investigated. A drawback of using an accelerometer is the mass added to the system. However, velocity sensors help measure mid-range frequencies, but it is less effective for frequencies below 10 Hz and above 2 kHz. Another limitation of the velocity sensor is that it is expensive, bulky and a very sensitive instrument that does not fit into routine vibration monitoring [56]. It is advisable to use the accelerometer to measure both low and high frequencies, which is a focus of this study [189].

A simple description of vibration motion can be represented in simple harmonic motion (SHM). Here there is a repetition of motion at equal intervals of time (periodic motion), so the SHM is a reciprocating motion. Assuming *y(t)* is the displacement of a vibratory system of mass, the mathematical representation of the vibration displacement is represented in equation 3.12 [190],

$$\text{Displacement, } \mathrm{y} = A\cos\omega t = A\cos 2\pi\frac{t}{T} \tag{3.12}$$

where *A* is the *amplitude* of vibration, *T* is the *period* of vibration (3.13) with its reciprocal *f* being the *frequency* (3.14). Such that [190];

$$Period, \quad T = \frac{2\pi}{\omega}\ sec/cycle \tag{3.13}$$

$$Frequency,\ f = \frac{1}{T} = \frac{\omega}{2\pi} cycle/sec\ \ or\ Hz \tag{3.14}$$

With ω as the angular frequency in rad/sec.

Velocity and acceleration of the harmonic motion can be achieved by differentiation of equation (3.15) so that [190];

$$Acceleration,\ \ a = -\omega^2 A\cos\omega t = \omega^2 A\cos\ (\omega t + \pi) \tag{3.15}$$

However, most vibration data are collected using accelerometers, making the signal easily processed as acceleration. These acceleration data are converted to velocity signals to investigate signals that may be effectively observed in machine conditions. Acceleration data is therefore integrated to obtain a velocity signal and a double integration to obtain displacement. The vibration acceleration signal can be integrated using either the hardware integration circuit or software integration. Even though many instruments can implement the integral circuit using recent versions, the performance parameters of the electronic components have large discreteness. Thus, there would be a reduction in the preciseness of the result. In order to ensure accuracy with the hardware circuit, calibration and correction would be needed for the signal with varying frequency and amplitude.

However, the software integration method is most suitable with recent advancements in computerisation and data processing. The software integration approach has two

basic principles, i.e., a time-domain integral principle, achieved by the Simpson summation approach and the frequency-domain integral principle.

3.7.1 Time domain integral principle

Direct integration of time domain vibration signal with zero drift and noise in the signal amplifier will cause a trend trim, producing some error in the result [110][191]. Consequently, it is expedient to remove direct current components as well as noise before integrating. Also, the trend trim that shows up after integration can be removed by polynomial fitting. The time domain integral principle is represented such that the acceleration time domain signal is defined as and the integration is expressed as velocity as seen in equation 3.16 [191]

$$v = \int_0^t a(t)dt = \bar{v}(t) + v_0 \tag{3.16}$$

Where $\bar{v}(t)$, is the dynamic velocity component after integration, v_0 is the static velocity component after integration, t is the time and dt is differential about t.

$$v(N) = v(k-1) + \frac{[a(k-1)+4a(k)+a(k+1)]T_s}{6} \tag{3.17}$$

where k is signal sampling points and T_s is sampling period, and N is the number of data point.

3.7.2 Frequency domain integral principle

Here, the Fourier transform converts the signal from the time domain into the frequency domain. After that, the integral operation carried out in the time domain is changed into an algebraic operation of the spectrum in the frequency domain [119,203]. This can be converted back to the time domain using the inverse fast Fourier transform (IFFT). This approach also helps to remove the trend trim. The acceleration and velocity FFT in discrete forms are represented as, and respectively, as can be seen in Equations 3.18 and 3.19 [110].

$$a(n) = \sum_{k=0}^{N-1} A(k)e^{j2\pi nk/N} \tag{3.18}$$

$$v(n) = \sum_{k=0}^{N-1} \frac{1}{j\omega_k} H(k)\, A(k)e^{j2\pi nk/N} \tag{3.19}$$

$$H(k) = \begin{cases} 1, & f_d \leq k\Delta f \leq f_{u,} \\ 0, & others \end{cases} \tag{3.20}$$

The algebraic operation relationship in frequency domain is computed as follows;

$$V(k) = \frac{A(k)}{j\omega_k} \tag{3.21}$$

Where $A(k)$ and $V(k)$ are the Fourier transforms of acceleration and velocity signal (3.21); the omega arithmetic, $\omega_k = 2\pi k\Delta f$, and *k=0,1,2…N/2 -1;* Δf is the frequency resolution; j is the imaginary unit; $H(k)$ being the frequency characteristics of the band-pass filter (3.20); f_d and f_u are the lower and upper cut off frequency range; N is the number of data points [110].

3.8 Combining acceleration and velocity for fault diagnosis

According to [192], displacement signal tends towards low-frequency components, while that acceleration tends toward high-frequency components. The velocity signal covers a frequency range of 10 Hz to 1000 Hz, which is most suitable for vibration severity indication. It can be seen that the acceleration range covers bearings and gear faults which occurs at high frequencies, and velocity covers a frequency range at which rotor-related fault occur [193]. Thus, a combination of acceleration and velocity features could significantly distinguish rotor-related and bearing faults in a single analysis.

3.9 Theory of poly-coherent composite bispectrum (pCCB)

In defining bispectrum, the second-order moment's power spectrum is considered the basis of its computation. For this chapter, the computation for the poly-coherent composite bispectrum (pCCB) was expressed, which is a build-up of both composite spectrum and bispectrum analysis.

3.9.1 Spectrum Analysis

Bispectrum analysis takes its root from the power spectral, which is a second-order moment [194]. A discrete time series *x(n)* of a power spectrum is represented mathematically by the signal's discrete Fourier Transform (DFT) as [11,207] as in (3.22);

$$\boldsymbol{S}_{xx}(f_k) = E[\boldsymbol{X}(f_k)\boldsymbol{X}^*(f_k)] \tag{3.22}$$

where *k* is the discrete frequency variable i.e., k = 1, 2, 3, …., N and *E*[] is the expectation operator.

3.9.2 Composite spectrum Analysis

Like the power spectrum density (PSD), the cross-power spectral density (CSD) between two signals was computed with the DFT of these signals as shown in equation (3.23) [24];

$$CSD, \boldsymbol{S}_{x_1x_2}(f_k) = E[\boldsymbol{X}_1(f_k)\boldsymbol{X}_2^*(f_k)] \tag{3.23}$$

Where $S_{x_1x_2}(f_k)$ denotes the CSD and k = 1, 2, 3, …, N. The computation of the CSD is such that there is correlation of features between two signals in the frequency domain analysis. However, the signals may contains some noises as can be observed in vibration analysis, thus a modification of the CSD produced the coherent composite spectrum (CCS)[196]. The CCS is computed as [25,24,208] in equation (3.24);

$$S_{CCS}(f_k) = \sum_{r=1}^{n_s} \frac{X_{CCS}^r(f_k)X_{CCS}^{r*}(f_k)}{n_s} \tag{3.24}$$

Where $X_{CCS}^r(f_k)$ and $X_{CCS}^{r*}(f_k)$the coherent composite Fourier transform and its complex conjugate respectively for the *rth* segment of the measured vibration data from *'b'* bearing locations at frequency f_k. The n_s represents the number of equal segments used for Fourier transform computation. So that $X_{CCS}^r(f_k)$ is computed as [21],[25];

$$X_{CCS}^r(f_k) = \sqrt{(S_{X_1\gamma_{12}^2X_2}^r(f_k)S_{X_2\gamma_{23}^2X_3}^r(f_k) \dots S_{X_{b-1}\gamma_{(b-1)b}^2X_b}^r(f_k))^{\frac{1}{(b-1)}}} \tag{3.25}$$

Here, γ_{12}^2, γ_{23}^2,…. $\gamma_{(b-1)b}^2$ are the respective coherence between bearing 1 - 2, 2 - 3,…. (b - 1)b where b=1, 2, ….b. Also, $S_{X_1\gamma_{12}^2X_2}^r(f_k)$, $S_{X_2\gamma_{23}^2X_3}^r(f_k)$, … $S_{X_{(b-1)}\gamma_{(b-1)b}^2X_b}^r(f_k)$ are the respective coherent cross-power spectrum between bearing 1 - 2, 2 - 3, …, (b-1)b, which was computed thus [25,24];

$$S_{X_q\gamma_{q(q+1)}^2X_{q+1}}^r(f_k) = \left[X_q^r\gamma_{q(q+1)}^2X_{(q+1)}X_q^{r*}\gamma_{q(q+1)}^2X_{(q+1)}\right] \tag{3.26}$$

Where q = 1, 2, …., (b-1).

As seen in the computation of equations (3.22), (3.23), (3.24), (3.25) and (3.26), the phase information was not retained from the signals from intermediate bearing location. This is due to both the combination of the Fourier transform and its complex conjugate [11], and the cross-power spectrum density (CSD).

3.9.3 Bispectrum Analysis

The bispectrum of the discrete Fourier transform (DFT) can be represented as [194]:

$$B_{xxx}(f_l, f_m) = E[X(f_l)X(f_m)X^*(f_l + f_m)], \quad l + m \leq N \tag{3.27}$$

The computation of bispectrum (3.27) was done in such a way that there is coupling between two frequencies f_l and f_m with a third frequency $f_l + f_m$ that is equal to the sum of the two frequencies, considering the given time domain signal. Also, given bispectrum component $B_{xxx}(f_l, f_m)$ may be represented as B_{pq} if the frequencies f_l and f_m are the pth and qth harmonics of the machines rotating speed frequency, respectively. The bispectrum is a complex quantity, so that both amplitude and phase were calculated for the B_{pq} components. Therefore, this ability of the bispectrum to combine harmonics component of several frequencies with the retention of their phases, make it useful for a robust and effective fault diagnosis.

3.9.4 Poly-coherent composite bispectrum (pCCB) analysis

The poly-coherent composite bispectrum **B** (3.28) is represented mathematically as [21][25] as;

$$\mathbf{B}(f_l f_m) = \frac{\sum_{r=1}^{n_s} (\mathrm{X}^{\mathrm{r}}_{\mathrm{pCCS}}(f_l)\mathrm{X}^{\mathrm{r}}_{\mathrm{pCCS}}(f_m)\mathrm{X}^{\mathrm{r}^*}_{\mathrm{pCCS}}(f_l+f_m))}{n_s} \tag{3.28}$$

where X^r_{pCCS} in equation (6.7) is the poly-coherent composite Fourier Transform (FT) for the *rth* segment of the measured vibration data from 'b' bearing location at frequency f_k and n_s is the number of equal segments used for the FT computation. Hence X^r_{pCCS} is computed as in equation (3.29) [22,24];

$$X_{pCCS}^{r}(f_k) = \left(\sum_{r=1}^{n_s} X_1^r(f_k)\gamma_{12}^2\, X_2^r(f_k)\gamma_{23}^2 X_3^r(f_k)\gamma_{34}^2 X_4^r(f_k) \ldots X_{(b-1)}^r(f_k)\gamma_{(b-1)b}^2 X_b^r(f_k)\right)^{\frac{1}{b}} \quad (3.29)$$

where $X_1^r(f_k), X_2^r(f_k), X_3^r(f_k), X_4^r(f_k), \ldots, X_{b-1}^r(f_k)$ *and* $X_b^r(f_k)$ respectively represents the FT of the rth segment at frequency f_k of the vibration responses at bearings 1, 2, 3, 4, …, (b-1) and b [8]. Also, $\gamma_{12}^2, \gamma_{23}^2, \ldots\ \gamma_{(b-1)b,}^2$ respectively represents the coherence between bearing 1-2, 2-3…, (b-1)b (where b = 1, 2, …, b), and the $S_{pCCS}(f_k)$ is the pCCS at frequency f_k [22,24]

The measure of the combination of the frequencies at f_l, f_m, and $f_l + f_m$ explains the characteristics of the bispectrum. The correlation of various harmonic components in bispectrum is found to be useful for robust and effective diagnosis especially in rotating machines [22,24].

3.10 Data matrix for condition classification

The data matrix in this study is a build-up of selected features which are sensitive to fault diagnosis from both time (*T)* domain, frequency (*F*) domain and bispectrum components (B_{xx}), obtained from signals of all machine conditions (C), collected at various machine running speeds (S), from of all sensors or bearing location (Bg1 to Bg4). Assuming the simulated conditions ($C_{k)}$ are $C_{RMRU,}$ $C_{Unb,}$ $C_{M,}$ $C_{CBg1,}$ $C_{RubD2,}$ $C_{Bg1Cg,}$ $C_{Bg2Cg,}$ the running speeds (S_p) are $S_{450\,RPM,}\, S_{900\,RPM}, and\ S_{900\,RPM},$ and the selected features are $T_{rms,}\, T_{CF,}\ T_{Ku,}\, F_{1x,}\, F_{2x,}\, F_{3x,}\, F_{4x,}\, F_{5x,}\, F_{SE.}$The measured data per bearing has data set from $D_{1,}\, D_{2,}\, D_3$ *to* D_m for the particular simulated machine condition $C_{k,}$ and at the particular rotating speed $S_{p,}$ where *k is 1, 2, 3, …, k* (representing the different simulated conditions) and *p 1, 2, 3, …, p* (representing the number of speeds), and *m = 1, 2, 3, …, m* (representing the number of data set collected). The data matrix is presented in equation (3.30) to (3.50).

Data matrix build up for dFAVF model

The build-up matrix for proposed dFAVF approach is presented from equation 3.30 - 3.41. Here, data matrix for rotor conditions was computed based on time domain and frequency domain of acceleration and velocity features (3.30). So that,

$$D_m = [T_{rms}\ T_{CF}\ \ T_{Ku}\ F_{1x}\ F_{2x}\ F_{3x}\ F_{4x}\ F_{5x}\ F_{SE}]_{Bg1-Bg4} \tag{3.30}$$

Equation 3.30 shows the features build-up for each dataset from the four Bearing locations. However, equations (3.31) to (3.36) represents rotor related conditions feature matrix.

$$F_{C_1S_1} = \begin{bmatrix} aT_{rms_{D_1}} & a\,T_{CF_{D_1}} & aT_{Ku_{D_1}} & vF_{1x_{D_1}} & vF_{2x_{D_1}} & vF_{3x_{D_1}} & vF_{4x_{D_1}} & vF_{5x_{D_1}} & vF_{SE_{D_1}} \\ aT_{rms_{D_2}} & aT_{CF_{D_2}} & aT_{Ku_{D_2}} & vF_{1x_{D_2}} & vF_{2x_{D_2}} & vF_{3x_{D_2}} & vF_{4x_{D_2}} & vF_{5x_{D_2}} & vF_{SE_{D_2}} \\ \vdots & \vdots & \vdots & \vdots & \vdots & \vdots & \vdots & \vdots & \vdots \\ aT_{rms_{D_m}} & aT_{CF_{D_m}} & aT_{Ku_{D_m}} & vF_{1x_{D_m}} & vF_{2x_{D_m}} & vF_{3x_{D_m}} & vF_{4x_{D_m}} & vF_{5x_{D_m}} & vF_{SE_{D_m}} \end{bmatrix}_{C_{RMRU}S_{450\ RPM}} \tag{3.31}$$

$$F_{C_1S_2} = \begin{bmatrix} aT_{rms_{D_1}} & a\,T_{CF_{D_1}} & aT_{Ku_{D_1}} & vF_{1x_{D_1}} & vF_{2x_{D_1}} & vF_{3x_{D_1}} & vF_{4x_{D_1}} & vF_{5x_{D_1}} & vF_{SE_{D_1}} \\ aT_{rms_{D_2}} & aT_{CF_{D_2}} & aT_{Ku_{D_2}} & vF_{1x_{D_2}} & vF_{2x_{D_2}} & vF_{3x_{D_2}} & vF_{4x_{D_2}} & vF_{5x_{D_2}} & vF_{SE_{D_2}} \\ \vdots & \vdots & \vdots & \vdots & \vdots & \vdots & \vdots & \vdots & \vdots \\ aT_{rms_{D_m}} & aT_{CF_{D_m}} & aT_{Ku_{D_m}} & vF_{1x_{D_m}} & vF_{2x_{D_m}} & vF_{3x_{D_m}} & vF_{4x_{D_m}} & vF_{5x_{D_m}} & vF_{SE_{D_m}} \end{bmatrix}_{C_{RMRU}S_{900\ RPM}} \tag{3.32}$$

$$F_{C_1S_3} = \begin{bmatrix} aT_{rms_{D_1}} & a\,T_{CF_{D_1}} & aT_{Ku_{D_1}} & vF_{1x_{D_1}} & vF_{2x_{D_1}} & vF_{3x_{D_1}} & vF_{4x_{D_1}} & vF_{5x_{D_1}} & vF_{SE_{D_1}} \\ aT_{rms_{D_2}} & aT_{CF_{D_2}} & aT_{Ku_{D_2}} & vF_{1x_{D_2}} & vF_{2x_{D_2}} & vF_{3x_{D_2}} & vF_{4x_{D_2}} & vF_{5x_{D_2}} & vF_{SE_{D_2}} \\ \vdots & \vdots & \vdots & \vdots & \vdots & \vdots & \vdots & \vdots & \vdots \\ aT_{rms_{D_m}} & aT_{CF_{D_m}} & aT_{Ku_{D_m}} & vF_{1x_{D_m}} & vF_{2x_{D_m}} & vF_{3x_{D_m}} & vF_{4x_{D_m}} & vF_{5x_{D_m}} & vF_{SE_{D_m}} \end{bmatrix}_{C_{RMRU}S_{1350\ RPM}} \tag{3.33}$$

$$F_{C_2S_1} = \begin{bmatrix} aT_{rms_{D_1}} & a\,T_{CF_{D_1}} & aT_{Ku_{D_1}} & vF_{1x_{D_1}} & vF_{2x_{D_1}} & vF_{3x_{D_1}} & vF_{4x_{D_1}} & vF_{5x_{D_1}} & vF_{SE_{D_1}} \\ aT_{rms_{D_2}} & aT_{CF_{D_2}} & aT_{Ku_{D_2}} & vF_{1x_{D_2}} & vF_{2x_{D_2}} & vF_{3x_{D_2}} & vF_{4x_{D_2}} & vF_{5x_{D_2}} & vF_{SE_{D_2}} \\ \vdots & \vdots & \vdots & \vdots & \vdots & \vdots & \vdots & \vdots & \vdots \\ aT_{rms_{D_m}} & aT_{CF_{D_m}} & aT_{Ku_{D_m}} & vF_{1x_{D_m}} & vF_{2x_{D_m}} & vF_{3x_{D_m}} & vF_{4x_{D_m}} & vF_{5x_{D_m}} & vF_{SE_{D_m}} \end{bmatrix}_{C_{Unb}S_{450\ RPM}} \tag{3.34}$$

$$F_{C_2S_2} = \begin{bmatrix} aT_{rms_{D_1}} & a\,T_{CF_{D_1}} & aT_{Ku_{D_1}} & vF_{1x_{D_1}} & vF_{2x_{D_1}} & vF_{3x_{D_1}} & vF_{4x_{D_1}} & vF_{5x_{D_1}} & vF_{SE_{D_1}} \\ aT_{rms_{D_2}} & aT_{CF_{D_2}} & aT_{Ku_{D_2}} & vF_{1x_{D_2}} & vF_{2x_{D_2}} & vF_{3x_{D_2}} & vF_{4x_{D_2}} & vF_{5x_{D_2}} & vF_{SE_{D_2}} \\ \vdots & \vdots & \vdots & \vdots & \vdots & \vdots & \vdots & \vdots & \vdots \\ aT_{rms_{D_m}} & aT_{CF_{D_m}} & aT_{Ku_{D_m}} & vF_{1x_{D_m}} & vF_{2x_{D_m}} & vF_{3x_{D_m}} & vF_{4x_{D_m}} & vF_{5x_{D_m}} & vF_{SE_{D_m}} \end{bmatrix}_{C_{Unb}S_{900\,RPM}} . \quad (3.35)$$

$$F_{C_2S_3} = \begin{bmatrix} aT_{rms_{D_1}} & a\,T_{CF_{D_1}} & aT_{Ku_{D_1}} & vF_{1x_{D_1}} & vF_{2x_{D_1}} & vF_{3x_{D_1}} & vF_{4x_{D_1}} & vF_{5x_{D_1}} & vF_{SE_{D_1}} \\ aT_{rms_{D_2}} & aT_{CF_{D_2}} & aT_{Ku_{D_2}} & vF_{1x_{D_2}} & vF_{2x_{D_2}} & vF_{3x_{D_2}} & vF_{4x_{D_2}} & vF_{5x_{D_2}} & vF_{SE_{D_2}} \\ \vdots & \vdots & \vdots & \vdots & \vdots & \vdots & \vdots & \vdots & \vdots \\ aT_{rms_{D_m}} & aT_{CF_{D_m}} & aT_{Ku_{D_m}} & vF_{1x_{D_m}} & vF_{2x_{D_m}} & vF_{3x_{D_m}} & vF_{4x_{D_m}} & vF_{5x_{D_m}} & vF_{SE_{D_m}} \end{bmatrix}_{C_{Unb}S_{1350\,RPM}} . \quad (3.36)$$

Considering a scenario where two machine conditions, i.e., baseline RMRU and Unbalance (Unb), with three machine running speeds, i.e., 450 rpm, 900 rpm and 1350 rpm, are being used to build the data matrix, equation (3.31) to (3.36) represents the computation of the matrix. Equation (3.31) represents the matrix *C1S1* with condition one (**RMRU**) and speed one (450 rpm). Equation (3.32) represents the matrix *C1S2* with condition one (**RMRU**) and speed two (900 rpm), and equation (3.33) represents the matrix *C1S3* with condition one (**RMRU**) and speed three (1350 rpm). Similarly, equation (3.34) represents the matrix *C2S1* with condition two (**Unb**) and speed one (450 rpm). Equation (3.35) represents the matrix *C2S2* with condition two (**Unb**), and speed two (900 rpm) and equation (3.36) represents the matrix *C2S3* with condition two (**Unb**) and speed three (1350 rpm). His computation was done for all rotor-related conditions. A concise representation for single condition single speed is represented in equation (3.37), while equation (3.38) represents the data matrix for the improved acceleration-based time domain and velocity-based frequency domain classification for rotor faults.

$$F_{C_kS_p} = \begin{bmatrix} F_{aT1_{D_1}} & \cdots & F_{aTn_{D_1}} & \cdots & F_{vF1_{D_1}} & \cdots & F_{vFn_{D_1}} \\ \vdots & \ddots & \vdots & \ddots & \vdots & \ddots & \vdots \\ F_{aT1_{D_m}} & \cdots & F_{aTn_{D_m}} & \cdots & F_{vF1_{D_m}} & \cdots & F_{vFn_{D_m}} \end{bmatrix}_{C_1S_1} \quad (3.37)$$

$$\mathbf{F} = \begin{bmatrix} F_{C_1S_1} & F_{C_1S_2} & \cdots & F_{C_1S_p} \\ F_{C_2S_1} & F_{C_2S_2} & \cdots & F_{C_2S_p} \\ \vdots & \vdots & \ddots & \vdots \\ F_{kS_1} & F_{C_kS_2} & \cdots & F_{C_kS_p} \end{bmatrix} \tag{3.38}$$

Given a data matrix **K**, features *kaT1, kaT2, kaT3 …kaTn* represents acceleration-based time domain parameter for bearing defects. The data matrix in equation (3.39) represents the single speed for a particular condition for bearing defects. However, equation 3.40 represents the data matrix computed using acceleration-based time domain bearing features and velocity-based frequency domain rotor features at a single condition and speed. After that, incorporation of all speeds and all conditions was represented in equation (3.41)which was for the proposed data fusion of the acceleration and velocity feature (dFAVF) model.

$$\mathbf{K} = \begin{bmatrix} k_{aT1_{D_1}} & \cdots & k_{aT2_{D_1}} & \cdots & k_{aT3_{D_1}} & \cdots & k_{aTn_{D_1}} \\ \vdots & \ddots & \vdots & \ddots & \vdots & \ddots & \vdots \\ k_{aT1_{D_m}} & \cdots & k_{aT2_{D_m}} & \cdots & k_{aT3_{D_m}} & \cdots & k_{aTn_{D_m}} \end{bmatrix}_{C_1S_1} \tag{3.39}$$

$$M_{C_kS_p} = \begin{bmatrix} k_{aT1_{D_1}} & \cdots & k_{aTn_{D_1}} & \cdots & F_{vF1_{D_1}} & \cdots & F_{vFn_{D_1}} \\ \vdots & \ddots & \vdots & \ddots & \vdots & \ddots & \vdots \\ k_{aT1_{D_m}} & \cdots & k_{aTn_{D_m}} & \cdots & F_{vF1_{D_m}} & \cdots & F_{vFn_{D_m}} \end{bmatrix}_{C_1S_1} \tag{3.40}$$

$$\mathbf{C} = \begin{bmatrix} K_{C_1S_1} & K_{C_1S_2} & \cdots & K_{C_1S_p} \\ F_{C_2S_1} & F_{C_2S_2} & \cdots & F_{C_2S_p} \\ \vdots & \vdots & \ddots & \vdots \\ F_{kS_1} & F_{C_kS_2} & \cdots & F_{C_kS_p} \end{bmatrix} \tag{3.41}$$

Data matrix build up for ATpCCB

The build-up matrix for the proposed AT-pCCB approach is presented from equations 3.42 - 3.50. Furthermore, the data matrix for rotor-related faults using pCCB components is developed, such that the pCCB components ***B11,***

B12, ***B13*** and ***B22*** represent the rotor-related pCCB components. In equation (3.42), the matrix comprises the selected pCCB amplitude components at a single condition and speed. Bpq is the number of pCCB components, *Dn* is the number of data sets, *C* is the machine condition, *S* is the operating speed and equation (3.43) shows the combination of all conditions and all speeds. However, equation (3.44) represented the initial pCCB computation at a single speed and single condition, while equation (3.45) represented the combined computation of all conditions and all speeds for the initial pCCB classification. Similarly, equation (3.46) represents the data matrix for the improved pCCB classification and equation (3.47) represents the data matrix for the combination of all conditions and all speeds.

$$B_{C_1S_1} = \begin{bmatrix} b_{11_{D1}} & b_{12_{D1}} & \cdots & b_{pq_{D1}} \\ \vdots & \vdots & \ddots & \vdots \\ b_{11_{Dn}} & b_{12_{Dn}} & \cdots & b_{pq_{Dn}} \end{bmatrix}_{C_1S_1} \tag{3.42}$$

$$\mathbf{B} = \begin{bmatrix} B_{C_1S_1} & B_{C_1S_2} & \cdots & B_{C_1S_p} \\ \vdots & \vdots & \ddots & \vdots \\ B_{C_kS_1} & B_{C_kS_1} & \cdots & B_{C_kS_p} \end{bmatrix} \tag{3.43}$$

$$B_{C_1S_1} = \begin{bmatrix} b_{11_{D1}} & \cdots & b_{13_{D_1}} \\ \vdots & \ddots & \vdots \\ b_{11_{D10}} & \cdots & b_{13_{D10}} \end{bmatrix}_{C_1S_1} \tag{3.44}$$

$$\mathbf{B}_{ini} = \begin{bmatrix} B_{C_1S_1} & \cdots & B_{C_1S_3} \\ \vdots & \ddots & \vdots \\ B_{C_4S_1} & \cdots & B_{C_4S_3} \end{bmatrix} \tag{3.45}$$

$$B_{C_1S_1} = \begin{bmatrix} b_{11_{D1}} & \cdots & b_{13_{D_1}} & b_{22_{D_1}} \\ \vdots & \ddots & \vdots & \vdots \\ b_{11_{D10}} & \cdots & b_{13_{D10}} & b_{22_{D10}} \end{bmatrix}_{C_1S_1} \tag{3.46}$$

$$\mathbf{B}_{imp} = \begin{bmatrix} B_{C_1S_1} & \cdots & B_{C_1S_3} \\ \vdots & \ddots & \vdots \\ B_{C_4S_1} & \cdots & B_{C_4S_3} \end{bmatrix} \tag{3.47}$$

By extending **B** in equation (3.43), the complex number (a + jb) of each pCCB component is used to create a data matrix $\mathbf{B}_{\boldsymbol{RI}}$ as seen in equation 3.48.for real and imaginary, such that Real **(B) = B** *R* and Imaginary **(B) = B** *Img***,** thus;

$$\mathbf{B}_{\boldsymbol{RI}} = \begin{bmatrix} (\mathbf{B}\ R) \\ (\mathbf{B}\ Img) \end{bmatrix} \tag{3.48}$$

The matrix build-up for the proposed AT-pCCB approach was represented in equations (3.49) and (3.50). Data matrix **D** in equation (3.49) represents the sub-model AT-ApCCB. It was computed by fusing the matrix **B** as in equation (3.43) and **K** as in equation (3.39) which are those of amplitude of pCCB rotor components and acceleration-based time domain bearing features. Similarly,

$$\mathbf{D} = \begin{bmatrix} (\mathbf{B}\ ) \\ (\mathbf{K}) \end{bmatrix} \tag{3.49}$$

The fusion of matrix and **K** is represented by the computation of the real and imaginary pCCB rotor components and the acceleration-based time domain bearing features. This combination represented in data matrix **E** is equation (3.50) which provides the classification of machine conditions for the AT-RIpCCB model.

$$\mathbf{E} = \begin{bmatrix} (\mathbf{B}\ R) \\ (\mathbf{B}\ Img) \\ (\mathbf{K}) \end{bmatrix} \tag{3.50}$$

3.11 Normalisation approach

Normalisation makes all elements in the matrix dimensionless quantities. It helps to make all data appear similar across the field, leading to cohesion and higher-quality data. Normalisation is achieved by computing each row's standard deviation and mean and subtracting the mean from each element within a row. After that, divide the standard deviation of the row. Equation 3.51 gives the formula to perform normalisation on every value in a dataset:

$$\text{Normalised value} = (\mathrm{D} - \mu)/\sigma \tag{3.51}$$

Where D is the original value, μ is the mean data and σ is the standard deviation.

3.12 Principal Component Analysis (PCA-based) Approach

Principal component analysis (PCA) can be defined as "an orthogonal linear transformation that converts a data set to a new coordinate system where the greatest variance by any projection of the data comes to lie on the first coordinate and the second greatest variance on the second coordinate" [20,96,93]. PCA is a multivariate statistical tool that reduces large interrelated datasets to a small number of variables while retaining the variability in the original data [20,24].

PCA has been used in this study because it uses simple matrix operations obtained from linear algebra and statistics in computing the projection of an original data set but into the same number with fewer dimensions. PCA focuses on the dimensionality reduction of a data set. Here, large and complex variables are transformed into a new set of uncorrelated variables where significant variations in the data set are retained in the first few variables called principal components (PCs) [20,45,93]. The first few PCs retain the variability of the original data [20,87,198]. PCA reveals the existing variance in the original data, which is identified by observations (e.g., the quantity of measured vibration signal) and variables (e.g., CF, Ku, 1x-5x). According to Brownlee [199] operation of PCA as applied to a data set may be represented by a n x m matrix called **A**, and the projection of **A** is called **B** so that,

$$\boldsymbol{A} = \begin{pmatrix} a11, & a12 \\ a21, & a22 \\ a31, & a32 \end{pmatrix} \tag{3.52}$$

$$\boldsymbol{B} = PCA(A) \tag{3.53}$$

Consider a number of samples (observation) *p*, and random variables (features) *m*, represented by a data matrix **G** = [*m* x *p*], the principal components of **G** can be computed as the reduced solution of an eigenvalue-eigenvector problem [87]. Comprehensive studies of the steps as well as application of PCA can be found in the work of Jolliffe [87], Vidal et al. [200], Bishop [88], Brownlee [199], Jaadi [201], Nembhard and Sinha [20], Yunusa-Kaltungo and Cao [202] Nembhard et al. [51] and so on. PCA has been used in this study to investigate the relationship of an extensive range of experimentally simulated rotating machine faults in a single analysis [16,213,86,87].

3.12.1 Observation of increased principal components for improved fault diagnosis

As stated earlier, Principal Component Analysis (PCA) reduces the number of variables in a data set by dimensionality reduction. This approach helps to simplify analysis as smaller sets of data can be easily explored and visualised. The principal components (PCs) are the new variables constructed linearly or mixed with the initial variable in the data set. The combination is such that the PCs are uncorrelated, with most information retained within the first few variables (PCs).

Jaadi [201] tried to simplify the process of PCA and gave an example of how the PCs are formed so that, given 10-dimensional data, there are 10 principal components (PCs). However, PCA transfers as much information as possible to the first component; the remaining maximum information is transferred to the second component. This is represented in Figure 4.2, where the percentage of the variance of each PC is shown. This approach for computing the PCs helps to reduce dimensionality while retaining most of the information from the data set. Thus, PCs with low information are ignored, while the first few PCs with the most information are considered for further investigation.

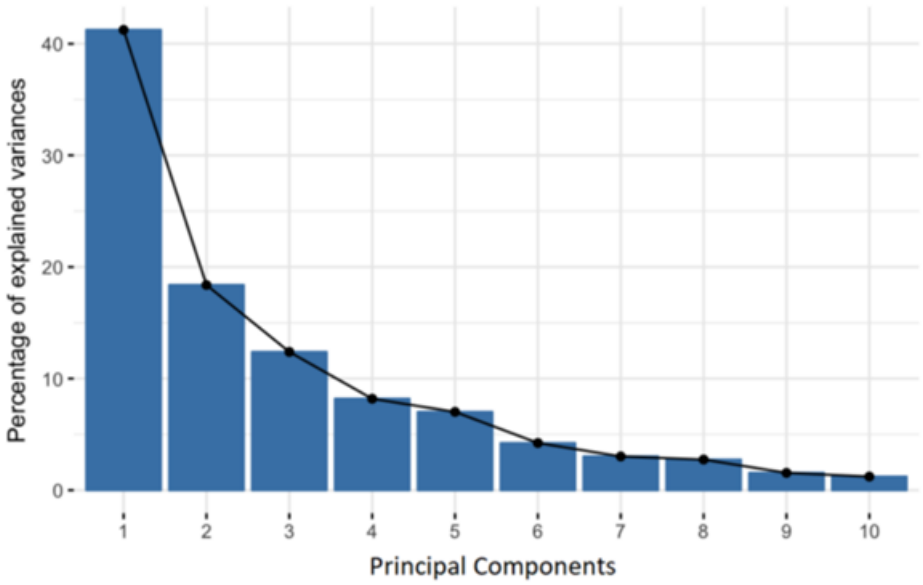

Figure 3. 5 Bar chart showing percentage of variance for each Principal Component accessed from [201]

The eigenvector and eigenvalue form the significant computation aspect of PCA. According to Jaadi [201], “the eigenvectors of the covariance matrix are actually the directions of the axes where there is most variance, and that is called Principal Component. Moreover, the eigenvalues are simply the coefficient attached to eigenvectors, giving the amount of variance carried in each Principal Component”. Thus, principal components are gotten in their order of importance by rearranging the eigenvector in order of their eigenvalues, i.e., from highest to lowest. Once the PCs are obtained, the percentage of information (variance) present in each component is done by dividing the eigenvalue of each component by the sum of eigenvalues.

However, various studies [212-217] used multiple PCs to investigate and analyse machine identification. Yunusa-Kaltungo and Cao [202] observed various PCs in pattern recognition and classification of gear faults. Prieto-Moreno, Llanes-Santiago and Garcia-Moreno [205] proposed a new approach to developing the principal components and compared it with the traditional method; observation showed further PCs also retained more information than the first few PCs in the new method. Cao and Yunusa-Kaltungo [206] computed the percentage of variance for various principal components to investigate machine faults. Manassas, El Adel and Ouladsine [207] proposed two new machine fault identification methods using various PCs.

Wang and Xiao [204] used the optimal number of PCs in machine fault detection. These studies show that other principal components may contain important information that may be useful in classifying various machine conditions. It should be noted that when plotting the principal components (PCs), each PC has a single direction with a midpoint at zero. A positive or negative PC gives the direction of the variable in that PC with reference to a single-dimension vector [87].

3.13 Clustering, and pattern recognition

Clustering and pattern recognition are achieved using the principal components (PCs). [87] A plot of the first few PCs against each other would produce either a 2D or 3D view cluster, and the patterns could be used for investigating machine conditions. In this study, plots of PC1vsPC2 and PC1vsPC2vsPC3 were used to showcase clustering and the patterns observed were used to classify various machine conditions [206]. This

approach is advantageous in observing results as the separation between clusters would help predict machine dynamic behaviour.

3.14 Quantification method using differentiation between baseline and faulty condition

A mean of each condition is obtained from the various scenarios to achieve a definite value for the separation between the baseline RMRU and faulty conditions. This is achieved by plotting the mean of PC1 against PC2 and PC3 to generate the specific mean in x, y and z coordinates, respectively. Mathematically, the mean is calculated as in equation 3.54 for the PC1vsPC2 classification and PC1vsPC2vsPC3 as in equation (3.55).

$$cX = \sum_{i=1}^{nc} \frac{c(Xi)}{nc} \quad \text{and} \quad cY = \sum_{i=1}^{nc} \frac{c(Yi)}{nc} \tag{3.54}$$

$$cX = \sum_{i=1}^{nc} \frac{c(Xi)}{nc} \quad \text{and} \quad cY = \sum_{i=1}^{nc} \frac{c(Yi)}{nc} \quad cZ = \sum_{i=1}^{nc} \frac{c(Zi)}{nc} \tag{3.55}$$

Where *c* represents the conditions (RMRU and faulty), *cX* is the mean of condition at *PC1, cY* is the mean of condition at *PC2, cZ* is the mean condition at PC3 *nc* is the number of data set at condition *c. Xi and Yi* are the sum of *X and Y* datasets, respectively. Applying Pythagorean's theorem, the distance between each faulty and RMRU condition is obtained and recorded.

3.15 Summary of research methodology

This chapter discusses the methodology for this research. It presented a background for this study inspired by work from earlier PhD students, Dr Akilu Yunusa-Kaltungo and Dr Adrian Nembhard. The study of Dr Nembhard proposed the unified multispeed analysis (UMA), which considered only acceleration data and rotor faults with the test rig operated below its first critical speed. This study improved the UMA by fusing acceleration-based time and velocity-based frequency domain parameters and thus proposed the dFAVF model. The model could classify rotor and bearing faults in a single analysis when the test rig operated below and above its first critical speed. Also, the study of Dr Yunusa-Kaltungo proposed the poly-coherent composite bispectrum (pCCB) for rotor fault classification using rotor faults when the rig operated below its

first critical speed. This study also affirmed and improved the pCCB classification approach and went further to observe the complex number representation of the pCCB component in the real and imaginary representations. It then proposes the AT-pCCB classification model, which is made up of AT-ApCCB and AT-RIpCCB sub-models. Both sub-models classified a consolidated rotor and bearing faults in a single analysis. A description of the research process and the various method employed was presented. Reference was made to chapter three, which extensively covered this study's experimental approach. The methods were discussed in detail and included the time domain analysis (root mean square, crest factor and kurtosis), frequency domain analysis (Fast Fourier transform and spectrum energy), envelope analysis, conversion of acceleration to velocity signals, poly-coherent composite bispectrum (pCCB) theory, data matrix, principal component analysis, clustering, and patterning recognition and finally data quantification approach. This chapter presented tools for this research and discussed the reason for selecting most of the tools, the limitations of the selected method, and the work in general. The framework of the methodology, the analysis and the results from the research are discussed in chapters 5 to chapter 9. Since the study is hugely experimental based, a detailed description of the test rig and experiment was presented in chapter 4.

CHAPTER 4

EXPERIMENTAL MODEL APPROACH

This chapter considers an aspect of the methodology of this research work. Since this is experimental research, much focus is given to the description of the experimental approach. This covers the existing flange-based test rig (FFTR) the improved spring-based test rig one and two (SFTR-1&2) which were built in the dynamic laboratory of the University of Manchester. Instrumentation and modal test of the test rig is presented to help determine the natural frequencies and thus select the machine running speed to avoid resonance. The mode shape is observed to understand the dynamic behaviours of the test rig. Thereafter, description of the simulated fault, data collection and storage are presented.

4.1 Overview

This research observes vibration signals from various test rigs based on the foundation flexibility. Here, the flexibility relates to the natural frequency of the entire system, not 'rotor flexibility'. The observation is to understand the dynamic behaviour of the different rotating machines while investigating the proposed fault identification approaches for the various health conditions that may appear during their operation in a single analysis. Thus, three rotating test rigs are considered, with their details presented in this chapter. These are the flange-based flexible test rig (FFTR) and the spring-based flexible test rig 1 & 2 (SFTR-1 & 2).

Furthermore, discussions on the instrumentation, modal testing, fault simulation, data acquisition and signal processing for storage as applied in this research are presented. Usage of these tools followed suggestions in Sinha's book [45], where a detailed explanation of the general approach to carrying out vibration-based condition monitoring is presented.

4.2 Test Rig Setup

Three experimental rigs, i.e., the flange-based flexible test rig (FFTR) and the spring-based flexible test rig 1 and 2 (SFTR-1&2), were used to measure vibration data for this study. The FFTR is from earlier research work built by two former PhD students, i.e., Dr Akilu Yunusa-Kaltungo and Dr Adrian Nembhard. This study improved their rig design from flange-base to spring-base in order to reduce the natural frequency of the rig. Data collected for their study was used in the preliminary phase of this research. However, the SFTR-1 and SFTR-2 are improved versions of the FFTR, all with similar structures but a variation of their bearing pedestal, supporting their various foundation flexibilities. Although, the SFTR may be used in this chapter to represent SFTR-1 and SFTR-2 unless otherwise stated.

These three test rigs are very relevant in achieving the objectives set out in this research and providing data for investigations to address some of the gaps already identified in the literature. The data from FFTR will help to develop an initial approach for observing an extensive range of rotating machine faults. After that, data from the SFTR will be considered to understand the machine's behaviour while it runs over its

critical speed and to investigate multiple consolidated machine critical part faults in a single analysis. These test rigs give a good representation of industrial-scale rotating machines having multiple shafts and multiple bearings. However, the bearing used in this study was the available component at the time, which brought limitations to the bearing defect simulation.

Pictures of the FFTR and SFTR are shown in Figures 4.1 - 4.2 and 4.3 - 4.4, respectively. FFTR and SFTR are similar in their configuration except for the foundation flexibility and bearing pedestal. The setup of both rigs comprises two rigidly coupled 20 mm diameter shafts (S1 and S2) with lengths of 1000 mm and 500 mm. They are connected by a rigid coupler (C2). The coupled shaft is supported by four ball bearings (Bg1 – Bg4) with a 20 mm internal diameter installed at the four bearing pedestals. Three machined steels with 125 mm diameter and 14 mm thickness used as balancing discs were mounted on the shaft, with two discs placed on the long shaft (S1) and one on the short shaft (S2). A flexible coupler (C1) connects the long shaft with a three-phase 0.75 kW 3000 rev/min electric motor. A detailed description of these components is in section 4.2.3, where a comparison between components of the FFTR and SFTR is carried out. The whole system is mounted on a lathe bed, which rests on vibration dampers.

For emphasis, the difference between the three test rigs is the foundation flexibility related to the machine stiffness and its natural frequencies, which are influenced by the bearing pedestal. Each bearing has four holes flange unit and is connected to the bearing pedestal using this hole. The FFTR makes this connection using a 10 mm diameter flange rod for each of the four holes. However, the improved SFTR-1&2 have spring connections at these holes with spring stiffness of 4.69 N/mm and 14.4 N/mm, respectively, for each spring. Figure 3.7 gives a pictorial representation of this description. The adjustments in the foundation flexibilities come from the understanding that a change in either stiffness or mass affects the machine's natural frequency, which in turn alters its overall dynamics behaviour [11]. Thus, the test rigs' dynamic characterisation (modal analysis) and mode shape were presented in subsections 3.4.2 and 3.4.3. The experiment is the same as explained in section 3.5.

4.2.1 Flange-based flexible test Rig (FFTR)

Figure 4.1 and Figure 4.2 shows a pictorial and schematic representation of the flange-based flexible test rig (FFTR). These figures are based on a photograph from the lab and schematics from an earlier study [26].

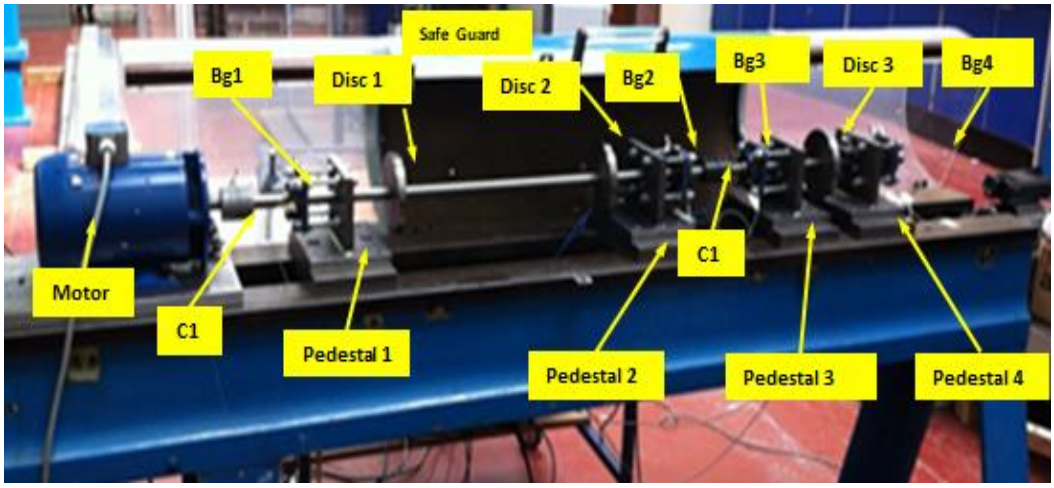

Figure 4. 1Experimental set up for flanged-based flexible test rig (FFTR).

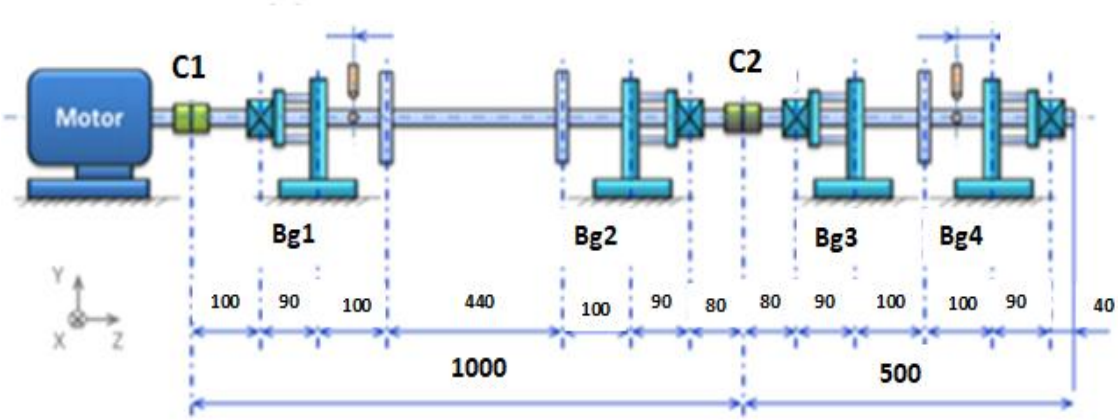

Figure 4. 2 Schematic of flange-based flexible test rig (FFTR) [26].

4.2.2 Spring-based Flexible Test Rig (SFTR)

The pictorial and schematic representation of the spring-based flexible test rig (SFTR) is seen in Figure 4.3 and Figure 4.4, respectively. These figures are photographed from the dynamic lab of the University of Manchester and the schematics developed for the thesis report.

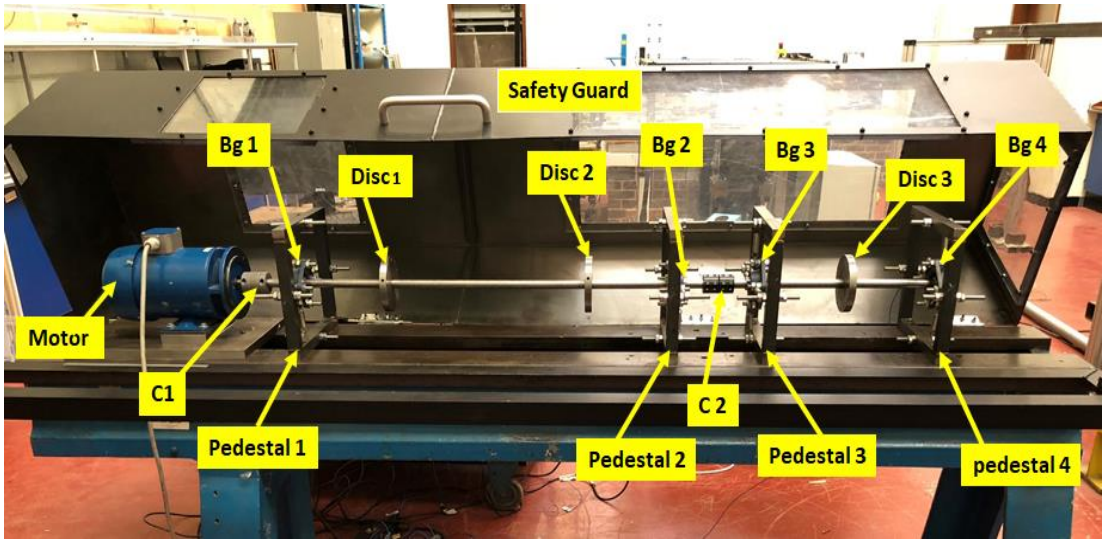

Figure 4. 3 Experimental set up for Spring-based flexible test rig (SFTR).

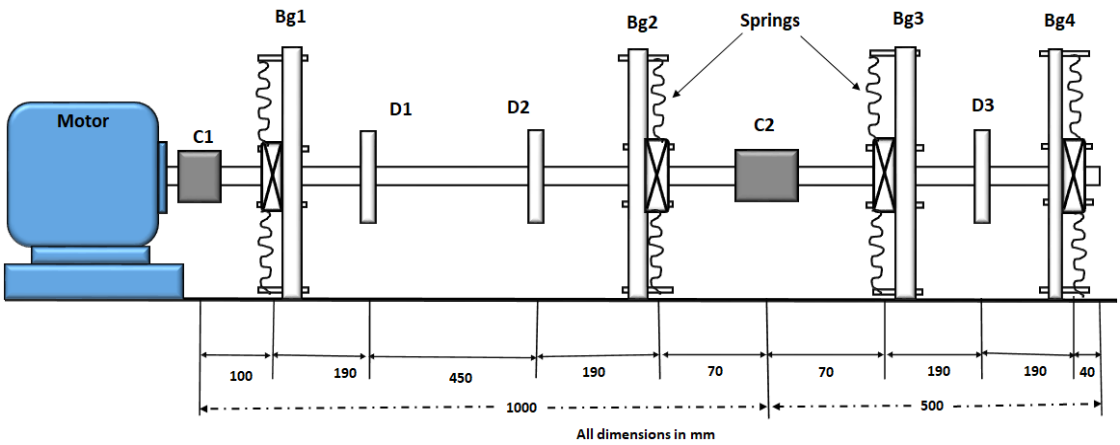

Figure 4. 4 Schematic of Spring-based flexible test rig (SFTR).

4.2.3 Some fundamental elements of the test rig

Some of the fundamental elements of the test rigs used in this study are discussed in this section. Given the modification of the FFTR to SFTR, major part of the test rig remains the same while a few were adjusted. Thus, similar and adjusted elements for the FFTR and SFTR are presented in the subsections below. While Table 4.1 shows similar components in the test rigs, Table 4.2 shows the difference in the components that make up FFTR and SFTR.

4.2.3.1 Rotating shaft

The shaft or rotor is one of the critical components in a rotating machine. In this study, two shafts (rotors) are used to build up the test rigs. These are the long shaft, which is 1000 mm and the short shaft, which is 500 mm, with a diameter of 20 mm. Another shaft in this study is the one from the motor. This shaft connects the motor to the long shaft using the flexible coupler (C1), and the long shaft is connected to the short shaft by the rigid coupler (C2). The shaft is made of mild steel, which is a mix of iron and carbon. Its benefit is the low price and suitability for most engineering applications. Views of the shafts are in the pictures in Figure 4.1 and Figure 4.3.

4.2.3.2 Electric motor

The manufacturer of the electric motor drives the test rig is Crompton Greaves Ltd, India. It is a 3-phase, 0.75kW, 3000 rpm induction motor, with model number GF 79654. Figures 4.5 shows a picture of the electric motor. The motor can run at various speeds as programmed and controlled by a speed controller.

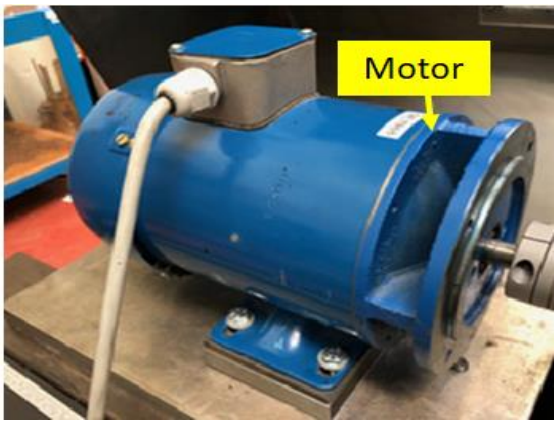

Figure 4. 5 Picture of electric motor.

4.2.3.3 Couplers

The test rig is connected by two couplers, i.e., flexible coupler (C1) Ruland/ FCMR 38-16-16-A and rigid coupler (C2). The flexible coupler (C1), as seen in Figure 4.6 (a) and (b), holds the long shafts (1000 mm) and the motor together, while the rigid coupler (C2), as seen in Figure 4.6 (c) and (d), connects the long shaft and short shaft (500 mm).

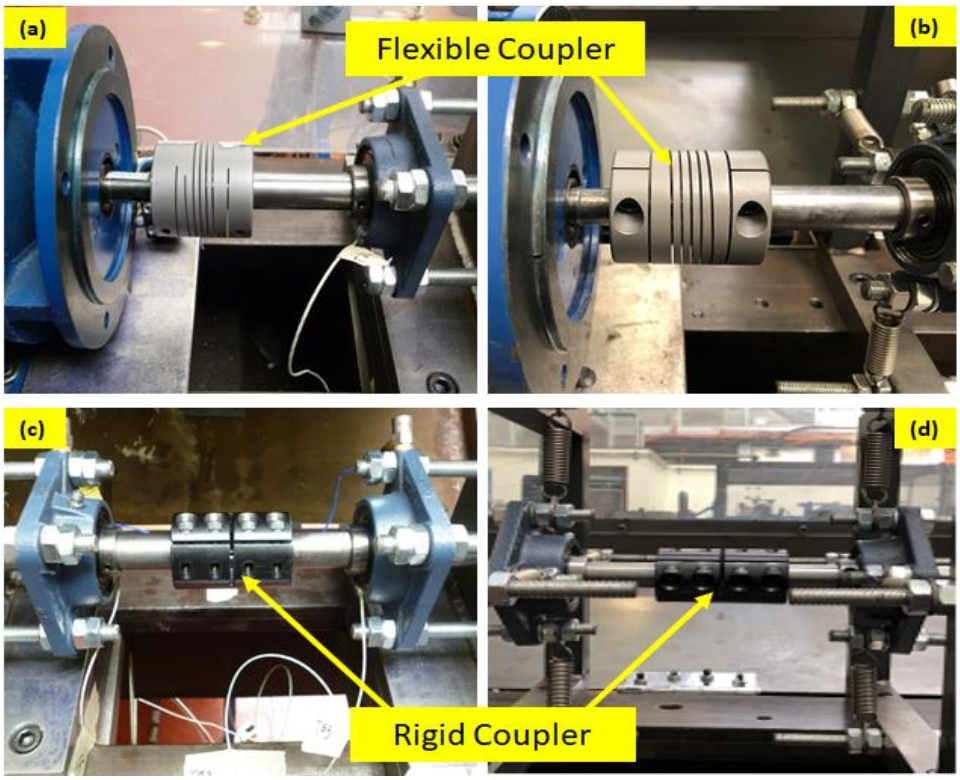

Figure 4. 6 Pictures showing similar configuration of various sections of couplers (a) soft coupler FFTR [26] (b) soft coupler SFTR (c)rigid coupler FFTR [26] (d) rigid coupler SFTR.

4.2.3.4 Bearing and bearing pedestal

The bearing and bearing pedestals are significant components in this test rig and central industrial rotating machinery. The bearing pedestal in this study uses flange rods for the FFTR and springs for the SFTR. The bearings have a model number of SKF FY 20 TF with eight (8) rolling elements or balls, each with a diameter of 7.938 mm. The internal diameter of the bearing is 20 mm, which fits into the shaft's internal diameter. The bearing's width, external, and pitch circle diameter are 31 mm, 47 mm, and 33.5 mm, respectively. The bearing pedestal for the FFTR is made up of a 10 mm threaded rod connected by a flange approach. In contrast, the SFTR bearing pedestal is built up of springs of length 5.5 mm connected to the pedestal, as seen in Figure 4.7, (a) and (b), respectively, and Figure 3.7 (c) is a schematic of the bearing pedestal. A detail of this design diagram is shown in the appendix section.

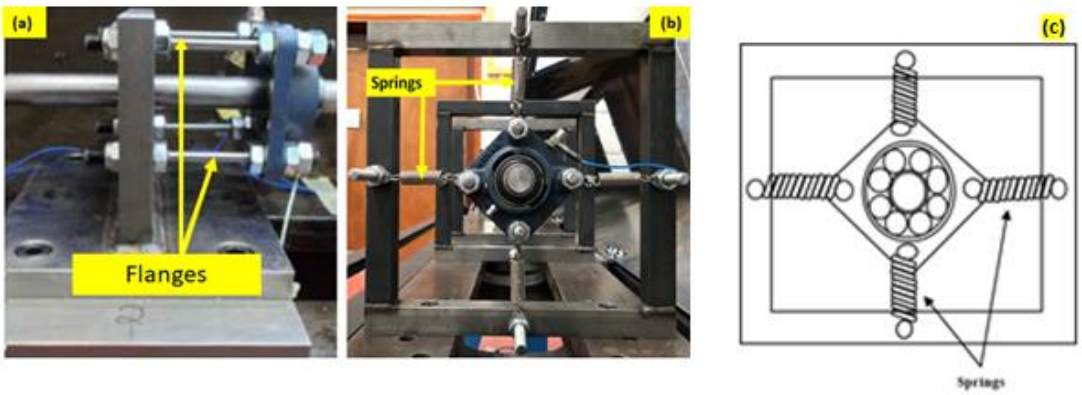

Figure 4. 7 Bearing pedestal of experimental rig set at (a)picture of FFTR [26] (b)picture of SFTR (c) schematics of SFTR.

4.2.3.5 Balance disc

Balance discs are essential in the test rig as they help to correct unbalance. Three machined mild steel with 125 mm diameter and 14 mm thickness are used as balance discs. Two balance discs were mounted on the long shaft (S1) and one on the short shaft (S2). Each of the discs contained 12 tapered holes (M5) with a pitch diameter of 125 mm with an angle of 300 degrees between any two adjacent holes. These holes help to simulate the unbalance fault by inserting a mass unbalance in them. Figure 4.8 shows a picture of one balance disc close to Bg1.

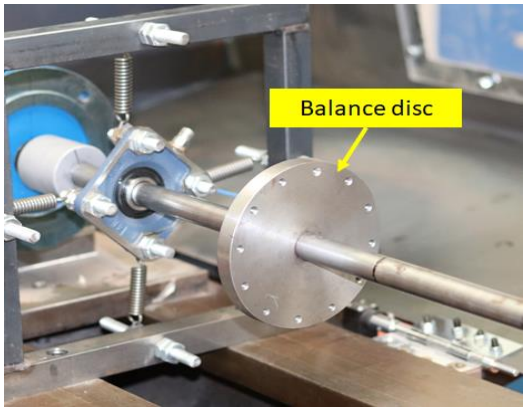

Figure 4. 8 Picture of balance disc.

4.2.3.6 Rig cover/safety guard

The test rig cover for the FFTR and SFTR serves the same purpose: protecting the machine from external interference during operation and keeping the operator safe. A sensing device is set between the test rig and cover so that an attempt to open the cover during operation triggers the operation to stop. This device is a safety initiative that keeps the operator and test rig safe. On the other hand, due to the design of the bearing pedestal, the covers of FFTR and SFTR are different. Figures 4.1 and 4.3 show views of the different test rigs, including their covers.

Table 4. 1 showing detail of similar components that made up the FFTR and SFTR.

NAME	ID	MODEL	DESCRIPTION
Motor	Motor	Crompton Greaves/ GF7965	3 phase, 0.75kW, 3000 rpm.
Shaft 1	S1	Nil	20 mm diameter X 1000 mm length mild steel rod.
Shaft 2	S2	Nil	20 mm diameter X 500 mm length mild steel rod.
Coupler 1	C1	Ruland/ FCMR 38-16-16-A	20 mm bore flexible coupling 16 mm x 20 mm.
Coupler 2	C2	Nil	Rigid Coupling.
Balance Disc	D1, D2, D3	Nil	125 mm outer diameter X 14 mm thickness section machined steel with 20 mm inner diameter.
Bearing	Bg1, Bg2, Bg3, Bg4	SKF FY 20 TF	

Table 4. 2 showing detail of different components that made up the FFTR and SFTR.

NAME	***ID***	***MODEL***	***DESCRIPTION***		
			FFTR	*SFTR-1*	*SFTR-2*
Bearing Pedestal	*Bg1, Bg2, Bg3, Bg4*	*SKF FY 20 TF*	*Flange mounted grease lubricated bearings with 10 mm diameter per flange*	*Spring mounted grease lubricated bearings with a 4.69 N/mm stiffness per spring.*	*Spring mounted grease lubricated bearings with a 14.4 N/mm stiffness per spring.*
Test rig covers	*Nil*	*Nil*	*Curved metallic sheet*	*Rectangular metallic sheet*	*Rectangular metallic sheet*

4.3 Instrumentation

Instrumentation is vital in recording vibration signals as it determines the quality of signals acquired [11]. The selection of an instrument is dependent on various factors such as the output required, the accuracy level of output, signal resolution, measurement range, managing excess measurement parameters and mounting arrangement. In order to achieve any of these, some technical considerations would have to be considered [11]. Instrumentation in this research include accelerometers, impact hammer, signal conditioner, data acquisition system (DAQ), and speed controller. The various instruments' descriptions and functions are presented in subsections 4.3.1 to 4.3.5.

4.3.1 Accelerometers

Vibration responses can be obtained in acceleration, velocity and displacement using an accelerometer, velocity pick-ups and displacement probes [11]. In this study, accelerometers have been used to obtain vibration signals. The accelerometers are also called transducers and can measure a vibrating system's dynamic acceleration.

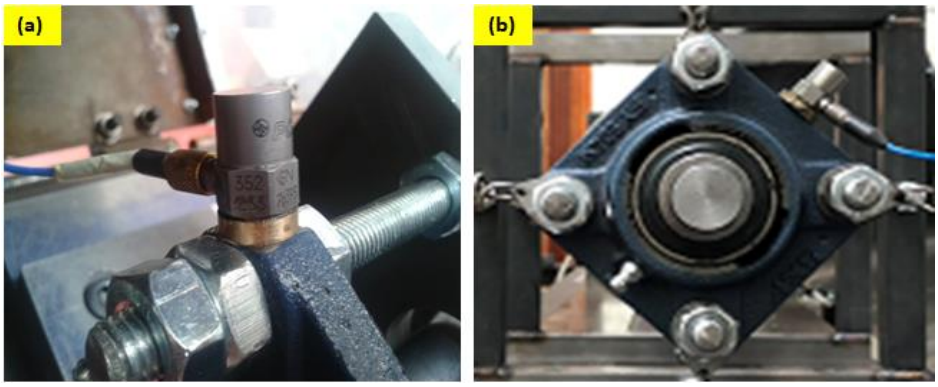

Figure 4. 9 Position of Accelerometer in (a) FFTR [26] and (b) SFTR.

In this research, four accelerometers have been used, each with a sensitivity of 100 mV/g. Their model number is 352C33, ECN number is 28610, the frequency range is (+/-5%) 0.5 – 10000 Hz and resonant frequency ≥ 50 kHz, temperature range of -65 to +200 oF, excitation voltage is 18 to 32 VDC, mounting torque 10 to 20 in-lb with a 10-32 coaxial jack connector. The four accelerometers, with one on each bearing pedestal, are installed on the various test rigs in this study. Each accelerometer was mounted on the bearing housing at 450 radially using stud mounting. This mounting angle gives measurements that account for the accelerometer's horizontal and vertical responses. Figure 4.9 (a) and (b) show the accelerometer mounted on the bearing pedestal of FFTR and SFTR, respectively.

4.3.2 Impact hammer

An ICP-PCB 086C03 impact hammer was used for this research, as shown in Figure 4.10. This hammer is to identify the test rig's natural frequencies and mode shapes. Experimentally, the natural frequencies of rotating machines or other structures are obtained using impact hammer testing by hitting the machine with a hammer and collecting the response with an accelerometer.

Figure 4. 10 Impact hammer for modal testing.

The impulse from the hammer contains an almost steady force over a broad frequency range, which is why it can excite all resonant frequencies within that range. The hammer senses the force applied through an integrated ICP quartz element mounted on the striking head. The impact force is transferred to the analogue-to-digital converter (ADC) through the signal conditional. Also, the impact hammer is designed so that the frequency range to be excited varies based on the impact tip of the hammer, i.e., the soft tip excites a lower frequency range, and the hard tip excites frequency ranges that are higher than those for soft tip.

The impact hammer has a sensitivity of 10 mV/N, and the sensing element is quartz, measurement range of ±224 npk resonant frequency of ≥22 kHz. The excitation voltage is 20-30 VDC, and the current excitation is 2 to 20 mA and a BNC jack connector. The impact hammer has a mass of 0,16 kg, a head diameter of 157 mm, and a tip diameter of 63 mm, the length of the hammer is 216 mm, and the mass is 75g.

4.3.3 Speed controller

The speed controller helps operate the test rig and is used to vary the speed of the motor. It is manufactured by Newton Tesla, model CL 750 and has a 0.75kW with an input frequency of 50/60 Hz and output frequency of 5-60 Hz. The output voltage is 0-200 Volts, and the AC output current is 4.1 A. The power rating is 0.75 kW.

Figure 4. 11 Figure 4. 11 Picture showing speed controller.

The speed controller can be operated manually using the nubs, as seen in Figure 4.11. It is also connected to the personal computer and operated by manually inputting the required speed.

4.3.4 Signal conditioner

The PCB 482C signal conditioner, as pictured in Figure 4.12, was used in this study. Its function supplies electrical power to the accelerometer and impact hammer. Also, the output signals typically have very low magnitudes and may carry various forms of contamination. Thus, these signals need amplification and filtration before digitising them [11,29]. Some of these signal conditioners have low pass filters, which can stop frequencies higher than the desired frequency range to be measured to increase the accuracy of measured signals [11,200].

Figure 4. 12 Photograph of PCB 482C signal conditioner.

The signal conditioner also provides this function of signal amplification, linearisation, isolation, multiplexing and filtration. It should be noted that almost all signals from the transducers carry a certain amount of noise. Thus, signal conditioning is needed to get the vital signal. This signal conditioner is a four-channel device with a BNC input connector from the sensor and BNC output connectors carrying signals to the data acquisition system.

4.3.5 Data acquisition (DAQ) system

The data acquisition (DAQ) system comprises the device and software, as seen in Figures 4.13 and 4.14, respectively. In this study, vibration outputs from the transducers go through the signal conditioner but are analogue signals. These analogue signals must be converted to digital signals to be stored and/or processed. Thus, an analogue to a digital converter (ADC) is used for this purpose. The ADC is the data acquisition device (DAQ) hardware, which makes the data readable on the personal computer. The ADC converts continuous time signatures into discrete forms [11, 29,200].

The DAQ used in this study for recording modal test and vibration data is shown in Figure 4.14. It was manufactured by National instruments Company, having model number NI USB-6229 BNC with a 16 bits ADC resolution, 16 channels and a sampling rate of 250 kS/s for a single channel; 250 kS/s for multiple channels. The input range is

±10 V, ±5 V; ±1 V, ±0.2 V. A data acquisition (DAQ) software is used to enable communication of the DAQ device with the personal computer.

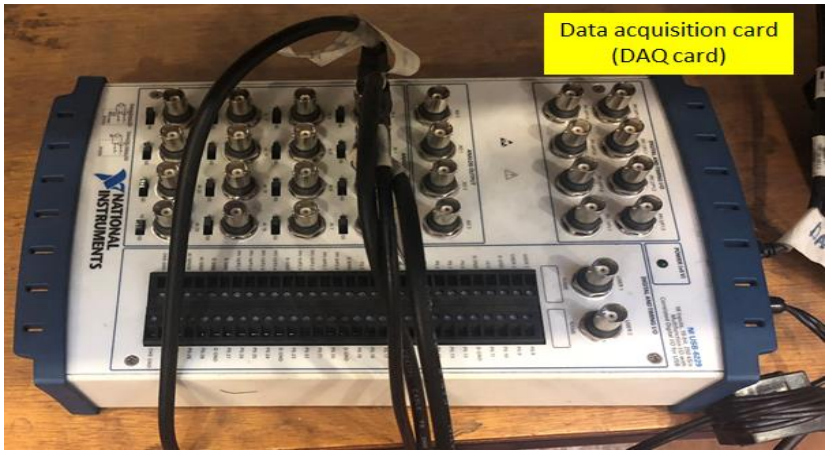

Figure 4. 13 Photograph of NI USB-6229/16-bit/16-channel ADC (DAQ hardware).

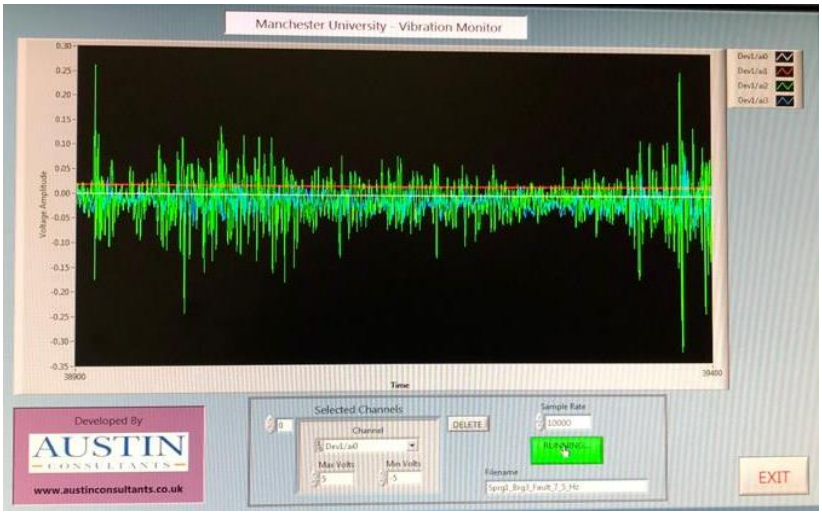

Figure 4. 14 Picture showing DAQ driver software.

The DAQ software used in this study is a customised LABVIEW data acquisition software developed by Austin Consultant for the University of Manchester dynamic lab. Figure 4.14 shows a picture of the DAQ software capturing vibration data. The software usage is straightforward, but care must be taken when inputting things like the sampling frequency, accelerometer channels and voltage ranges with the file name.

4.4 Modal Testing

Modal testing helps understand the structural dynamics of a system, as also as rotating machines. Dynamic characterisation through a modal test was achieved with accelerometers placed along the test rig shaft at nine different locations. The impact hammer was used on the test rig at two locations (impact locations 1 and 2), as shown in Figure 4.15. At each impact location, ten responses were collected in the vertical radial direction (x-plane) at all nine accelerometer locations. The rig shaft is rotated 90 degrees afterwards to align the accelerometers in the horizontal radial direction (y-plane). Accelerometers at the bearing pedestal location at P2, P6, P7, and P9 were all repositioned in the horizontal radial direction, and another ten-impact data was collected. This procedure was repeated for impact location 2, and the modal testing was done on the SFTR-1 and SFTR-2. The impact was carried out at an evenly spaced time interval with much caution to allow the free response on the test rig to decay fully before making another impact. The force response from the impact hammer and the signal response from the accelerometer are recorded.

Note that data acquisition for the modal test was started before the first impact and was stopped after the decay of the tenth impact. Moreover, care was taken to ensure the exact impact location was stuck for all ten impacts, and a double hit was avoided at all costs.

The data acquired were processed and used to compute the Frequency Response Function (FRF) and construct the mode shape from the detected modes with a MATLAB-based algorithm. The computation of the FRF was achieved by applying a rectangular window, averaging the ten responses acquired and applying a 0.16 Hz frequency resolution from the signal with a 5000 Hz sampling frequency. The vertical and horizontal radial direction for obtaining the natural frequencies is to observe the direction in which the natural frequency is dominant, which helps to understand the machine's behaviour. FRF amplitude and phase representation of the modal test at accelerometer location two in the vertical direction is observed to obtain the correct natural frequencies free of biases from the mass of other accelerometers. Section 4.4.1 presents the FRF, natural frequency and mode shape for FFTR, while Section 4.4.2

presents the FRF, natural frequency and mode shape for SFTR-1, and that of SFTR-2 is presented in section 4.4.3. Table 4.3 shows the accelerometer location along the test rig for modal test and mode shape.

Note that nine locations were used for the modal test to observe the mode shape, while four sensor locations at the four bearing pedestals were used for vibration data collection for analysis.

Table 4. 3 Accelerometer location for modal test and mode shape.

Location on the rig	***P1***	***P2***	***P3***	***P4***	***P5***	***P6***	***P7***	***P8***	***P9***
Dist. From mid of coupler 1(in mm)	*0*	*100*	*190*	*515*	*740*	*930*	*1070*	*1260*	*1450*

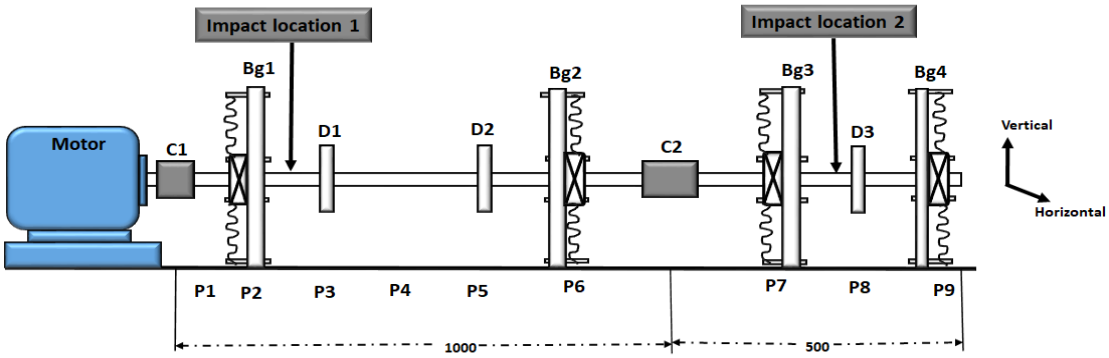

Figure 4. 15 SFTR for modal testing with impact and accelerometer locations.

4.4.1 Modal Testing for FFTR

The FRF from the modal analysis of the FFTR is represented in Figure 4.16. Also, Table 4.4 shows the first four natural frequencies in the vertical and horizontal directions. These figures were obtained from the study of Nembhard and Yunusa-Kaltungo [26-27]. Nembhard and Yunusa-Kaltungo [26-27] stated that natural frequencies in the vertical direction were dominant. Thus, they used it in their study. The mode shape is presented in Figure 4.17. It helps to understand the machine's dynamic behaviour and faults that may show up during its operation.

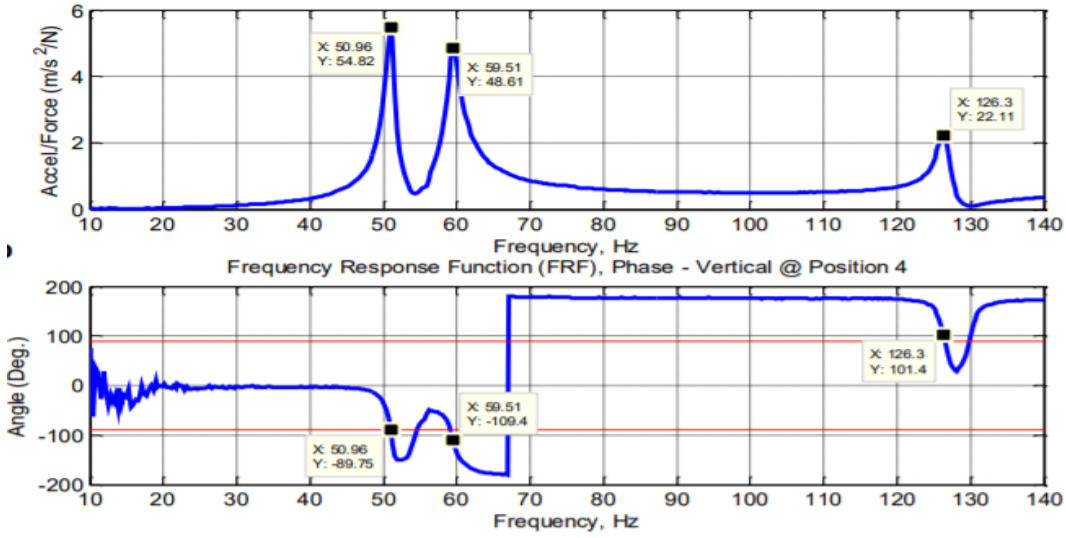

Figure 4. 16 Typical Frequency Response Function (FRF) plot of the measured acceleration response to the applied force in the modal tests for FFTR at location 2 accessed from [27,26].

Table 4. 4 Showing the first four natural frequency of FFTR [25].

1st Nat Freq	***2nd Nat Freq***	***3rd Nat Freq***	***4th Nat Freq***
50.66 Hz	*56.76 Hz*	*59.20 Hz*	*127 Hz*

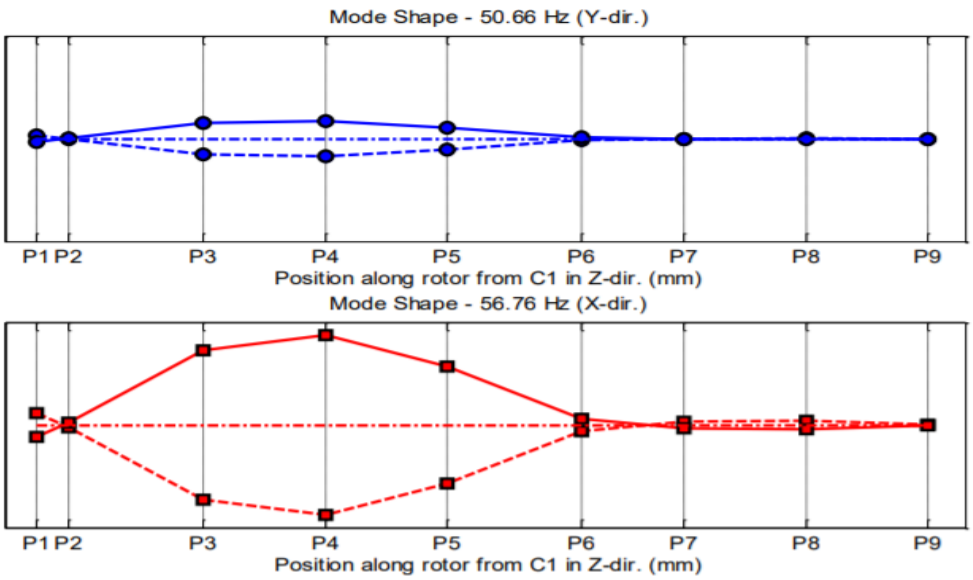

Figure 4. 17 The mode shape of FFTR for the first two natural frequencies accessed from [27,26]in (a) 50.66 Hz dominant in vertical direction (b) 56.76 Hz dominant in horizontal direction.

The natural frequencies of the FFTR are all above the nameplate running speed of the motor, which is 3600 rpm (50 Hz). Thus, the three machine running speeds selected are below the machine's first critical speed, i.e., at 1200 RPM (20 Hz), 1800 RPM (30 Hz) and 2400 RPM (40 Hz), all below the machine's first critical speed. Note that the speed was selected in the study by Yunusa-Kaltungo [27].

4.4.2 Modal Testing for SFTR-1

Similarly, the FRF of specific impact location and accelerometer position in both vertical and horizontal directions is presented in Figure 4.18. For better understanding, Figure 4.18 (a) shows both the FRF amplitude and phase plot at the vertical axis, while Figure 4.18(b) shows both the FRF amplitude and phase plot at the horizontal axis, respectively. Each of the plots has a legend that shows what they represent. The plots on each figure show the presence of the natural frequencies and their validations. Details are found in [11]. The first five natural frequency obtained in both direction is recorded in Table 4.5. The first three mode shapes are presented in Figure 4.19 and 4.20. However, Figure 4.19 is a combination of vertical and horizontal modes and impact location one, while that of impact location two is presented in Figure 4.20. represented the first three modes.

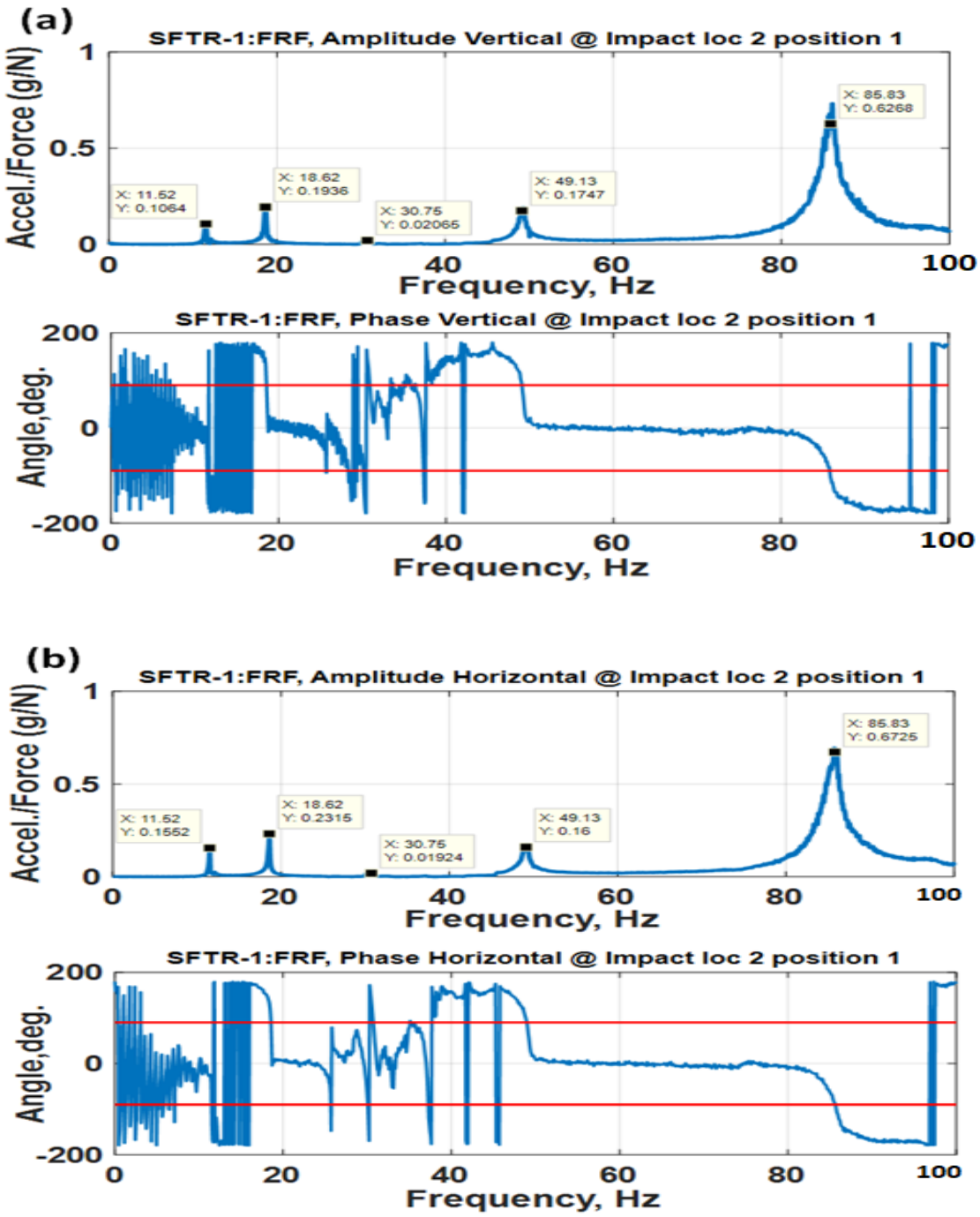

Figure 4. 18 A typical Frequency Response Function (FRF) plot of the measured acceleration response to the applied force in the modal tests for SFTR-1 at location 2 accelerometer position 1 in (a) Vertical (b) Horizontal.

Table 4. 5 Showing the first five natural frequency of SFTR-1.

Natural frequency	***1st***	***2nd***	***3rd***	***4th***	***5th***
Vertical	*11.52 Hz*	*18.62 Hz*	*30.75 Hz*	*49.13 Hz*	*85.83 Hz*
Horizontal	*11.52 Hz*	*18.62 Hz*	*30.75 Hz*	*49.13 Hz*	*85.83 Hz*

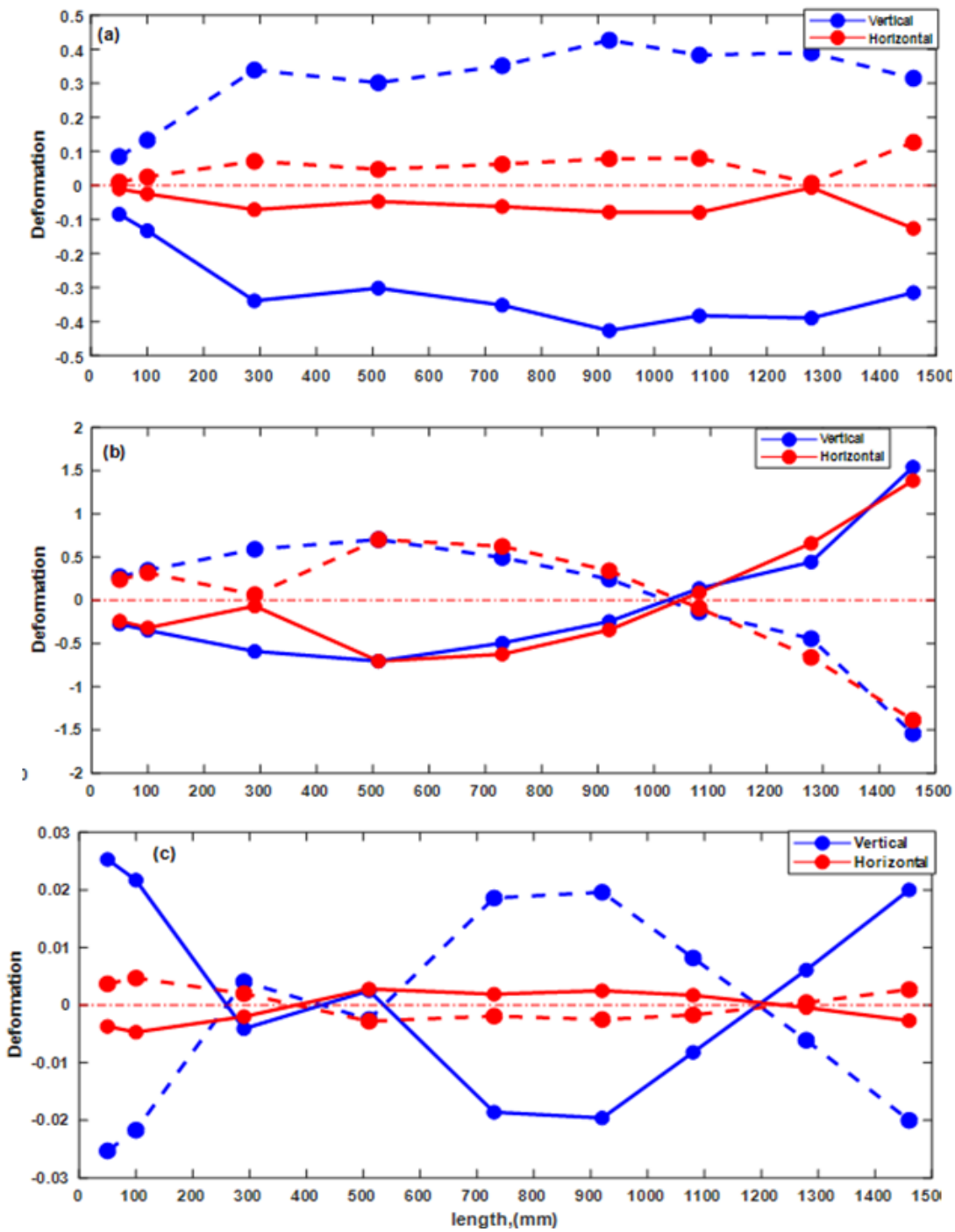

Figure 4. 19 The mode shape of SFTR-1 for the first five natural frequencies at vertical and horizontal impact location 1 in (a) mode 1 (b) mode 2 (c) mode 3.

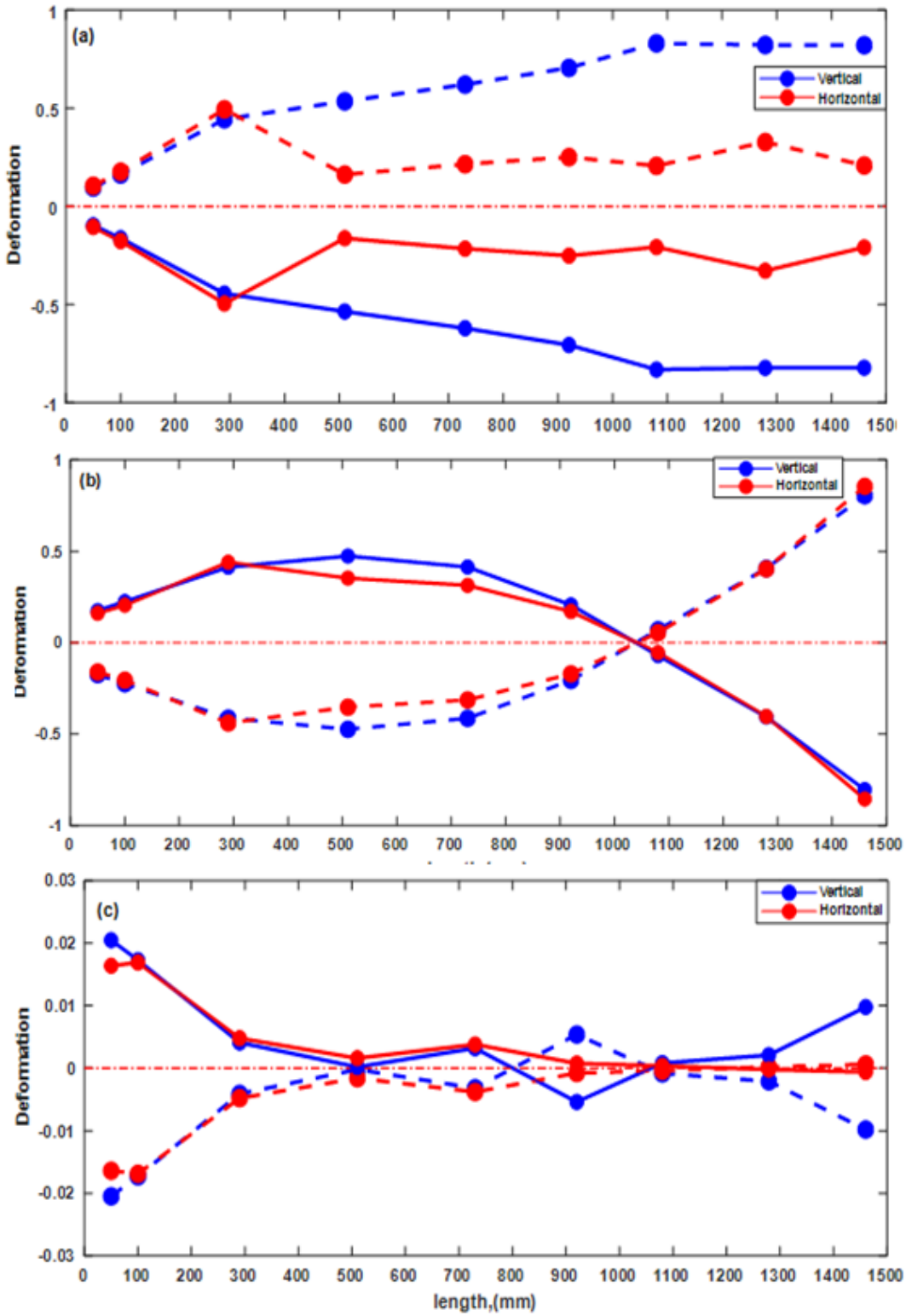

Figure 4. 20 The mode shape of SFTR-1 for the first five natural frequencies at vertical and horizontal impact location 2 in (a) mode 1 (b) mode 2 (c) mode 3.

Based on the natural frequencies, three running machine speeds were selected (one below and two above its first critical speed), i.e., 450 RPM (7.5 Hz) below the first critical speed, 900 RPM (15 Hz) above the first critical speed and 1350 RPM (22.5 Hz) above second critical speed. The selections were made to avoid resonance.

4.4.3 Modal Testing for SFTR-2

THE SFTR-2 was built to compare experimental result outcomes, transfer fault identification methods on similar machines with variation in their foundation flexibilities and strengthen earlier studies [45,22] where vibration data can be used on fault identification without any historical data. Here, the Frequency Response Function (FRF) is presented in Figure 4.21. Like Figure 3.18, plots are observed in Figure 4.21 (a) vertical amplitude and phase, while in Figure 3.21 (b) are horizontal amplitude and phase. Table 4.6 shows the first five natural frequencies of the SFTR-2 in the vertical and horizontal directions. However, in Figure 4.22 and Figure 4.23, only the vertical mode shape at impact locations one and two are presented. Horizontal mode shapes were not added as the experiment was not completed on both impact locations.

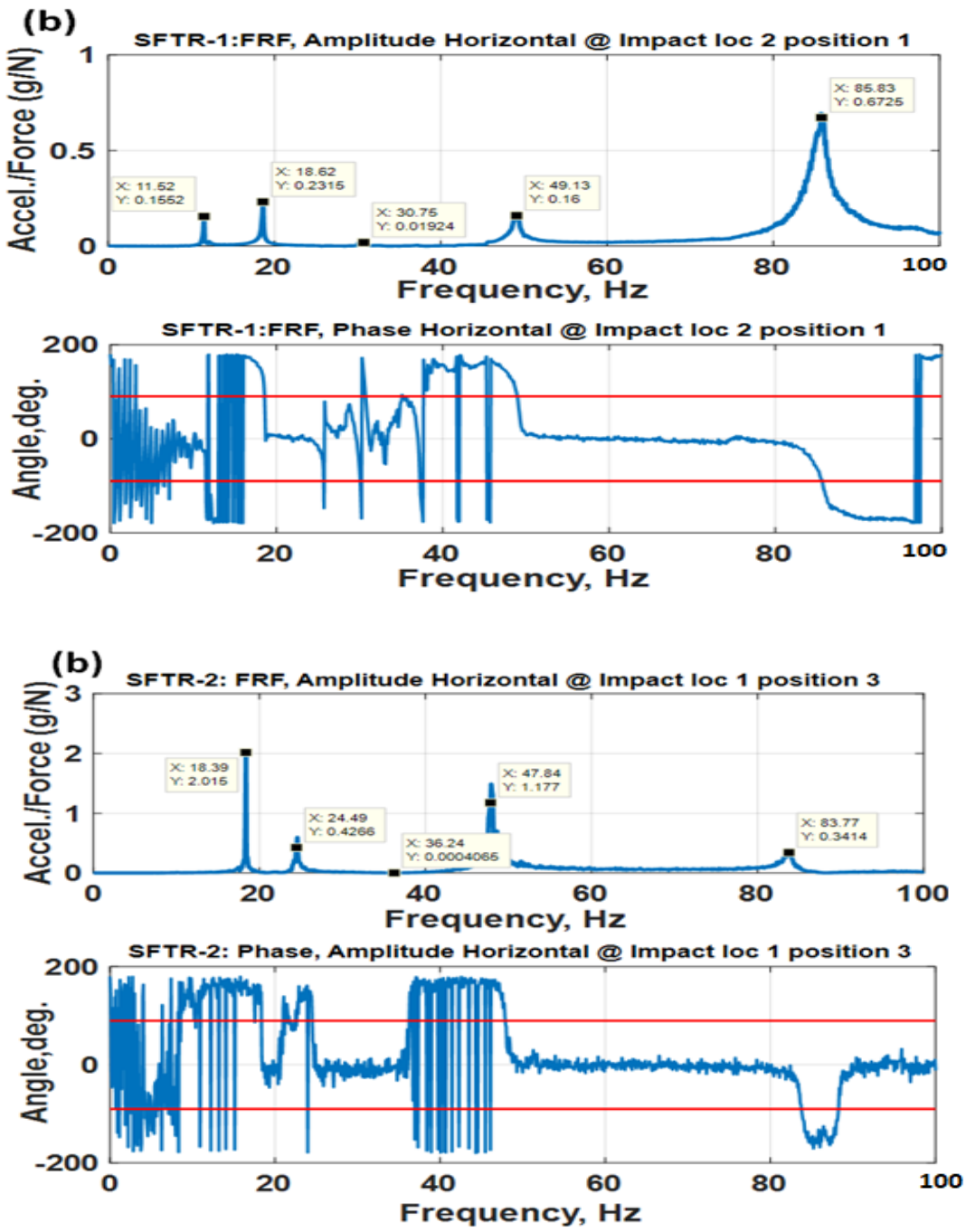

Figure 4. 21 A typical Frequency Response Function (FRF) plot of the measured acceleration response to the applied force in the modal tests for SFTR-2 at location 2 at accelerometer position 3 in (a) Vertical (b) Horizontal.

Table 4. 6 Showing the first five natural frequency of SFTR-2.

Natural frequency	***1st.***	***2nd***	***3rd***	***4th***	***5th***
Vertical	*17.78 Hz*	*23.88 Hz*	*32.65 Hz*	*51.19 Hz*	*86.36 Hz*
Horizontal	*18.39 Hz*	*24.49 Hz*	*36.24 Hz*	*47.84 Hz*	*83.77 Hz*

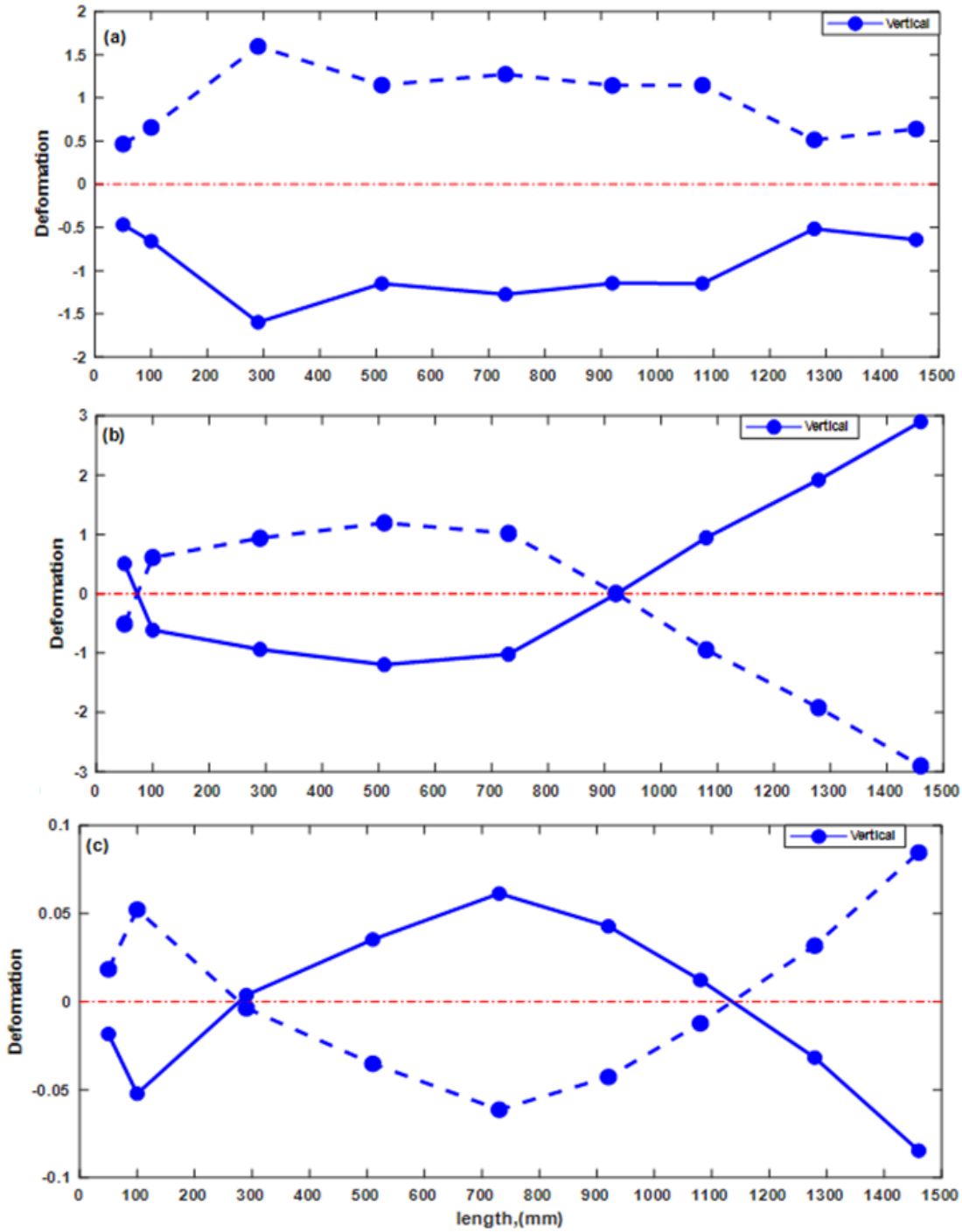

Figure 4. 22 The mode shape of SFTR-2 for the first five natural frequencies at vertical impact location 1 in (a) mode 1 (b) mode 2 (c) mode 3.

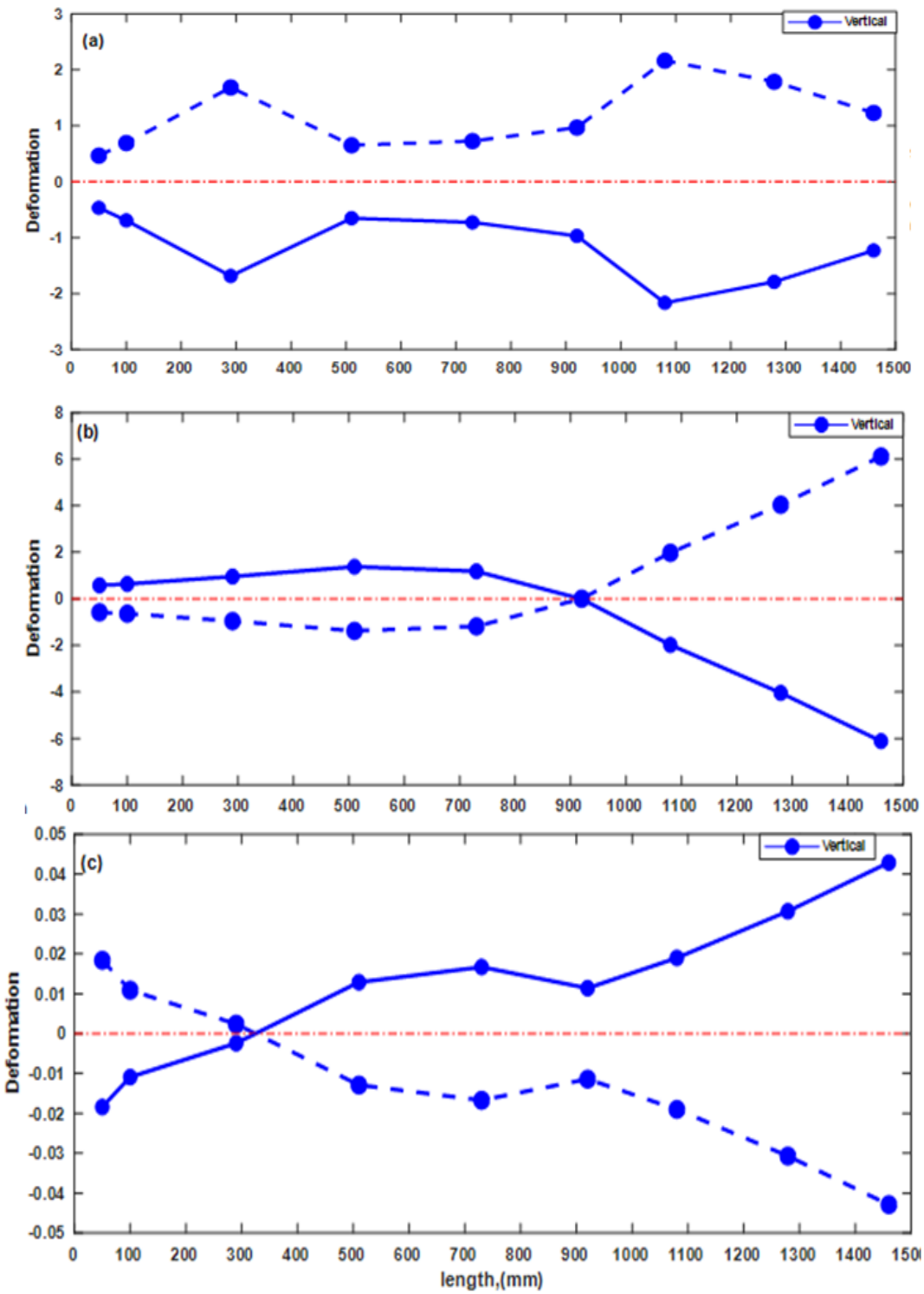

Figure 4. 23 The mode shape of SFTR-1 for the first five natural frequencies at vertical impact location 2 in (a) mode 1 (b) mode 2 (c) mode 3.

Similarly, the same machine condition is maintained except for a change in its foundation flexibility to compare vibration data effectively. The three machine running speeds selected in the SFTR-2 are two below and one above its first critical speed, i.e., at 450 RPM (7.5 Hz) below the first critical speed, 900 RPM (15 Hz) below the first critical speed and 1350 RPM (22.5 Hz) above first critical speed. However, the third machine's running speed is close to the second natural frequency. Investigation into such conditions would be helpful in fault identification.

4.5 Experiments conducted

This section looks at the experimentally simulated conditions with vibration data from the different test rigs recorded, i.e., for FFTR (below the machine's critical speed) and SFTR-1 & 2 (below and above the machine's first critical speed). The reason for such measurement is provided in the modal testing section. Various faults were simulated for the different experimental rigs based on the investigation this research is focused on. The FFTR had only rotor-related faults simulated as per earlier research work, i.e., misalignment, shaft bow, mechanical looseness and shaft rub, as seen in Figure 4.24. The SFTR-1 & 2 had both rotor and bearing faults simulated, with the rotor faults being unbalanced, misalignment, crack, looseness and rub, while that of the bearing was a cage defect, as shown in Figure 4.25.

It should be noted that each simulated condition was done one after the other. The healthy or baseline simulation was carried out first, with the test rig in good condition. However, there may be some residual misalignment, and residual unbalance (RMRU) [21-20]. Table 4.7 shows the various simulated machine condition for each test rig. Detail of each simulated condition is presented in subsections 4.5.1 to 4.5.8, and Table 4.8 gives a description of the all the faults simulated on the relatively flexible test rigs and figure 4.26 shows the faults simulated and their locations.

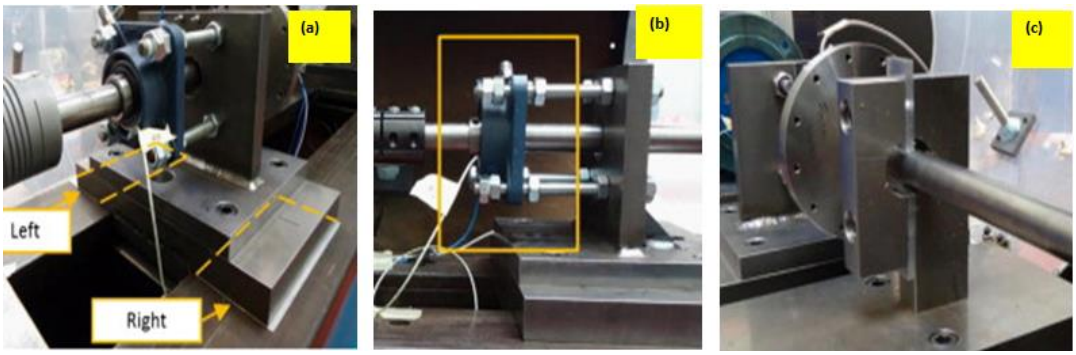

Figure 4. 24 FFTR Simulated Fault (a) Misalignment (b) Looseness (c) Rub all accessed from [51]

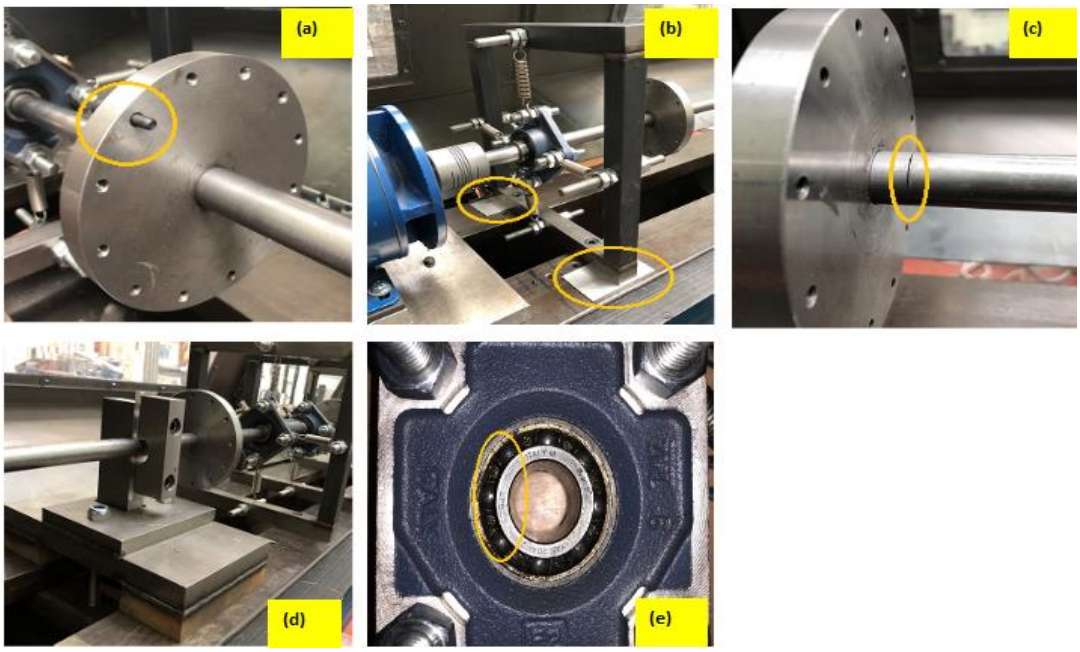

Figure 4. 25 SFTR Simulated Faults (a)Unbalance (b)Misalignment (c Crack (d)Rub (e)Bearing cage defect.

Table 4. 7 Various simulated conditions for the three-test rigs.

	FFTR	SFTR-1	SFTR-2
1.	RMRU	RMRU	RMRU
2.	Misalignment	Unbalance	Unbalance
3.	Shaft bow	Misalignment	Misalignment
4.	Mechanical looseness	Crack shaft	Crack shaft
5.	Shaft rub	Shaft rub	Shaft rub
6.		Bearing cage defect	Bearing cage defect

4.5.1 Residual Misalignment Residual Unbalance (RMRU)

The residual misalignment residual unbalance (RMRU) is the baseline or healthy state of the test rig. At this point, the assumption is that no fault is present in the machine. However, since the test rigs are not aligned perfectly due to multiple shafts and multiple bearing pedestals, some misalignment and unbalance may appear during their operation. This trend can be seen from the spectrum plots having 1x component operational speed and multiple harmonics. Three different speeds for all machine configurations in the baseline RMRU were operated, and vibration data was collected.

4.5.2 Unbalance

Unbalance occurs when there is an unequal distribution of mass in the shaft. Unbalance is one of the common rotor faults encountered by rotating machines. This study introduced the unbalance faults by creating 1.5 x 10-3 kgm unbalance using a 2.0g M5 x 25 mm screw, which is 55 mm in radius at D1. Having seeded, the unbalance fault measurement of vibration data was carried out.

4.5.3 Misalignment

Misalignment fault was simulated in this study by the displacement of the bearing (Bg1) pedestal using two 0.8mm shims from its original position in the vertical direction. The shim is placed between the bearing pedestal and the lathe bed. This arrangement causes a parallel misalignment along coupler 1 between the long shaft and the motor. Once the misalignment fault was seeded, recorded vibration signals were obtained.

4.5.4 Shaft bow

Shaft bow fault was introduced in this study by replacing the 1000 mm shaft with a long-bowed shaft which has a 3.2 mm displacement from the rotational axis (run out). Like in earlier studies [28,29], the shaft fault is intended to create a framework resembling a deflected rotor. Unbalance will be created in the rig, and there may be an increase or no increase in the vibration from the rotor. The collection of the vibration signal was done immediately after the shaft bow fault was set up.

4.5.5 Crack shaft

The crack shaft is simulated in this study at two locations, i.e., crack near bearing one (CBg1) and crack near bearing two (CBg2). The simulation was done on the long shaft with a 0.34 mm wide and 4 mm deep notch and a 0.33mm shim glued, thus creating a breathing crack with a width of 0.01 mm. An electro-discharge machining (EDM) device was used to cut the notch. CBg1 was created at 165 mm from bearing 1 (Bg1) and 655 mm from bearing 2 (Bg2). While CBg2 was created at 655 mm from bearing 1(Bg1) and 165 mm from bearing 2 (Bg2). Vibration data was collected after each configuration was set.

4.5.6 Shaft rub

Shaft rub fault was simulated using a gadget which houses a Perspex disc. The effect of the rub is felt when the upper part of the Perspex material rubs on the shaft creating a minor interference between the shaft and Perspex disc due to unbalance. This interference is achieved by setting a 0.1 mm gap between the Perspex disc and the shaft. The rub shaft on FFTR was simulated near bearing 2. Two rub shaft faults were simulated in SFTR, i.e., rub near disc one (RubD1) and rub near disc two (RubD2). RubD1 is 77 mm from D1, 119 mm from Bg1, 365 mm from D2, and 556 mm from Bg2. RubD2 is simulated at 77 mm from D2, 265 mm from Bg2, 365 mm from D1, and 556 mm from Bg2. Once each configuration was set up, vibration data were obtained at different speeds.

4.5.7 Mechanical looseness

Mechanical looseness fault was simulated in FFTR for this study. Nuts connecting the flange at the bearing pedestal were loosened. The nuts moved along the flange, and the bearing movement was about the axis of the shaft. However, the bearing pedestal was secured firmly to the lathe bed. Once this was set, vibration signals were collected when the machine operated at different speeds.

4.5.8 Bearing cage defect

A bearing cage defect was carried out on one anti-friction rolling element bearing. Initially, the intention was to seed a ball fault in the bearing using a Dremel grinder. However, due to the ball material's hardness and the greasing's slippery nature, the intended scratches from the Dremel affected the bearing cage. So, from analysis, a

cage defect was diagnosed. Once the defect was established, the same bearing was used but interchanged in all four locations, while three other bearings were healthy. For emphasis, while the defective bearing was at bearing pedestal 1 (Bg1), Bg2 to Bg4 were healthy. Also, while the defective bearing was at the Bg3 pedestal, Bg1, Bg2, and Bg4 were healthy. Vibration data at different speeds were collected during each configuration. It was challenging to simulate other bearing faults, such as inner race and outer race defects, as any effort in this line will destroy the bearing total due to its type. The grease on the balls made it extremely difficult to scratch any defect. So, measurement of the exact size of the bearing defect was not done but could be pursued in future work.

Table 4. 8 Showing description of fault in relative flexible foundation.

No	Condition	Code	Description
1	Baseline	RMRU	Residual Misalignment Residual Unbalance.
2	Unbalance	Unb	2.0 g of M5 screw to create 1.5 x 10^{-3} kgm unbalance at 30^0.
3	Misalignment	M	Parallel Misalignment with Bg1 displaced 0.8mm in vertical direction.
4	Shaft bow	S-Bow	3.2 mm displacement of the long shaft from the axis of rotational
5	Crack near Bearing1	CBg1	0.34mm wide x 4mm deep notch with 0.33mm shim glued (on rotor near Bg1).
	Crack near Bearing2	CBg2	0.34mm wide x 4mm deep notch with 0.33mm shim glued (on rotor near Bg2).
6	Rub near Disc1	RubD1	Perspex blade on rotor near Disc1.
6	Rub near Disc2	RubD2	Perspex blade on rotor near Disc2.
7	Mechanical looseness	M-Loose Bg3	Unfastening of the four nuts that secures that secures bearing 3 to the pedestal.
8	Bearing cage defect (Bg1-4)	Bg1Cg - Bg4Cg	Bearing cage defect at bearing 1-4, scratched using a Dremel grinder.

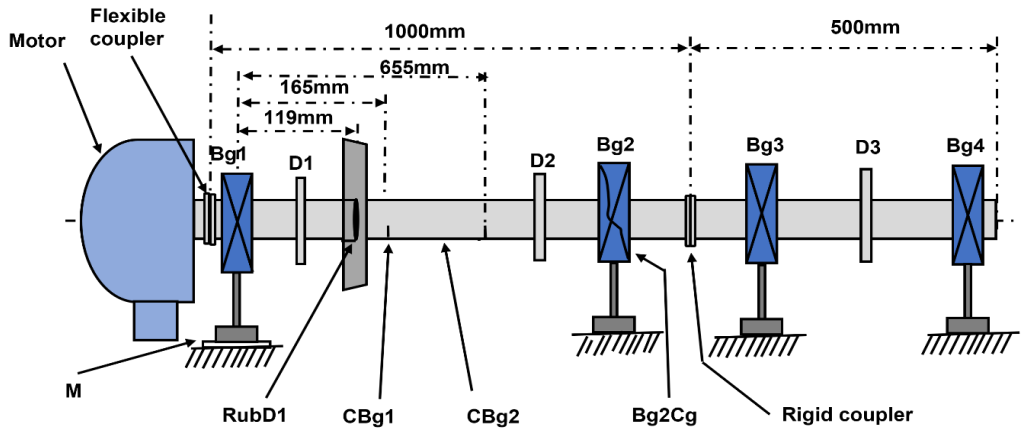

Figure 4. 26 Schematics of experimental test rig showing some of the simulated faults and their locations.

4.6 Data acquisition and processing

The test rig is controlled by the speed controller, which is operated from the personal computer and speed. The speed can be varied by manually inputting the intended speed into the speed controller. Vibration dynamic responses were measured and received by the signal conditioner from the accelerometer placed on the bearing.

The data acquisition system helps to convert the data from analogue to digital. The signal conditioner helps to amplify the filtering of the signal received from the accelerometer. It also supplies power to the accelerometer. Amplified signals in the conditioner are transferred to the data acquisition system (DAQ). This DAQ contains 16 bits, 16 channels with 16 outputs data-card. Analogue data collected and amplified are converted to digital in this system. The accelerometer is pk-pk which is 2 to -2 at point [0-3], as seen in the channels of the data acquisition system.

The digital signal is stored in data logging software on a personal computer. Figure 4.27 shows the set-up of the signal conditioner, DAQ and personal computer, while Figure 4.28 show a schematic of the data acquisition process. It should be noted that the data acquisition for both the FFTR and SFTR in this research employed the same approach.

Figure 4. 27 Data acquisition, personal computer, and other processing equipment.

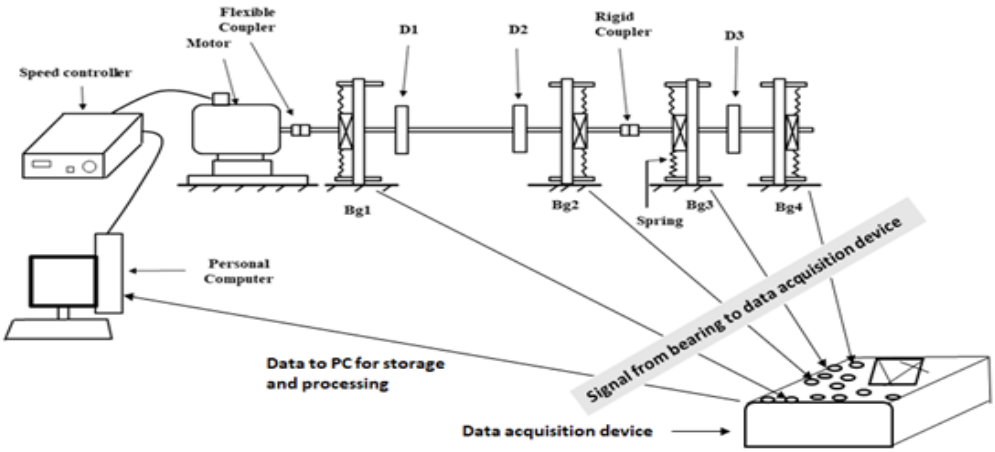

Figure 4. 28 Schematics of data acquisition from the test rig to personal computer.

4.7 Summary of experimental approach model

An extensive description of the three different test rigs used in this research study has been presented in this chapter, i.e., the flanged-based flexible test rig (FFTR) and the spring-based flexible test rig 1 and 2 (SFTR-1&2). The FFTR was built by two former PhD students (Dr Akilu Yunusa-Kaltungo and Dr Adrian Nembhard) in the dynamic lab of the University of Manchester. These PhD students built the FFTR with a flange-based bearing pedestal to accommodate the excitation speeds below the machine's first critical speed. The set-up was due to the foundation flexibility of the rig based on the natural frequency. The improved SFTR has a spring-based bearing pedestal and represents a typical industrial system in which the excitation speeds are below and

above its first critical speeds. Another area of interest is the modal testing for each test rig to determine their natural frequencies, and the mode shape for selected natural frequencies is discussed. Modal testing for FFTR is obtained from earlier studies of the PhD students. However, SFTR-1 and SFTR-2 are represented and discussed as original versions of this study. The modal test and mode shape help to understand the rotating machine's dynamics and to investigate the dynamic behaviour of the various faults simulated in the test rig. The simulated faults were also discussed in detail. After that, data acquisition, storage and signal processing approach were presented. With a clear presentation of the experimental approach, this study considered investigations and results in subsequent chapters.

CHAPTER 5

IMPROVED FAULT IDENTIFICATION APPROACH USING ACCELERATION-BASED TIME AND VELOCITY-BASED FREQUENCY DOMAIN FEATURES FOR ROTOR FAULTS DIAGNOSIS

Acceleration and velocity signals have provided useful diagnosis in rotating machine critical part. Rotor faults exist around the low frequency range (0 – 500 Hz) while bearing defect can be detected around the high frequency range (over 1000 Hz). Rotor fault can be effectively identified using velocity-based analysis while bearing fault identification is well achieved with acceleration-based analysis. The aim of the chapter is to understand rotor-related fault behaviour using acceleration and velocity features and thus using a combination of acceleration-based time and velocity-based frequency domain to create a fault identification model for classification of an extensive range of rotating machine faults. Principal component analysis (PCA) pattern recognition-based approach was useful in classifying machine conditions on the flange-based flexible test rig (FFTR). To quantify the observed fault classification, a mean representation of each condition was done and the observation of each fault with respect to the baseline RMRU condition were carried out.

5.1 Overview

This chapter presents the use of features of acceleration and velocity from vibration signals for improved fault diagnosis. Preliminary studies employed vibration data from the existing flanged-based flexible test rig (FFTR) that a former PhD student measured during his research. The improved approach is developed from an earlier study which proposed the unified multi-speed analysis (UMA) from the work of Nembhard and Sinha [20].

For clarity, a discussion of the earlier unified multi-speed approach is in section 5.2. After that, section 5.3 in the current study investigates time domain parameter analysis. Furthermore, observation of spectrum plots and data trending, all of which are from acceleration-based vibration signals. The time and frequency domain features from the acceleration signal were selected, and the classification of each condition was observed. The same analysis was repeated for the velocity-based vibration signal, obtained by conversion of acceleration signals, and the result was discussed. The improved acceleration and velocity features approach was observed and discussed. In order to show the novelty, a statistical approach used to distinguish each faulty condition from the baseline **RMRU** help quantifies the faulty condition.

The various simulated conditions are shown in chapter 4, Figure 4.24 and a brief description of the selected faults obtained from FFTR is seen in Table 5.1.

Table 5. 1 Description of fault obtained in FFTR data.

No	*Condition*	*Description*
1	*RMRU*	*Residual Misalignment Residual Unbalance.*
3	*Misalignment*	*Parallel Misalignment with Bg1 displaced 0.8 mm in vertical direction.*
5	*Shaft bow*	*3.2 mm bow on the 1000 mm shaft*
6	*Mechanical looseness*	*Loosening of the bolts on the flange in bearing pedestal three (Bg3).*
7	*Shaft rub*	*Perspex blade on rotor near Disc2.*

5.2 Earlier Unified Multi-Speed Approach

The unified multi-speed analysis (UMA) tool was developed to address challenges posed by machines with continuous changes in speed and dynamics in overall machine behaviour [20]. This tool presents a single analysis of features obtained from a machine at different speeds, all below the machine's first critical speed using acceleration signal only. Feature selection employed both time and frequency parameters from the acceleration signal. Complete detail of the selected features is in [20].

The selection aimed to produce diagnostic features representing a complex machine that can provide a simplified and robust tool. Principal component analysis was used to classify the conditions. Observation showed four separate analyses, i.e., "single speed and single bearing, an integrated feature from multiple speed at a single Bearing, single speed for integrated feature from multiple Bearing and the unified multi-speed analysis" [20]. The unified multi-speed analysis showed clear identification and separation of all conditions tested. In order to gain a clearer understanding of this work, more details can be accessed in [20].

5.3 Preliminary investigation for current study

This study used existing vibration data from a flanged-based flexible test rig (FFTR) for preliminary analysis. Data was trended on the acceleration-based vibration signals based on time and frequency domain parameters. The data trend showed how various parameters could contribute to indicating the presence of different faults in a signal. This work and previous studies [16, 19] carried out similar data trending, which showed that individual parameters provide a sensitive indication of a particular fault based on benchmarks and standards but may not give an exact indication of faults, as different faults could show similar indications. Also, the indications may not be consistent in various parameters. For instance, the kurtosis's indication of a bearing defect may not be observed in the **RMS**. Therefore, the data trending helps show how different parameters show sensitivity in the machine dynamics. Section 5.4.1 and 5.4.3 gives details of the analysis showing the data trending. Thus, this study proposed a

data fusion approach using various sensitive features from analysing vibration signals' time and frequency domain parameters.

Three speeds were considered for analysis, i.e., 1200 rpm (20 Hz), 1800 rpm (30 Hz) and 2400 rpm (40 Hz), all of which were obtained below the machine's first critical speed. Single and multi-speed analysis using acceleration features is carried out to validate the existing unified multi-speed approach (UMA) [20]. After that, further analysis using velocity features was presented to observe existing UMA. In order to improve the approach, a combination of acceleration and velocity features for single and multiple speeds was done. This improved approach was investigated to develop a diagnostic tool that can cover various faults associated with rotating machines' critical parts.

5.4 Acceleration Signal for fault Diagnosis

This section employs the measured acceleration signal for fault diagnosis and test rig condition classification to understand the machine's health. Time domain and frequency domain analyses were carried out. The measured data were obtained from an earlier research study from the flanged-based flexible test rig (FFTR) at a 10 kHz sampling rate with 11 samples (observations) collected at three different speeds, i.e., 1200 rpm (20 Hz), 1800 rpm (30 Hz) and 2400 rpm (40 Hz) below the machines' first critical speed as stated in section 5.3.

Time and frequency domain parameters presented useful features for further analysis. However, for detailed investigation, only figures from the 1200 rpm (20 Hz) speed are presented in both time and frequency domain analysis. This consideration was because representation at other bearings may not vary so much from what was observed from the 1200 rpm (20 Hz) analysis. Feature selection and data trending provided an understanding of the need for further signal analysis. Features extracted from the time domain include **RMS, CF, and Ku**, while that from the frequency domain had **SE** and harmonics of **1x, 2x, 3x, 4x,** and **5x**. The selected feature has various significance in machine fault diagnosis. For instance, **RMS** and **SE** reveal the energy state of the entire machine condition, while harmonics, **CF** and **Ku** indicate the signals' impulsiveness and transient nature. More details on the selected signal can be

accessed in [20]. Clustering analysis was achieved using a principal component analysis (PCA) based pattern recognition approach. Results, observations, and discussions are also presented.

5.4.1 Data trending using acceleration-based time domain parameter analysis

In order to achieve an efficient trend analysis, the bar chart plot considered the time domain parameter for RMRU and faulty conditions, which includes misalignment, shaft bow, mechanical looseness, and shaft rub. Figure 5.1 (a) – (c) shows the bar chart comparing the RMRU to the simulated faulty condition for all bearings at 20Hz. The comparison is to check for variation and consistency in different conditions to observe any helpful information.

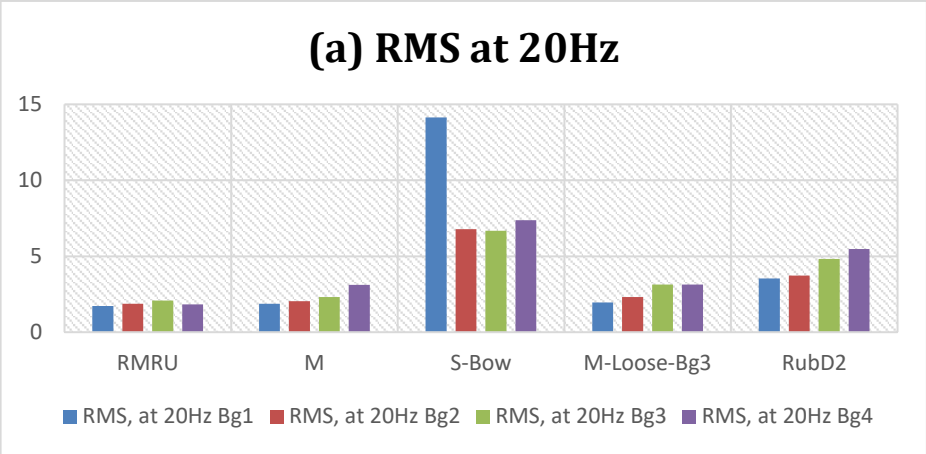

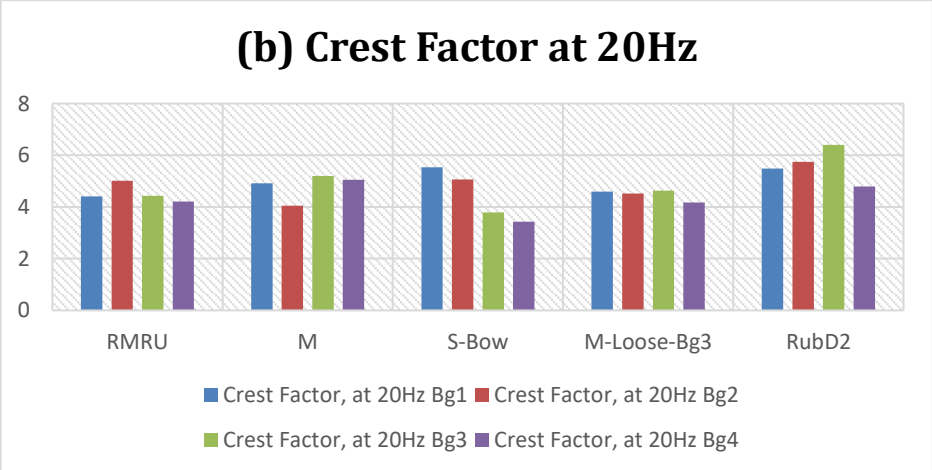

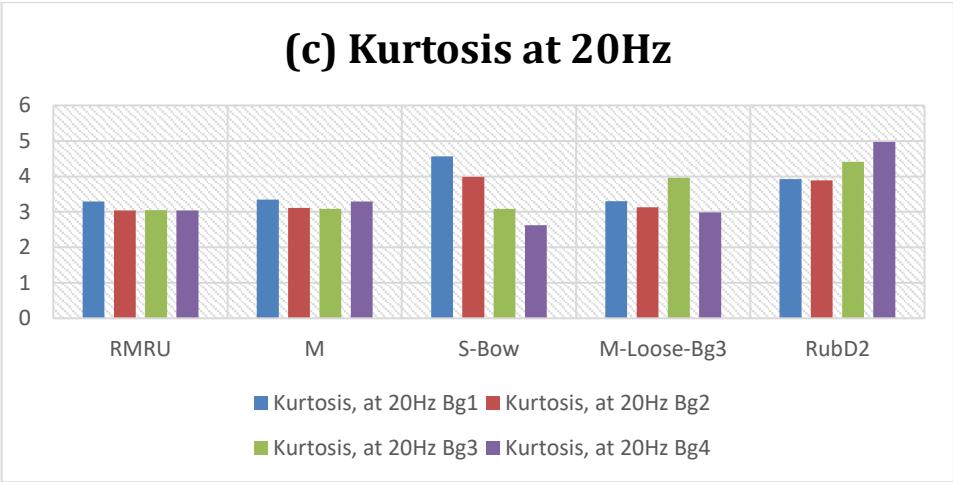

Figure 5. 1 Bar chart showing comparison of all faults with respect to healthy at all Bearings with machine speed 20Hz for (a) Root mean square (b) Crest Factor (c) Kurtosis.

Figure 5.1 shows the bar chart representation for all conditions for the four bearings at 20Hz. Observation shows that RMRU conditions tend to be reasonably low overall; however, the higher amplitude of shaft bow and shaft rub indicate their presence, as seen in Figure 5.1 (a) – (c). In figure 5.1 (c), the amplitude at bearing 3 is reasonably high, indicating the presence of mechanical looseness.

The time domain parameter analysis using RMS, CF and Ku has been attempted to detect the rotor-related fault in a rotating machine. The result showed the presence of some of these faults. RMS was able to detect shaft bow and rub. CF and Ku, which gives transient responses, could not clearly distinguish the RMRU from faulty. This observation leads to the conclusion that though time domain analysis retains useful analysis features, however, it cannot effectively detect all faults easily. Therefore, the frequency domain technique is employed for further investigation.

5.4.2 Observation of spectrum plot of measured acceleration signal

In this section, the frequency domain analysis is employed for more analysis as the time domain analysis could not effectively identify all conditions. Here, the Fast Fourier Transform (FFT) has been applied to convert signals from the time to frequency domain. A 16-bit data acquisition card was used to obtain signals, and the FFT could convert signals from a time domain to a frequency domain. The spectrum plot represents the conversion by FFT in the frequency domain and is used for analysis. The

representation shows that the data obtained is fine. Details of basic signal processing parameters are presented below.

The data were obtained at a sampling frequency (fs) of 10000 Hz or 10 kHz. Frequency resolution df = fs/N =10,000/2 16 = 0.15258 Hz, where N is the number of spectral lines, which is 16384 used to compute the Fourier transform. Sampling time = 1/fs = 1/10,000 = 0.0001 s. An average of 147. Filtering = high pass at 2 Hz and low pass at 1 kHz, and the reason for selecting this filter is to remove frequency content such as direct current (d.c.) components and low-frequency noise at the high pass and frequencies that a related to high-frequency range such as bearing are cut off at the low pass. Note that the Nyquist frequency is 5 kHz.

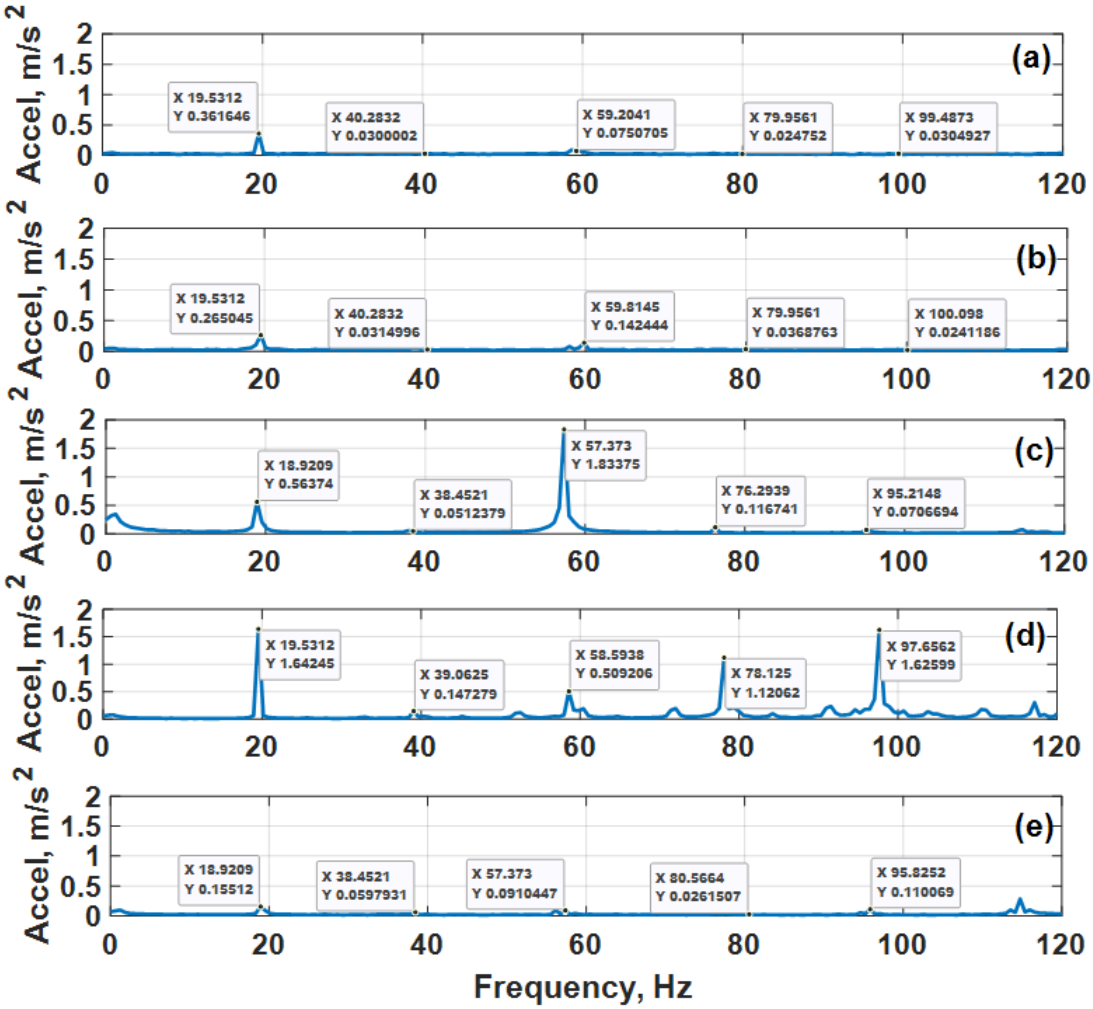

Figure 5. 2 Typical acceleration spectrum plots at 20Hz Bg3 for (a) RMRU (b) M (c) S-Bow (d) M-looseBg3 (e) RubD2.

In figure 5.2 (a), the baseline case appeared to show some residual misalignment due to the presence of other harmonics components. Introducing other simulated faults led to an increase in shaft unbalance, which can be seen from the increase in 1x in most cases. In the RMRU and misalignment cases, 1x and 3x were prevalent but with a very low 2x. The shaft bow in figure 5.2 (c) showed the presence of 1x to 5x harmonic components. However, there is a dominant peak at 3x with a frequency of 60 Hz. The peak could either be from a bow in the shaft or mode 3, indicated in the FRF plot with a natural frequency of 59.2 Hz. In figure 5.2 (d), mechanical looseness showed an increased 1x, 3x, 4x, and 5x with some sub-harmonics, which may be due to vibrations due to the loosed nuts in the flanged connection at bearing 3. Figure 5.2 (e) is a typical shaft rub spectrum with the presence of all harmonics at a low amplitude.

Observation of figure 5.2 (a) – (e) shows the presence of all harmonics in all four bearings. 1x harmonic seems to be prevalent at all bearings. However, the peaks of 2x, 3x, 4x, and 5x, which were also observed, were not consistent in their trend for the different bearings. The presence of an increased 3x harmonic in all cases may be due to the second mode at 59.2 Hz. Observations show a 1x amplitude of misalignment lower than that of RMRU, and this could be because of the complexity of fault simulation.

According to Nembhard and Sinha [20], fault diagnosis using the amplitude of a spectrum from steady-state vibration data is somewhat challenging. It was observed that different faults showed the same harmonic components. Also, the spectral features for the same faults at the same speed may differ at the exact bearing locations. It was also observed that some spectra plots could generate features like a baseline case even with the physical presence of a fault, thus, making fault identification difficult, as shown in Figure 5.1 (a) and (b). In order to validate some of these observations, data trending of the various spectra at 1200 rpm (20 Hz) speed for the first five harmonic components (1x – 5x) and the spectrum energy is presented in sub section 5.4.3 below.

5.4.3 Data trending using acceleration-based frequency domain features

Figure 5.3 (a) – (d) shows the data trending plot from analysis for RMRU and faulty conditions. It shows the relative changes between all conditions at various harmonics. This change is good for the precise detection of fault when compared to healthy. Figure 5.3 (a) – (d), representing 20 Hz, had Bg1 indicate shaft bow condition at 1x, 3x and SE. Bg2 showed the shaft bow at 1x, 3x and SE with mechanical looseness and rubbed at 4x. At Bg3, mechanical looseness was observed at 1x, 3x, 4x, and 5x with the shaft bow at SE. Bg4 showed the presence of bow at 1x, 3x, and SE with mechanical looseness at 2x, 4x and 5x. In as much as some faults were prevalent, the machine's overall condition could not be distinguished, making diagnosis cumbersome. Further work will need to show clarity of overall machine condition, feature selection and classification considered as proposed by Nembhard and Sinha [20].

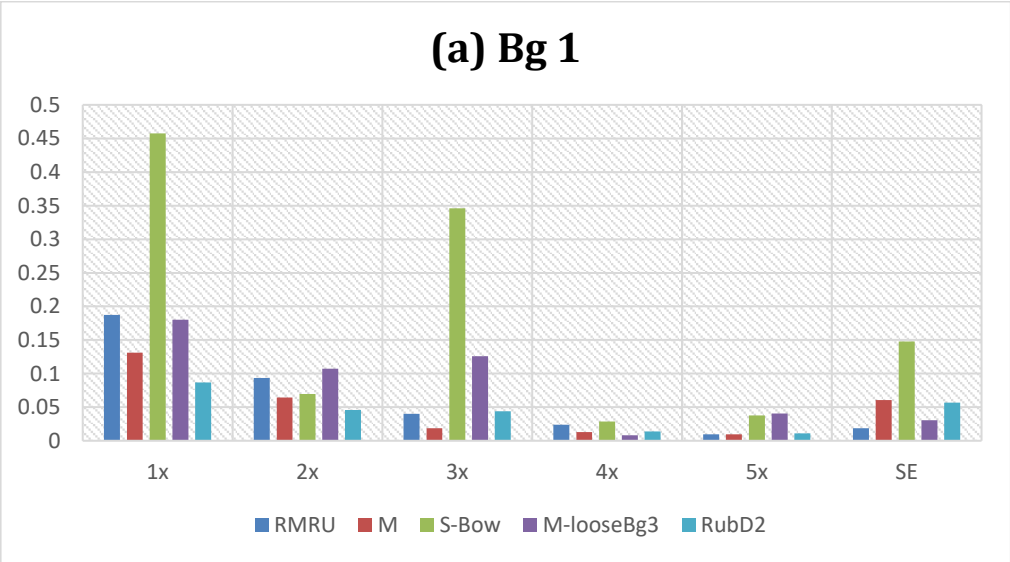

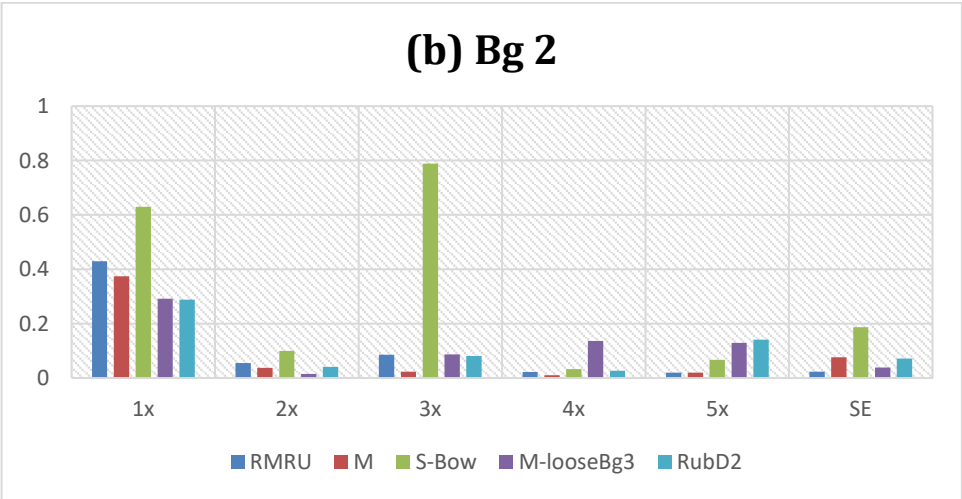

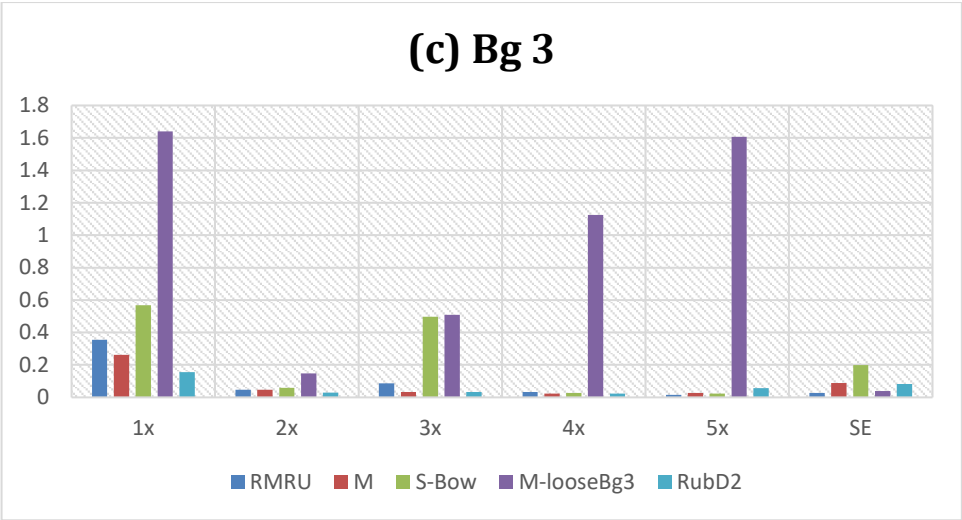

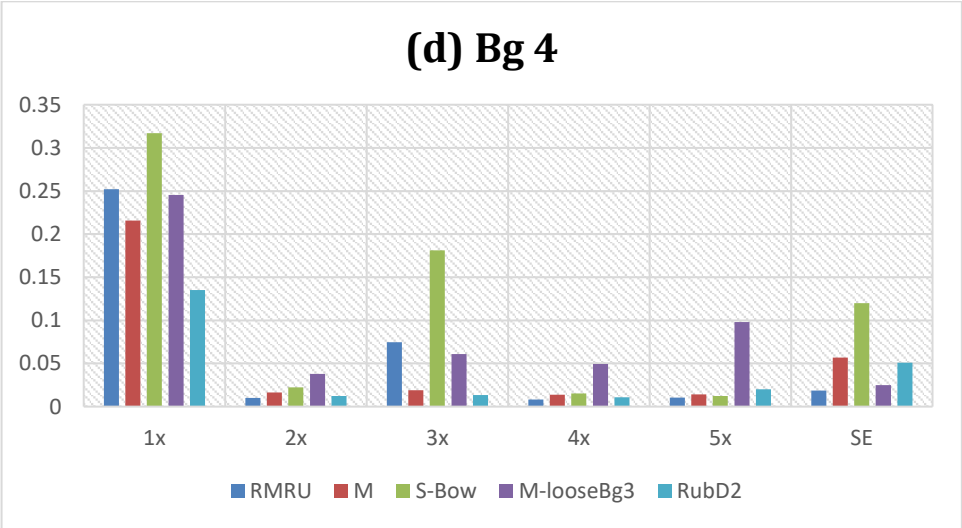

Figure 5. 3 Data trending for simulated conditions with 20 Hz at (a) Bg1 (b) Bg2 (c) Bg3 (d) Bg4.

5.4.4 Acceleration data model

Following the observation from data trending with time and frequency domain features, where conclusive diagnosis could not be achieved, further investigation was carried out using clustering analysis. The selected features are used to build a data matrix that is eventually fed into PCA for condition identification and classification. The Data matrix, analysis, observation, and result are discussed.

The matrix is built up in a structure such that the 1200 rpm (20Hz) feature from the RMRU condition at Bg1 gives a 9 x 11 matrix. Still computing the RMRU condition, a matrix of 36 x 11 is built with the combination of Bg1 to Bg4. After that, a 36 x 55 data

matrix is computed, comprising all five simulated conditions. This computation is repeated for 1800 rpm (30Hz) and 1800 rpm (40Hz) signals. Features from multiple speeds are combined and give a 108 x 55 data matrix inputted to PCA for classification. However, before the data matrix is inputted into the PCA-based classification tool, normalisation is done by computing each row's standard deviation and mean. The mean is subtracted from each element within a row and divided by the row's standard deviation. The normalisation is done to make all elements in the matrix dimensionless quantities [20].

5.4.5 Condition classification using Acceleration features

Analysis of machine condition using acceleration features extracted from time and frequency domain parameters of the measured vibration data is presented in Figure 5.4 (a) – (d)**.** This scenario represents both single and multi-speed analysis using acceleration features. Figure 5.4 (a) – (c) are all single-speed analyses, while Figure 5.4 (d) is a multi-speed analysis. Observation showed some overlap between the baseline RMRU, misalignment and mechanical looseness in Figure 4.5 (a). Figure 4.5 (b) and (c) showed separation for all conditions except for minimal overlap between RMRU and misalignment. The overlap suggests a faulty condition, possibly because of residual misalignment in the measured vibration data. Figure 5.4 (d), the multi-speed analysis, presents a good separation between all conditions. This representation gives a similar result to the earlier unified multi-speed diagnosis except for the variation in some faulty conditions.

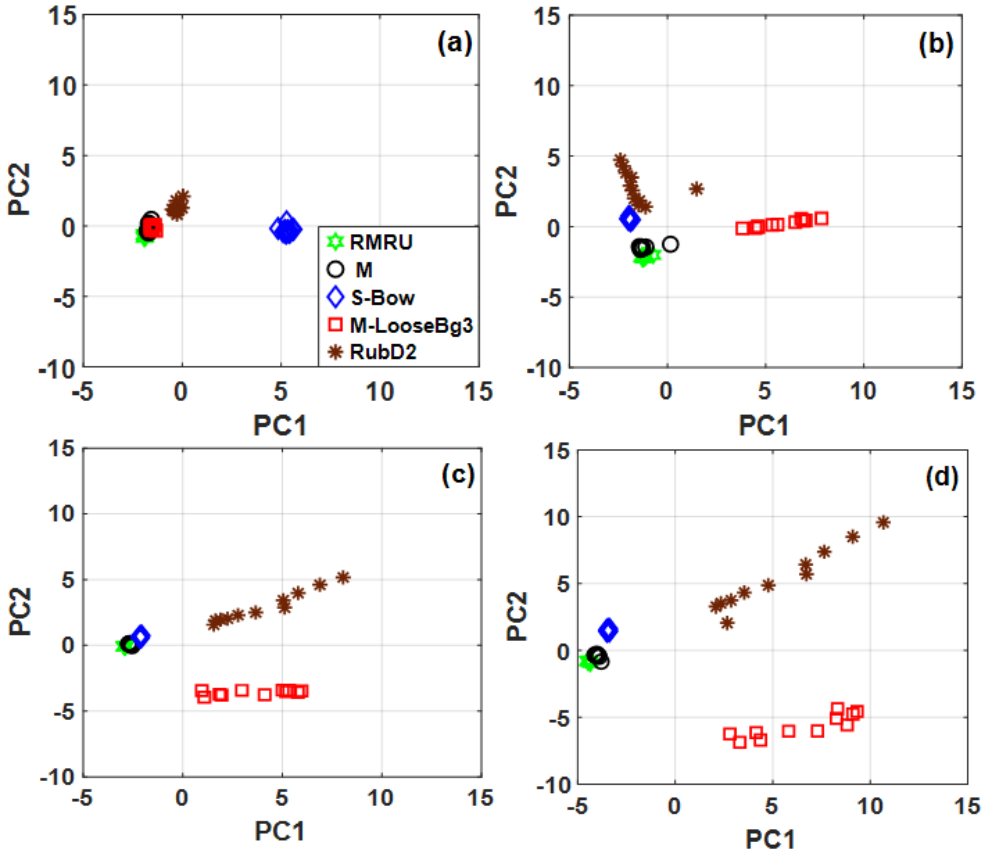

Figure 5. 4 Acceleration feature analysis at (a) 20Hz (b) 30Hz (c) 40Hz (d) multiple speed.

5.4.6 Observation and discussion

The time and frequency domain analysis gave beneficial results in its investigation. It detected some faults; however, obtaining helpful analysis during data trending was challenging as observation did not show consistency between the faulty and baseline RMRU condition. In applying the previously existing work [20] method, various plots were generated for all individual speeds and multi-speed. Observation showed a significant overlap between RMRU and some faulty conditions at 20Hz. This improved with increased speed as only little overlap between RMRU and misalignment was observed. Observation from the multi-speed plot showed distinct separation for all conditions. However, there seem to be dispersed clustering in some faulty condition, i.e., shaft rub and mechanical looseness, especially at 40Hz and multi-speed plots. This data spread was adjudged because the severity of these two cases could have progressed between the instances of acquiring different data sets. As stated earlier, some faults in this work vary significantly from those of earlier studies.

5.5 Velocity signal for rotor fault diagnosis

In section 5.4, a beneficial result was achieved in identifying faulty and baseline RMRU conditions when the unified multi-speed analysis tool was employed. However, further research to enhance the application of this tool for practical analysis is looked at in the section. Acceleration features were employed for analysis yielding valid results in previous work [20]. However, the improved tool focuses on employing velocity features for further analysis. The improved tool came from observation in [193] and [208], where the velocity gives a good representation of most parameters. In order to obtain velocity signals, measured vibration acceleration data obtained at 10 kHz with 11 samples (observations) used in the previous section are integrated [45].

This section briefly looks at time and frequency domain analysis, where similar features selected for acceleration analysis are then extracted for velocity analysis. Observation and discussion of analysis are expressed in the subsequent sub-sections. Note that data trending for velocity features is not presented in this study as observation shows similar trends with those of acceleration.

5.5.1 Time and frequency domain parameter analysis for velocity

Observation from the time and spectrum plot of velocity data is seen to have a similar trend with those of acceleration. Much discussion on its comparison, as well as data trending, is not presented in this section. The acceleration data is represented in m/s2, while that of velocity is in mm/s. Figure 5.5 (a) – (e) shows velocity spectrum plots for both baseline RMRU and faulty conditions as simulated in the flanged-based flexible test rig (FFTR). The presence of 1x up to 5x can be seen in the velocity spectra plot. However, velocity spectra amplitudes are much higher than acceleration spectra for all conditions due to the representation in mm/s.

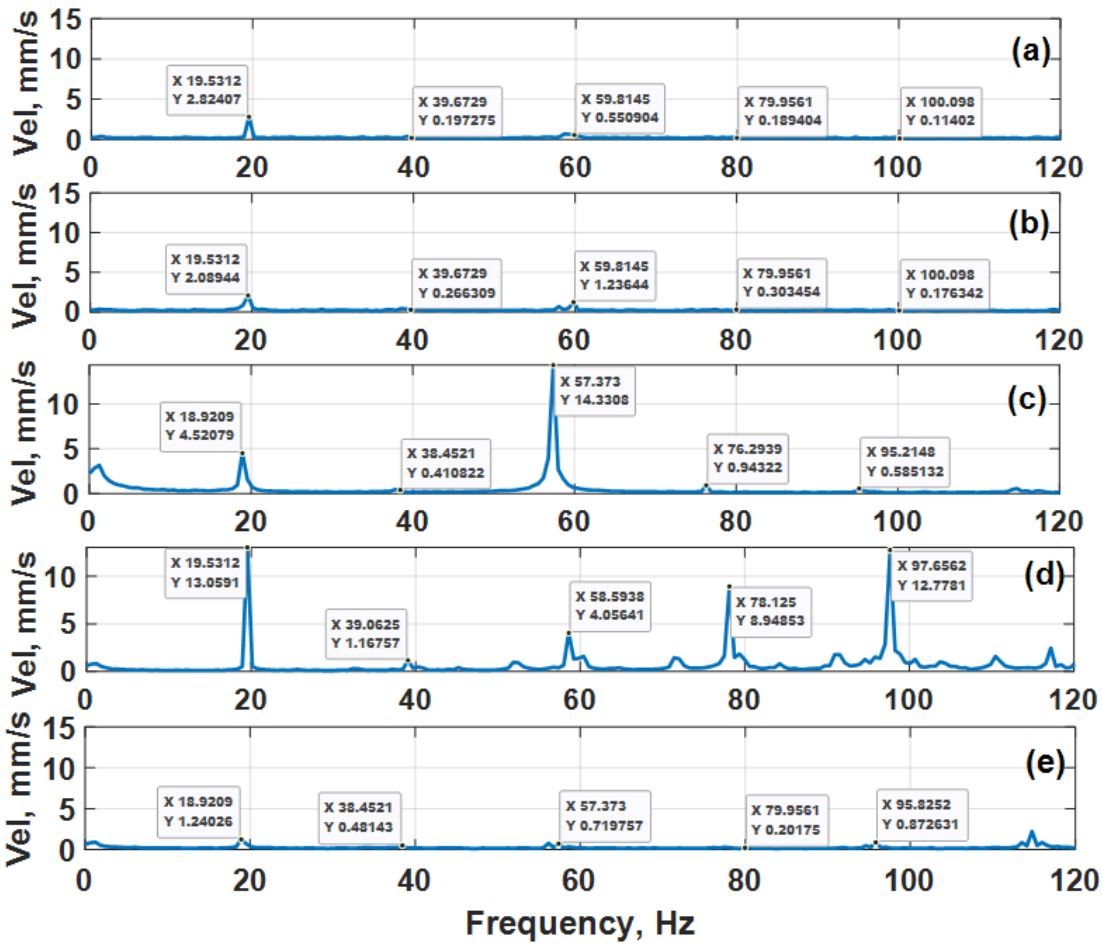

Figure 5. 5 Typical velocity spectrum plot at 20Hz Bg3 for (a) RMRU (b) M (c) S-Bow (d) M-looseBg3 (e) RubD2.

5.5.2 Velocity features arrangement

Velocity features are good indicators of rotor faults, mainly RMS and CF features expressed in [193] and [11]. Features obtained are the same as that from acceleration analysis, including RMS and CF for the time domain, while the harmonics of 1x, 2x, 3x, 4x, 5x, and SE were extracted from the frequency domain. A similar data matrix was built using the velocity features such that for 1200 rpm (20Hz), features from the RMRU condition at Bg1 produces a matrix of 9 x 11. Further computation includes Bg1 to Bg4, which presents a 36 x 11 matrix. Adding all five conditions gives a 108 x 55 data matrix set up for input into PCA for machine conditions identification. Normalisation which makes all elements in the matrix dimensionless quantities, is carried out.

5.5.3 Condition classification using velocity features

Investigation into velocity features where time and frequency parameters are selected from the analysed vibration data with velocity signal is shown in figure 5.6 (a) – (d). This analysis is based on improving the existing diagnosis tool in the earlier section. Figure 5.6 (a) – (c) represents single-speed analysis, while Figure 5.6 (d) shows the analysis for multi-speed. Figure 5.6 (a) showed an overlap between baseline RMRU, misalignment and mechanical looseness. Figure 5.6 (b) and (c) showed separation for all conditions except for the little overlap between RMRU and misalignment conditions. However, the multi-speed analysis in Figure 5.6 (d) showed separation for all conditions. Mere observation of the PCA plots showed a more distinct separation of conditions in velocity analysis, as seen in Figure 5.6 (d), even when compared with acceleration classification in figure 5.4 (d).

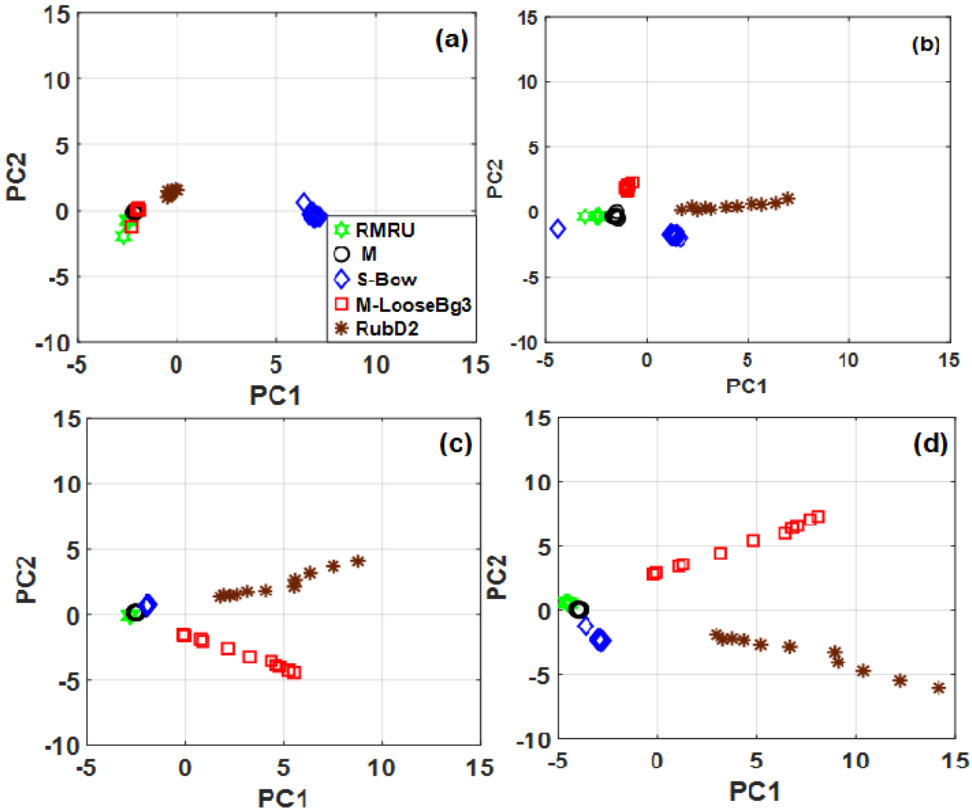

Figure 5. 6 Velocity feature analysis at (a) 20Hz (b) 30Hz (c) 40Hz (d) multiple speed.

5.5.4 Observation and discussion

Measured vibration signals in time waveform and spectrum plot were presented, and observation showed close similarity with that of acceleration plots except for higher amplitude, about three times that of acceleration. The plots cannot be compared directly, as the amplitudes of acceleration were in m/s2 while those of velocity were in mm/s. The single and multi-speed analysis using velocity features gave valuable results. The 20Hz speed analysis showed a significant overlap between RMRU and some faulty conditions. The 30Hz and 40Hz speed analysis showed separation for most conditions except for the little overlap between RMRU and misalignment conditions. The multi-speed analysis showed much separation for all conditions without any overlap. Even in comparison to acceleration classification, the velocity classification appeared to have a more apparent separation of each condition. It should be noted that mechanical looseness and shaft rub exhibited some dispersed clustering, especially in the 40Hz and multi-speed plots.

5.6 Improved approach using acceleration and velocity features for rotor faults diagnosis

Acceleration parameters are valid for diagnoses of bearing faults, while velocity parameter has helped diagnose rotor faults [53]. With these findings from the literature [28-29,46,219-220], the combination of different acceleration and velocity features is proposed in this work to develop a robust fault diagnosis tool that can effectively and efficiently classify machine health conditions for a broader range of rotating machine faults. This section selected features from time domain acceleration features (RMS, CF, KU) and frequency domain velocity features (1x – 5x and SE). These were used to build the data matrix of 108 x 55 for input into PCA. Normalisation is carried out to make all elements in the data matrix dimensionless quantities.

5.6.1 Classification of machine condition using combine acceleration and velocity features

Figure 5.7 (a) – (d) presents the combined acceleration and velocity features analysis for single and multi-speed. This analysis further pursues to achieve an improved and robust diagnostic tool for a broader range of machine conditions. In Figure 5.7 (a), a significant overlap was observed between RMRU and some faulty conditions, such as

misalignment and mechanical looseness. Figure 5.7 (b) and (c) presented separation in all conditions with a slight overlap between RMRU and misalignment. The multi-speed analysis in Figure 5.7 (d) gave much separation of all conditions, indicating a better diagnosis and identification of machine conditions when compared to the single speed and the individual acceleration and velocity multiple speed analysis.

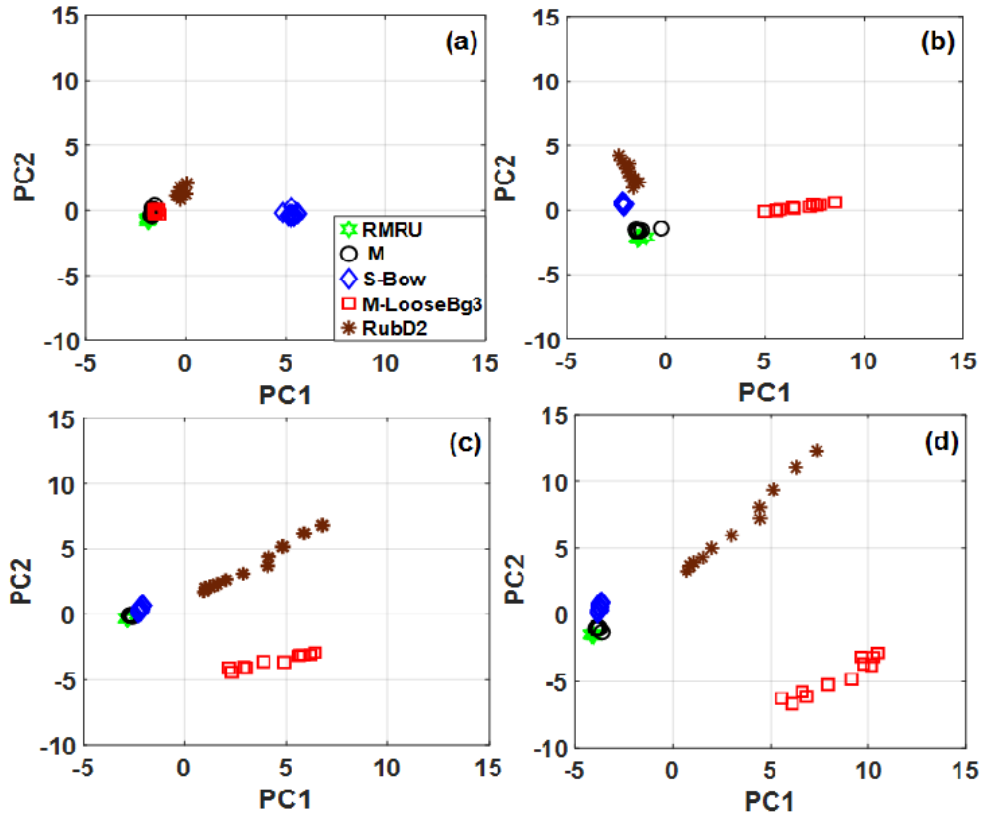

Figure 5. 7 Combine acceleration and velocity feature analysis at (a) 20Hz (b) 30Hz (c) 40Hz (d) multiple speed.

5.6.2 Observation and discussion

Investigation into improving the existing techniques has shown reasonable advancement in this work. Observation showed that all conditions were classified in the analysis, and the various faults were identified. Some scenarios, like 20Hz analysis, showed much overlap between RMRU and faulty conditions, such as misalignment and mechanical looseness. However, as the speed increases, results were observed to show classifications with much separation for individual conditions. Also, some conditions had dispersed clustering, especially at 40Hz and multi-speed analysis plots,

i.e., mechanical looseness and shaft rub conditions, which may indicate the machine state when collecting data. The multi-speed analysis for the combined acceleration and velocity classification indicated clear separation for all conditions; compared to those of acceleration and velocity, the separation was even much more, indicating better diagnosis and individual fault identification. Overall, an impressive result is shown in the multi-speed analysis for combined acceleration and velocity features analysis, which indicates an overall improved analytical tool for machine health condition identification. Note that this presumption where the combined acceleration and velocity features for multi-speed analysis provide an improved diagnosis is based on observation from the PCA plots. A quantitative approach to determine the efficiency of the improved method is considered in section 5.7.

5.7 Distinguishing faulty conditions from baseline RMRU for data quantification of machine conditions

In order to determine the efficiency and robustness of the improved acceleration and velocity features for fault diagnosis, a quantitative comparison for acceleration, velocity and combined acceleration and velocity feature classification is presented. The quantitative comparison is achieved by getting the mean of individual conditions and distinguishing each faulty condition from the baseline RMRU condition. A more explicit description and theory have been presented in chapter 4, section 4.13. A comprehensive presentation showing all conditions and the various scenarios is presented in Figure 5.8. Four scenarios are represented, i.e., 20Hz, 30Hz, 40Hz and multi-speed analysis, with each having all conditions for the acceleration, velocity and the combined acceleration and velocity features analysis.

In Figure 5.8 at 20 Hz, Misalignment and rub at Disc 2 showed increased separation in velocity analysis compared to acceleration. However, it decreased in the combined acceleration and velocity feature analysis. The shaft bow and mechanical looseness at Bg3 increased separation as it progressed from acceleration to velocity and the combined acceleration and velocity features analysis. Figure 5.8 at 30 Hz showed increased separation for misalignment and RubD2 as it went from acceleration to velocity to combined analysis. S-Bow increased separation in velocity but decreased

even more than acceleration at the combined analysis. At the same time, M-LooseBg3 showed a decreased separation at velocity but a much more increased separation at the combined analysis. Figure 5.8 at 40 Hz showed increasing separation in M, S-Bow and RubD2 as it moved from acceleration to velocity to combined analysis, while M-LooseBg3 showed a decreased velocity from acceleration. However, the combined analysis showed a higher separation when compared to acceleration and velocity. In Figure 5.8, the multiple speeds increase in separation for all conditions as it goes from acceleration to velocity except for M-LooseBg3, showing a higher separation for all conditions in the combined analysis. Overall, the multiple showed better separation than the individual speed when the faulty conditions were distinguished with respect to the RMRU. However, the multi-speed combined acceleration and velocity features analysis deduces a much higher separation. This quantification approach helps to establish that the combined acceleration and velocity features analysis gives an improved diagnosis compared to just acceleration (the existing UMA) and velocity features analysis.

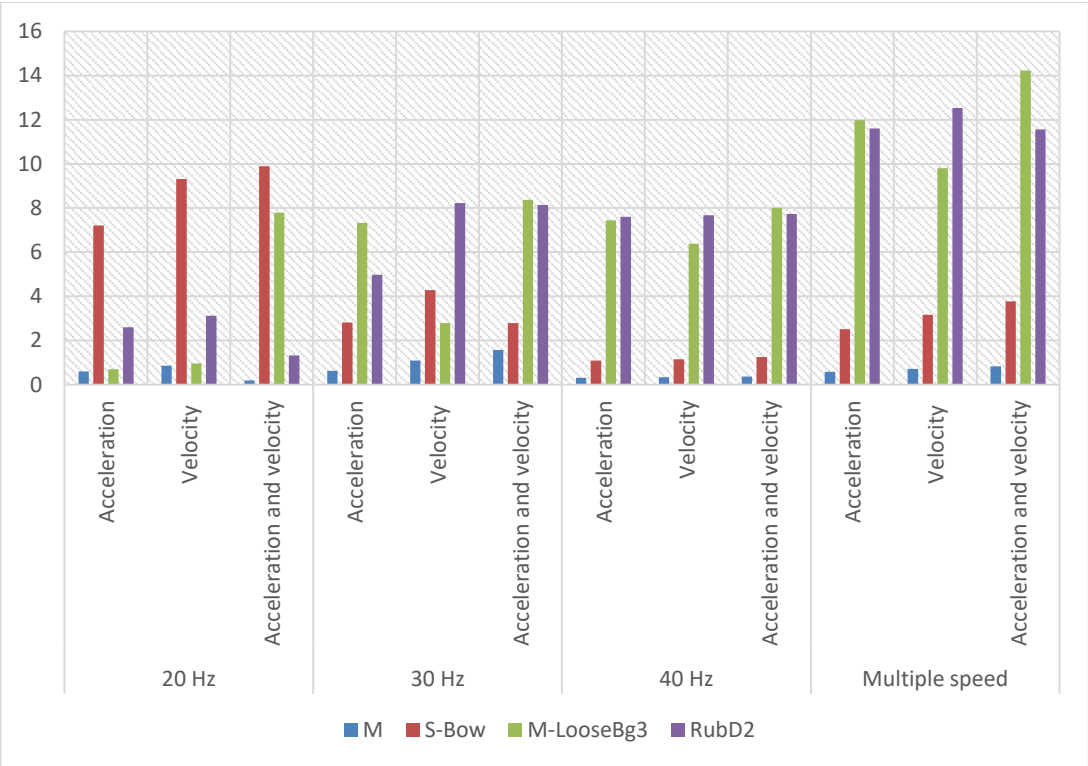

Figure 5. 8 Comprehensive plot showing separation of faulty conditions with respect to RMRU for all scenarios.

The first two scenarios, i.e., at 20 Hz and 30 Hz, tend to be random, and the last two, i.e., 40 Hz and multi-speed, had a better sequence. However, for the last two, the combined acceleration and velocity features showed a higher separation for each condition, with the last scenario having the highest. The last scenario, which represents the multi-speed, gave a higher separation, and the combined acceleration and velocity feature analysis gave the highest. The multi-speed scenarios suggest that the proposed improved approach in fault detection is adequate and robust and could be helpful in the diagnosis of a broader range of rotating machines' critical parts faults.

5.9 Chapter summary

The improved fault identification approach explored in this chapter is built from an earlier study that proposed the unified multi-speed analysis (UMA). The UMA used sensitive features from acceleration signals in fault classification, whereas the improved approach fused acceleration and velocity features in its analysis. Fusion acceleration and velocity features were explored to create a fault identification method to diagnose an extensive range of faults in a single analysis.

Data used in this study were collected from a previous research study by a former PhD student who constructed the FFTR that ran below the machines' first critical speed. The signal was acceleration based with rotor-related conditions only (**RMRU, M, S-bow, M-Loose** and **RubD2**). Data trending and condition classification using the acceleration features were carried out. The results obtained further validated the UMA. Since fault identification using time and spectra analysis may be helpful for individual conditions. However, with some extensive data set limitations, this thesis's analysis considered the data fusion approach.

Further work observed the velocity signals obtained by integrating the acceleration signals. Considering velocity signals came from studies that affirmed they presented better diagnoses of rotor faults, while the acceleration parameters are good in bearing fault diagnosis. However, velocity features classification showed more explicit clustering and separation of individual rotor conditions diagnosis than the acceleration features classification. This observation was evident, especially at the multiple speed analysis in a single analysis, thus satisfying the submission that the velocity signal gives a good diagnosis of rotor faults. Afterwards, the combined acceleration and velocity

features analysis were observed. The multi-speed analysis showed good clustering and more apparent separation of the machine conditions in a single analysis compared to individual speed.

A comparison of classification from acceleration, velocity and the fused acceleration and velocity features carried out through data quantification presented evidence that suggested a combination of acceleration and velocity features could improve fault diagnosis compared to only acceleration or velocity features. Data quantification was achieved by using the baseline RMRU as a reference to determine the separation of the faulty rotor cases. Observation showed that the combined acceleration and velocity features gave much more separation than velocity classification, and the velocity showed more separation than the acceleration for the single and multiple speeds. This result proves that the combined acceleration and velocity classification approach improved the analysis compared to the earlier UMA approach, which classified only acceleration features.

This preliminary investigation focused on rotor-related faults only, while the vibration data were measured below the machine's first critical speed. However, most industrial machines run at multiple speeds over their critical speeds during operation. In such situations, observing the machine's behaviour toward fault identification would help improve machine diagnosis. Thus, further work to understand diagnosis when a machine runs below and above its critical speed intending to classify an extensive range of rotating machines' critical parts faults, such as rotor and bearing faults, in a single analysis is investigated in the next chapter.

CHAPTER 6

DATA FUSION OF ACCELERATION AND VELOCITY FEATURES (dFAVF) FOR ROTOR-RELATED AND BEARING FAULTS INDENTIFICATION

This chapter presents the novel data fusion of acceleration and velocity features (dFAVF) for rotor and bearing fault identification using data from the improved spring-based flexible test rig one (SFTR-1). This is a build up from the improved approach using data from FFTR in chapter 5. The aim of this chapter is to observe the SFTR-1 which operates both below and above its first critical speed and the incorporation of bearing faults into the proposed classification model. Principal component analysis (PCA) pattern recognition approach has been able to provide useful classification of the fault using the first and second principal components (PCs). Incorporating the third PCs into the classification model provided a different observation platform for improved analysis. Further work looked at quantification of the faulty conditions with respect to the baseline RMRU, as this can help to understand the location and severity of the fault, although this is not validated yet.

6.1 Overview

This chapter proposes the data fusion of acceleration and velocity features (dFAVF) for rotor-related and bearing faults diagnosis in rotating machines. It is a build-up from chapter 5, where only rotor-related fault and acceleration vibration data below the first critical speed were considered during analysis. This chapter considers a broader range of machine faults, including several rotor-related and bearing defects, with acceleration signals obtained below and above the machines' first critical speed. As the introduction has established, 70 % of machine failure originates from rotor faults. Bearings are one of the most critical components in a rotating machine, with demand on their carrying capacity and reliability [152]. Much research has been done over the years on rolling elements bearing many benefits, one of which is calculating its life with reasonable accuracy [153]. In real life, Bearing may not operate up to its calculated life rating, which may be due to handling carelessly, heavy loading, and inadequate lubrication. Each of the factors causes peculiar damages to the Bearing [153]. In the previous chapter, the preliminary study presented an improved rotor fault identification approach using different acceleration and velocity features for machine diagnosis.

This chapter tends to validate the improved approach applied to the flanged-based flexible test rig (FFTR) by exploring results on the spring-based flexible test rig (SFTR) using the proposed dFAVF. The spring-based flexible test rig (SFTR) is a modification of earlier FFTR, i.e., modification of the bearing pedestal from flange connection to spring. The flexibility is focused on the test rig's foundation, enabling it to run below and above critical machine speeds. The foundation's flexibility was considered since several rotating machines in the industries run above their critical speed during operation [193,221]. Consideration of such machines brought about an understanding of their dynamic characterisation at various critical speed as well as challenges encountered when such type of machines undergoes condition monitoring. The design of most machines operating at high speeds is such that they pass through several critical speeds at which a high vibration level is encountered [212]. Assuming we have the same machine on the same foundation, the machine may be observed to either run below or above or through its critical speeds. Based on this, some recent studies

were examined with dynamic characterisation to identify critical speeds and mode shapes at various critical speeds and challenges in fault diagnosis for such scenarios [36,40, 202,222-224].

Data from the SFTR-1 were obtained and signal processing presented time and frequency analysis for acceleration and velocity signals. After that, selected feature extraction was carried out. Single and multiple speeds for acceleration and fused acceleration and velocity features classification were done with observation and discussions presented.

Table 6. 1 Fault simulated in SFTR-1 for current study.

No	Condition	Code	Description
1	Healthy	**RMRU**	Residual Misalignment Residual Unbalance.
2	Unbalance	**Unb**	1.5×10^{-3} kgm.
3	Misalignment	**M**	Parallel Misalignment with Bg1 displaced 0.8mm in vertical direction.
4	Crack near Bearing1	**CBg1**	0.34mm wide x 4mm deep notch with 0.33mm shim glued (on rotor near Bg1).
5	Crack near Bearing2	**CBg2**	0.34mm wide x 4mm deep notch with 0.33mm shim glued (on rotor near Bg2).
6	Rub near Disc1	**RubD1**	Perspex blade on rotor near Disc1.
7	Bearing 1 cage defect	**Bg1Cg**	Bearing cage at bearing 1 scratched using a Dremel grinder.
8	Bearing 2 cage defect	**Bg2Cg**	Bearing cage at bearing 2 scratched using a Dremel grinder.

6.2 Acceleration to velocity computation

Acceleration signal processing in the time and frequency domain was carried out in this study; a similar approach from chapter 5 was repeated here. However, this chapter's computation of the velocity frequency domain was carried out using the omega arithmetic approach. Time domain analysis for velocity signal was omitted as the focus was on the combination of acceleration-based features. These are helpful in high-frequency ranges such as bearing conditions and the velocity-based features, which are helpful for the frequency range between 10 Hz and 1000 Hz rotor conditions.

Much reference is made to the computation using some of the equations in chapter four.

Chapter 4 used the integration method to convert the acceleration signal to velocity before other parameters are computed both in acceleration and velocity. However, this chapter takes it further to use only the velocity frequency harmonic components and spectrum energy in its calculation. The spectra density of the Fourier transform of acceleration signal was transformed into its corresponding velocity spectra without going through the integration in time by applying the Omega Arithmetic (OA) approach [209]. This study uses the omega arithmetic method to convert the acceleration spectra to a velocity. In this correlative method, the frequency (Hz) significantly converts acceleration spectra density to velocity. Mathematically, omega (ω) is a Greek character used to represent frequency measured in radians/second. Therefore, the velocity spectra density is evaluated by dividing the acceleration spectra density with omega (ω).

6.3 Time and frequency domain parameter analysis (acceleration and velocity)

Signal processing for the current work presented time and frequency domain analysis using acceleration-based vibration data. After that, the omega arithmetic method achieved computation for velocity-based vibration data [219,225]. The computational parameter in this study was considered so that helpful comparison for rotor-related faults and bearing defect conditions can be achieved with the collection of equal data, similar time length and sampling frequencies. These computation parameters included data collected at a sampling frequency (*fs*) of 10 kHz; the number of data points N= 16384 used to compute the Fourier transform, frequency resolution (*df*) of 0.6104 Hz; and the number of averages was 287. Vibration signals were obtained at three speeds for all conditions, i.e., RMRU and faulty (rotor-related faults and bearing defect). Frequency domain analysis of various rotor faults with an observation of the machine running speed and its harmonics, as can be seen in the spectra plots where Figures 6.1 - 6.3 are acceleration plots and, Figures 6.4 – 6.6 are those for velocity.

6.3.1 Acceleration spectra analysis

Figure 6.1 to 6.3 shows typical acceleration spectra plots from the Bg2 bearing pedestal with the baseline-residual misalignment and residual unbalance (**RMRU**) and rotor faults, i.e., misalignment (**M**), unbalance (**Unb**), crack near bearing 1 (**CBg1**), crack near bearing 2 (**CBg2**) and rub near disc 1 (**RubD1**) conditions, when the machine ran at 450 rpm (7.5 Hz), below its first critical speed and 900 rpm (15 Hz), 1350 rpm (22.5 Hz), above its first critical speed. A high amplitude at 2x for all cases and all speeds may be due to residual misalignment, and residual unbalance [51][25]. The appearance of peaks and increase in amplitudes in these spectra plots is observed based on the position of the harmonic frequencies in the FRF and mode shape[11].

In Figures 5.4 to 5.6, there is the presence of 1x – 5x harmonic components for all cases at all speeds. Looking at Figure 5.4, which is a typical spectra plot at 450 rpm (7.5 Hz), Figure 5.4 (a) – (d) shows a small peak between 1x (7.5 Hz) and 2x (15 Hz), which may represent mode 1 (11.52 Hz). A small peak is also observed between 4x (30 Hz) and 5x (37.5 Hz) for all cases, and this peak may represent mode 3 (30.75 Hz). Other peaks that may be observed are not discussed as the focus of this study only considered up to 5x. In Figure 5.5, a typical spectra plot for vibration signal at 900 rpm (15 Hz), peaks which may be due to mode 4 (49.13 Hz), were observed just after 3x (45 Hz) harmonic for all cases but with increased amplitude in **CBg2** case. Figure 5.5 (d) – (e) showed small peaks just before the 1x (15 Hz) component, and it is most likely because of mode 1 (11.52 Hz). Figure 5.6 (a) – (f), a typical spectra plot at 1350 rpm (22.5 Hz), showed small peaks in front of 1x (22.5 Hz) in all cases and may be due to mode two (18.62 Hz). Figure 5.6 (a), which is **RMRU** has another peak in front of 1x, which may be due to mode 1 (11.52 Hz). This peak is also evident in Figure 5.6 (b), (c) and (f). Figures 5.6 (b) and (c) **M** and **Unb**, respectively, showed sub-harmonics components and sidebands around the various harmonic components observed. The sub-harmonics could have been from vibration that may show up due to inconsistency with the connection of the shaft and flexible coupler. The connection may not have been bolted firmly. Note that the adjustment in the bearing pedestal and shaft connector on some occasions when different faults are to be seeded in the test rig. Any peak observed after 1x in the spectra plot may be due to mode 3 (30.75 Hz). The peaks observed after

2x component (45 Hz) in Figure 5.6 (a) – (c) and (f) may be due to mode 4 (49.13 Hz). The 2x amplitude is seen to be very high in almost all the cases, with **Unb** and **RubD1** showing a more increased amplitude while **CBg1** and **CBg2**, even though they are high, showed amplitude lower than the other cases. Also, a small peak observed before 4x (90 Hz) in all the cases may be due to mode 5 (85.83 Hz). The spectra plots in Figure 5.6 showed sub-harmonics or sidebands around almost all the harmonic components. This effect could also be due to vibrations from the improper connection between the shaft and the soft coupler.

Observation shows that the amplitudes of the harmonics of particular faults vary at different speeds. It is also observed that in some cases, different faults may show similar harmonics with slightly different amplitudes.

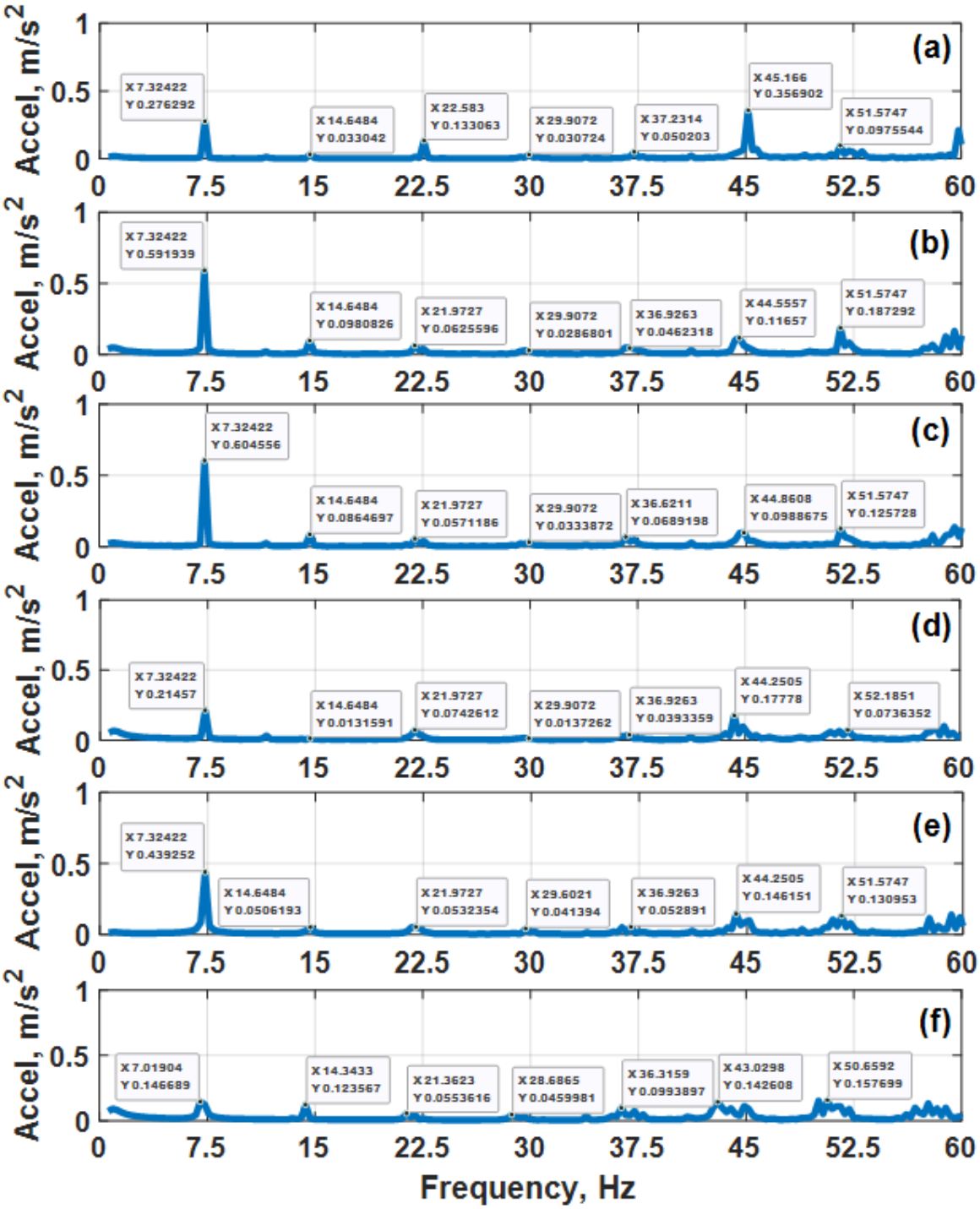

Figure 6. 1 Typical acceleration spectra plots at Bearing 3 450 rpm (7.5 Hz) for (a) RMRU (b) M (c) Unb (d) CBg1 (e) CBg2 (f) RubD1.

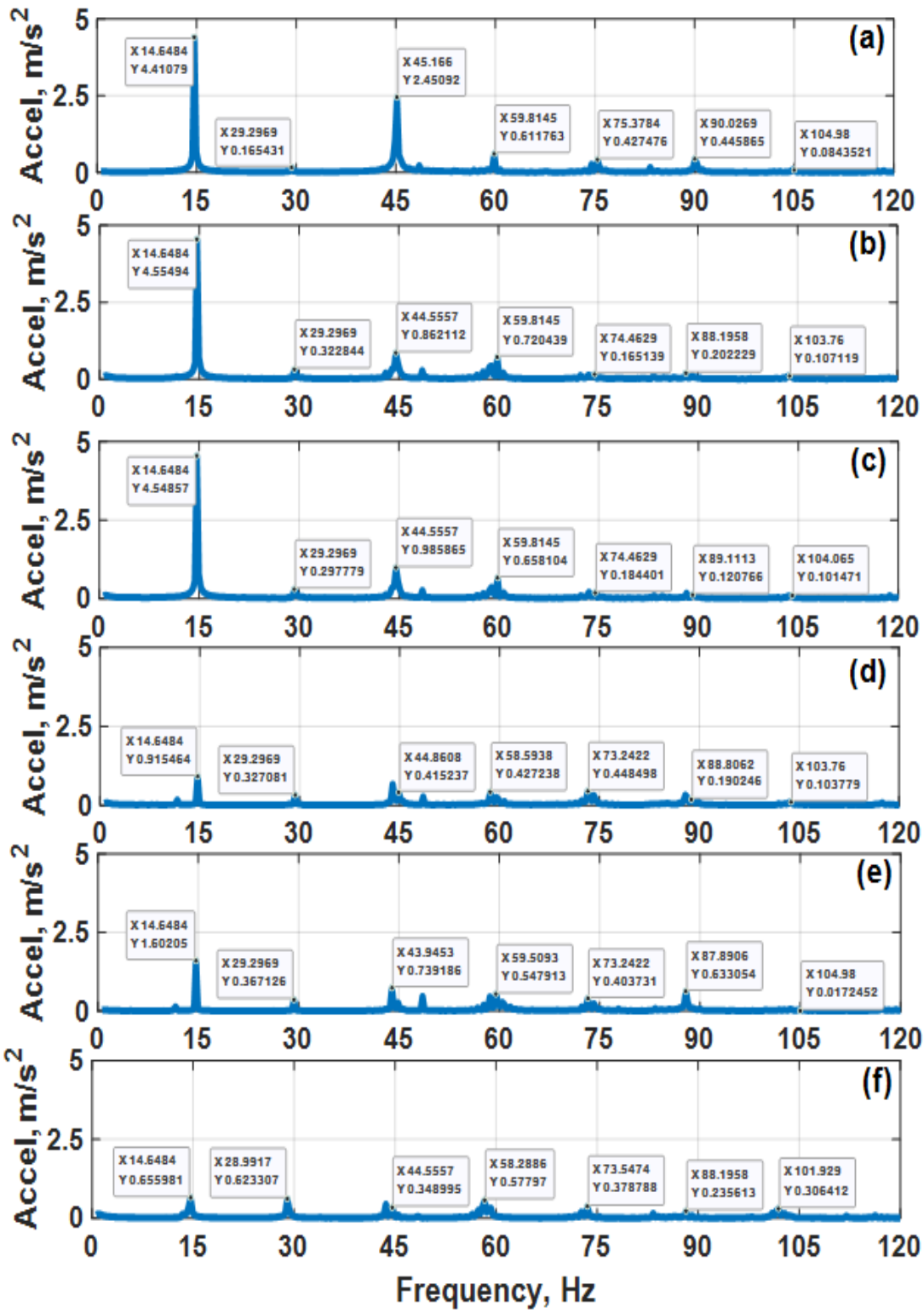

Figure 6. 2 Typical acceleration spectra plots at Bearing 3 900 rpm (15 Hz) for (a) RMRU (b) M (c) Unb (d) CBg1 (e) CBg2 (f) RubD1.

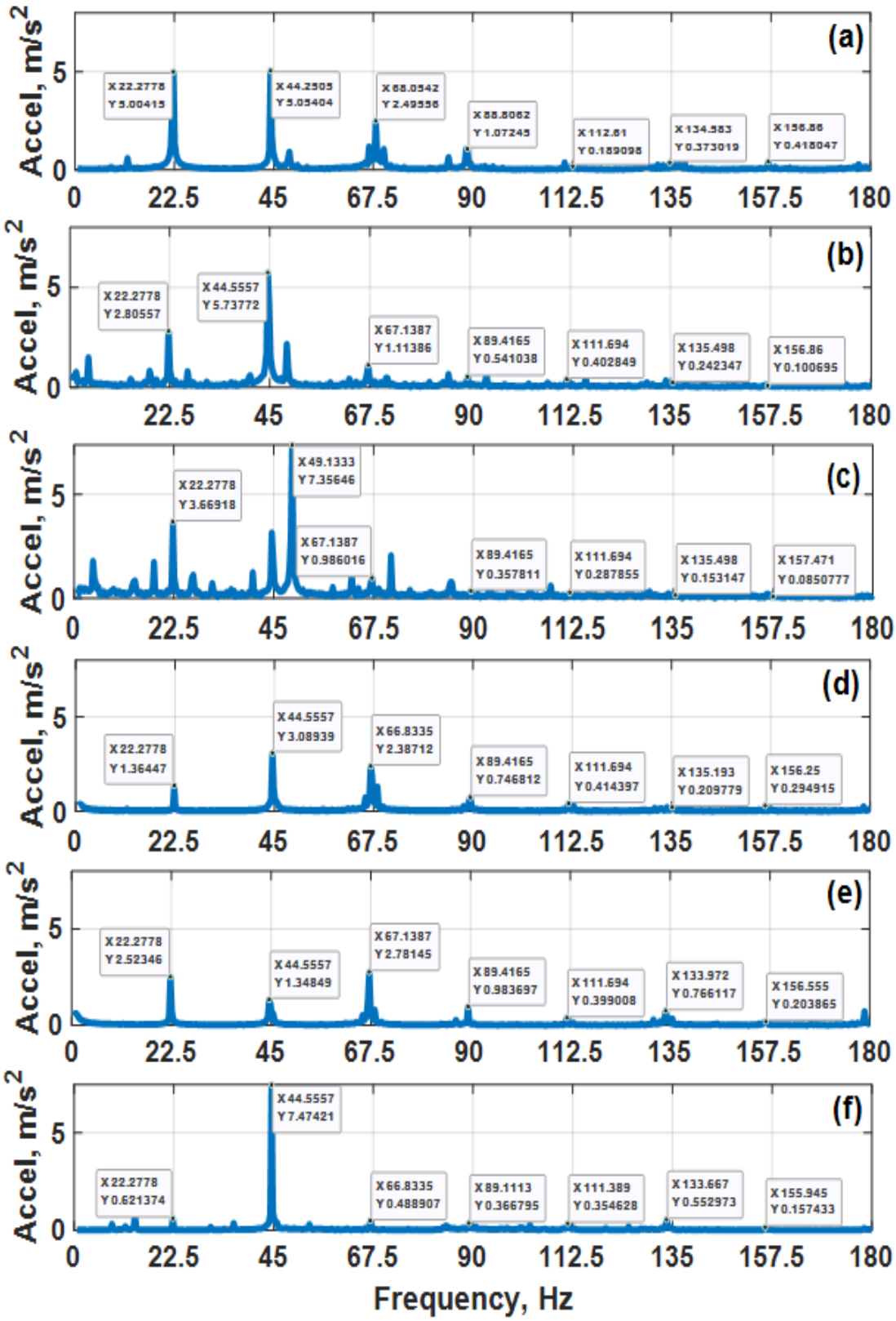

Figure 6. 3 Typical acceleration spectra plots at Bearing 3 1350 rpm (22.5 Hz) for (a) RMRU (b) M (c) Unb (d) CBg1 (e) CBg2 (f) RubD1.

6.3.2 Velocity spectra analysis

Various typical velocity spectra plots at bearing 2 locations are presented in Figure 6.4 – 6.6. All cases and speeds observed here are same with those observed in the acceleration spectra plots shown in Figure 5.4 to 5.6. An initial glance showed a higher 1x component in all cases and speeds as compared to their acceleration plots. However, the harmonic components seem to be lower and disappearing as the frequency increases. The velocity spectrum gives a nominal peak in its harmonics compared to the acceleration spectrum which highlights very high frequency range. Note the mathematical defining of velocity and acceleration is that "velocity is the rate of change of displacement with time" and "acceleration is the rate of change of velocity with time. However, all observation with respect to presence of harmonic components and appearance of peaks due to the mode in the FRF as discussed in the acceleration section, is also observed in the velocity spectra respectively.

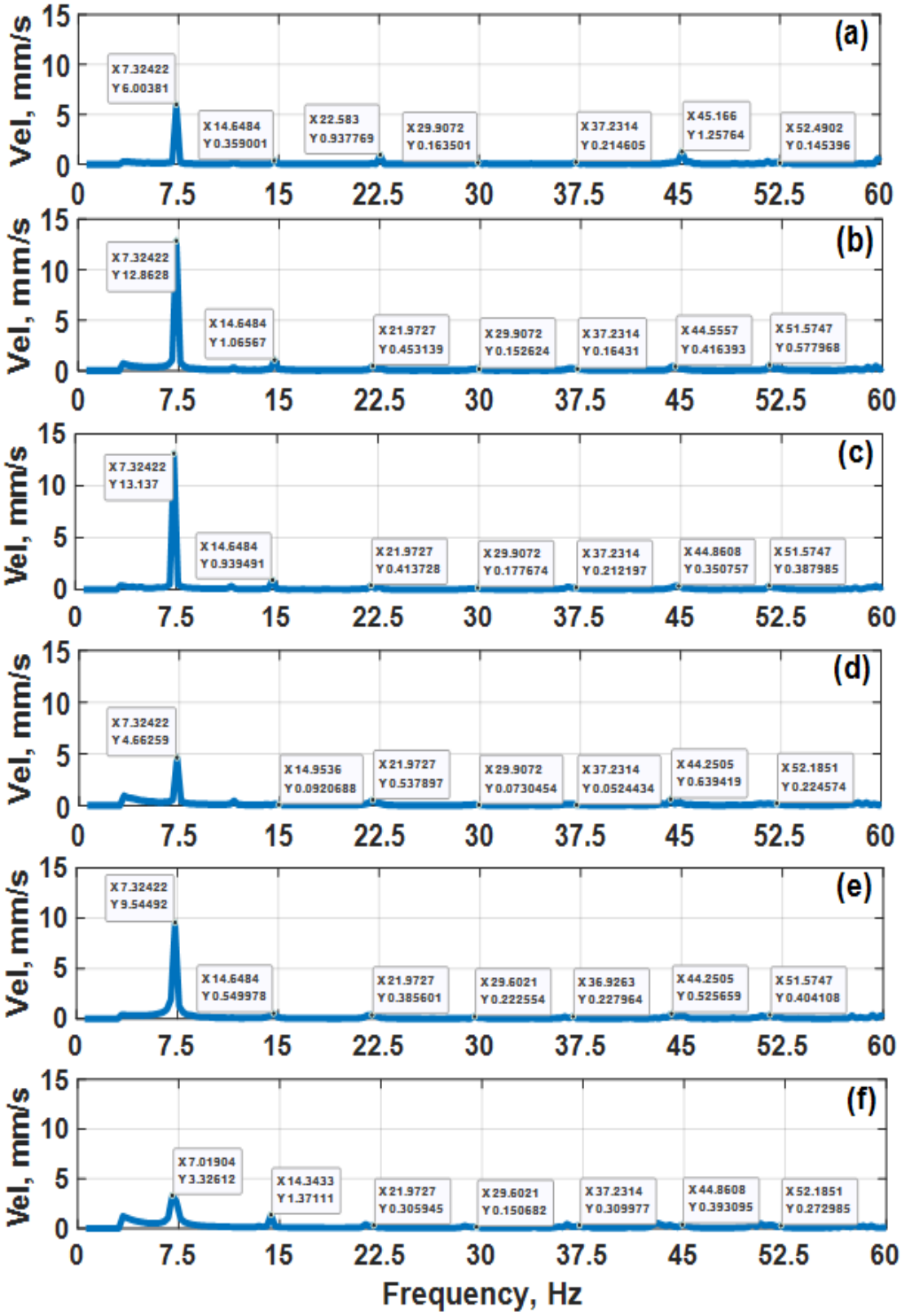

Figure 6. 4 Typical velocity spectra plot at Bearing 3 (a) RMRU (b) M (c) Unb (d) CBg1 (e)CBg2 (f) RubD1.

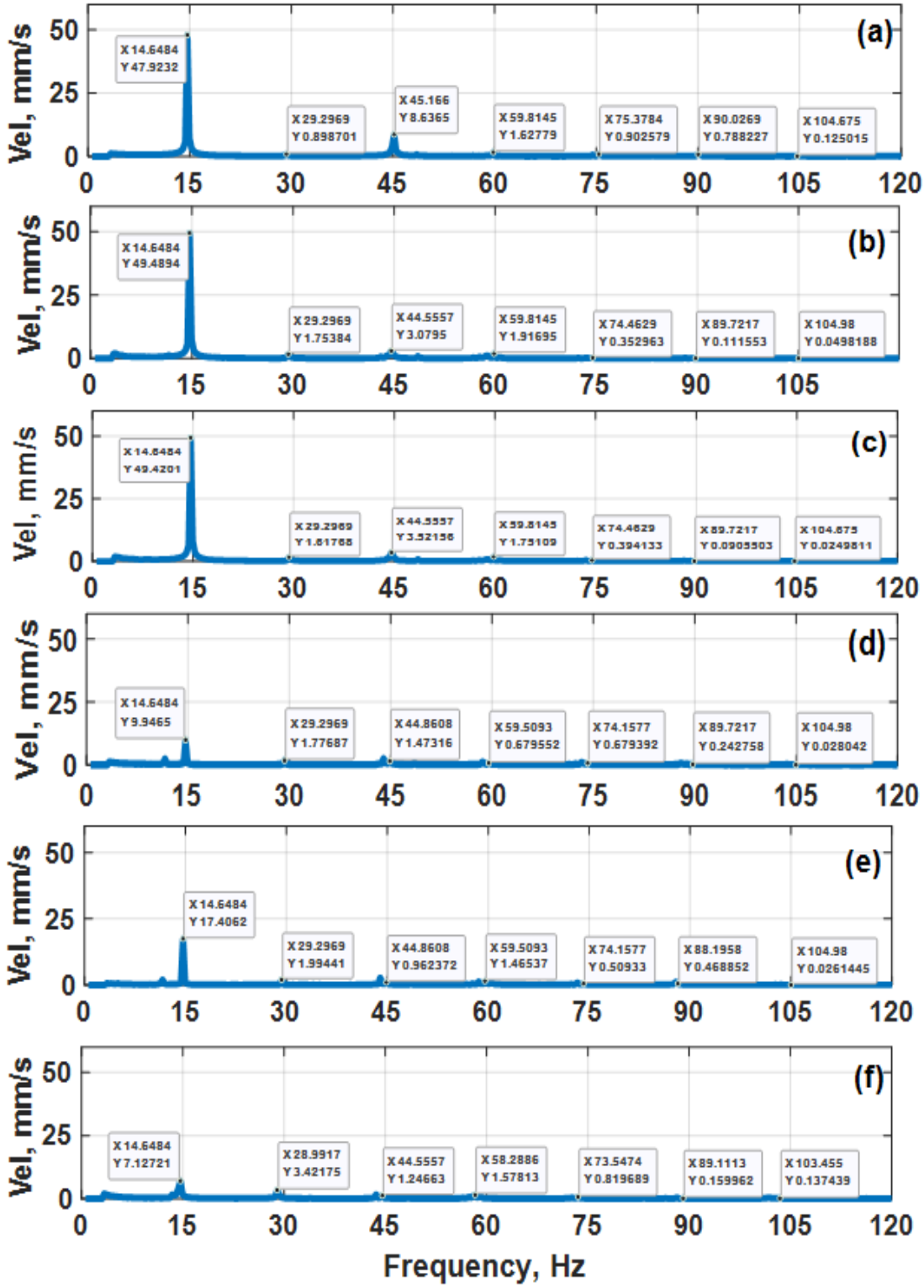

Figure 6. 5 Typical velocity spectra plot at Bearing 3 (a) RMRU (b) M (c) Unb (d) CBg1 (e)CBg2 (f) RubD1.

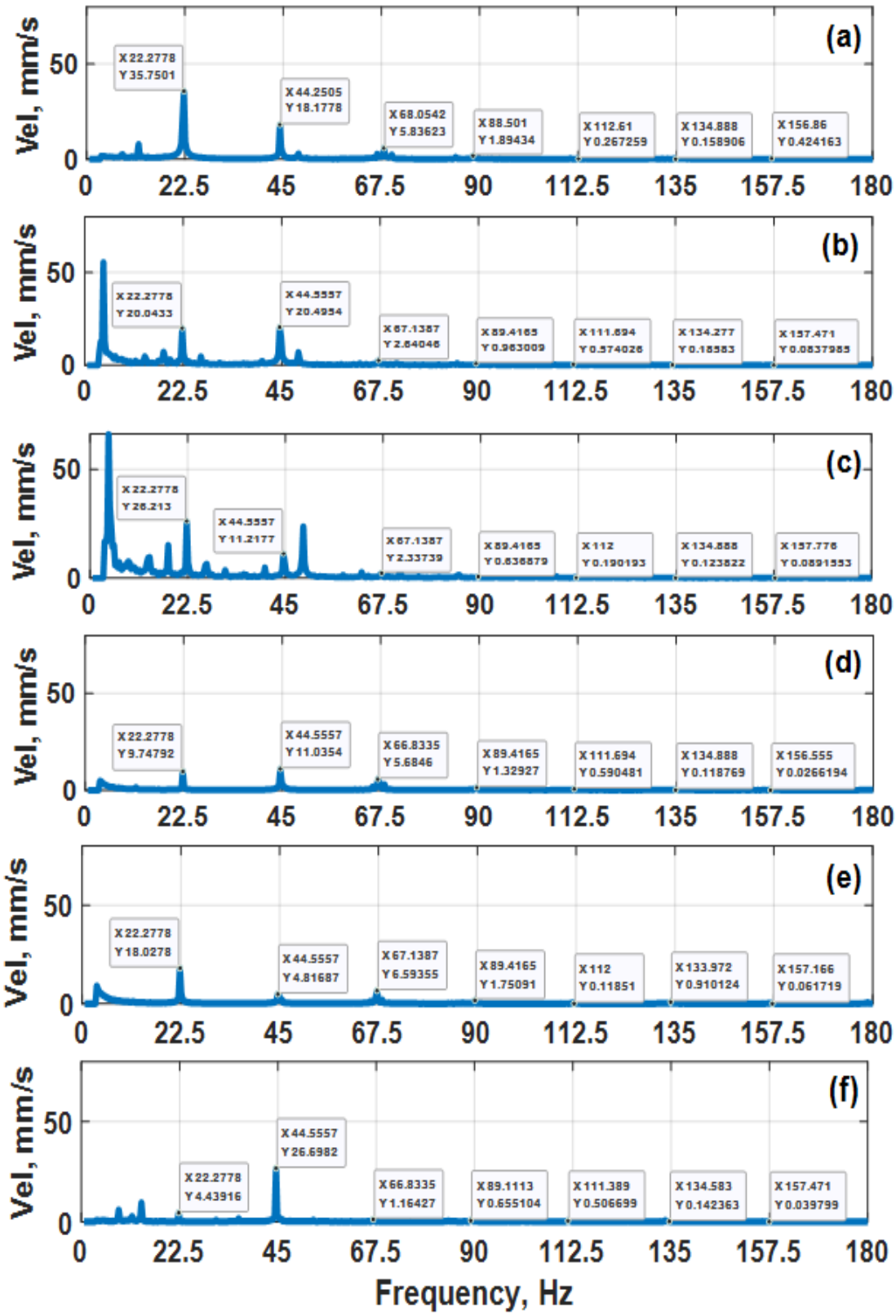

Figure 6. 6 Typical velocity spectra plot at Bearing 3 (a) RMRU (b) M (c) Unb (d) CBg1 (e)CBg2 (f) RubD1.

6.4 Discussion

Looking at fault identification using VCM approaches, typical time domain and frequency domain analysis typically gives valuable insight into the machine's behaviour [11]. However, data is continuously recorded as changes occur over a long period of machine operation with changing speeds. This situation makes large sets of VCM data available [15]. Analysis may become cumbersome for the vibration signal analyst, creating poor human judgment and incompetent fault diagnosis. Chapter 4 investigated time and frequency domain analysis (including bar chart and data trending), which pointed out specific faults due to their prominence. However, the overall machine condition could not be determined with total reliance on these analyses. So also, for the current study, much would not be said on observation from these analyses (time and frequency domain). In Figures 6.1 – 6.6, typical spectrum plots in acceleration and velocity, respectively, are presented. As can be seen, there are some differences between each plot, but based on the spectrum analysis only, it is generally difficult to make a diagnosis. Besides these inadequacies, there is also the challenge of generating several spectra for fault diagnosis. In order to improve fault diagnosis (FD), a data fusion-based approach has been considered in various studies [23,34,95,174,215] where functional fault diagnoses have been achieved with improved outcomes. Hence the earlier improved approach, based on data fusion of acceleration and velocity features for fault identification, is applied again to the current SFTR experimental data.

6.5 Feature arrangement for rotor faults

In this analysis, the feature arrangement is based on equation 3.30 to 3.38. Features *F* per bearing was 9, using four bearings (Bg1 – Bg4), the total number of features becomes 4 x 9 = 36. Similarly, the number of data sets m is 20 per machine condition k, and there are 7 machine conditions (*i.e., k=7*), so the total number of data sets for all cases equals 20 x 7 = 140. Thus, a fusion of acceleration and velocity features at all speeds and all experimentally simulated test conditions gave a 108 x 140 data matrix. PCA-based classification of machine conditions was employed in analysing the computed features. (PCs). [20]. Normalisation is carried out before inputting the data matrix into the PCA-based dFAVF model.

6.6 Data fusion analysis approach for fault diagnosis

Considerations of the improved approach from the earlier study in chapter five led to the proposed novel data fusion of acceleration and velocity features (dFAVF) model for fault identification in rotating machines. This model was based on single and multiple speed analysis from acceleration and then the proposed model. Exclusive analysis of each observation had three basic scenarios of single speed at 450 rpm (7.5 Hz), which is below the first critical speed, 900 rpm (15 Hz) and 1350 rpm (22.5 Hz), which is above the first critical speed and the fourth scenario multiple speeds. Note that all observations and scenarios were made up of multiple bearings (i.e., combining Bg1- Bg4). Plots of PC1 versus PC2 were done since they contained a more significant variance in the data matrix [20].

As presented in chapter five, considerations for principal component analysis were based solely on observations from principal component 1 and principal component 2 (PC1 vs PC2).

In order to expand understanding of the availability of relevant information on other PCs, the computation of the percentage variance for each PC should be carried out. However, variance computation is omitted in this study, whereas the PC3 was included for analysis. Thus, a plot of PC1vsPC2vsPC3 is generated, which shows a three-dimensional view of all cases and indicates additional PCs. The incorporation of PC3 in this analysis is to help retain any good variance in the analysis as well as to present a three-dimensional view of the clusters in the PCA for observation.

6.6.1 Acceleration features analysis at single and multiple speeds for rotor fault identification

Figure 6.7 (a) – (d) and Figure 6.8 (a) – (d) show the PCA classification of the simulated rotor condition for fault diagnosis in a rotating machine. The data fusion of acceleration-based time and frequency domain analysis is presented, where Figure 6.7 showed PC1vsPC2 PCA plots and Figure 6.8 showed PC1vsPC2vsPC3 PCA plots. These figures are a representation of single and multiple-speed analysis. Figure 6.7 and 6.8 (a) – (c) represent the single speeds at 450 rpm (7.5 Hz), 900 rpm (15 Hz) and 1350 rpm (22.5 Hz), respectively, for each scenario, Figures 6.7 and 6.8 (d) represents the

multiple speed analysis for each scenario. Observation of both figures shows similarities, except that Figure 6.8 gives a different angle of view due to its three-dimensional view.

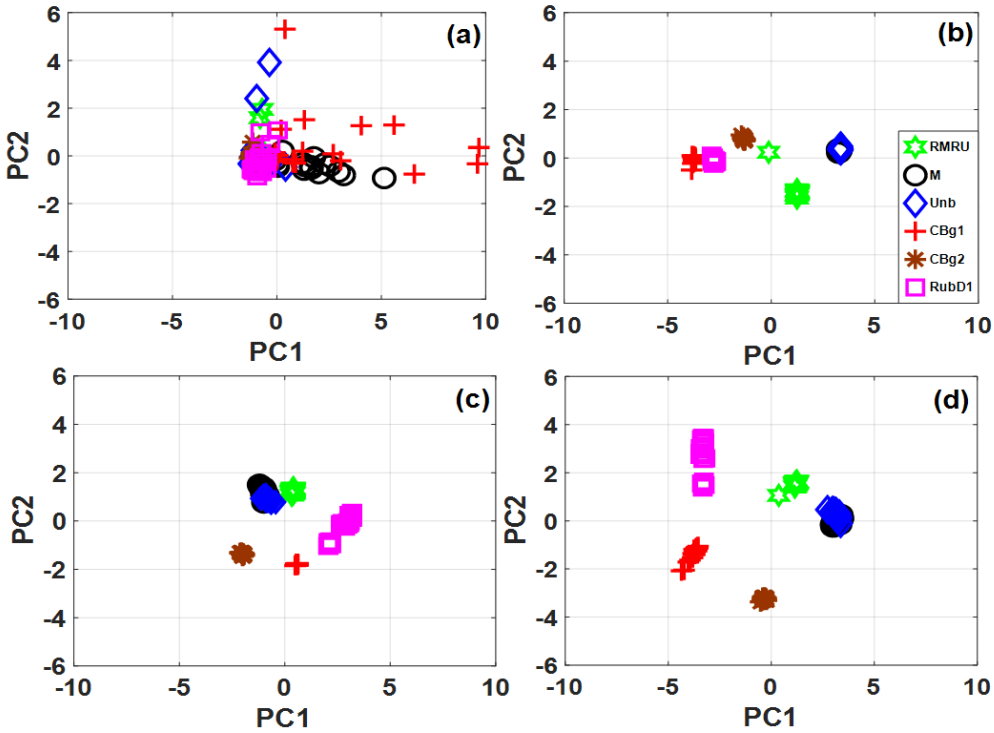

Figure 6. 7 Classification of SFTR rotor-related conditions acceleration-based features at (a) 450 rpm (b) 900 rpm (c) 1350 rpm (d) Multiple speeds.

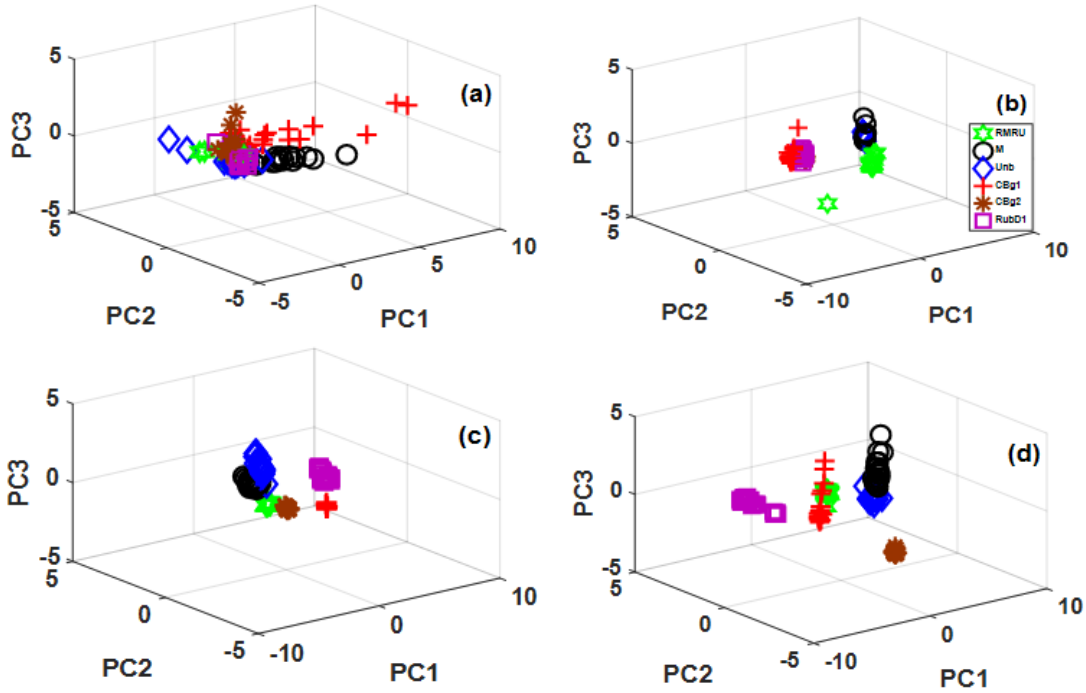

Figure 6. 8 Classification of SFTR rotor-related conditions for acceleration-based features at PC1vsPC2vsPC3 (a) 450 rpm (b) 900 rpm (c) 1350 rpm (d) Multiple speeds.

Figure 6.7 (a) shows an overlap between all the overall machine FD conditions. Some clustering was observed with the rotor faults. However, proper fault diagnosis was not achieved. Since 450 rpm (7.5 Hz) is a relatively low speed, an effective analysis may not be achieved for a robust fault diagnosis. Furthermore, in Figure 6.7 (b) – (c), individual conditions were clustered with overlap between unbalance and misalignment. In Figure 6.7 (b), reasonable separation was observed even though the RMRU was close to Unbalance and misalignment. For Figure 6.7 (c), RMRU is very close to overlapped unbalance and misalignment. Figure 6.7 (d) showed much separation between all conditions except for the overlap between unbalance and misalignment. Figure 6.8 (a) – (d) showed similar clustering and separation of the simulated conditions as in Figure 6.7 (a) – (d). However, the three-dimensional view provided a unique diagnosis approach which can help the vibration analyst make more explicit decisions on the identified faults. Note that the conditions in this investigation are all rotor-related faults. The investigation was done as a transference of diagnostic approach from the FFTR to the SFTR-1 to check for the insensitivity of the proposed method since earlier studies considered only rotor faults.

6.6.2 Data fusion of acceleration and velocity features (dFAVF) analysis at single and multiple speeds for rotor faults

Analysis of acceleration-based vibration features has been presented in subsection 6.6.1. in order to provide a comprehensive and robust fault diagnosis approach which is also effective and reliable, the single and multiple speed for fused acceleration and velocity features analysis was considered, as shown in Figure 6.9 (a) – (d) and Figure 6.10 (a) –(d). All conditions in Figure 6.9 (a), (b), (c) and (d) tend to cluster individually with good separation except for the overlap between unbalance and misalignment. However, Figure 6.9 (d) gave a much separation between all conditions compared to Figure 6.9 (a) – (c). Note, Figure 6.9 (d) is the multi-speed classification which represents to proposed dFAVF model for a single analysis of various machine faults. Similarly, Figure 6.10 (a) – (d) shows the representation as observed in Figure 6.9 (a) – (d); however, in a three-dimensional view for a more apparent diagnosis.

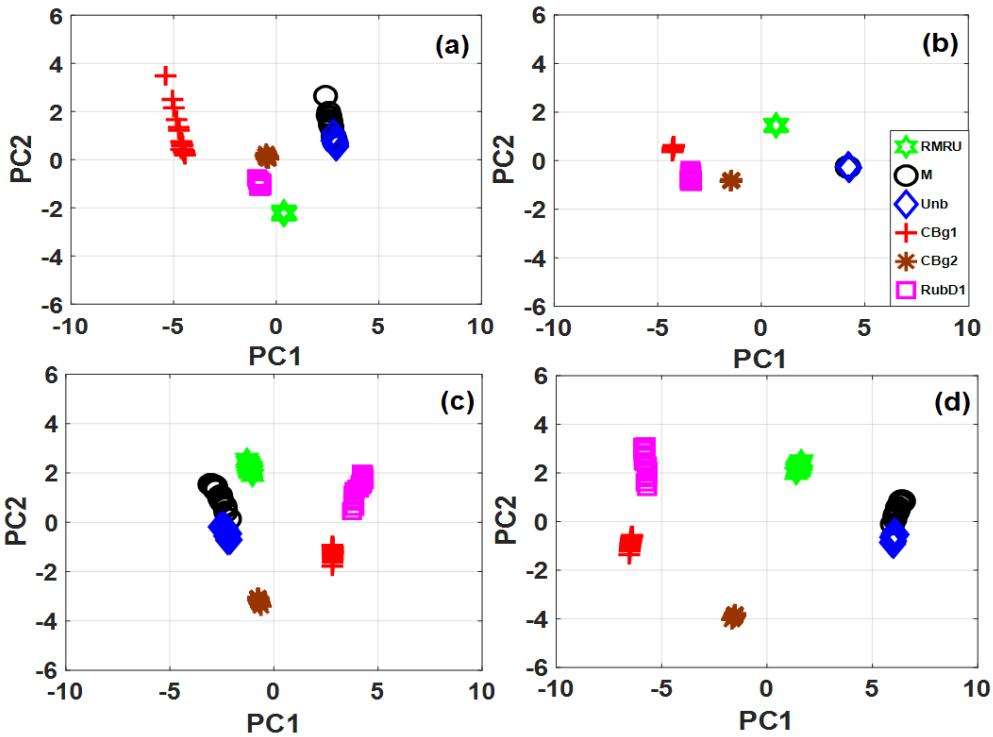

Figure 6. 9 Classification of SFTR rotor-related conditions acceleration-based time and velocity-based frequency domain features at (a) 450 rpm (b) 900 rpm (c) 1350 rpm (d) Multiple speeds.

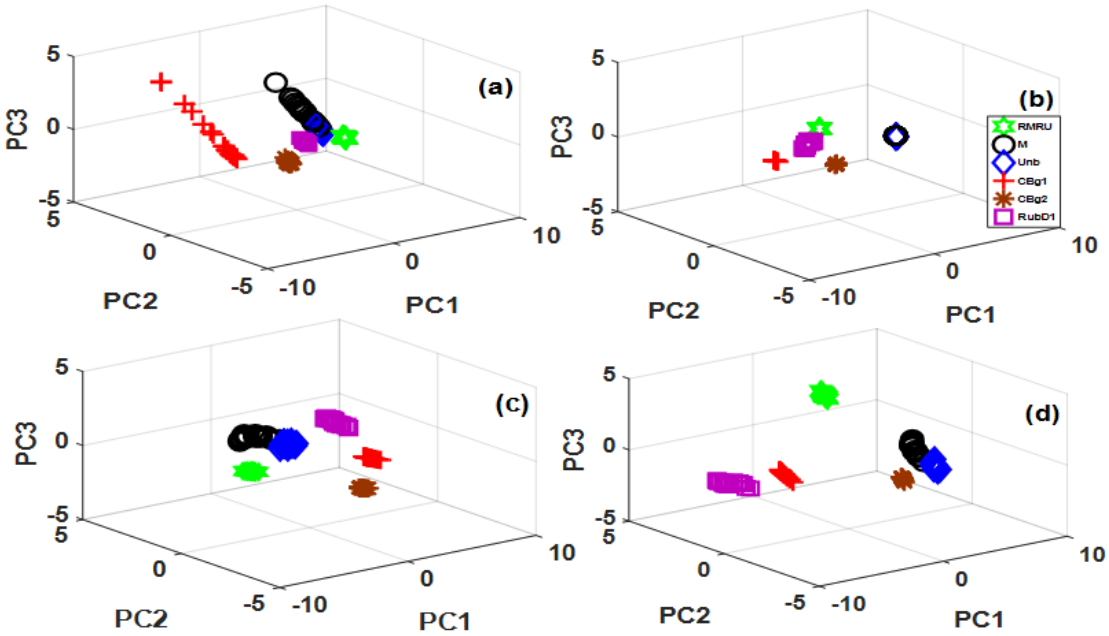

Figure 6. 10 Classification of SFTR rotor-related conditions for acceleration-based time and velocity-based frequency domain features at PC1vsPC2vsPC3 (a) 450 rpm (b) 900 rpm (c) 1350 rpm (d) Multiple speeds.

6.5.4 Observation and Discussion

There was a separation between all rotor faults with respect to the baseline RMRU. Notwithstanding the overlap between unbalance and misalignment in almost all cases, there was still a useful separation between them. Also, the overlap between the unbalance and misalignment could be from the residual unbalance and misalignment in the machine. Thus, the machine may show similar features around both conditions. Observation alone does not clearly indicate a better clustering or separation between individual conditions, so computation showing the separation between faulty with respect to the baseline RMRU conditions would be a helpful quantification approach. However, the bearing defect was analysed and seen in sections 6.6 and 6.7, and its diagnostic features were incorporated into the dFAVF model for observation of an extensive range of faults in a single analysis, as seen in sections 6.8 and 6.9.

6.6 Bearing fault diagnosis approach

During operation, the natural frequency of the bearing housing is excited due to impact loading per rotation [56]. It ranges from 1 to 5 kHz. However, this study's bearing housing natural frequency is around 2.4 kHz. Power spectrum density (PSD) analysis in bearing fault diagnosis may not show the related fundamental frequency, especially when the minor defect. The envelope analysis is used to mitigate such a situation by extracting impacts with low energy [56]. In this study, envelope analysis is employed on bearing signals to examine the behaviour of a damaged bearing cage.

The bearing cage defect was simulated at Bg1 to create a cage defect at bearing 1 (**Bg1Cg**), and data were collected at the three different machine running speeds. Thereafter, the faulty bearing was moved to Bg2, replacing Bg1 with a healthy bearing. Thus, creating a bearing cage defect at Bg2 (**Bg2cg**), data were collected at three machine's running speeds (450 rpm, 900 rpm and 1350 rpm). Observation of bearing defect signal before and after envelope analysis at Bg1 and Bg2 is presented in Figures 6.11 – 6.13.

6.7 Bearing faults time and frequency domain analysis

Figure 6.11 – 6.13 showed typical plots for bearing cage defect analysis at two bearing pedestal locations, i.e., Bg1 and Bg2, at the three machine running speeds (450 rpm,

900 rpm and 1350 rpm), respectively. Focusing on the spectra plots after envelope analysis showed some useful diagnosis features. Firstly, we observe the FTF 1x frequency, and its harmonic with the amplitude showing the effect of the damaged cage. Also, smaller peaks are seen around some harmonic components, which may be due to the natural frequency of the FRF. Figures 6.11 – 6.13 (a) and (d) give a typical spectrum plot of bearing defect after a high filter at 500 Hz. The filtering helps to remove the low frequencies, which may be rotor related. After that, envelope analysis is carried out on the signal with a time domain representation in Figure 6.11 – 6.13 (b) and (e). Here, **a** represents the original signal, while **up** and **lo** represent the upper and lower envelope signals. Figure 6.11 – 6.13 (c) and (f) shows the spectrum plot for the envelope signal.

The observation of Figure 6.11 – 6.13 provides a valuable understanding of the dynamics of the machine with respect to the appearance of cage defects during machine operation at different speeds. Investigation of the spectra after filtering before envelope analysis and the time domain analysis after envelope analysis could be helpful for fault diagnosis where relevant parameters are considered. However, observations of the typical plots may not give useful diagnosis features immediately.

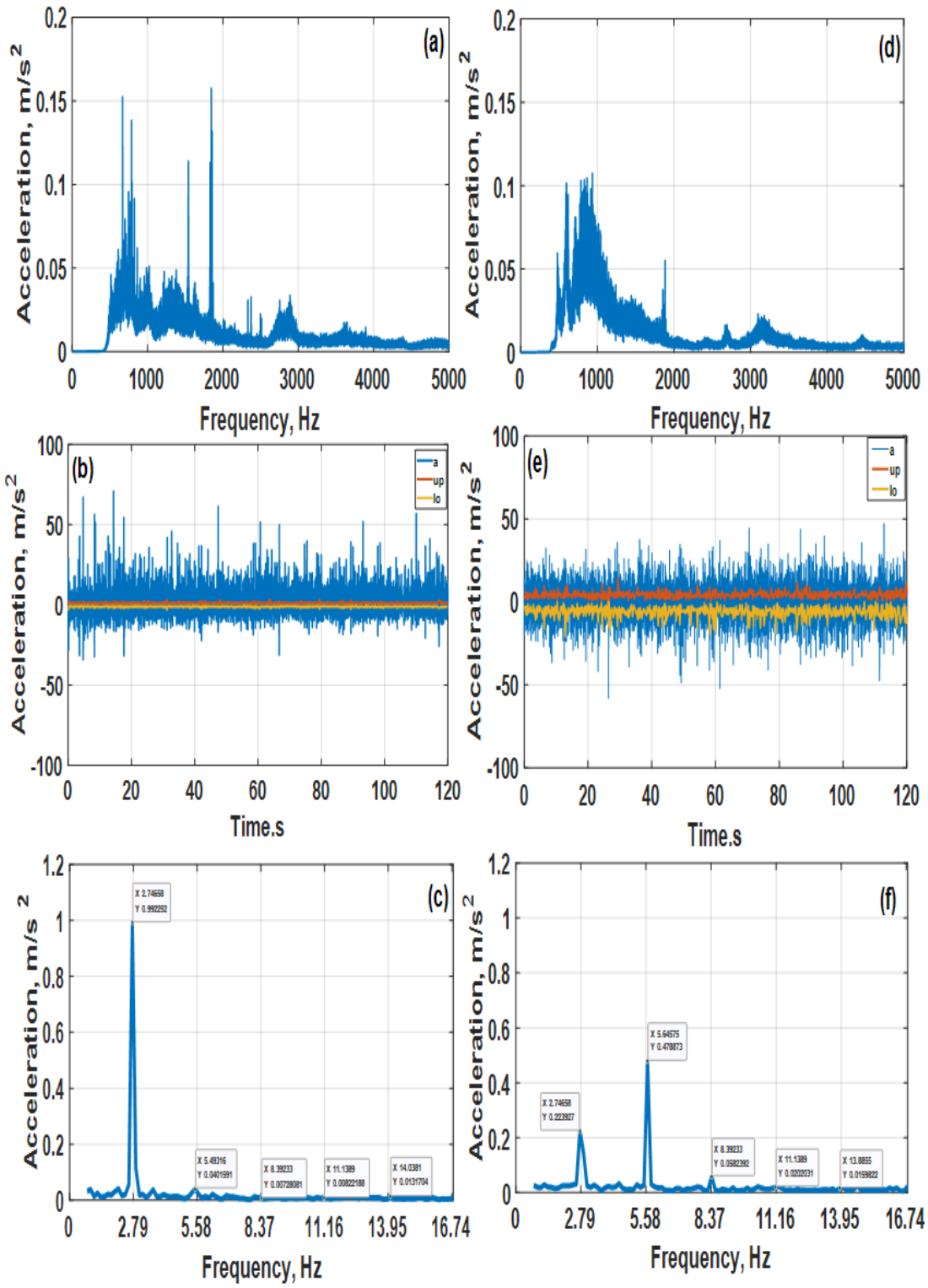

Figure 6. 11 Typical Bearing defect at 450 rpm for (a) Bg1Cg filtered Spectrum (b) Bg1Cg envelope time domain (c) Bg1Cg envelope spectrum (d) Bg2Cg filtered spectrum (e) Bg2Cg envelope time domain (f) Bg2Cg envelope spectrum.

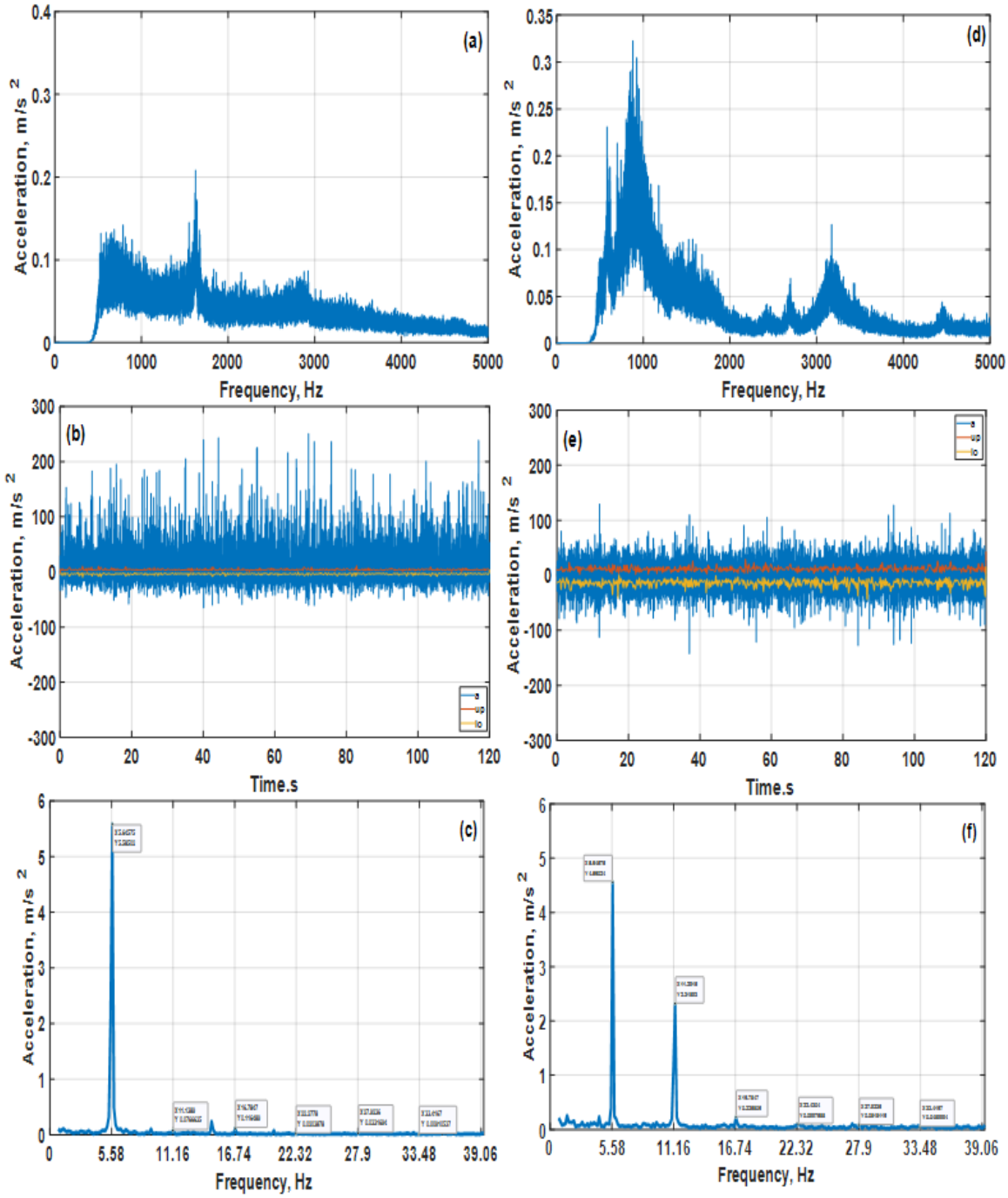

Figure 6. 12 Typical Bearing defect at 900 rpm for (a) Bg1Cg filtered Spectrum (b) Bg1Cg envelope time domain (c) Bg1Cg envelope spectrum (d) Bg2Cg filtered spectrum (e) Bg2Cg envelope time domain (f) Bg2Cg envelope spectrum.

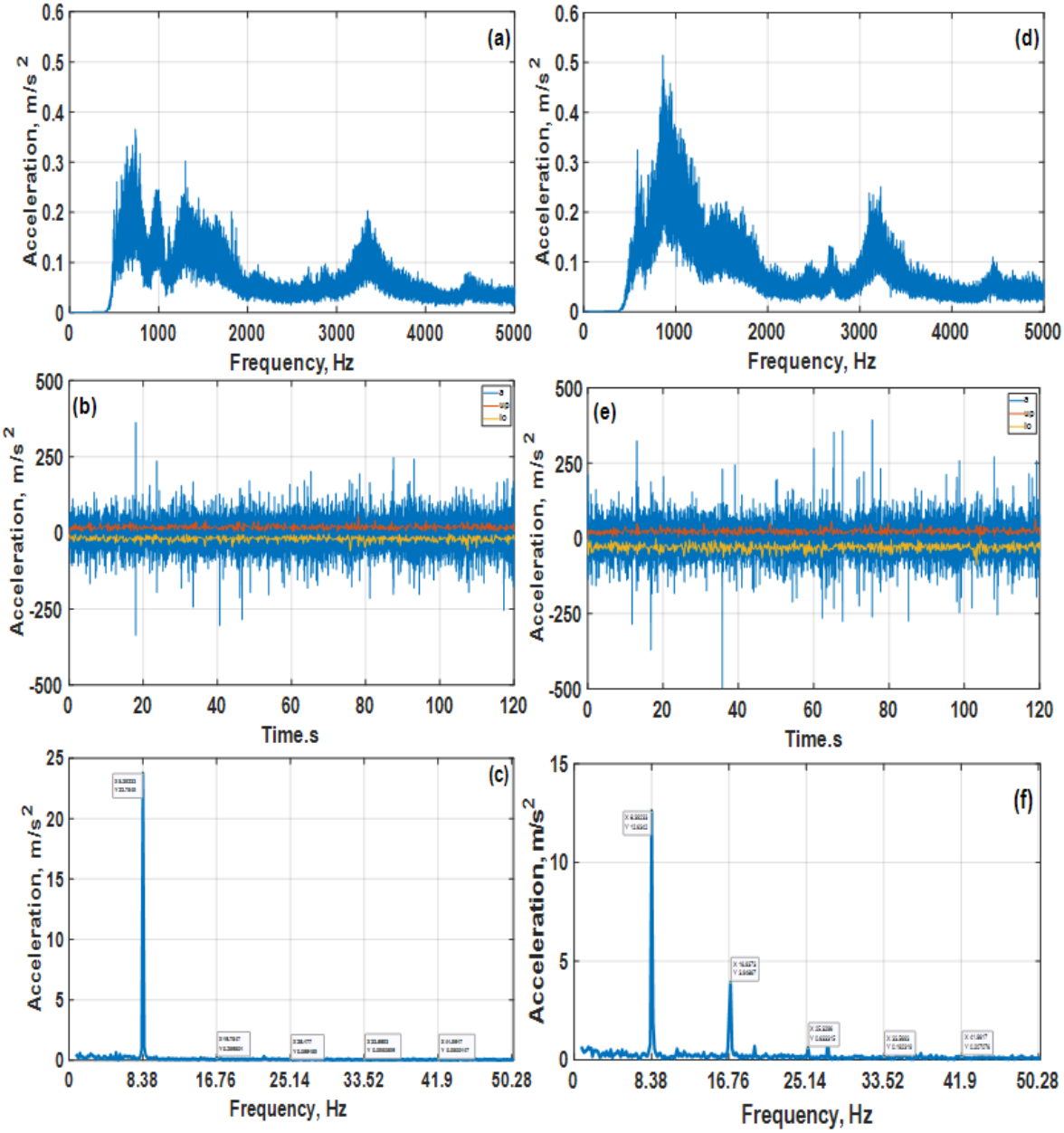

Figure 6. 13 Typical Bearing defect at 3550 rpm for (a) Bg1Cg filtered Spectrum (b) Bg1Cg envelope time domain (c) Bg1Cg envelope spectrum (d) Bg2Cg filtered spectrum (e) Bg2Cg envelope time domain (f) Bg2Cg envelope spectrum.

The values for the fundamental fault frequencies as calculated using the various machine running speeds are shown in Table 6.2 below.

Table 6. 2 Various fundamental frequencies at the three machine running speeds.

Machine running speed	***7.5 Hz***	***15 Hz***	***22.5 Hz***
BSF	*14.65 Hz*	*29.26 Hz*	*44.36 Hz*
BPFI	*37.11 Hz*	*74.21 Hz*	*111.32 Hz*
BPFO	*22.89 Hz*	*45.78 Hz*	*68.67 Hz*
FTF	*2.86 Hz*	*5.72 Hz*	*8.58 Hz*

It should be noted that calculations of the fundamental train frequencies (FTF) gave 2.86 Hz, 5.72 Hz and 8.58 Hz for each machine running speeds at 7.5 Hz, 15 Hz and 22.5 Hz, respectively. However, the experimentally generated envelope analysis spectrum plots showed the FTF to be 2.79 Hz, 5.58 Hz and 8.38 Hz, with the machine running speeds at 7.5 Hz, 15 Hz and 22.5 Hz, respectively. Table 6.3 shows the values of the calculated and experimentally obtained fundamental train frequency (FTF).

Table 6. 3 Table showing the calculated and experimental fundamental train frequency (FTF) at the three machine running speeds.

Machine running speed	***7.5 Hz***	***15 Hz***	***22.5 Hz***
Calculated FTF	*2.86 Hz*	*5.72 Hz*	*8.58 Hz*
Experimentally obtained FTF	*2.79 Hz*	*5.58 Hz*	*8.38 Hz*

Overall observation shows that significant fault-bearing cage defect identification may not be achieved with only the harmonic components. Therefore, this study tries to improve FD by developing a data combination model of acceleration-based time domain and velocity-based frequency domain features from the rotor and bearing parameters for a single analysis. This model incorporated bearing features into the already proposed dFAVF in section 6.6, where only rotor faults have been considered. The model was expected to effectively identify various machine faults in a single analysis.

6.8 dFAVF features arrangement for rotor and bearing fault

Equation (3.39) represents the initial data matrix build-up for only acceleration-based time domain features of bearing data, while equation (3.40) is the data matrix for fusion of acceleration-based time domain bearing defects and velocity-based frequency domain rotor-related faults is represented in equation (3.41). The test rig had 4 bearing pedestals (Bg1 – Bg4) with measurements done at 3 machines' running speeds. A total of 9 x 4 x 3 = 108 features was computed. Similarly, 20 datasets per machine condition were collected, forming the observation. Since 8 machine conditions were simulated, the total observation for all cases became 20 x 8 = 160. Thus, data fusion of acceleration and velocity features (dFAVF) at all speeds and all experimentally tested conditions gave a 108 by 160 data matrix. These data were normalised to create a common scale for easy interpretation of the data. Data normalisation is achieved here by converting each element in the matrix from equation (3.41) to zero mean and unit variance. [15]. After that, PCA-based pattern recognition was carried out to analyse the computed data matrix [198]. And thereby classify the machine conditions.

6.9 Pattern recognition using proposed dFAVF approach for a consolidated rotor and bearing fault diagnosis

In this analysis, only the multiple-speed approach is considered for analysis. Since it has been proven that the dFAVF is a valuable model for fault diagnosis, the aim is to have a single analysis where all machine conditions can be observed and diagnosis carried out efficiently. Figure 6.14 represents the PCA-based pattern recognition using the dFAVF model. A plot of PC1 versus PC2 was done as it contained a more significant variance in the data matrix [198]. The simulated conditions represented in Figure 6.14 (a) are the baseline residual misalignment and residual unbalance (baseline-**RMRU**), misalignment (**M**), Unbalance (**Unb)**, crack close to Bg1 (**CBg1**), crack close to Bg2 (**CBg2**), shaft rub near disc 1 (**RubD1**), bearing cage defect at Bg1 (**Bg1Cg)** and bearing cage defect at B2 (**Bg2Cg**). Observation showed clustering and separation of baseline-**RMRU, M, Unb, CBg1, CBg2, RubD1, Bg1Cg** and **Bg2Cg**. However, while the baseline-**RMRU, M, Unb, CBg1, CBg2** and **RubD1**, which are rotor conditions, stayed close to each other while **Bg1Cg** and **Bg2Cg** which are bearing defects, are separated from

other conditions while showing some spread in their cluster. This separation of the bearing case from other conditions may be due to differences in the frequency range [192], i.e., 'low' frequency faults cluster around the same region, which is further from the 'high' frequency faults. On the other hand, the spread seen in **Bg1Cg, and Bg2Cg** may be due to variations in the impact load during machine operation.

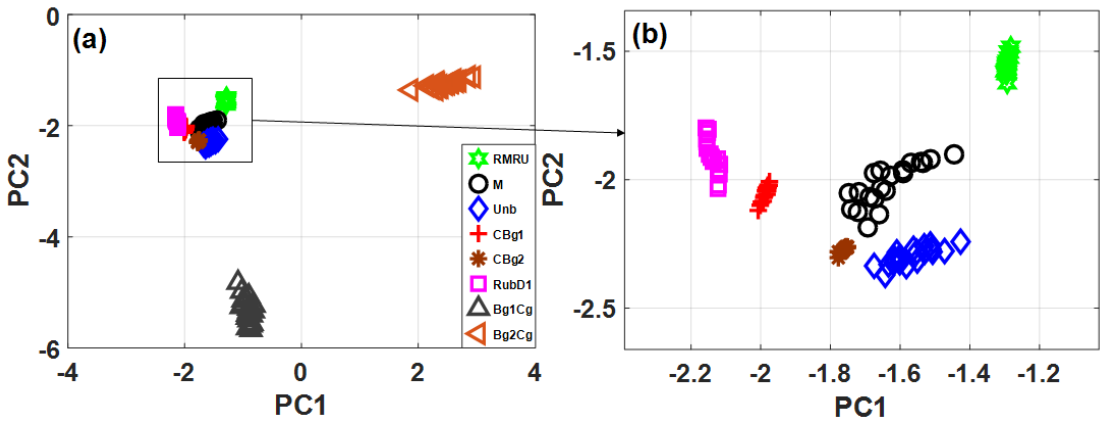

Figure 6. 14 Typical PC1 vs PC2 for single classification of a lab rotating rig for (a) rotor-related and bearing fault (b) zoomed view showing only rotor faults.

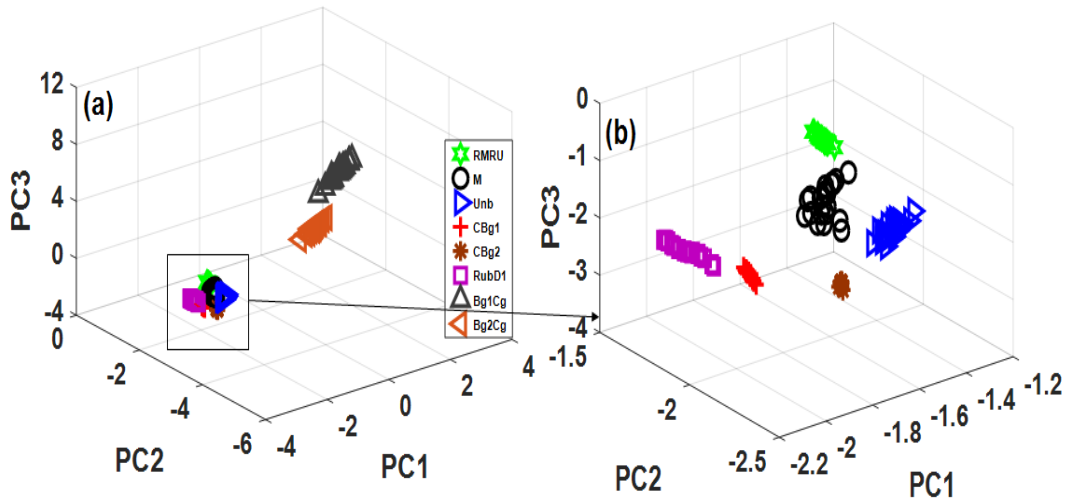

Figure 6. 15 Typical PC1 vs PC2 vs PC3 for single classification of a lab rotating rig for (a) rotor-related and bearing fault (b) zoomed view showing only rotor faults.

The data fusion of acceleration and velocity features (dFAVF) model using up to 3 PCs in the PCA-based pattern recognition approach is presented in Figure 6.15. A very outstanding clustering was observed for all conditions, and separation between each can be seen. It also gives another cluster view, which could help identify fault severity.

These outcomes give credence to the improved approach and present a comprehensive diagnostic approach for fault identification in rotating machines' critical parts. However, mere observation is not enough to determine the efficiency of the proposed dFAVF method both in the PC1vsPC2 and that PC1vsPC2vsPC3. Thus, a data quantification approach which distinguishes the baseline RMRU from faulty conditions is carried out to validate the proposed method, as shown in section 6.10.

6.10 Data quantification for discriminating faulty conditions from baseline RMRU with respect to dFAVF method on rotor and bearing faults diagnosis

This section discusses the separation of faulty conditions with respect to baseline RMRU for the dFAVF method. A comparison of PC1vsPC2 and PC1vsPC2vsPC3 for combining acceleration-based time and velocity-based frequency domains was achieved. The bar chart represents the result visually, as seen in Figure 6.16. This investigation tried to validate that computing more PCs in the fault classification is beneficial and improves fault identification in rotating machines.

An overall observation of the analysis showed the PC1vsPC2vsPC3 slightly higher than PC1vsPC2. This observation indicates that the incorporation of PC3 has provided useful variance for improved analysis. Thus, the PC1vsPC2vsPC3 classification approach will be helpful to vibration analysts for a prompt diagnosis and understanding of machine behaviour with respect to fault identification.

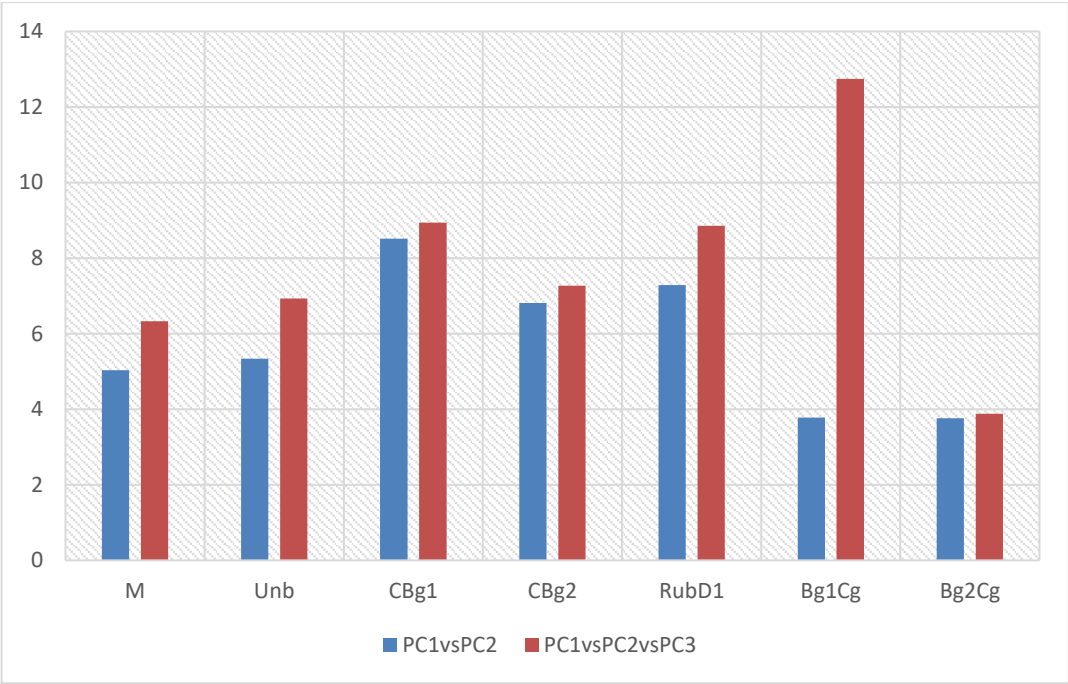

Figure 6. 16 Bar chart representing a comparison of the data from PC1vsPC2 and PC1vsPC2vsPC3.

A comparison of PCA-based pattern recognition plots using PC1vsPC2 and PC1vsPC2vsPC3 was achieved. The overall observation from Figure 6.16 shows much separation between RMRU and the faulty conditions using the PC1vsPC2vsPC3 compared to PC1vsPC2. The result supports that the increase in PCs shows improved analysis in clustering and separation of the investigated machine conditions.

6.11 Chapter summary

The proposed data fusion of acceleration and velocity features (dFAVF) method extends the improved unified multi-speed approach. It has been used to diagnose a broader range of rotating machine faults, i.e., several rotor faults (**M, Unb, CBg1, CBg2,** and **RubD**) and bearing defects (**Bg1Cg** and **Bg2Cg)**. This model was investigated using vibration data from the spring-based flexible test rig 1 (SFTR-1).

Acceleration and velocity spectra analysis was carried out, and the velocity spectra were achieved by converting acceleration data using the omega arithmetic approach. The PCA-based pattern recognition approach was used in classifying acceleration data for rotor-related faults. The results showed the clustering and separation of the

different machine conditions at individual and multiple-speed analyses. This investigation again reaffirmed the proposed UMA from an earlier study, using data from a modified test rig. After that, the proposed novel data fusion of acceleration and velocity features (dFAVF) approach was used to classify rotor faults. This model comprises acceleration-based time domain features and velocity-based frequency domain features. The result showed better clustering and separation of each machine condition observed for the dFAVF model compared to the earlier UMA. It also confirmed the effectiveness of the improved model from chapter 5.

The further investigation incorporated bearing fault into the dFAVF approach. The simulated bearing cage defects were analysed with an initial high pass filter at 500 Hz, which removed all rotor-related faults on the bearing fault signal. Acceleration-based time domain features were extracted to populate the dFAVF model for classification. This consolidated rotor and bearing faults classification showed good clustering and separation of the experimental machine condition in the individual and multiple speed analysis. Also, the rotor conditions were seen to be around a particular plot section, separated from the bearing conditions. This observation was because of the frequency range of occurrence, as the rotor tends to occur in low-frequency ranges while bearing faults happen in the high-frequency range. However, further investigation is needed to validate this observation.

The data quantification section compared PC1vsPC2 and PC1vsPC2vsPC3 to show that important diagnosis information may be present in other PCs besides the first two. The result showed that the PC1vsPC2vsPC3 gave more separation compared to PC1vsPC2. The result indicates that better fault diagnosis could be achieved with additional information from more PCs.

The contribution herewith is that even in a complex machine with varying speeds, the dFAVF approach could distinguish both rotor and bearing fault in a single analysis. The frequency range of the various machine faults could contribute to their location in the analysis. Data quantification validated the improvement in the classification approach with more PCs giving useful diagnosis information.

CHAPTER 7

POLY-COHERENT COMPOSITE BISPECTRUM (pCCB) APPROACH FOR DIAGNOSIS OF ROTOR FAULTS

This chapter looks at an earlier data fusion approach i.e., the poly-coherent composite bispectrum (pCCB) which is higher order spectrum (HOS) analysis. The pCCB has been applied in classification of rotor-related fault. However, the aim of this chapter is to use data from the SFTR-1 to investigate the pCCB fault identification method, improve the analysis using a combination of various pCCB components and the combination of various real and imaginary (complex number) pCCB components. Observation of the first few principal components is carried out to investigate the dynamics of the faults in the system. Thereafter, quantification of the faults is presented by comparing the faulty conditions to the baseline RMRU.

7.1 Overview

In chapter six, data fusion of acceleration and velocity features was considered for fault diagnosis in rotating machines. In as much as the fused approach gave good clustering, the novelty is that the approach could present a good diagnosis of the rotor and bearing fault in a single analysis. Notwithstanding the valuable diagnosis achieved in earlier chapters, it is worthy of note that the Fast Fourier Transform (FFT) employed in the analysis uses only amplitude in its diagnosis. Thus, much is not done with the signal phase [25,206]. However, the higher-order spectra (HOS) consider both amplitude and phase in their signal analysis. Therefore, this chapter focuses on a recent area of research for fault diagnosis (FD) in rotating machines: the higher-order bispectrum analysis. Bispectrum analysis has the potential to combine various frequency components in measured vibration signals. An earlier study [21,25,69] developed the poly-coherent composite bispectrum (*pCCB*) approach, which retains both amplitude and phase information and also reduces the rigour of analysing large vibration data due to data fusion of the individual bearings (sensor data fusion). These studies [22,24,25] focused on vibration data measured below the first critical speed. However, this work aims at classifying machine conditions using an earlier approach in diagnosing complex rotating machines (multiple bearings, multiple shaft couplings and running at multiple speeds) operating below and above the machine's first critical speed.

The experiment for this work was based on the same spring-based flexible test rig one (SFTR-1) from chapter six. Four conditions were considered for analysis in this preliminary study using some simulated faults investigated in chapter 6. These faults are a baseline state where no fault is simulated in the test rig, i.e. residual misalignment and residual unbalance (**RMRU**) [21], crack near bearing one (**CBg1**), crack near bearing two (**CBg2**) and rub near disc one (**RubD1**). Three speeds were considered based on the machine's natural frequencies observed from the FRF of the modal testing in chapter 3 subsection 3.4.2, Figure 3.15 and Table 5.3. i.e., 450 rpm (7.5 Hz), 900 rpm (15 Hz), and 1350 rpm (22.5 Hz).

Ten data sets were collected for each condition at three different speeds. The poly-coherent composite bispectrum (pCCB) plots at the three selected speeds and four

machine conditions, i.e., residual misalignment residual unbalance (**RMRU**), crack near bearing one (**CBg1**), crack near bearing two (**CBg2**), rub near disc one (**RubD1**) was investigated. The description of the theory of the poly-coherent composite bispectrum (pCCB) is presented in the methodology chapter in section 4.8.

7.2 Signal analysis and feature selection

This study collects the signals from four bearing pedestals (multiple bearing) using four accelerometers (multiple sensors). The poly-coherent composite bispectrum (pCCB) approach has been developed so that signals multiple sensors are fused during signal analysis [62,25]. The results of these analyses are the pCCB plots in figure 7.1 (a) – (d) to figure 7.3 (a) – (d), which are representations of the three selected speeds respectively, with each showing the four machine conditions that have been investigated (**RMRU**, **CBg1**, **CBg2**, **RubD1**).

Figure 7.1 – 7.3 shows very clear presence of pCCB components at B_{11}, $B_{12} = B_{21}$, $B_{13} = B_{31}$, others include B_{22}, $B_{23} = B_{32}$ and B_{33}. The pCCB component is a function of two frequency components from the pCCS, plotted in the **x**, **y**, and **z** orthogonal axes where **x** and **y** represent the frequencies and **z** is the amplitude of the pCCB components. The presence of B_{11} component shows the relationship between and as seen in equation (6.7), with both equal to the machine running speed, i.e., 1x harmonic. So the B_{11} component shows the relationship between f_l (1x), f_m (1x) and f_l+f_m (2x). Similarly, the presence of $B_{12} = B_{21}$ pCCB component shows the relationship between 1x, 2x and 3x frequency components, while that of $B_{13} = B_{31}$ shows a relationship between 1x, 3x and 4x frequency component[25].

In figure 7.1 (a), the **RMRU** case at 450 rpm, there is the presence of B_{11}, $B_{12} = B_{21}$, $B_{13} = B_{31}$ and a small presence of $B_{23} = B_{32}$ and B_{33}. Figure 7.1 (b) and (c) shows higher of the first few pCCB components, including B_{22} but minimal or no B_{33}. However, figure 7.1 (d) had a high presence of all pCCB components. Figure 7.2 shows the pCCB plots at 900 rpm (15 Hz) for the tested machine conditions. The first few pCCB components i.e., B_{11}, $B_{12} = B_{21}$ and $B_{13} = B_{31}$ were conspicuous. However, figure 7.2 (a) showed very little or no presence of other components. Figure. 7.2 (b), (c) and (d) showed a good presence of B_{22}, $B_{23} = B_{32}$ and B_{33} with the first few components. While figure 7.2 (b)

appeared slightly like figure 7.2 (c), there is a higher amplitude in figure 7.2 (c). On the other hand, Figure 7.2 (d) has B_{11} and other components, but the B_{33} is low. Looking at Figure 7.3, the pCCB plot at 1350 rpm (22.5 Hz), most pCCB components seem to be present. However, figure 7.3 (a) showed higher B_{11}, B_{12}= B_{21} and B_{23} with a low B_{31} and no obvious B_{33}. ***Figure*** 7.3 (b) and (c) had the presence of B_{22} without B_{33}. Figure 7.3 (d), however, had the presence of all components with no visible B_{33}.

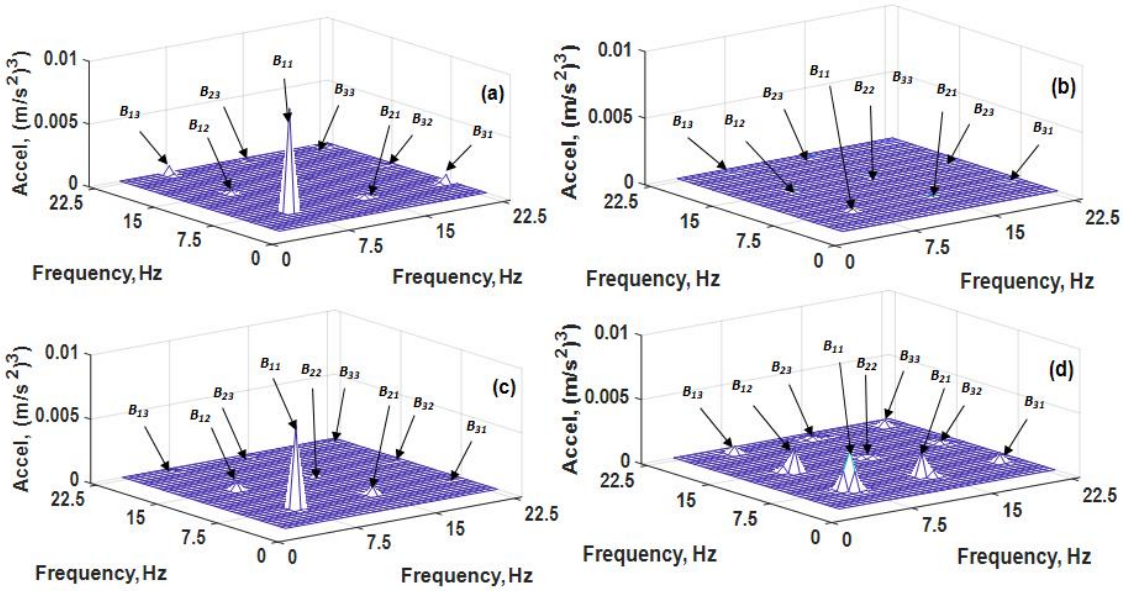

Figure 7. 1 Typical acceleration-based pCCB analysis plots at 450 rpm (7.5 Hz) for (a) RMRU (b) CBg1 (c) CBg2 (d) RubD1.

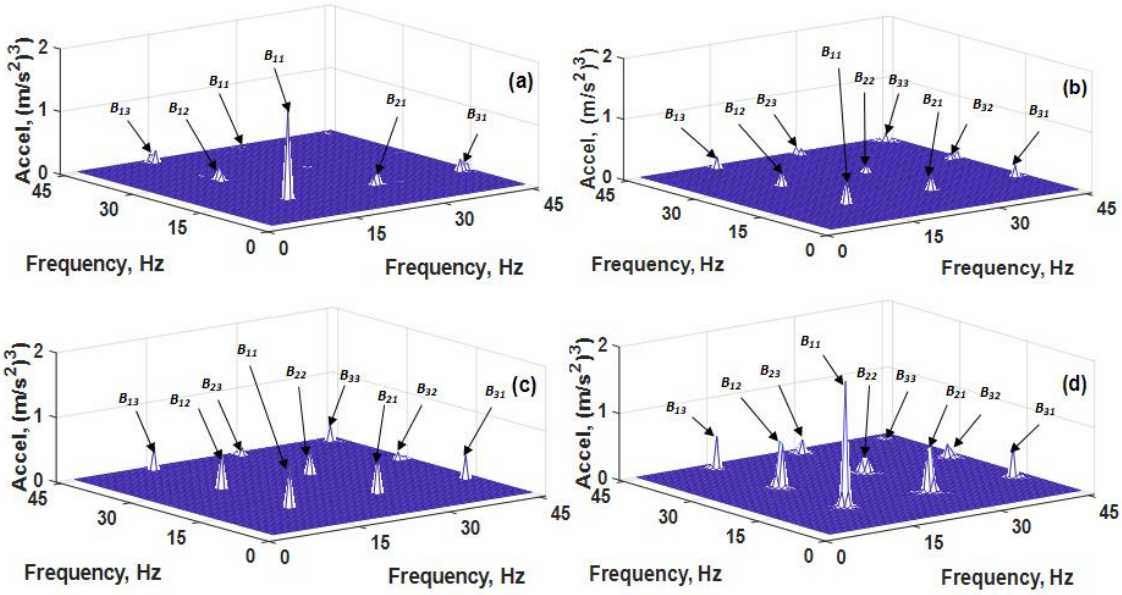

Figure 7. 2 Typical acceleration-based pCCB analysis plots at 900 rpm (15 Hz) for (a) RMRU (b) CBg1 (c) CBg2 (d) RubD1.

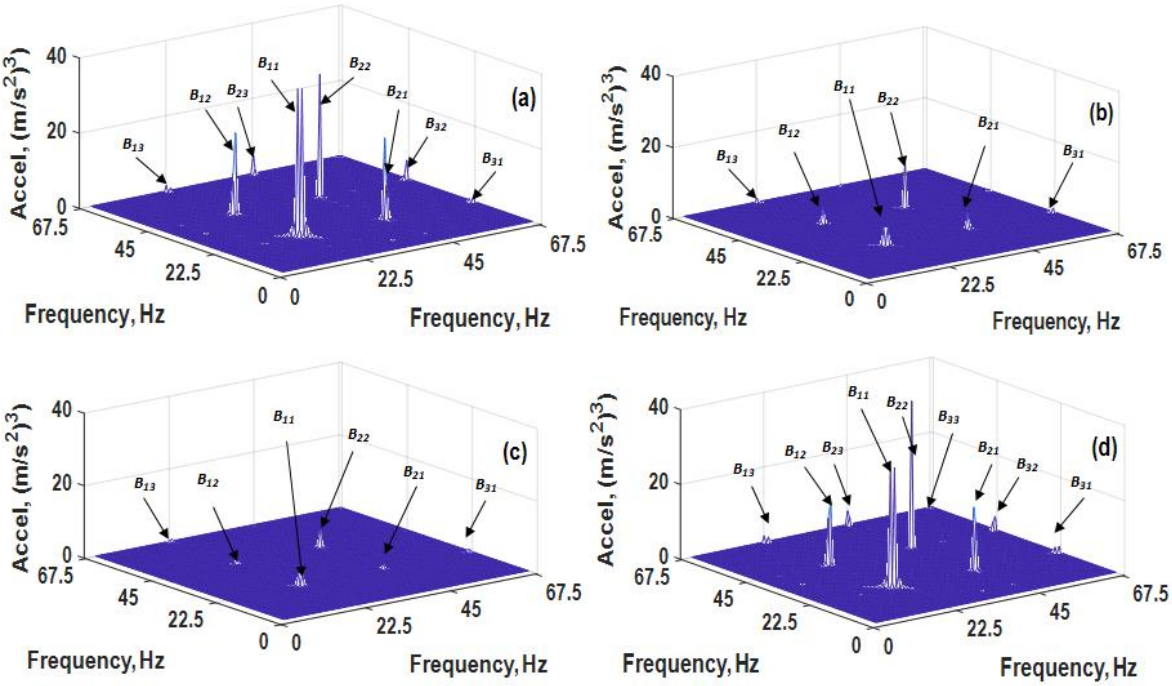

Figure 7. 3 Typical acceleration-based pCCB analysis plots at 1350 rpm (22.5 Hz) for (a) RMRU (b) CBg1 (c) CBg2 (d) RubD1.

The poly-coherent composite bispectrum (pCCB) plots showed the presence of B_{11}, B_{12}= B_{21}, and B_{13} = B_{31} at all speeds and all conditions. The RMRU at 450 rpm (7.5 Hz) and 900 rpm (15 Hz) had very little B_{12}, while that of 1350 rpm (22.5 Hz) had a higher B_{12} but a very small B_{13}. All other faults had the presence of B_{22}, B_{23} = B_{32}, and B_{33}.

The pCCB components gave helpful information about the presence of a particular fault; however, it did not represent the overall state of the machine. Also, with a large set of vibration data, observation of individual plots would be cumbersome, so the classification of the different conditions may give better diagnostic information on the overall machine's health.

7.3 Rotor fault classification using pCCB Components

In this initial study, three pCCB components were extracted for analysis i.e B_{11}, B_{12} = B_{21}, B_{13} = B_{31}. A PCA-based feature classification and fault identification model was developed using the extracted pCCB components. Data matrix developed in the investigation is generally represented in equation (3.42) and (3.43). However, the data matrix for the initial investigation which tried to reaffirm the earlier proposed approach is represented in equation (3.44) and (3.45). Since the 10 sets of vibration signals were measured for different simulated machine conditions, each at 3 speeds, the model contained components from individual conditions, with individual speeds, extracted for input into the matrix. So, with the individual condition and speed using 3 selected pCCB components, a data matrix is created. This model was extended to contain more conditions so that for four conditions, the matrix became 3 x 40, and with the three speeds all fused, a data matrix of 9 x 40 was developed. The built PCA-based model is used to classify the individual health condition of the machine where data were collected below and above the machines' first critical speed.

The classification of the PCA-based pattern recognition model of the various conditions using the data fusion approach at a single speed and multiple speeds is observed. A plot of PC1 versus PC2 helps observe the classification pattern. In the feature arrangement for the data model, no normalization was done since the pCCB components have similar dimensions.

Figure 7.4 shows the result for classifying simulated machine conditions using the developed data combination PCA-model. Figure 7.4 (a) shows the total overlap for all rotor conditions at 450 rpm. However, a zoomed view in Figure 7.5 (a) showed clear separation for all conditions except for overlap between **RMRU** and **CBg2**. As stated in chapter six, the data obtained at 450 rpm may not be the best in fault identification due to low speed.

Also, figure 7.4 (b) showed good clustering and separation for all conditions with little overlap between **RMRU** and **CBg1**. The **RubD1** condition was also observed to have some spread creating a partial overlap in other cases.

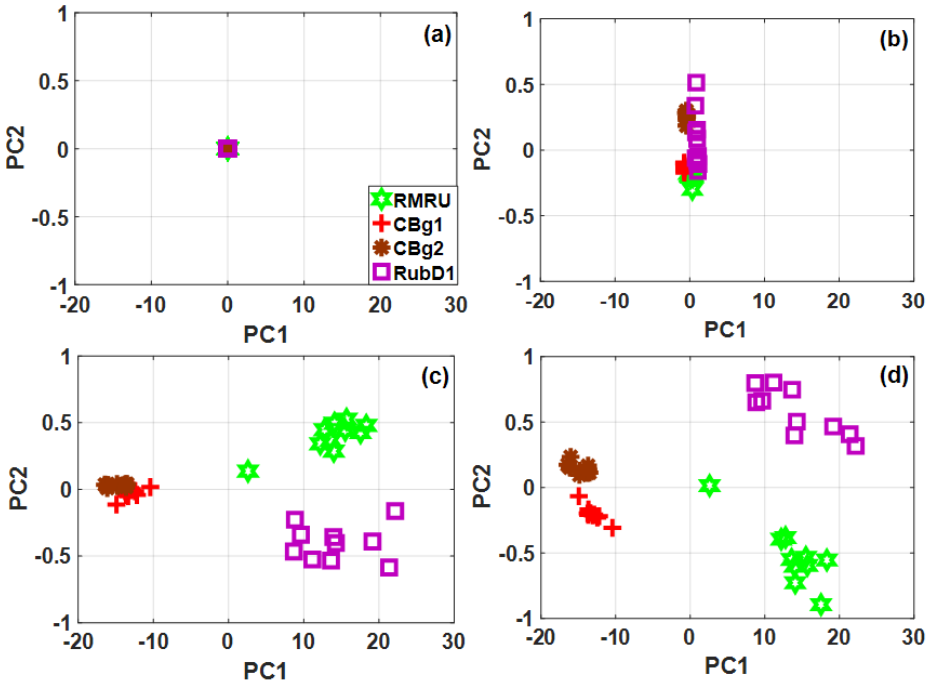

Figure 7. 4 Classification of test rig conditions using pCCB components at (a) 450 rpm (b) 900 rpm (c) 1350 rpm (d) Multiple speeds.

Figure 6.5 (b) is a zoom representation of Figure 6.5 (a). All cases are separated from each other with good clustering and a better view of the spread on **RubD1**. This spread may be because of the touch and run between the Perspex and the shaft during machine operation. Furthermore, Figure 6.4 (c) showed significant clustering and separation for all cases except for the overlap between **CBg1** and **CBg2**. **RMRU** had good clustering, but one data set singles itself to the middle of the plot. The reason for

this is not apparent, as such may be an exception. However, more observations would aid in better understanding such behaviour.

Similarly, Figure 6.4 (d) showed a cluster for all conditions and a better separation than others observed in the UMA and improved approach. The **CBg1** and **CBg2** are still close to each other and around the same region of the plot. The outcome may be due to the similarity in their condition. RMRU at the lower part toward the right of the plot has particular data still seen separated. RubD1 is on the right topmost part of the plot. Thus, the multiple-speed approach for fault diagnosis in rotating machines gave a good and robust classification and fault identification. Normalisation is carried out on the data matrix for the pCCB components, and a plot of the normalised PC1 vs PC2 is presented in Figure 7.6.

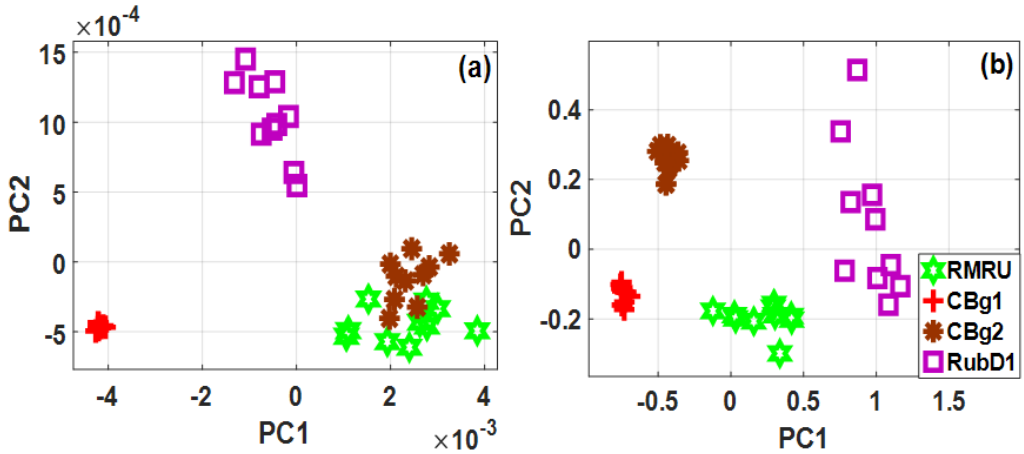

Figure 7. 5 Zoomed view of classified test rig conditions using pCCB components at (a) 450 rpm (b) 900 rpm.

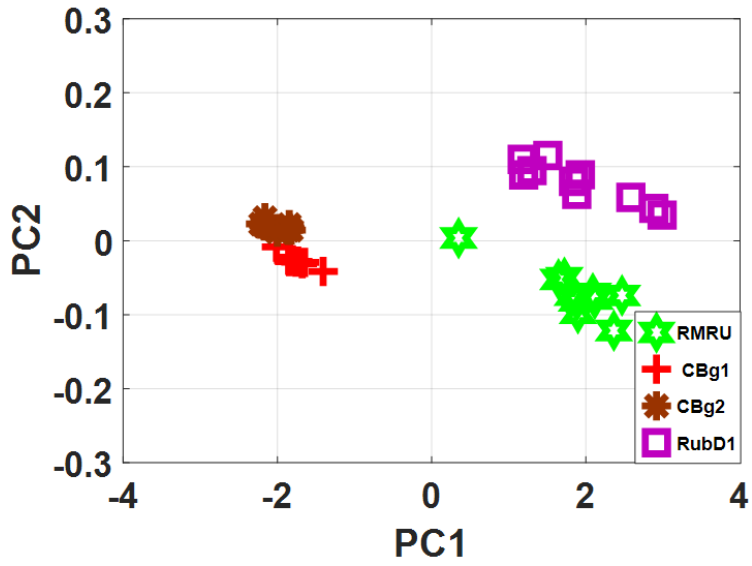

Figure 7. 6 Classification of test rig conditions using normalised pCCB component at multiple speed in a single analysis.

9.6.1 Investigation to improve diagnosis of rotor faults observing the amplitude of pCCB components

Initial investigation extracted only the first 3 pCCB components for its analysis. However, observation from the pCCB plots showed the presence of up to six components. In order to improve the fault identification model, an investigation was carried out on individual pCCB components, checking for their sensitivity to particular machine conditions for effective fault identification. This was done by extracting the various components, as seen on the plots where observation of the most sensitive component helped select features to be used in building up the data matrix for a better diagnosis approach.

7.4.1 Analysis of magnitude of individual pCCB components

Due to pCCB components B_{11} up to B_{33} in the pCCB plots, as shown in Figure 7.1 – 7.3, six pCCB components are selected and investigated to get the most valuable components that present a better understanding of machine dynamic behaviour for fault diagnosis. The pCCB components being investigated are B_{11}, B_{12}, B_{13}, B_{22}, B_{23}, and B_{33}.

The bar charts in figure 7.7 show the plots of the amplitude of the six pCCB components for the selected machine conditions at the three machine running speeds. The bar charts have representations in both 2D and 3D, presenting clear observation,

especially in figures where the component's amplitudes did not appear in the 2D representation. Figure 7.7 (a) showed the 2D representation of pCCB amplitude at 450 rpm (7.5 Hz), Figure 7.7 (b) showed the 3D representation of pCCB components at 450 rpm (7.5 Hz), and Figure 7.7 (c) showed the 2D representation of pCCB components at 900 rpm (15 Hz), Figure 7.7 (d) showed the 3D representation of pCCB components at 900 rpm (15 Hz), Figure 7.7 (e) showed the 2D representation of pCCB components at 1350 rpm (22.5 Hz) and Figure 7.7 (f) showed the 3D representation of pCCB components at 1350 rpm (15 Hz). Observation of Figure 7.7 showed useful amplitude at B_{11} and B_{12} at all running speeds. Overall, some components showed reasonable amplitudes that indicate particular faults, and others showed no useful components for indicating other faults due to their almost insignificant amplitude. Therefore, the amplitude of the components may not be enough to make a judgement on components that is sensitive enough to distinguish machine condition.

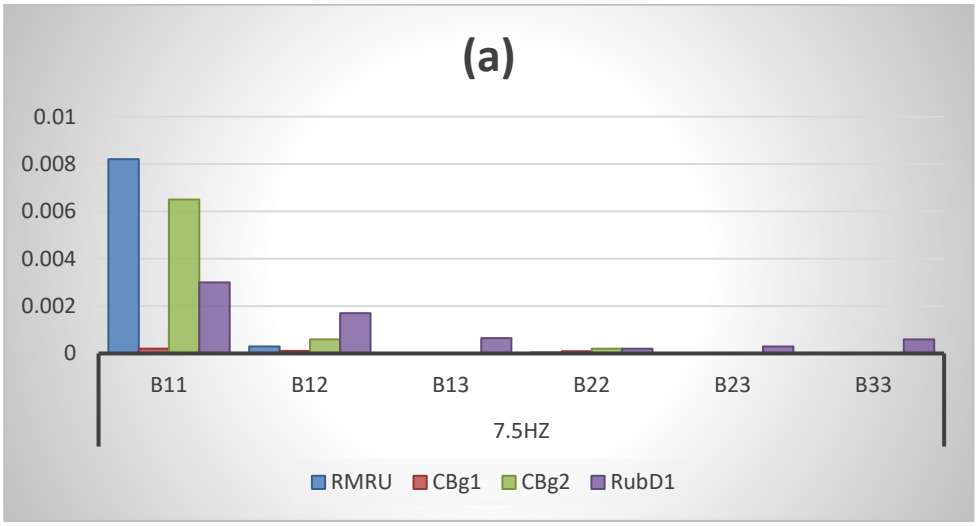

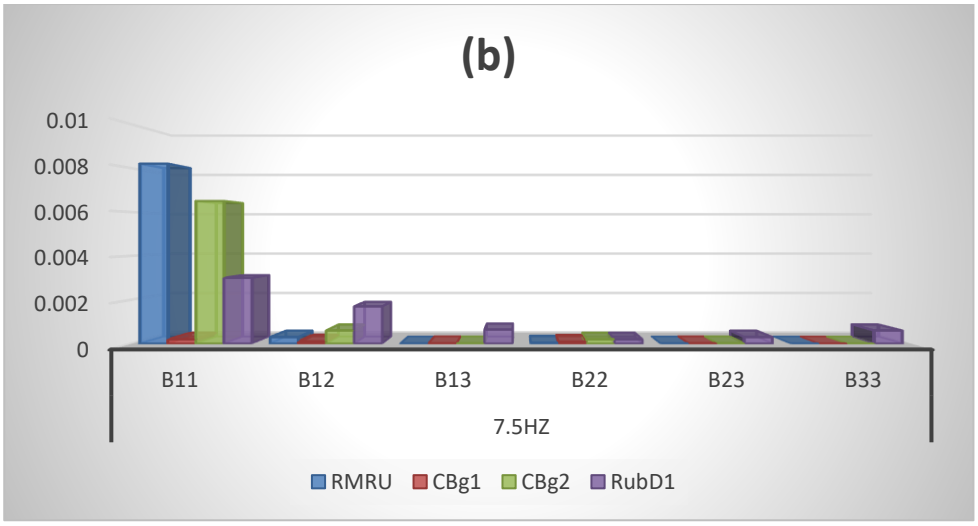
(b)
0.01
0.008
0.006
0.004
0.002
0
B11
B12
B13
B22
B23
B33
7.5HZ
RMRU
CBg1
CBg2
RubD1

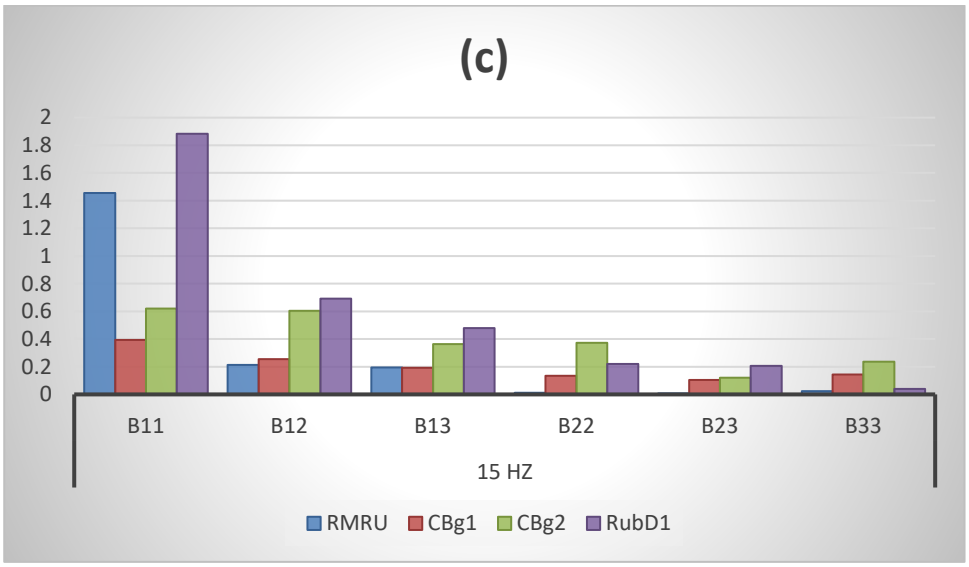
(c)
2
1.8
1.6
1.4
1.2
1
0.8
0.6
0.4
0.2
0
B11
B12
B13
B22
B23
B33
15 HZ
RMRU
CBg1
CBg2
RubD1

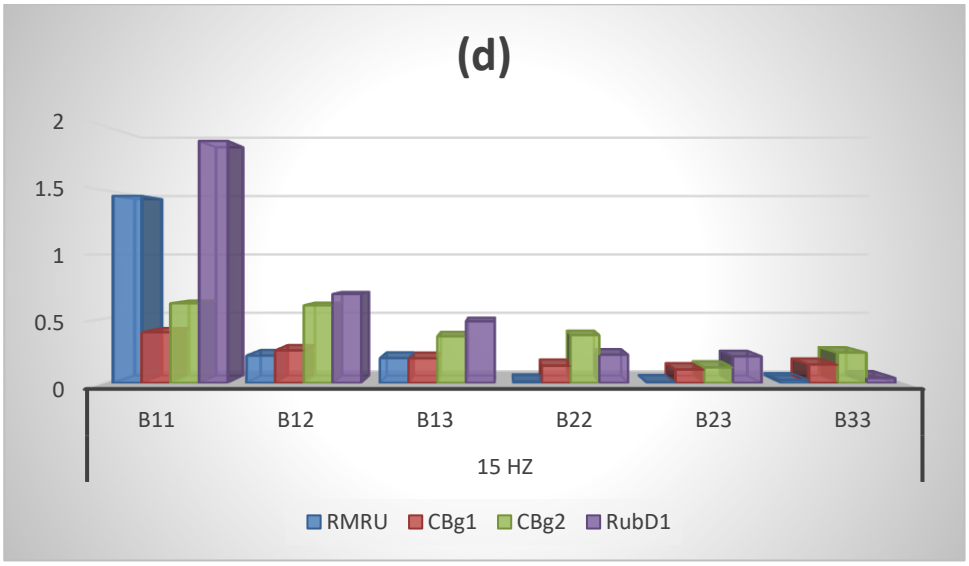
(d)
2
1.5
1
0.5
0
B11
B12
B13
B22
B23
B33
15 HZ
RMRU
CBg1
CBg2
RubD1

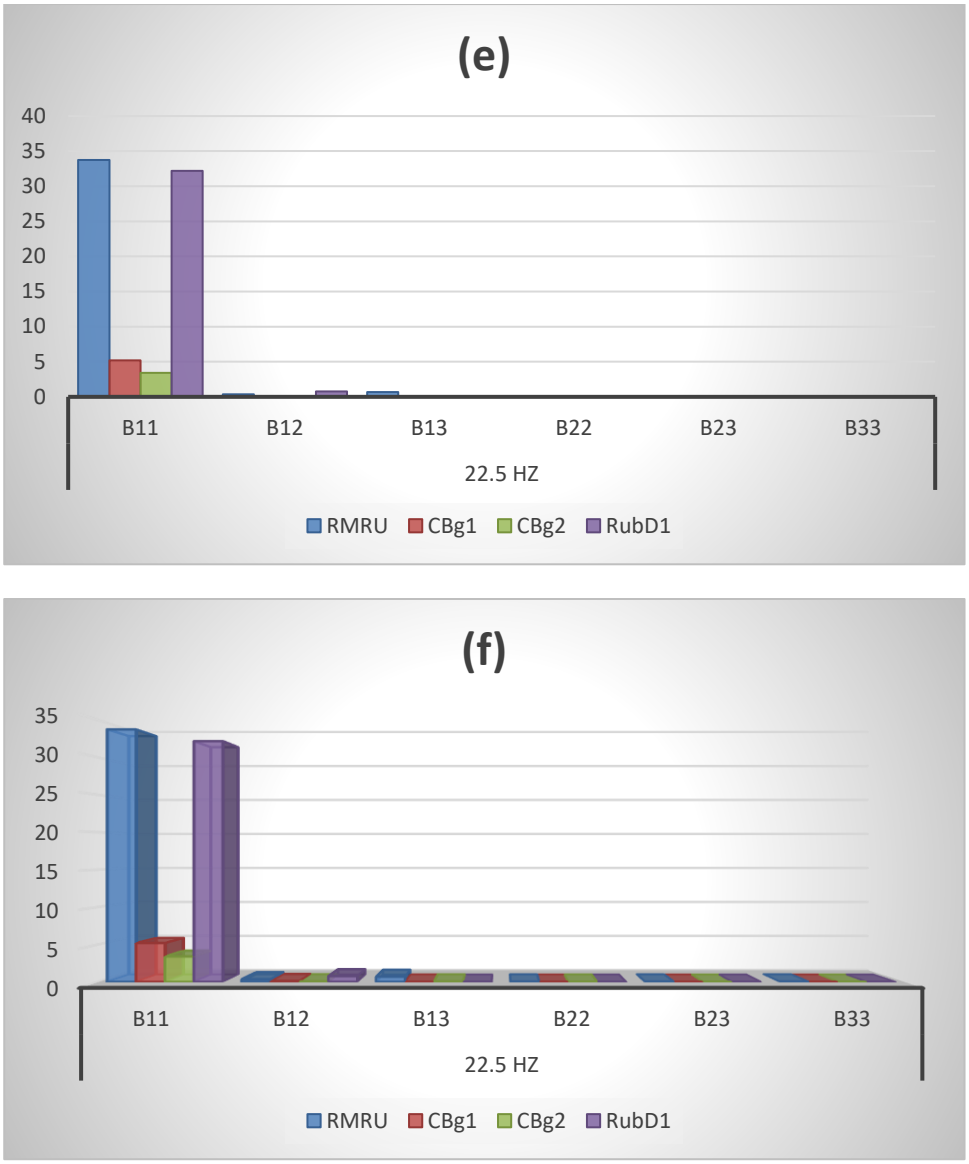

Figure 7. 7 Amplitude of pCCB at (a) 2D representation of 450 rpm (b) 3D representation of 450 rpm (c) 2D representation of 900 rpm (d) 3D representation of 900 rpm (e) 2D representation of 1350 rpm (f) 3D representation of 1350 rp

In order to create a better understanding of the selection of the pCCB components that provide helpful information for fault identification, a PCA-based classification of each pCCB component from the 10 data sets at the multiple speed with PC1 vs PC2 is done. This classification is presented in Figure 7.8 (a) – (f). Observation of Figure 7.8 (a) – (c) showed good separation of the faulty conditions from the healthy ones. Figure 7.8 (b) had some overlap between **CBg1** and **RMRU**, Figure 7.8 (c) showed overlap of all faulty conditions with good separation from **RMRU**, Figure 7.8 (d) showed

separation of all conditions except for the overlap between **CBg2** and **RubD1**. Figures 7.8 (e) and (f) showed an overlap of all conditions. From the observation, B_{11}, B_{12}, B_{13}, and B_{22} showed reasonable separation that makes them useful for further investigation in fault diagnosis. However, quantifying these analyses by distinguishing the faulty condition from RMRU will help establish particular components that show useful sensitivity in machine condition indication. It is presented in subsection 7.42.

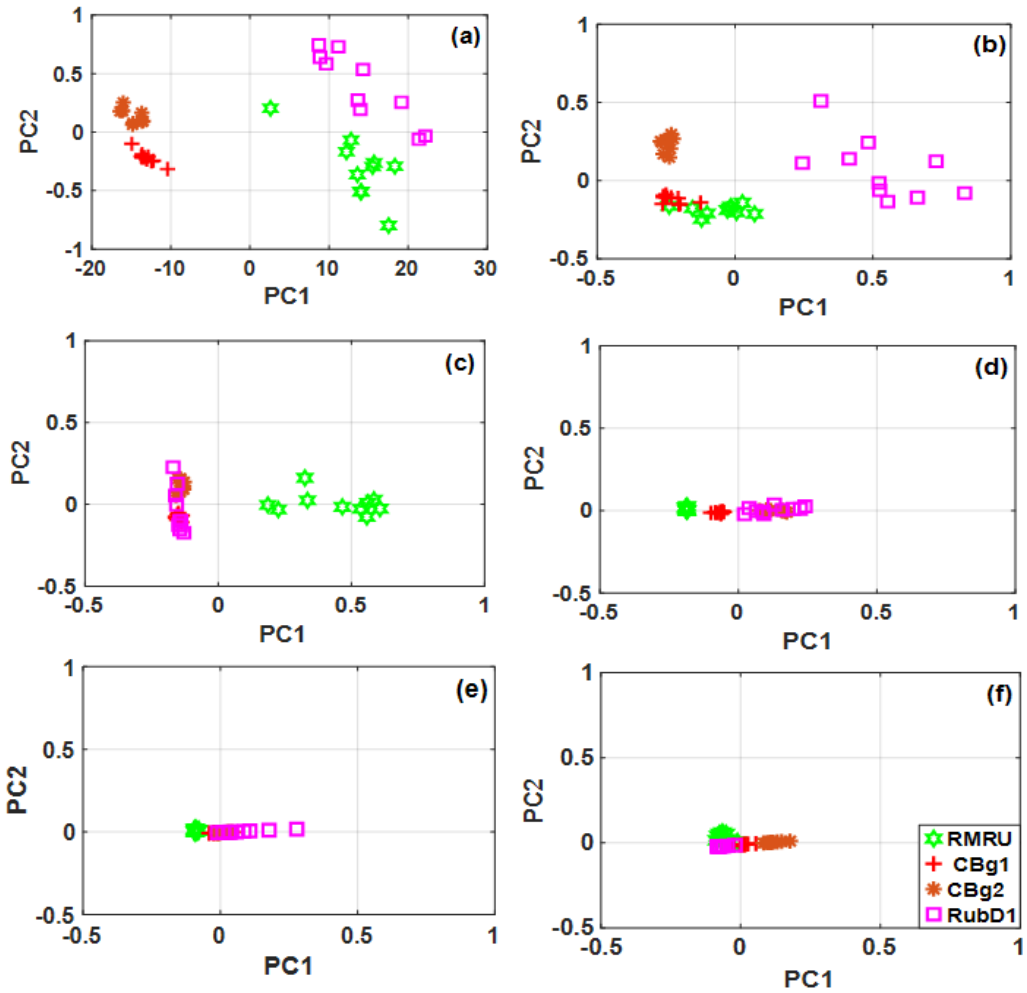

Figure 7. 8 Classification of individual pCCB components at multiple speed for (a) B11 (b) B12 (c) B13 (d) B22 (e) B23 (f) B33.

7.4.2 Data quantification for discriminating faulty conditions from baseline RMRU for the observed pCCB components

Table 7.2 is populated with the values from This has been used to create bar charts in Figure 7.9 presents the results of the separation observed between the faulty and the

baseline RMRU condition. Figure 7.9 (a) showed the bar chart plot for all pCCB components when the faulty separation with respect to RMRU was done. B_{11} gave a very good indication for retaining helpful information. Since the other values are small, a zoomed view with the exemption of B_{11} is presented in Figure 7.9 (b). Observation showed higher values at B_{12}, B_{13} and B_{22}, which makes them useful for fault diagnosis. The separation at B_{23} and B_{33} is very low, so its amplitude would be insignificant in indicating any fault.

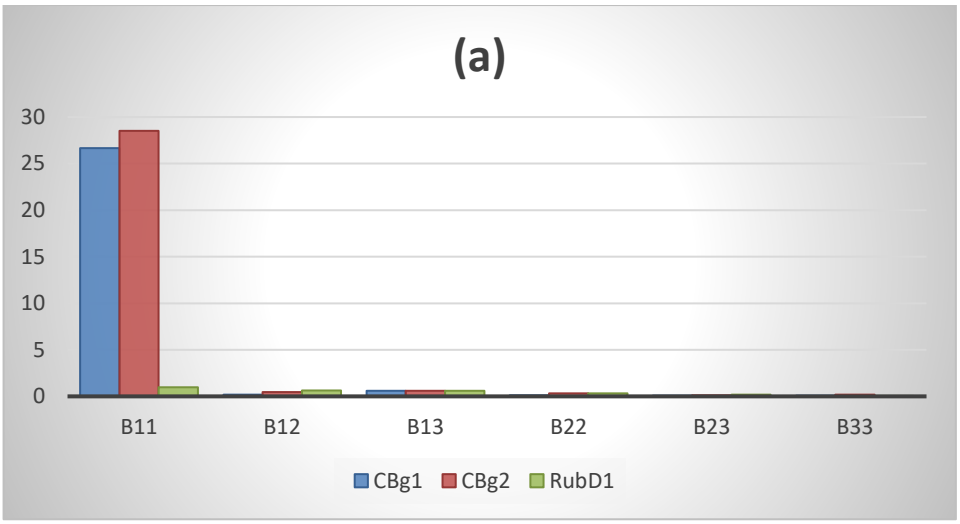

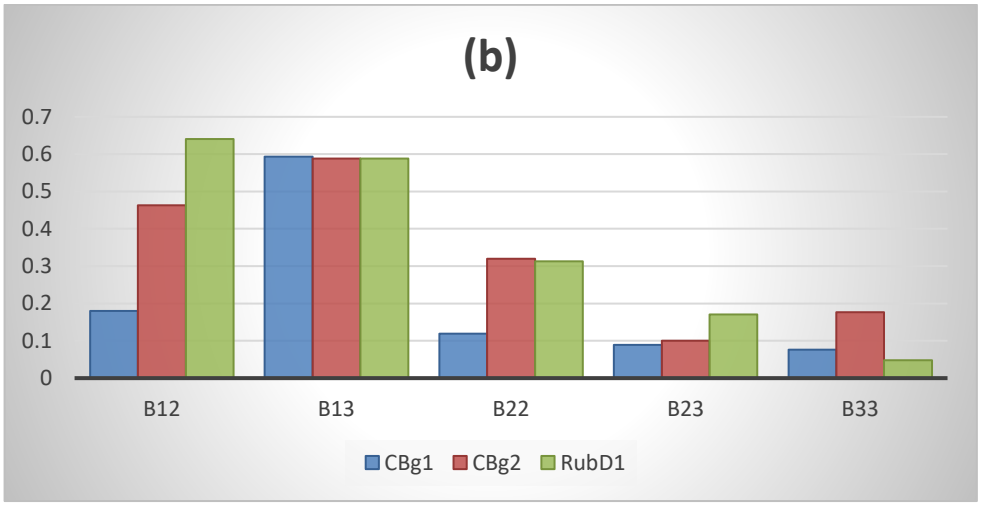

Figure 7. 9 Bar chart showing the comparison of faulty to RMRU for individual pCCB components at multiple speed for (a) All pCCB components selected (b) zoomed view of pCCB components without B11.

Therefore, the investigation thus far has selected the B_{11}, B_{12}, B_{13} and B_{22} for improved rotor fault identification. On the other hand, most rotor faults, such as crack and rub, exhibit 1x and 2x harmonics components. With the combination of two frequencies in the computation of the bispectrum, the 2x harmonic frequency will combine to produce useful diagnosis information in the bispectrum analysis. Thus, adding B_{22}, a combination of 2x, 2x and 4x, is expedient.

7.4.3 Improved fault diagnosis approach using the amplitude of pCCB components

A data matrix was built up for the improved pCCB analysis as represented in equation (3.46), so that with the individual condition and individual speed using 4 selected pCCB components, a data matrix say is created. This model was extended to contain more conditions so that for four conditions, the matrix became 4 x 40, and with the three speeds all fused, a data matrix of 12 x 40 was developed as represented in equation (3.47).

The data matrix was normalised and inputted into PCA-based pattern recognition and a plot of PC1 vs PC2 carried out. Figure 7.10 shows the improved classification of pCCB components for rotor fault identification in rotating machines. This classification was also normalised, and observation showed improved analysis compared to the initial investigation using three pCCB components. This improvement is seen by comparing the earlier pCCB classification in Figure 7.6 with the increased pCCB component classification in Figure 7.10. The latter showed increased separation between the investigated conditions. Quantification of the various condition would help establish this observation. Since the pCCB components have been used to improve fault classification, the complex number (real and imaginary) components which retain the phase information are also considered to improve fault identification.

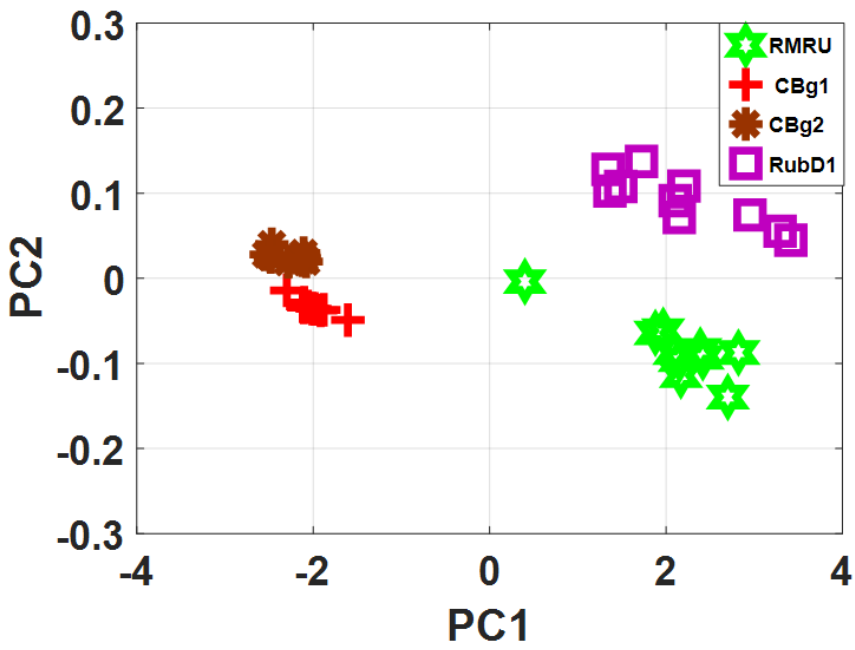

Figure 7. 10 Improved classification of machine condition using increased pCCB components.

7.5 Comparison of magnitude to real and imaginary improved pCCB components analysis

The improved classification of machine conditions with an increased number of pCCB components for rotor fault identification has been achieved in section 7.4. However, pCCB is a complex number which retains both amplitude and phase in its computation and has a real and imaginary component. Therefore, an investigation into the classification pCCB real and imaginary components was carried out. Afterwards, a comparison of the amplitude of pCCB components with this complex number component is observed.

7.5.1 Feature arrangement for real and imaginary pCCB component for rotor faults

In this study, selected features are based on the frequency coupling corresponding to the machine rotating frequency components and higher components that show sensitivity in rotor fault detection. The selected features are $\boldsymbol{B_{11}}$, $\boldsymbol{B_{12}}$, $\boldsymbol{B_{13}}$ and $\boldsymbol{B_{22}}$.

Equation. (3.46) and (3.47) represents the pCCB amplitude components having a data matrix of 12 x 40 and equation. (3.48) represents the real and imaginary pCCB components with a matrix of 12 x 80 at integrated multiple speeds for all conditions. The computed data matrix was normalised and inputted into a PCA-based

algorithm where a plot of PC1 vs PC2 gives a representation for rotor fault identification and classification.

7.5.2 Rotor fault classification and observation

Figures 7.11 (a) and (b) show the PCA-based pattern recognition and classification approach, comparing the amplitude with the real and imaginary pCCB components. The plots show a clear separation between individual components for both the amplitude and the real and imaginary plots observed for each rotor condition. However, the real and imaginary pCCB component plots showed further separation from individual conditions than the amplitude pCCB components.

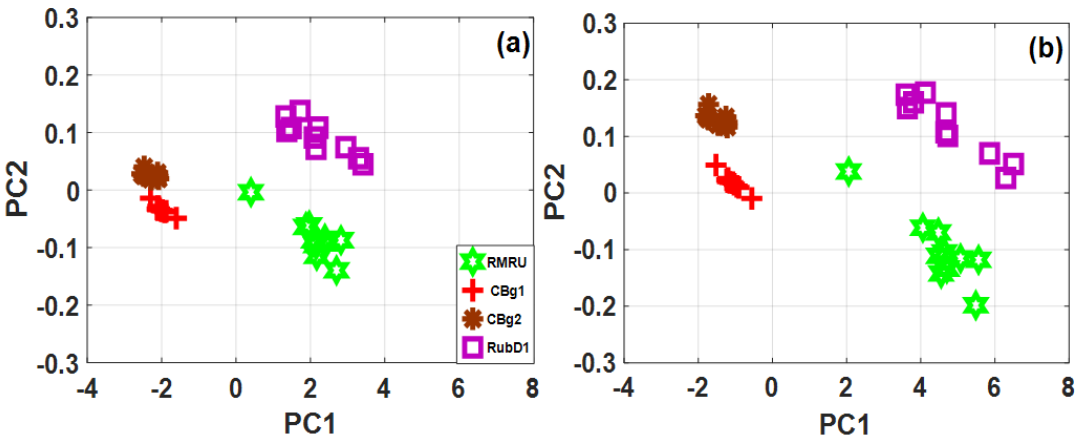

Figure 7. 11 Improved classification of test rig conditions in a single analysis for (a) Amplitude of pCCB components (b) Real and Imaginary of pCCB components.

7.6 Overall comparison of PCA-based rotor faults diagnosis using pCCB components for improved classification

This section compares the initial, the improved and the real and imaginary pCCB component analysis with a comparison of the PCA-based classifications, i.e., PC1vsPC2 and PC1vsPC2vsPC3 plots. Figures 7.12 (a), (c) and (e) showed the PC1vsPC2 plots for the initial, the improved and the real and imaginary pCCB component analysis, and Figures 7.12 (b), (d) and (f) showed the PC1vsPC2vsPC3 plots for the three pCCB components configuration. Overall observation showed that the real and imaginary pCCB component plots had further separation for the individual rotor conditions than the initial and improved analysis. However, it is not clear from the plots between PC1vsPC2 and PC1vsPC2vsPC3, which gives better separation. Therefore subsection

7.6.1. discussed the quantification approach, where the differentiation between the faulty case and the baseline RMRU condition was observed.

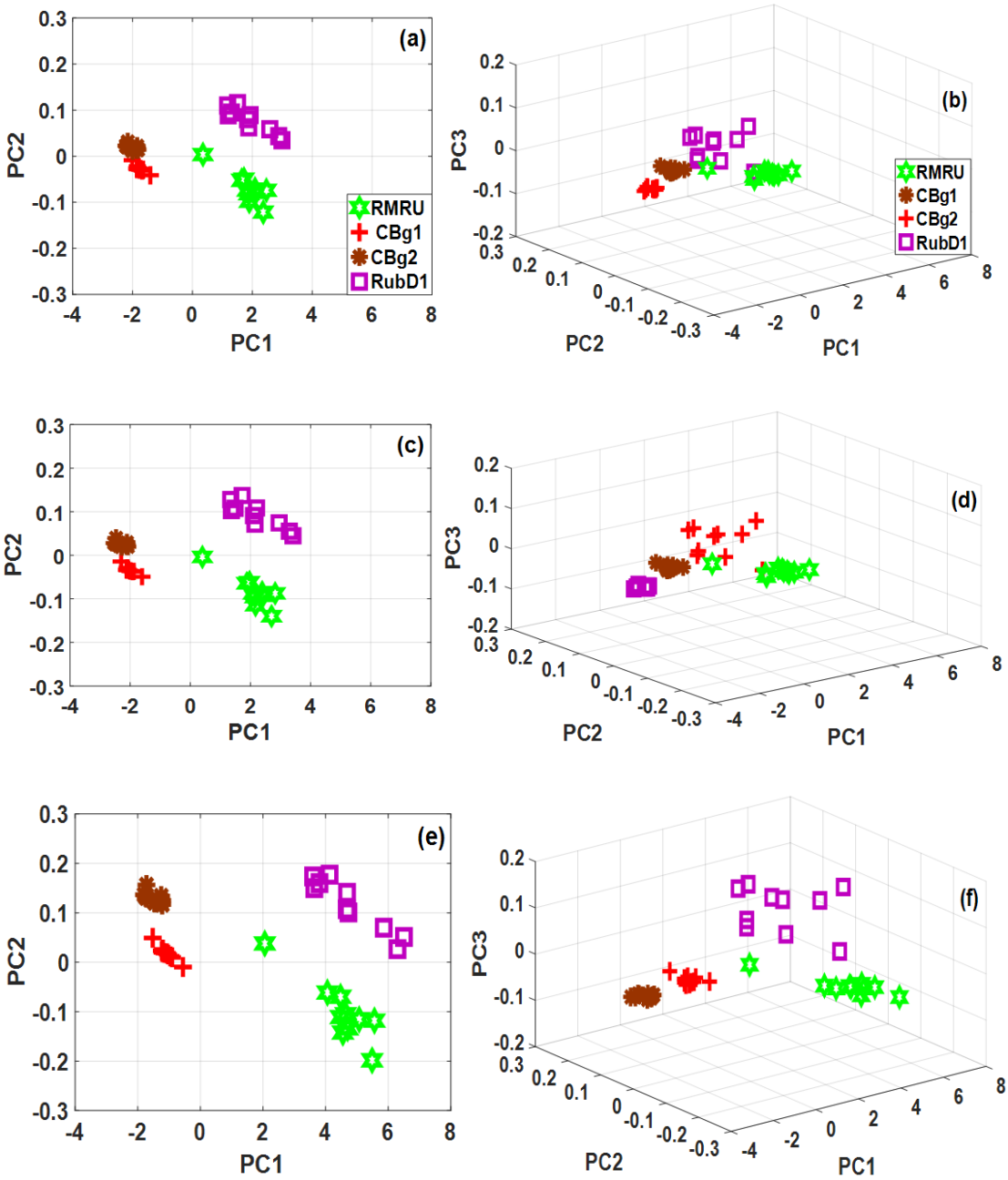

Figure 7. 12 Comparison of test rig conditions using classification of selected pCCB components at multiple speed for single analysis at (a) Initial amplitude of pCCB component for PC1vsPC2 (b) Initial amplitude of pCCB component for PC1vsPC2vsPC3 (c) Improved amplitude of pCCB components for PC1vsPC2 (d) Improved amplitude of pCCB component for PC1vsPC2vsPC3 (e) Real and imaginary pCCB components for PC1vsPC2 (f) Real and imaginary pCCB component for PC1vsPC2vsPC3

7.6.1 Differentiating faulty conditions from baseline RMRU for data quantification

The differentiation between the faulty and RMRU conditions is presented in this section. Figure 7.13 shows the differentiation of the faulty from baseline RMRU condition for PC1vsPC2 and PC1vsPC2vsPC3. The figure represents the quantification of the simulated fault by comparing the separation between RMRU and each fault in the single analysis. In Figure 7.13, the classification for PC1vsPC2 showed increased separation at real and imaginary pCCB components compared to the improved and initial approach. Similarly, the classification for PC1vsPC2vsPC3 showed increased separation at the real and imaginary pCCB than those of the improved and initial pCCB classification. Also, the PC1vsPC2vsPC3 classification showed more separation in all cases than in PC1vsPC2. Thus, the real and imaginary pCCB classification at PC1vsPC2vsPC3 gave a better indication for fault identification in diagnosing rotating machines.

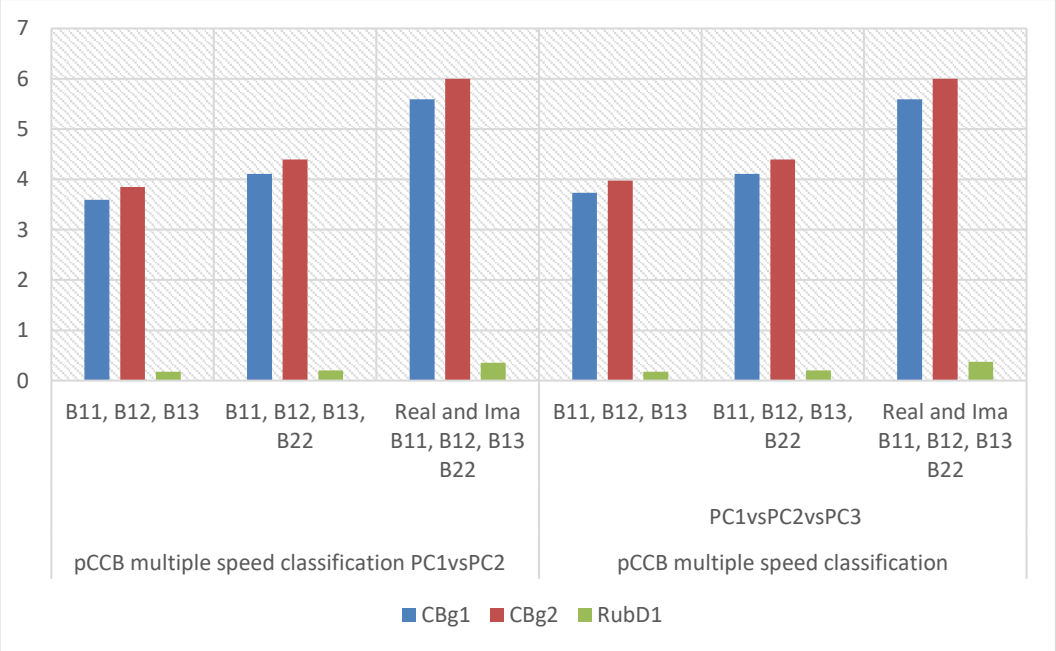

Figure 7. 13 A comprehensive bar chart representing a differentiation of faulty from RMRU condition at PC1vsPC2 and PC1vsPC2vsPC3.

7.7 Chapter summary

This Initial investigation considered an earlier proposed poly-coherent composite bispectrum (pCCB) analysis in diagnosing rotor-related faults in rotating machines. Vibration data used in this study were obtained from the spring-based flexible test rig 1 (SFTR-1) focusing on four conditions, i.e., **RMRU**, **CBg1**, **CBg2** and **RubD1**.

Poly-coherent composite bispectrum (pCCB) plots were generated using measured vibration acceleration data when the test rig ran below and above its first critical speed for all four conditions. There were visible peaks at $\boldsymbol{B_{11}}$***,*** $\boldsymbol{B_{12}}$***, and*** $\boldsymbol{B_{13}}$**.** These were considered to build a matrix for input to PCA. Investigation shows reasonable separation and clustering between each condition. The classification showed the usefulness of this diagnosis approach, as indicated in an earlier study.

Further investigation improved the classification approach using more pCCB components, which now had $\boldsymbol{B_{11}}$***,*** $\boldsymbol{B_{12}}$***,*** $\boldsymbol{B_{13}}$ and $\boldsymbol{B_{22}}$**.** The improved pCCB components classification showed further separation than the initial pCCB components classification. Since the pCCB is a complex number, its real and imaginary aspect was considered for analysis to improve its diagnosis capability further. The result showed that the real and imaginary PCCB component analysis gave much more separation of all conditions. Thus, producing a better diagnosis of rotor faults than the other pCCB classification methods. A comparison of varying PCA plots, i.e., PC1vsPC2 to PC1vsPC2vsPC3, was observed to check for diagnosing information with more PCs, but the outcome did not expressly show distinct separation. However, the real and imaginary pCCB classification showed more separation of the simulated conditions than the initial and improved approach. Hence, more diagnostics information could be present in the real and imaginary pCCB classification features. In order to establish this observation, a data quantification approach was made to represent the value of each fault by differentiating them with respect to the baseline RMRU. However, their values showed that the PC1vsPC2vsPC3 had a slightly high value for the real and imaginary pCCB component classification than the others.

Thus, the efficiency of the pCCB approach from an earlier study has been validated in this study. The improved pCCB approach also indicated the likelihood that additional pCCB components improve the diagnosis model. Such as the harmonic components on

the faults being investigated. For instance, the presence of 2x and 4x components in rub faults can be easily indicated in the $\boldsymbol{B_{22}}$ pCCB component. The real and imaginary pCCB classification approach shows some novelty as it retained useful indication for the diagnosis of rotor faults in rotating machines from the comparison with the earlier and improved pCCB approach.

These classification approaches can be transferred to the industry for validation. However, since this study aims to cover an extensive range of rotating machines' critical parts faults in a single analysis, the incorporation of bearing faults into these approaches is considered in the next chapter.

CHAPTER 8

ACCELERATION-BASED TIME DOMAIN AND POLY-COHERENT COMPOSITE BISPECTRUM (AT-pCCB) APPROACH FOR ROTOR AND BEARING FAULT IDENTIFICATION

This chapter proposes a novel acceleration-based time domain and poly-coherent composite bispectrum (AT-pCCB) in the identification of rotating machines' critical parts (rotor and bearing) faults. This is a build-up from chapter 7 where only rotor faults were investigated using poly-coherent composite bispectrum (pCCB) approach. This chapter incorporates bearing acceleration time domain features into the model. Acceleration features from time domain analysis and pCCB components are fused to carry out diagnosis of an extensive range of faults. In the proposed dFAVF method, features of acceleration and velocity were combined for classification, however, a robust but simple fault identification approach is in continuous demand. This chapter therefore advances investigation with the aims of applying feature reduction approach to the fusion of hybrid data in classification of extensive range of faults in rotating machine critical parts. The fusion of acceleration features and pCCB components was observed in two sub-scenarios i.e., the acceleration-based time domain and amplitude of the pCCB (AT-ApCCB) and the acceleration-based time domain with real and imaginary pCCB components (AT-RIpCCB). Observation of the first few principal components (PCs) and quantification of machine conditions by comparing faulty to baseline RMRU was investigated.

8.1 Overview

Studies in chapter seven presented a new approach to the analysis of poly-coherent composite bispectrum (pCCB), which developed from composite spectrum [25,63] and bispectrum [29,34,53,64-65] analysis in earlier research. This chapter considers a new feature reduction hybrid model where data fusion is done using acceleration-based time domain features and pCCB components from vibration signals for a consolidated rotor and bearing fault identification. Section 8.2 gives an overview of the novel approach, i.e., data fusion of acceleration and velocity features (dFAVF) and poly-coherent composite bispectrum (pCCB) approach, both improved and combined real and imaginary components. A proposed novel acceleration-based time-domain and poly-coherent composite bispectrum (AT-pCCB) component are discussed and investigated in section 8.3. The novel approach was from studies in chapter six, where the fusion of the time domain and frequency domain parameters was carried out. Pattern recognition and fault classification is presented with results and observations in section 8.4. After that, the differentiation of faulty conditions with respect to baseline RMRU condition is presented in section 8.5.

8.1.1 Previous studies with analysis using dFAVF and pCCB components

In the current research, initial work proposed the novel data fusion of acceleration and velocity features (dFAVF) model for consolidated rotor and bearing fault identification in analysing a single with outstanding classification using signals from the spring-based flexible test rig 1 (SFTR-1). This model consisted of an acceleration-based time domain, i.e., **RMS, CF, Ku**, and velocity-based frequency domain parameters **1x** – **5x** harmonic components and the SE. These parameters were seen to possess sensitive features for various machine condition classifications, even though they may not give the best diagnosis on an individual basis. The acceleration features are useful for bearing fault diagnosis, and the velocity features gave good rotor-related fault diagnosis. Observation of results showed good clustering of individual conditions and separation between not just rotor and bearing but amongst most of the faults. The dynamics of these faults may be better understood from their frequency range. The distinct separation between the rotor-related and bearing fault may be because of their

frequency ranges which are a low-frequency range for the rotor and a high-frequency range for bearing faults.

The further investigation focused on higher order poly-coherent composite bispectrum (*HOpCCB*) analysis of the signal from the spring-based flexible test rig 1 (SFTR-1). The pCCB plots for three selected speeds were observed. Amplitude from selected pCCB components was used to classify rotor faults with helpful diagnosis. Further investigation improved the classification of pCCB components where additional components provided useful diagnostic features, especially for crack shaft and shaft rub faults. Since pCCB retains both amplitude and phase, it thus has a complex number representation. Consideration of the complex number of the pCCB component led to a proposed real and imaginary pCCB components classification. Comparing the amplitude to real and imaginary features showed that the latter had further separation of the tested faulty condition compared to the improved or initial approach. Worthy of note is that only rotor faults, i.e., crack and rub faults, were considered in this diagnosis. Also, the pCCB analysis involves the fusion of signals from multiple sensors (multiple bearing pedestal) and the combination of two frequency components. It makes available more diagnostics information than the simple spectrum. Also, bearing diagnosis is effective using time domain kurtosis (Ku) and crest factor (CF) due to their ability to indicate impulsiveness, which is the characteristic of bearing defects.

8.1.2 Current study and newly proposed approach

Considering the usefulness of the acceleration time domain parameter for bearing diagnosis and the improved pCCB components for rotor diagnosis, a combination of acceleration-based time-domain features and pCCB frequency domain components could provide improved diagnostic information for identifying both rotor and bearing faults in a single analysis. This combination is used to propose a novel fault identification approach. Data preparation and model setup for principal component analysis (PCA) classification for the proposed fault identification approach is presented in section 8.3. The result from the observation of PCA plots is further quantified in section 8.4. The quantification is done to establish the usefulness of the proposed method.

8.2 Feature selection and organisation for combine acceleration-based time domain and frequency-based pCCB for fault diagnosis

As discussed in section 8.1, the proposed novel acceleration-based time domain and poly-coherent composite bispectrum (AT-pCCB) model would provide a consolidated machine critical part (rotor and bearing) fault identification in a single analysis. The data matrix in this section was represented in chapter three, section 3.10. In this study, the following features are considered, i.e., acceleration-based time domain kurtosis (Ku), crest factor (CF) and root mean square (RMS) and poly-coherent composite bispectrum (pCCB) frequency domain features, i.e., $\boldsymbol{B_{11}}$, $\boldsymbol{B_{12}}$, $\boldsymbol{B_{13}}$ and $\boldsymbol{B_{22}}$. The model is developed so that acceleration-based time domain bearing defect features and poly-coherent composite bispectrum components (AT-ApCCB) are fused for classification as represented in equation (3.49). On the other hand, the bearing defect features are fused with the real and imaginary poly-coherent composite bispectrum component (AT-RIpCCB) as represented in equation (3.50). This fusion is done to observe the most suitable approach for a consolidated rotor and bearing fault identification. It should be noted that only 10 sets of vibration data and six machine conditions were considered in this chapter. The six conditions are **RMRU**, **CBg1**, **CBg2**, **RubD1**, **Bg1Cg**, **Bg2Cg**.

These matrices are individually normalised and inputted into a PCA-based algorithm where a plot of PC2vsPC1 and PC2vsPC1vsPC3 gave a representation for a consolidated rotor and bearing fault identification and classification using the acceleration-based time domain with pCCB component (AT-pCCB) model.

8.3 Pattern recognition using proposed AT-pCCB approach for a consolidated rotor and bearing fault diagnosis

The PCA-based pattern recognition approach is used in classifying machine conditions using the acceleration-based time domain with a poly-coherent composite bispectrum (AT-pCCB) model. This model was developed to have alternatives called sub-models for this study. The sub-model comprises the combined acceleration-based time-domain features with amplitude of poly-coherent composite bispectrum components (AT-ApCCB) and the combined acceleration-based time-domain features with real and imaginary poly-coherent composite bispectrum components (AT-RIpCCB). These two sub-models are developed to compare both approaches for the consolidated rotor and

bearing fault identification. The user can determine which is suitable for their diagnosis based on the available parameters. Subsection 8.3.1 and 8.3.2 presents the diagnostics approach for AT-ApCCB and AT-RIpCCB models, respectively. Data matrix **B** which is made up of rotor pCCB components is 9 x 40 while that of **K** which is made up of bearing time domain features is 9 x 20. The integration of **B** and **K** gives a data matrix **D** which is 18 x 60. This matrix **D** provides classification of machine condition for the AT-ApCCB model. Therefore, equation (3.50) which is data matrix **E,** is made up of 27 x 100. The computed data matrix **D** represents the acceleration-based time-domain with amplitude of pCCB components (AT-ApCCB) while **E** represents the acceleration-based time-domain with real and imaginary pCCB components (AT-RIpCCB).

8.3.1 Machine condition classification using AT-ApCCB

This section investigated machine conditions such as baseline **RMRU**, **CBg1**, **CBg2, RubD1**, **Bg1Cg** and **Bg2Cg** using the proposed AT-ApCCB sub-model. Here, signal processing has been carried out based on analysis from chapters six and seven. Figure 8.2 and Figure 8.3 shows the PCA-based pattern recognition of the combined acceleration-based time-domain with amplitude of the pCCB (AT-ApCCB) model for the selected rotor and bearing faults classification in a single analysis. Figure 8.1 shows clustering for all conditions with overlap between **RMRU** and **RubD1** and, **CBg1** and **CBg2,** all of which are rotor conditions. Also, clusters of **Bg1Cg** and **Bg2Cg,** the bearing faults, appeared towards the right of the plot, separated from the rotor faults. However, the overlap between **CBg1** and **CBg2** may show good separation when the cases are viewed closely.

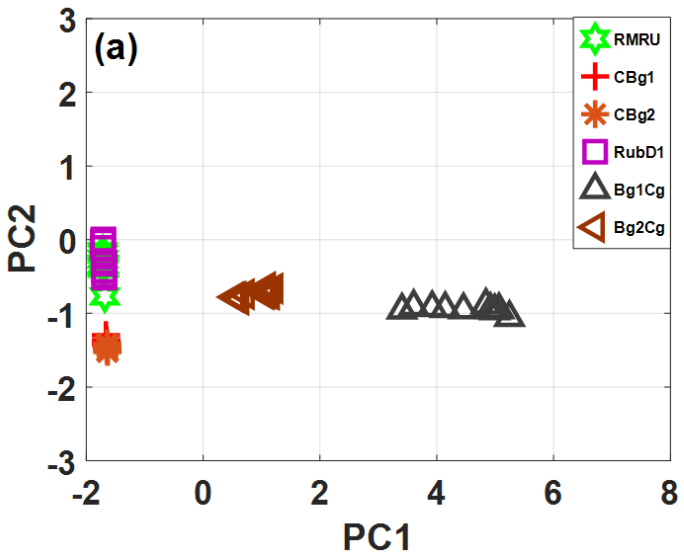

Figure 8. 1 Classification of acceleration-based time domain with amplitude of pCCB (AT-ApCCB) for rotor-related and bearing faults (PC1sPC2).

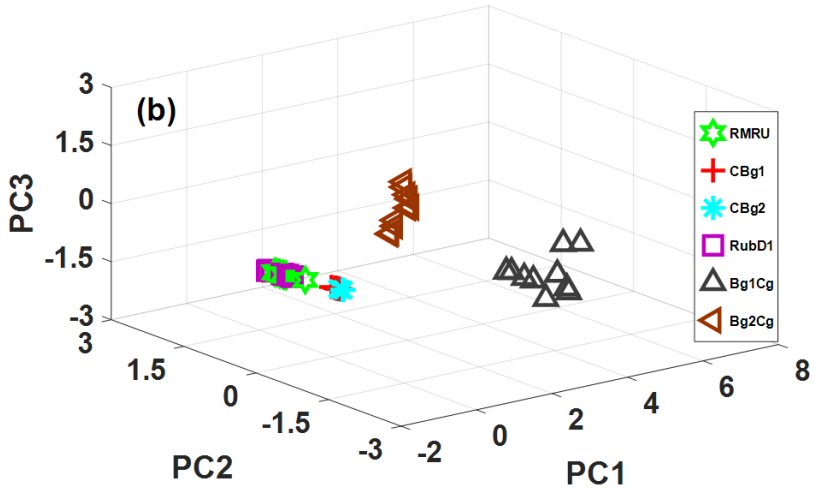

Figure 8. 2 Classification of acceleration-based time domain with amplitude of pCCB (AT-ApCCB) for rotor-related and bearing faults (PC1sPC2vsPC3).

Figure 8.2 represents the pattern recognition PCA-based approach with the inclusion of more PCs in its classification. Observation gives the 3D view PC1vsPC2vsPC3 of the classified condition. The two bearing cases are behind towards the back of the plots, and the rotor faults are in front. As can be observed, the plot in Figure 8.2 gave a different perspective from the plot in Figure 8.1. They both contributed to understanding the behaviour of the fault even with the use of hybrid features from

time and frequency domain parameters. In order to clarify which plots gave a better indication of a machine fault condition, differentiation of faulty with respect to **RMRU** condition is investigated in section 8.4.

8.3.2 Machine condition classification using AT-RIpCCB

This sub-section is an extension of the study in sub-section 8.3.1. However, it shows the analysis of PCA-based pattern recognition with the incorporation of the real and imaginary components of the pCCB into the model. This incorporation, seen as a sub-model for this study, is the combined acceleration-based time-domain with real and imaginary poly-coherent composite bispectrum (AT-RIpCCB) model. Figure 8.3 and Figure 8.4 showed the PCA-based pattern recognition for the AT-RIpCCB model. Observation of Figure 8.3 showed some difference from that of 8.1. The clustering was observed in all cases, like in Figure 8.2, and the overlap of the rotor cases is similar. However, the **Bg1Cg** case seems to spread out more and tends towards the bottom of the right side of the plot. Overall, observation showed a separation between individual cases.

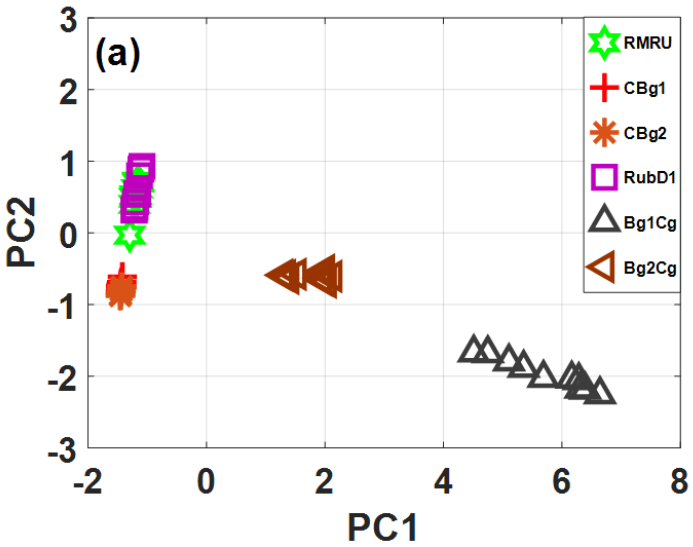

Figure 8. 3 Classification of consolidated rotor-related and bearing faults for acceleration-based time domain to real and imaginary pCCB (AT-RIpCCB) (PC1sPC2).

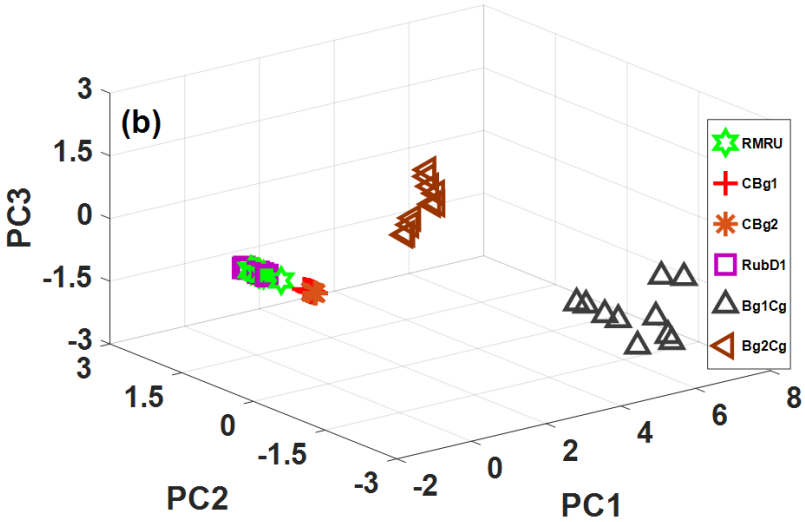

Figure 8. 4 Classification of consolidated rotor-related and bearing faults for acceleration-based time domain to real and imaginary pCCB (AT-RIpCCB) (PC1sPC2vsPC3).

The observation of Figure 8.4 is like that of Figure 8.3. However, in comparison with Figure 8.3, there seemed to be a further separation between the bearing conditions with more spread in **Bg1Cg**. As stated above, the 3D view in Figure 8.4 helps to give a different view of the PCA plot, which also provides some improved diagnostic features as the plots with more PCs tend to give better separation between some cases. Observation of the separation of faulty with respect to RMRU conditions while

comparing the separation for PC1vsPC2 and PC1vsPC2vsPC3 is carried out in section 8.4 for both sub-models.

8.4 Data quantification for differentiation of faulty conditions with from baseline RMRU for AT-pCCB fault identification approach

The comparison of the separation of faulty to RMRU conditions has proven to show the usefulness of various approaches in this study. It has also helped to imply how severe a fault may be considering its distance from the baseline state. The bar chart in Figure 8.5 is a graphical representation of the differentiation of faulty from baseline RMRU condition for the proposed AT-ApCCB and AT-RIpCCB when classified using PC1vsPC2 and PC1vsPC2vsPC3.

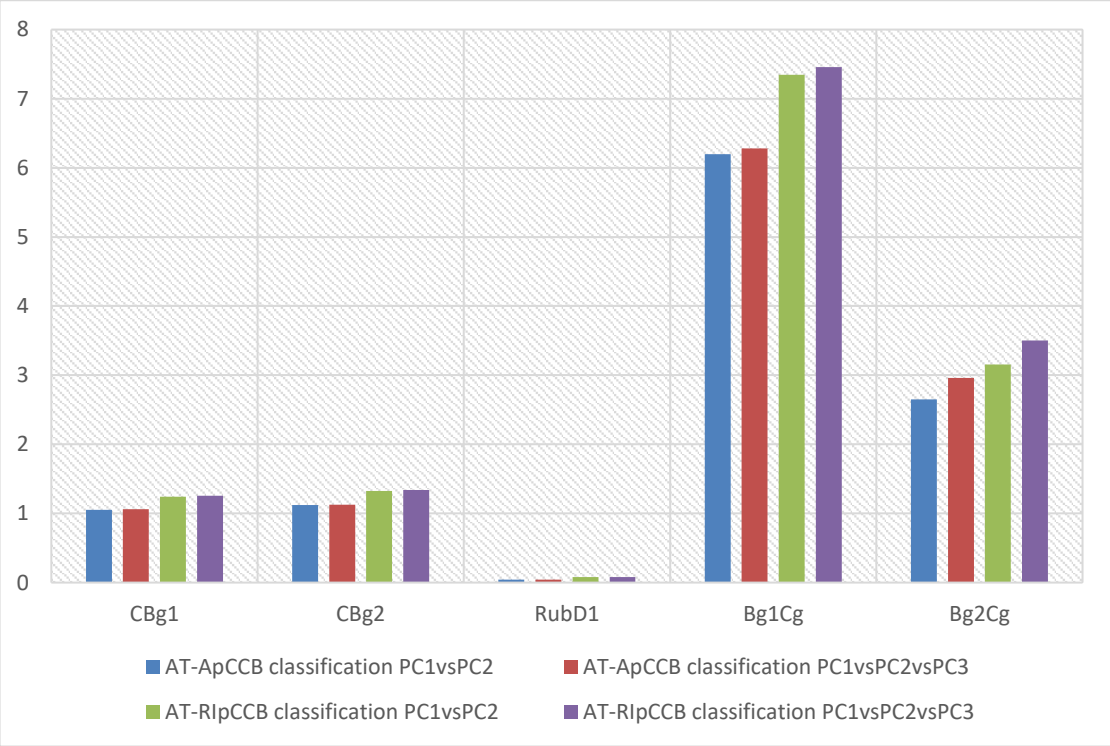

Figure 8. 5 Comprehensive bar chart plot comparing the separation between RMRU and faulty condition for a hybrid acceleration-based time domain and pCCB (AT-pCCB) components and a hybrid acceleration-based time domain with real and imaginary pCCB (AT-RIpCCB) components at PC1vsPC2 and PC1vsPC2vsPC3

This figure compared the AT-ApCCB and AT-RIpCCB approach for the PC1vsPC2 and PC1vsPC2vsPC3 with the differentiation of faulty conditions considered with respect to the RMRU case. A glance at the plot showed that for both approaches, the

PC1vsPC2vsPC3 has a slightly higher magnitude than those of PC1vsPC2 for individual cases, indicating better separation. This separation indicates that adding more PCs may help to distinguish the faults further, even if most of the data information is retained in PC1 and PC2. Thus, more PCs also signify useful diagnosis.

8.5 Chapter summary

This chapter investigated a proposed novel approach for a consolidated rotor-related and bearing fault diagnosis in a single analysis. The approach combined acceleration-based time-domain with poly-coherent composite bispectrum (AT-pCCB) components. It is a hybrid feature reduction approach having less frequency domain features fused with time domain parameters.

The proposed approach stems from the earlier novel data fusion of acceleration and velocity features (dFAVF) and the improved poly-coherent composite bispectrum (pCCB) fault diagnosis methods. Acceleration-based bearing data in the dFAVF model included **RMS**, **CF,** and **Ku,** and the pCCB components input in the improved models included $\boldsymbol{B_{11}}$, $\boldsymbol{B_{12}}$, $\boldsymbol{B_{13}}$ and $\boldsymbol{B_{22}}$. This hybrid fault diagnosis approach contained acceleration-based time-domain features and poly-coherent composite bispectrum components (AT-pCCB). The AT-pCCB is the umbrella model for the acceleration-based time domain with amplitude of pCCB (AT-ApCCB) and acceleration-based time domain with real and imaginary pCCB (AT-RIpCCB). These sub-methods helped to present a diagnostic approach based on finding from the initial investigation, where a comparison of amplitude to real and imaginary pCCB components for rotor fault diagnosis was made in chapter 7. Since the bearing parameters were incorporated in improved pCCB models, observing both models' results would help vibration analysts better judge based on the parameters used. With a PCA-based pattern recognition approach with an observation from PC1vsPC2 and PC1vsPC2vsPC3, both models were clustered and separated conditions. However, the AT-RIpCCB showed better representation than the AT-ApCCB.

A quantification approach which helps to establish this observation further involves the differentiation of faulty with respect to the **RMRU** condition. The AT-RIpCCB showed a slightly higher magnitude than the AT-ApCCB, thus better separating individual cases in a single analysis. Also, the comparison of the PC1vsPC2 and

PC1vsPC2vsPC3 in this analysis showed the latter had a slightly higher magnitude than the former, indicating the PC1vsPC2vsPC3 have more diagnostics information.

The improved pCCB has shown exceptional rotor faults classification due to amplitude and phase information. The time domain feature, especially from acceleration data, is excellent in indicating bearing defect primarily due to their indication of impulsiveness (**CF**) and peakedness (**Ku**). This data fusion model also showed the rotor-related faults clustering around the same region while the bearing defect clusters are separated from the rotor conditions. The proposed model again shows occurrence around their fault frequency ranges where the rotor is low-frequency range faults, and the bearing is high-frequency range faults. Therefore, the results present an improved vibration-based fault identification approach in rotating machines' critical parts where an extensive consideration of rotor and bearing faults can be diagnosed in a single analysis.

CHAPTER 9

ENHANCED "ROTATING MACHINES' CRITICAL PARTS" FAULT IDENTIFICATION APPROACH FOR SIMILAR MACHINES WITH DIFFERENT FOUNDATION FLEXIBILITY

Various rotating machines are similar in structures, dimensions, and models due to standardisation; however, they may exhibit difference in dynamics due to installation foundation or/and location. Others may be old and lack baseline data for classification of the machine condition. These dynamics when properly investigated is useful in understanding machine condition diagnosis, such that fault identification parameters may be insensitive for the different machine. Thus, machine dynamics and fault identification approach can be successfully carried out so that data from one machine can support fault identification in another. The aim of this chapter is to enhance fault identification of an extensive range of faults in rotating machines' critical parts (rotor and bearing) for different foundation flexibilities using the propose dFAVF and AT-pCCB. Observation and comparison of the first three principal components and quantification of machine condition was carried out.

9.1 Overview

Vibration-based fault identification (VFI) techniques are popular for detecting rotor-related and bearing faults in rotating machines. Time and spectrum analysis tools are helpful in signal diagnoses of many rotating machine conditions. However, this individual parameter from time and frequency analysis may not be enough in fault identification. Thus, the data fusion approach is considered where various parameters with sensitive information that indicates the state of a machine are used in fault identification. This chapter considered more rotor-related and bearing faults from the spring-based flexible test rig one (SFTR-1) and Spring-based flexible test rig two (SFTR-2) in presenting further investigation into the proposed novel data fusion of acceleration and velocity features (dFAVF) and acceleration-based time-domain and poly-coherent composite bispectrum (AT-pCCB) components. Vibration data were collected when both test rigs ran below and above their first critical speed, i.e., 450 rpm (7.5 Hz), 900 rpm (15 Hz) and 1350 rpm (22.5 Hz). However, for the SFTR-2, its 3rd running speed is close to the 2nd natural frequency, i.e., the 1350 rpm (22.5 Hz) machine running speed and 23.88 Hz natural frequency. So, analysis from spectrum plots and pCCB plots from signals recorded from the SFTR-2 was observed to understand the dynamics of the proximity of the 3rd running speed and the 2nd natural frequency in fault identification. Also, the mode shape was useful in understanding the dynamic behaviour of the faults simulated with the machine operating around the such frequency. After that, a combination of features from both test rigs is studied to strengthen the proposed novel dFAVF and AT-pCCB approach and determine how insensitive the proposed approaches would be when transferred to different machines.

The vibration data collected here is the same as the earlier study. The dFAVF had 20 sets of data for each condition, while AT-pCCB had 10 sets of data for each condition in their diagnostics models. All data were collected with a sampling frequency of 10 kHz. The faults simulated in this study are **RMRU**, **M**, **Unb**, **CBg1**, **CBg2**, **RubD1**, **RubD2**, **Bg1Cg**, **Bg2Cg**, **Bg3Cg**, and **Bg4Cg**. Results from the investigation of SFTR-1 data are presented in section 9.2. Section 9.3 covers the investigation of STFR-2 data in time and frequency domain analysis for

rotor-related faults, envelope analysis for bearing defects and the poly-coherent composite bispectrum (pCCB). After that, the proposed models were observed. In section 9.4, the investigation of combined analysis for SFTR-1 and SFTR-2 was presented. Section 9.5 presents observations and a discussion of the results. Section 9.6 presented a comprehensive comparison of results from SFTR-1, SFTR-2 and combined analysis.

9.2 Individual foundation analysis for spring-based flexible test rig 1 (SFTR-1)

Time and frequency domain analysis from tested conditions from SFTR-1 has been presented in chapter six. The analysis covered the main rotor and bearing faults simulated for this research. The bearing faults analysed in chapter six were those at locations one and two. This chapter included an analysis of bearing three and four. Since the envelope spectrum analysis helped to identify the fundamental train frequency indicative of bearing faults, with only time domain features included in building the data matrix, observation of the envelope analysis at bearing three and bearing four was not presented. The data matrix was based on representation from equation (3.41) for dFAVF model and equation (3.49) and (3.50) for AT-pCCB model. This section considered the classification of machine conditions using the proposed dFAVF and AT-pCCB methods with a PCA pattern recognition plot at PC1vsPC2 and PC1vsPC2vsPC3. Also, in the investigation of the AT-pCCB method, a comparison of the improved amplitude and the real and imaginary components of the pCCB with integrated classification involving bearing defect.

9.2.1 Application of novel dFAVF and AT-pCCB fault identification method on spring-based flexible test rig (SFTR-1)

The classification of machine conditions with the proposed dFAVF and AT-pCCB for SFTR-1 is presented in Figure 9.1 and Figure 9.2. Figure 9.1 (a) is the PC1vsPC2 classification for dFAVF and Figure 9.1 (b) is the PC1vsPC2vsPC3 classification for dFAVF. Figure 9.2 (a) is the PC1vsPC2 classification of AT-pCCB amplitude components only (AT-ApCCB) and Figure 9.2 (c) is the PC1vsPC2 classification of AT-pCCB real and imaginary components (AT-RIpCCB). Figure 9.2 (b) is the PC1vsPC2vsPC3 classification of AT-pCCB amplitude components (AT-ApCCB) and Figure 9.2 (d) is the

PC1vsPC2vsPC3 classification of AT-pCCB real and imaginary components (AT-RIpCCB). All plots are multiple-speed single analyses of the consolidated rotor and bearing faults classification.

In Figure 9.1 (a), the dFAVF method for multiple speed classification in a single analysis showed clustering and separation for all conditions. Overlap amongst the rotor faults was conspicuous while those of bearing were further apart. However, the rotor conditions seem convergent, close to the zero-point. In contrast, the bearing conditions are shown to be further away from the rotor but in strategic areas around the rotor conditions. Figure 9.1 (b) is a 3D PCA-based plot for the same conditions in Figure 9.1 (a). A better view of the clustering and separation for the conditions was observed. In Figure 9.1 (b), the rotor conditions overlap ahead of the bearing conditions. All bearing conditions though separated clearly, were behind the rotor conditions. This observation indicates the low and high-frequency regions in the rotor and bearing faults analysis, respectively.

Figure 9.2 (a) and (b) present the AT-ApCCB method for a multiple-speed classification in a single analysis which also showed clustering and separation of each condition. The rotor conditions show separations, especially **M**; **CBg1** and **CBg2** appeared in the same region in the plot and seemed to overlap. **RMRU**, **Unb** and **RubD1** tend to overlap each other. The bearing conditions showed separations except for the spread at **Bg4Cg**, which overlapped **Bg3Cg**. The spread in **Bg4Cg** could be due to the machine's state during data collection. Another important observation is the separation of the bearing from the rotor conditions. All rotor conditions were seen towards the left part of the plot, while the bearing conditions had a good space around the plot. Figure 9.2(b), a 3D representation of Figure 9.2(a) having additional PCs in its analysis, presented a different view from observation. Notwithstanding the overlap and separation of the various conditions as observed in Figure 9.2 (a), the rotor faults in the plots are somewhat in front of the bearing faults, which were seen behind the rotor faults indicating low and high-frequency range for rotor and bearing faults, respectively.

Figure 9.2 (c) and (d) present the AT-RIpCCB method for a multiple-speed classification in a single analysis which also showed clustering and separation of each condition. The

AT-RIpCCB is another sub-approach for the classification of machine conditions. The investigation here is similar to Figure 9.2 (a) and (b), except that the former considered the magnitude of the pCCB components and the latter incorporated the real and imaginary components of pCCB. Figure 9.2 (c) Observation showed similar clustering and separation between machine conditions, as seen in Figure 9.2 (a). However, the separation in Figure 9.2 (c) is further apart from the observation. Similarly, Figure 9.2 (d) observation showed the further separation of conditions.

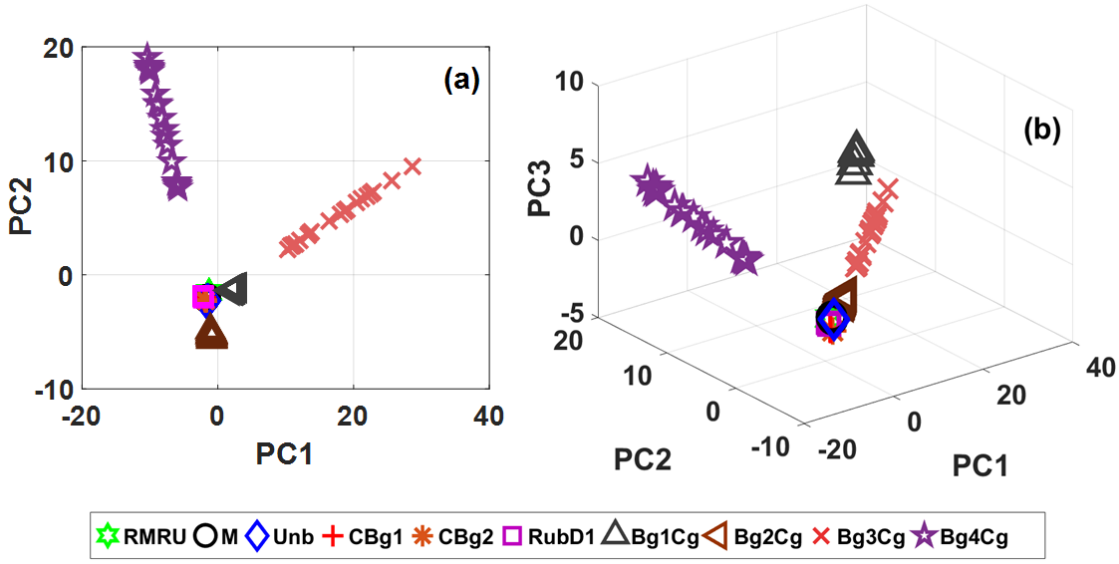

Figure 9. 1 dFAVF Classification of SFTR-1 conditions at(a) PC1vsPC2 (b) PC1vsPC2vsPC3.

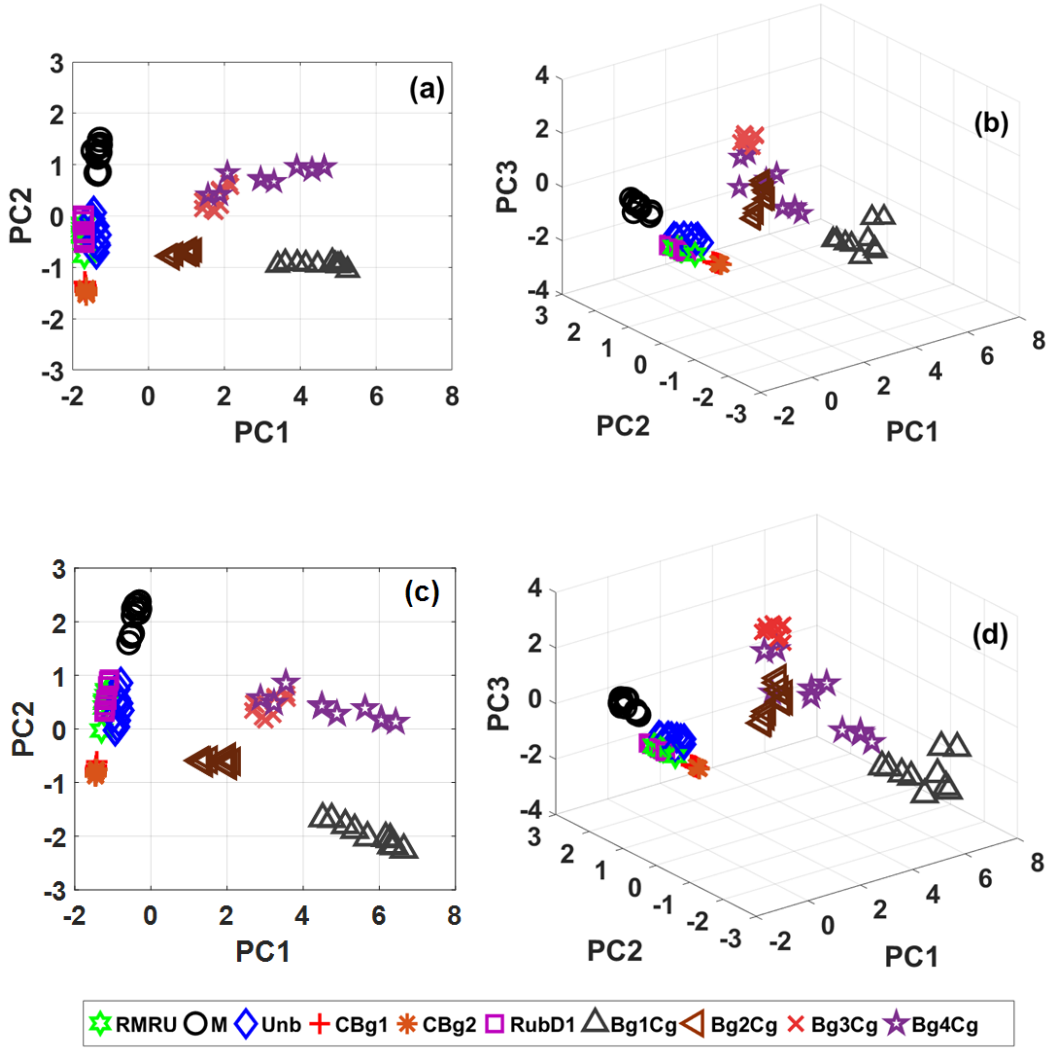

Figure 9. 2 Classification of combined SFTR-1 conditions for multiple speed single analysis with (a) AT-ApCCB (PC1vsPC2) (b) AT-ApCCB (PC1vsPC2vsPC3) (c) AT-RIpCCB (PC1vsPC2) (d) AT-RIpCCB (PC1vsPC2vsPC3).

9.2.2 Observation/ Discussion

Results from fault identification and diagnosis using the proposed methods, dFAVF, and sub-methods AT-ApCCB and AT-RIpCCB, have been presented in sub-section 9.2.1. Fault classification was achieved in all scenarios; however, the classification at dFAVF showed much overlap between the rotor conditions, except when viewed closely, the separation is seen. The AT-pCCB, on the other hand, showed a more apparent separation in the rotor conditions. The uniqueness of all the methods is how the rotor faults separate from the bearing conditions. This observation could indicate the faults' frequency range, i.e., low and high-frequency ranges for rotor and bearing faults,

respectively. The applicability of these methods in industrial scenarios where an extensive range of rotating machine faults can be diagnosed in a single analysis is highly recommended. However, the transference of the diagnostics approach from one machine to another with similar foundation flexibility is tested in this study to show the insensitivity of the methods and usefulness of fault diagnosis for machines without prior baseline data.

9.3 Individual foundation analysis for spring-based flexible test rig 2 (SFTR-2)

The analysis of the novel dFAVF and AT-pCCB methods using data from SFTR-1 gave useful diagnostic information for a consolidated rotor and bearing fault detection. To check for transferability and validate the approaches, data from a second test rig is investigated, i.e., the SFTR-2 using the proposed approaches (dFAVF and AT-pCCB). The spring-based flexible test rig 2 (SFTR-2) is built to modify the foundation flexibility of a similar test rig (SFTR-1), where the natural frequencies of the test rig are increased by increasing the stiffness of the rig [45]. Thus, the SFTR-2 had four bearing pedestals Bg1 – Bg4, with each bearing pedestal having four springs connected to a bearing and stiffness of 14.4 N/mm per spring. The first few natural frequencies obtained from modal testing of SFTR-2 are 17.78 Hz, 23.88 Hz, 32.65 Hz, 51.19 Hz and 86.36 Hz. Thus, the first natural frequency for SFTR-2 is higher than that of SFTR-1 by a difference of about 6.26 Hz. Vibration data was collected using the same parameters as was done in SFTR-1. Signals from rotor-related and bearing defects were collected one after the other. Time and frequency analysis of the vibration signal collected from the SFTR-2 was carried out. Time domain **RMS**, **Ku** and **CF** and frequency domain **1x** – **5x** harmonic components and **SE** was useful in observing the dynamic behaviour of the SFTR-2. Nevertheless, the discussion of the time domain features is minutely considered in this chapter as the focus is already on the validation and improvement of the developed methods. Subsection 9.3.1 gave a detailed observation of the acceleration spectra,

velocity spectra, pCCB spectra and bearing analysis (with and without envelope analysis).

9.3.1 Vibration signal analysis from SFTR-2

Figure 9.3 to Figure 9.8 showed both acceleration and velocity spectrum analysis for the various rotor faults selected for this study. Typical bearing diagnosis plots are represented in Figure 9.9 to Figure 9.11. Poly-coherent composite bispectrum (pCCB) plots are seen in Figure 9.12 to Figure 9.14. The observation and discussions of these plots and their usefulness in rotating machine fault identification and detection are presented.

9.3.1.1 Acceleration signal analysis

Time and frequency domain analysis is carried out using acceleration signals. However, the time domain parameter in this study is discussed extensively in chapter 4, so nothing is discussed in this section on the time domain analysis. On the other hand, the frequency domain analysis for acceleration data is presented in Figures 9.3 to 9.5. As stated earlier in chapter five, the presence of an increased 2x component in a spectrum plot could be due to the presence of misalignment and unbalance, which is already in existence in the test rig, so that the baseline case is referred to as residual misalignment and residual unbalance |(RMRU). The frequency location of a particular harmonic component is dependent on its position on the FRF, and the amplitude of the harmonic component will be based on one or a combination of two of the mode shapes of the rig [20].

In the acceleration spectrum plot in Figure 9.3 – 9.5, there is the presence of **1x** to **5x** harmonic components for all cases and all measurement speeds. The zoomed version of the spectrum plot was done to capture each plot's first five harmonic components. Figure 9.3 shows the spectrum for rotor conditions at 450 rpm (7.5 Hz). Small peak is observed between **2x** (15 Hz) and **3x** (22.5 Hz) in all the cases, which may be due to 1st mode (17.78 Hz). The amplitude in Figure 9.2 (f), which is the **RubD1** case, was seen to be very high compared to others which may be due to effects from the rubbing apparatus adjusting the machine's natural frequency. Also, peaks seen before **5x** (37.5 Hz) for all conditions may be due to 3rd mode (36.24 Hz). In the case of rub, the peak

also showed a higher amplitude. Observation of Figure 9.3 (a) – (e) showed all cases had the **1x** aligned with the machine running speed at 7.5 Hz. However, Figure 9.3 (f), the RubD1, has a **1x** machine running speed of around 7.34 Hz. This condition can be due to the manual setting of the speed during operation, as the exact running speed may not be obtained.

In Figure 9.4 (a), (b), (d), (e), small peaks were observed just after **1x** (15 Hz), which may be due to the 1st mode (17. 78 Hz). Peaks observed between **2x** (30 Hz) and **3x** (45 Hz) at **RMRU, Unb, CBg1, CBg2** and **RubD1** may be due to the 3rd mode (32.65 Hz). Also, peaks between **3x** (45 Hz) and **4x** (60 Hz) for all conditions may be due to the 4th mode (47.84 Hz) and the peaks just after **5x** (75 Hz) for all conditions may be due to the 5th mode (86.36 Hz).

Figure 9.5 (a) –(f) has **1x** – **5x** harmonic components in the spectra. Peaks observed before **1x** (22.5 Hz) component for all conditions except **RubD1** may be due to 1st mode (17.78 Hz). An increased **1x** (22.5 Hz) component in all conditions except RubD1 may be because of an operation close to the critical speed at 2nd mode (23.88 Hz). The second peak in **CBg1** may be due to its proximity to the 2nd mode (23.88 Hz). The peaks observed between **1x** (22.5 Hz) and **2x** (45 Hz) at **RMRU, CBg1,** and **CBg2** may be due to the 3rd mode (32.88 Hz). The peak observed between **3x** and **4x** (60 Hz) at **RMRU**, **M, CBg1, and CBg2** may be due to the 4th mode (47.84 Hz). Peaks observed

for **RMRU, Unb, CBg1**, and **CBg2** may be due to a combination of the 4th mode vertical (51.19 Hz) and 5th mode.

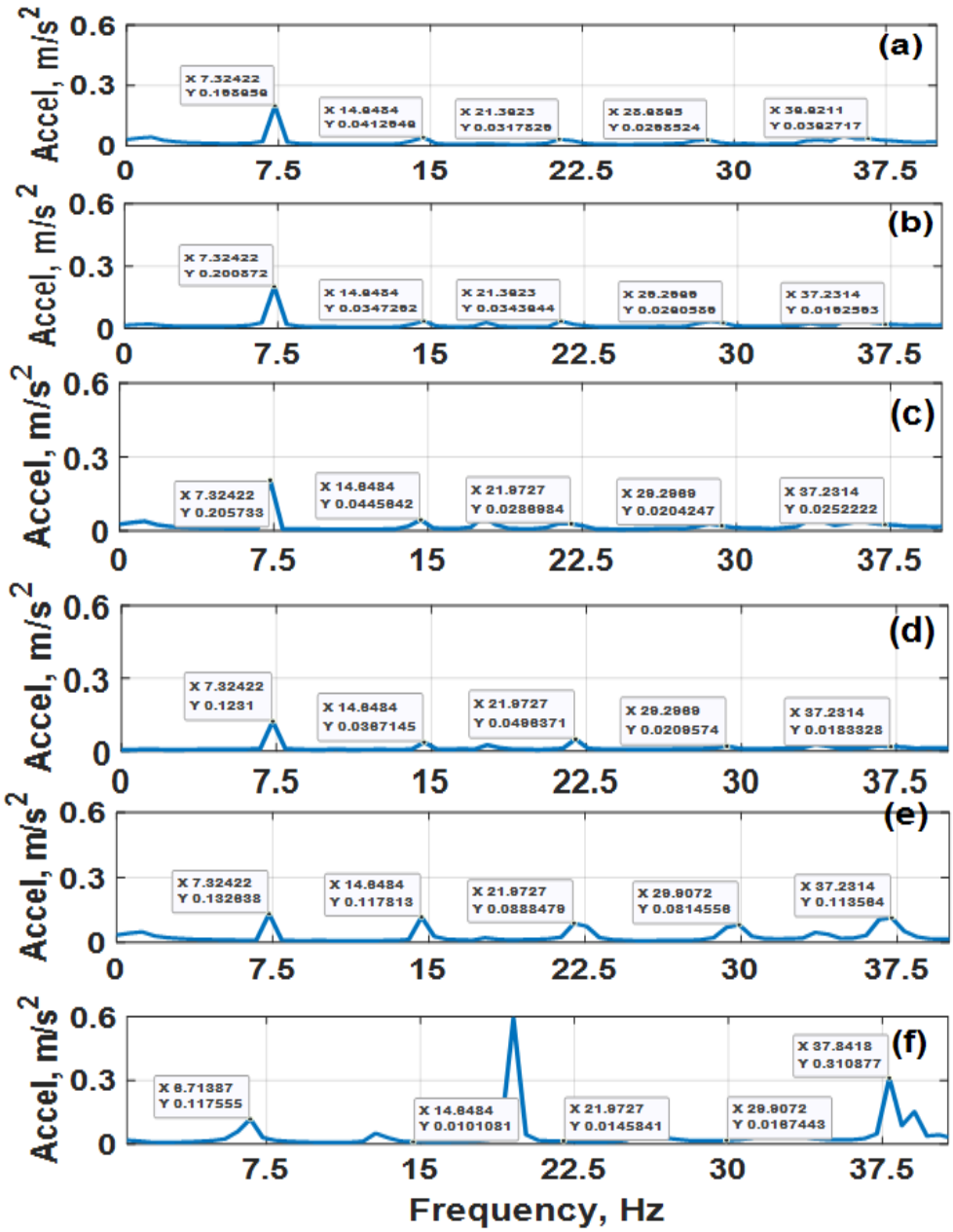

s

Figure 9. 3 SFTR-2 measured acceleration spectra plot at 7.5 Hz Bearing 2 (a) RMRU (b) M (c) Unb (d) CBg1 (e) CBg2 (f) RubD1.

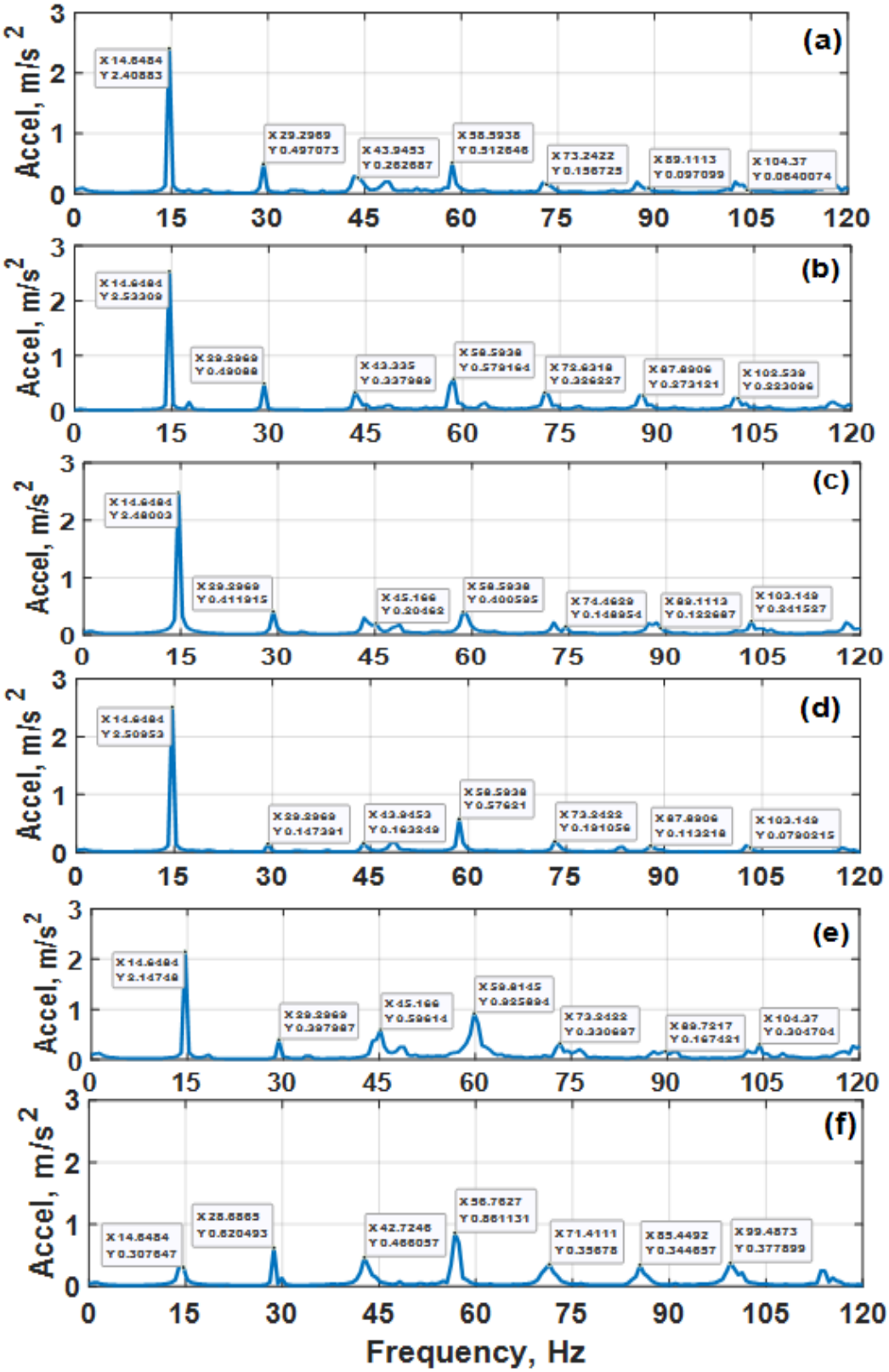

Figure 9. 4 SFTR-2 measured acceleration spectra plot at 15 Hz Bearing 2 (a) RMRU (b) M (c) Unb (d) CBg1 (e) CBg2 (f) RubD1.

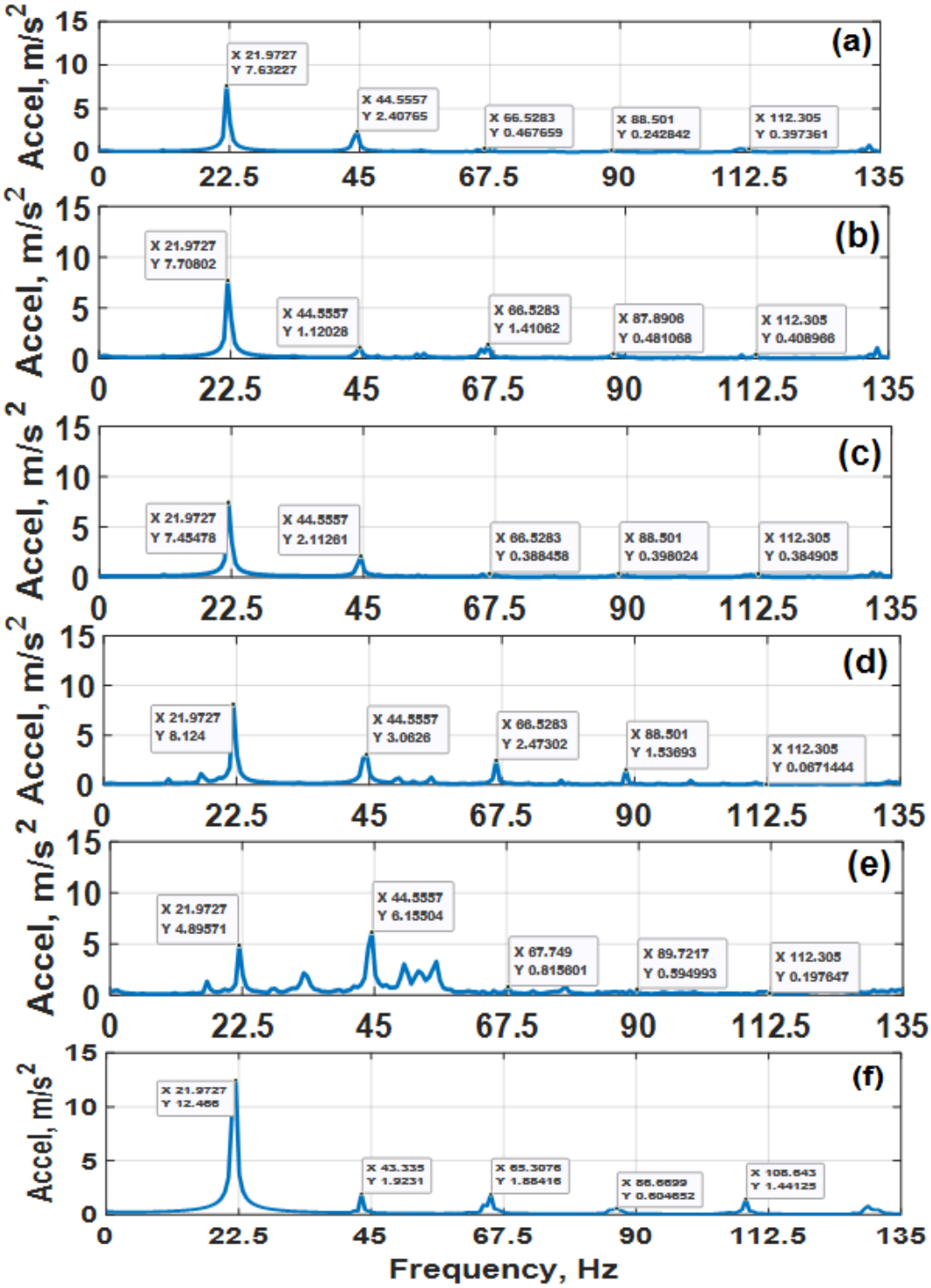

Figure 9. 5 SFTR-2 measured acceleration spectra plot at 22.5 Hz Bearing 2 (a) RMRU (b) M (c) Unb (d) CBg1 (e) CBg2 (f) RubD1.

9.3.1.2 Velocity signal analysis

The spectra plots shown in Figure 9.6 – 9.8 are those of velocity obtained from acceleration signals using the omega arithmetic method [209]. Observations of the Figures showed an increased **1x** amplitude in all cases, as seen for the acceleration spectra (Note there cannot be a direct comparison between the amplitude of acceleration and velocity as their units are different). Similar to observations from chapter six, the velocity spectra showed a reduction or disappearance of harmonic components as the frequency increased for each spectrum [209]. The appearance of harmonic components in the velocity spectra is like the respective acceleration spectra; the difference is the increased peak.

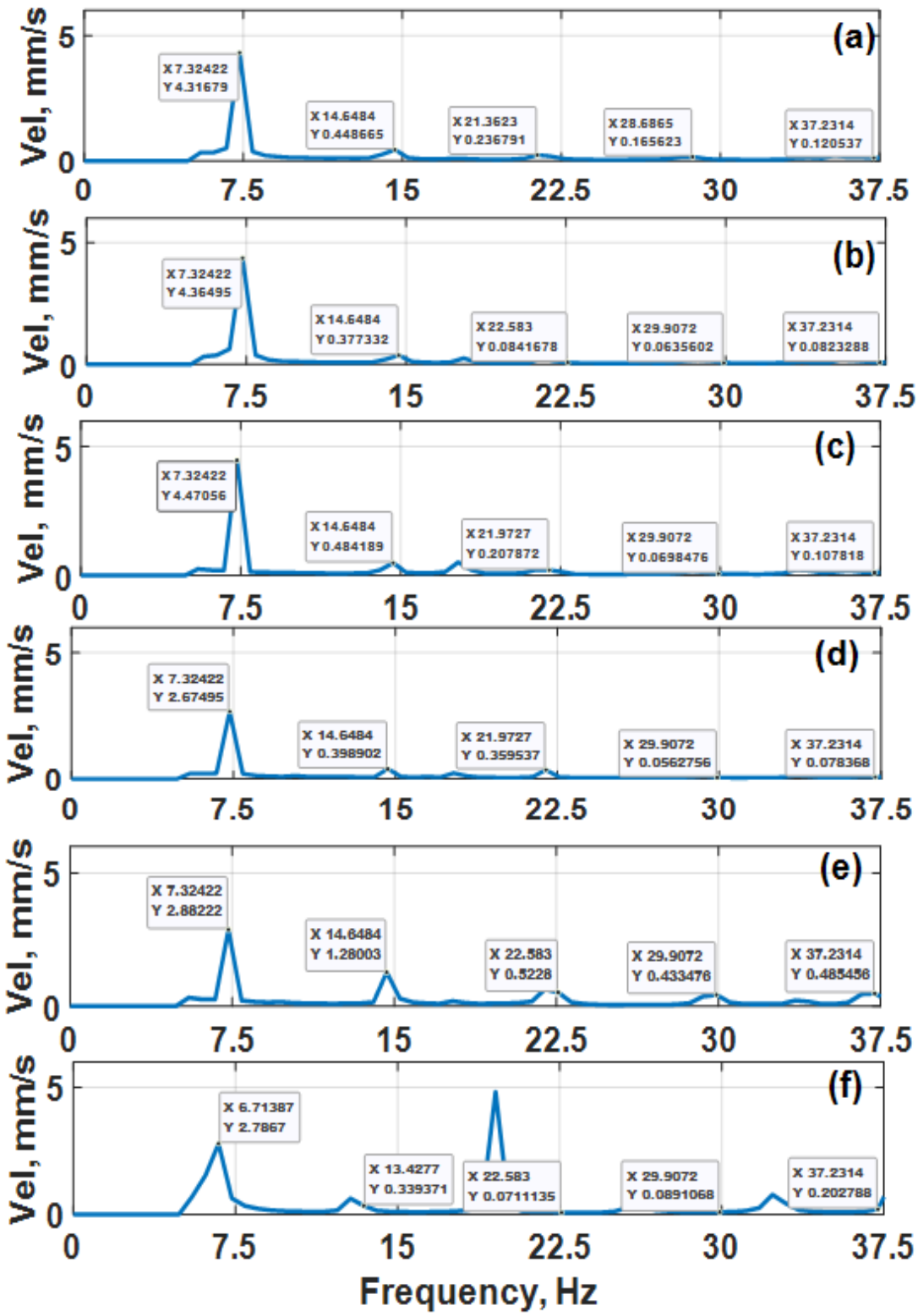

Figure 9. 6 SFTR-2 measured velocity spectra plot at 7.5 Hz Bearing 2 (a) RMRU (b) M (c) Unb (d) CBg1 (e) CBg2 (f) RubD1.

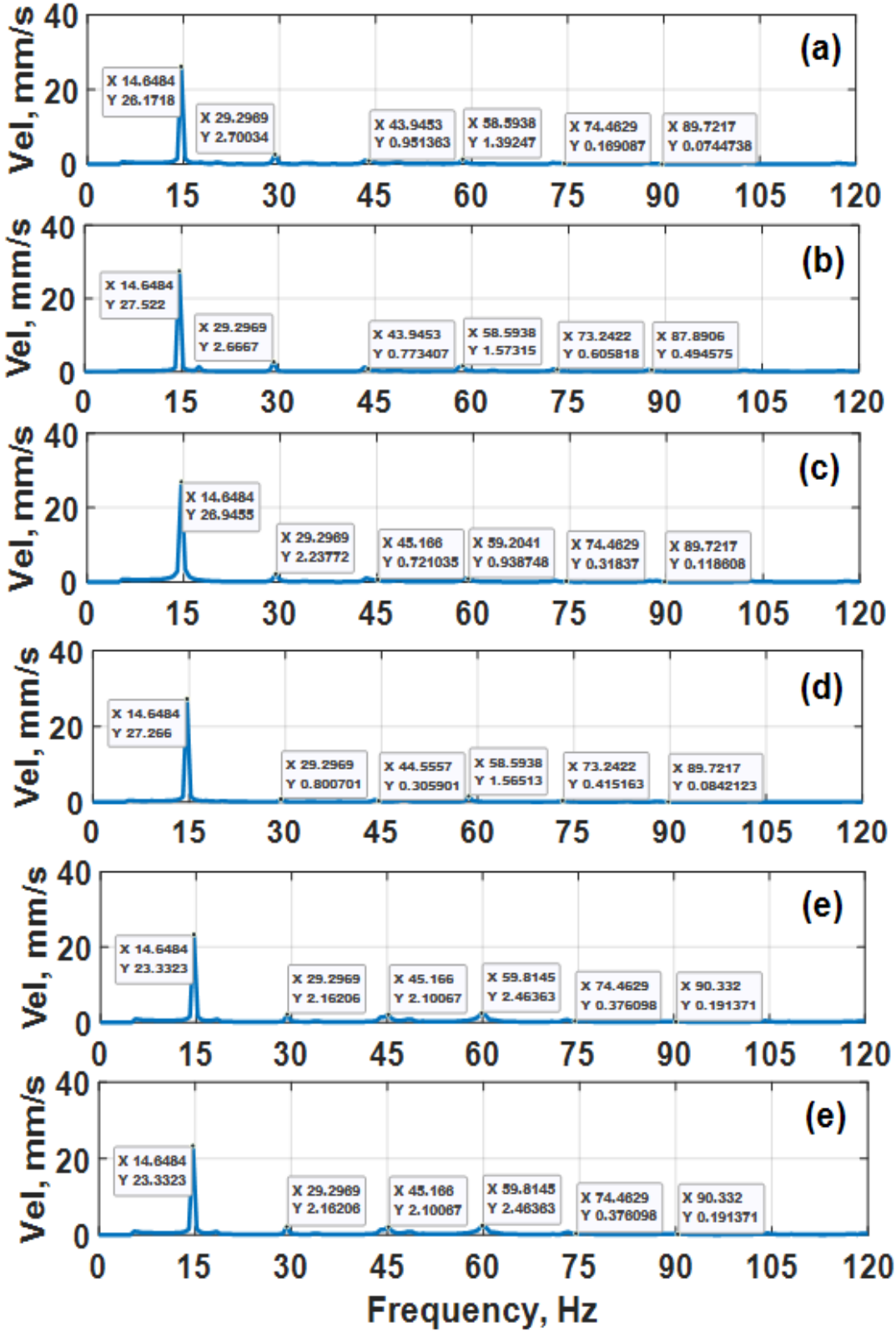

Figure 9. 7 SFTR-2 measured velocity spectra plot at 15 Hz Bearing 2 (a) RMRU (b) M (c) Unb (d) CBg1 (e) CBg2 (f) RubD1.

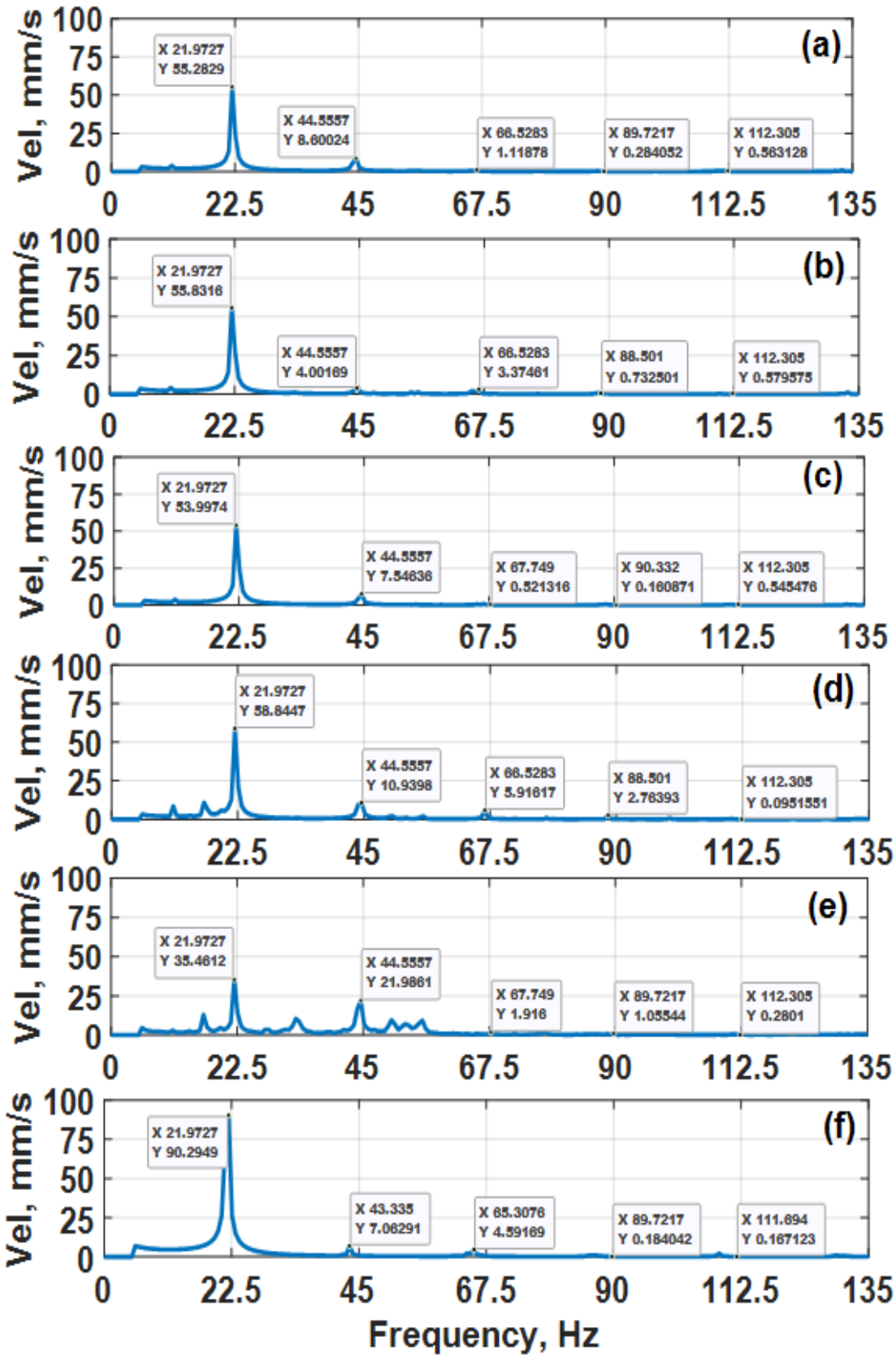

Figure 9. 8 SFTR-2 measured velocity spectra plot at 22.5 Hz Bearing 2 (a) RMRU (b) M (c) Unb (d) CBg1 (e) CBg2 (f) RubD1.

9.3.1.3 Bearing analysis

Figure 9.9 – 9.11 shows typical plots for bearing cage defect analysis at all four bearing pedestal locations, i.e., Bg1 – Bg4, at the three machine running speeds (450 rpm, 900 rpm and 1350 rpm). The bearing cage defect was simulated at Bg1 to create a cage defect at bearing 1 (**Bg1Cg**), and data were collected at the three different machine running speeds. After that, the faulty bearing was moved to Bg2, replacing Bg1 with a healthy bearing. Thus, data were collected at three running machine speeds, creating a bearing cage defect at Bg2 (**Bg2cg**). This was repeated at Bg3 and Bg4, creating bearing cage defects at Bg3 (**Bg3cg**) and (**Bg4cg),** respectively, while placing a healthy bearing at other locations at each experiment. Figure 9.9 – 9.11 (a) - (d) gives a typical spectrum plot of bearing defect after a high pass filter at 500 Hz. The filtering helps to remove the low frequencies, which may be rotor related. After that, envelope analysis is carried out on the signal with a time domain representation as in Figure 9.9 – 9.11 (e) - (h). Here, **a** represents the original signal, while **up** and **lo** represent the upper and lower envelope signals. Figure 9.9 – 9.11 (i) - (l) shows the spectrum plot for the envelope signal.

It should be noted that the fundamental train frequencies for the bearing cage in SFTR-2 are the same as those for SFTR-1. Thus, reference should be made to chapter six for clarity. However, the calculated fundamental train frequencies (FTF) gave 2.86 Hz, 5.72 Hz, and 8.58 Hz for each machine running speeds at 7.5 Hz, 15 Hz and 22.5 Hz, respectively and the experimentally generated envelope analysis spectrum plots showed the FTF to be 2.79 Hz, 5.58 Hz and 8.38 Hz with the machine running speeds at 7.5 Hz, 15 Hz and 22.5 Hz respectively.

Observation from Figure 9.9 – 9.11 provided a useful understanding of the dynamic behaviour of the machine to the appearance of cage defects during the machine operating at different speeds. Investigation of the spectra after filtering before envelope analysis and the time domain analysis after envelope analysis may be helpful for fault diagnosis where particular parameters are considered. However, observations of the typical plots may not give useful diagnosis features instantly. Focusing on the spectra plots after envelope analysis showed some useful diagnosis features. Firstly, we observe the FTF 1x frequency and its harmonic with the amplitude

showing the effect of the damaged cage. Also, smaller peaks are seen around some harmonic components, which may be due to the natural frequency of the FRF. On overall observation, significant detection of bearing cage defect is not achieved using only the harmonic components.

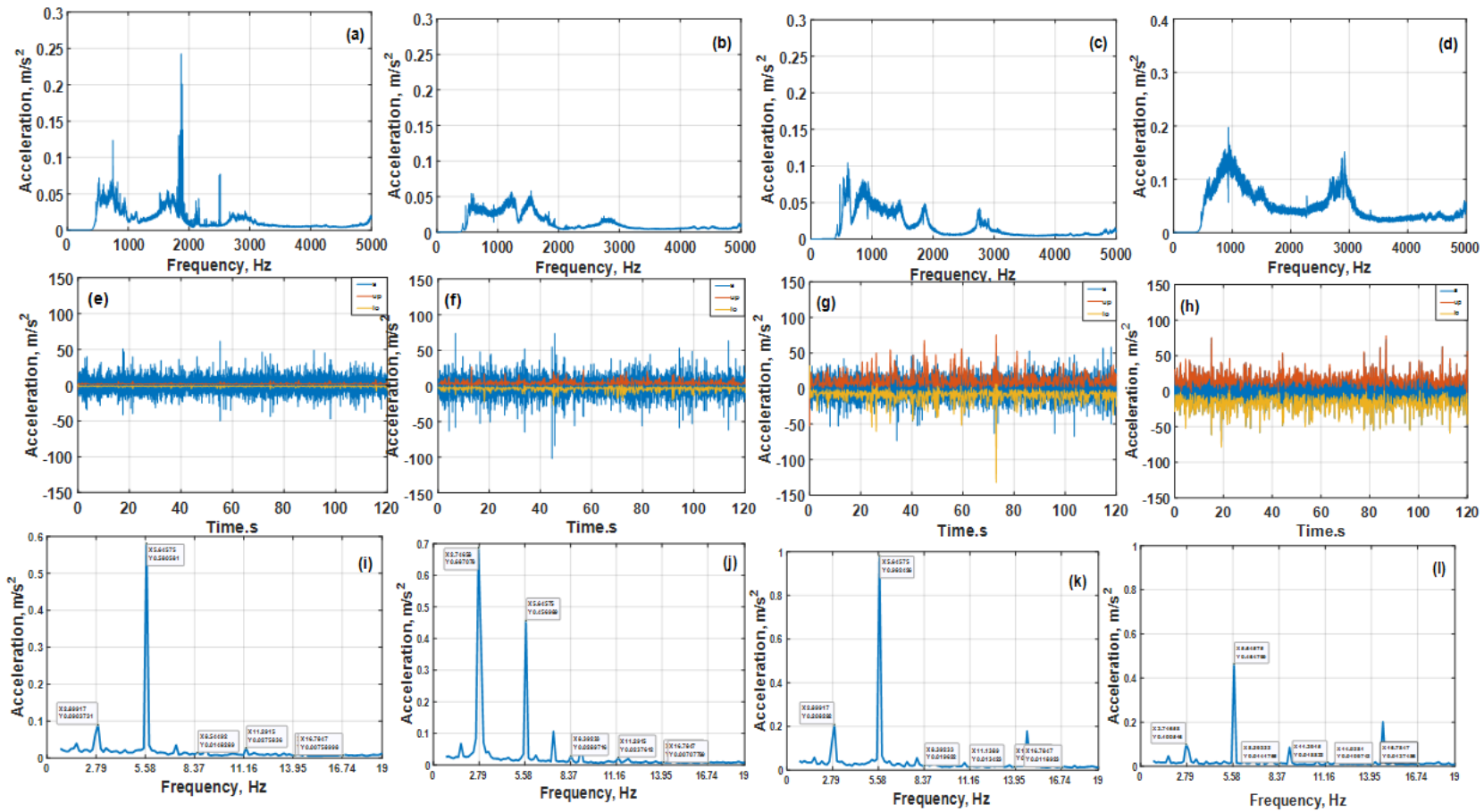

Figure 9. 9 Typical Bearing defect at 450 rpm for (a) Bg1Cg filtered Spectrum (b) Bg2Cg filtered spectrum (c) Bg2Cg filtered spectrum (d) Bg4Cg filtered spectrum (e) Bg1Cg envelope time domain (f) Bg2Cg envelope time domain (g) Bg3Cg envelope time domain (h) Bg4Cg envelope time domain (i) Bg1Cg envelope spectrum (j) Bg2Cg envelope spectrum (k) Bg3Cg envelope spectrum (l) Bg4Cg envelope spectrum.

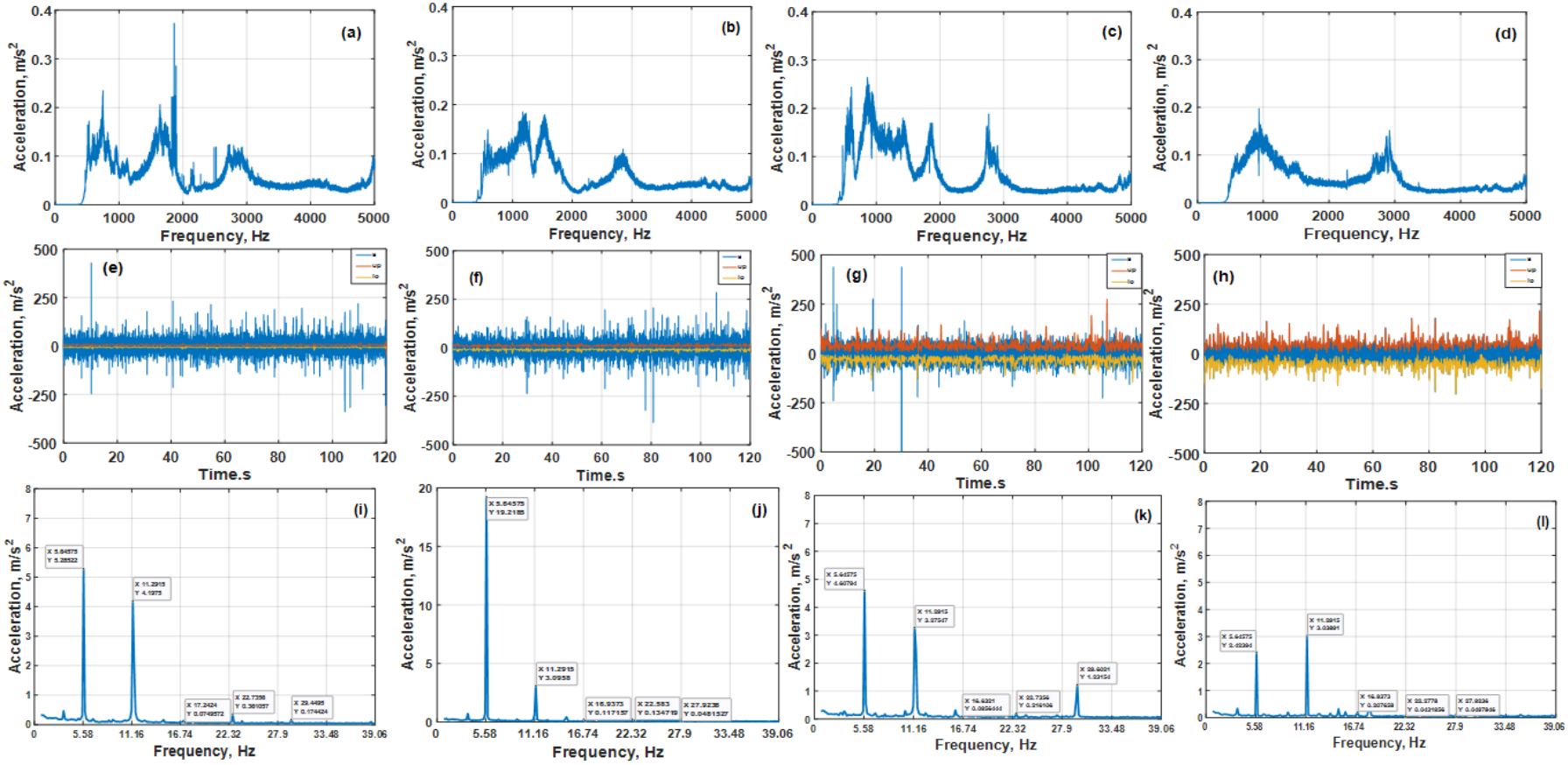

Figure 9. 10 Typical Bearing defect at 900 rpm for (a) Bg1Cg filtered Spectrum (b) Bg2Cg filtered spectrum (c) Bg2Cg filtered spectrum (d) Bg4Cg filtered spectrum (e) Bg1Cg envelope time domain (f) Bg2Cg envelope time domain (g) Bg3Cg envelope time domain (h) Bg4Cg envelope time domain (i) Bg1Cg envelope spectrum (j) Bg2Cg envelope spectrum (k) Bg3Cg envelope spectrum (l) Bg4Cg envelope spectrum.

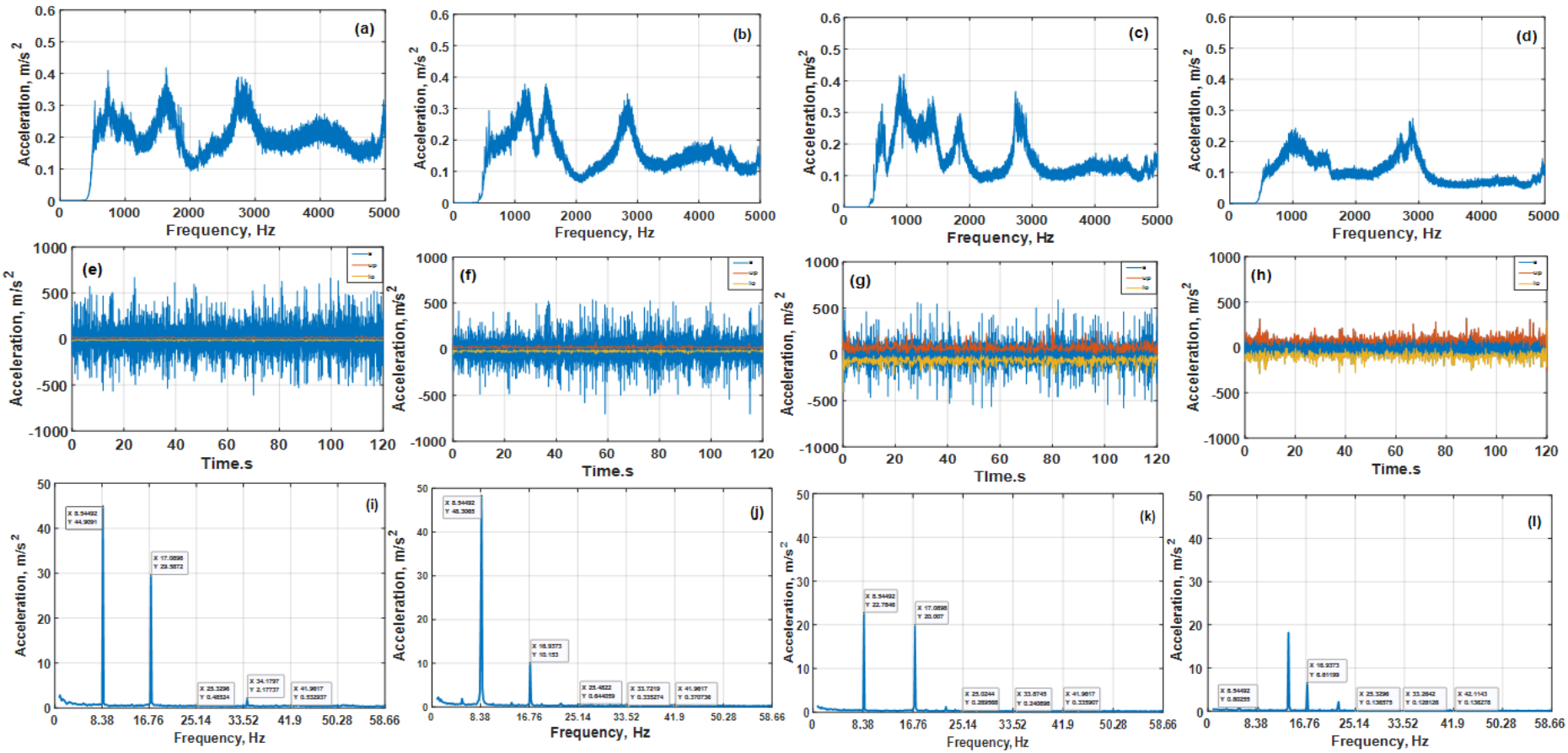

Figure 9. 11 Typical Bearing defect at 1350 rpm for (a) Bg1Cg filtered Spectrum (b) Bg2Cg filtered spectrum (c) Bg2Cg filtered spectrum (d) Bg4Cg filtered spectrum (e) Bg1Cg envelope time domain (f) Bg2Cg envelope time domain (g) Bg3Cg envelope time domain (h) Bg4Cg envelope time domain (i) Bg1Cg envelope spectrum (j) Bg2Cg envelope spectrum (k) Bg3Cg envelope spectrum (l) Bg4Cg envelope spectrum.

9.3.1.4 Poly-coherent composite bispectrum (pCCB) analysis

This study presents a poly-coherent composite bispectrum (pCCB) analysis for the SFTR-2. The pCCB bispectra plots, as shown in Figure 9.12 (a) – (g) to Figure 9.14 (a) – (g), are representation at the three selected speeds respectively, with each plot showing the machine conditions that has been investigated (**RMRU**, **M**, **Unb**, **CBg1**, **CBg2**, and **RubD1**). Figure 9.12 – 9.14 shows very clear presence of pCCB components at B_{11}, $B_{12} = B_{21}$, $B_{13} = B_{31}$, others include B_{22}, $B_{23} = B_{32}$ and B_{33}. In Figure 9.12 (a), the **RMRU** case at 450 rpm, there is the presence of B_{11}, $B_{12} = B_{21}$, $B_{13} = B_{31}$ and a small presence of B_{22}. Figure 9.12 (b), (c) and (e), which are **M**, **Unb**, **and CBg2**, shows the higher amplitude of the first few pCCB components, including B_{22}, but minimal $B_{23} = B_{32}$. Also, Figure 9.12 (d), which is **CBg1**, show very little of the first few pCCB components. The amplitude of the pCCB components here is minimal compared to others in the figures. However, Figure 9.12 (f), which is **RubD1**, had a high presence of all pCCB components.

Figure 9.13 shows the pCCB plots at 900 rpm (15 Hz) for the tested machine conditions. The first few pCCB components i.e., B_{11}, $B_{12} = B_{21}$ and $B_{13} = B_{31}$ were seen. However, figure 9.13 (a) showed high B_{11} and very little or no presence of other components. Figure. 9.13 (b) - (g) showed good presence of B_{11}, $B_{12} = B_{21}$ and $B_{13} = B_{31}$ and B_{22}, $B_{23} = B_{32}$ with only Figure 9.13 (g) showing B_{33}. While figure 9.13 (b) appeared slightly similar to Figure 9.13 (c) and (e), there is a higher amplitude in Figure 9.13 (b).

In Figure 9.14, which is the pCCB plots at 1350 rpm (22.5 Hz), there seems to be the presence of all components but mostly very low amplitude. However, figure 9.14 (a) showed the presence of B_{11}, B_{12}= B_{21} and B_{23}, with low B_{31} and no obvious B_{33}, and Figure 9.14 (d) - (e) had the presence of B_{22} without B_{33}. Figure 9.14 (e) showed some forms of subharmonics which could be due to the crack faults. The low amplitude of some pCCB components was adjudged to be a result of a high B_{11} component, which is due to the operational speed close to the 2nd critical speed, i.e., B_{11} is at 22.5 Hz, and the 2nd mode is at 23.88 Hz.

Observation of the machine condition using data from SFTR-2 showed the presence of pCCB components, which may be suitable for understanding machine faults. However,

comparing SFTR-1 to SFTR-2 using pCCB plots at similar speeds, the presence of a particular component may be similar. Overall, the pCCB plot showed variation in the appearance of components and their amplitude for a particular fault at a particular speed.

In as much as the pCCB components gave useful information about the presence of a particular fault, the overall state of the machine is not clearly represented by it. Also, with a large set of vibration data, observation of individual plots would be cumbersome, so the classification of the different conditions may give better diagnostic information on the overall machine's health.

As stated in chapters seven, the spectrum harmonic components or pCCB components alone may not provide exceptional information for fault identification, so a combination of various sensitive features may be useful. Thus, further investigation using the dFAVF and AT-pCCB model was carried out and presented in section 9.3.2.

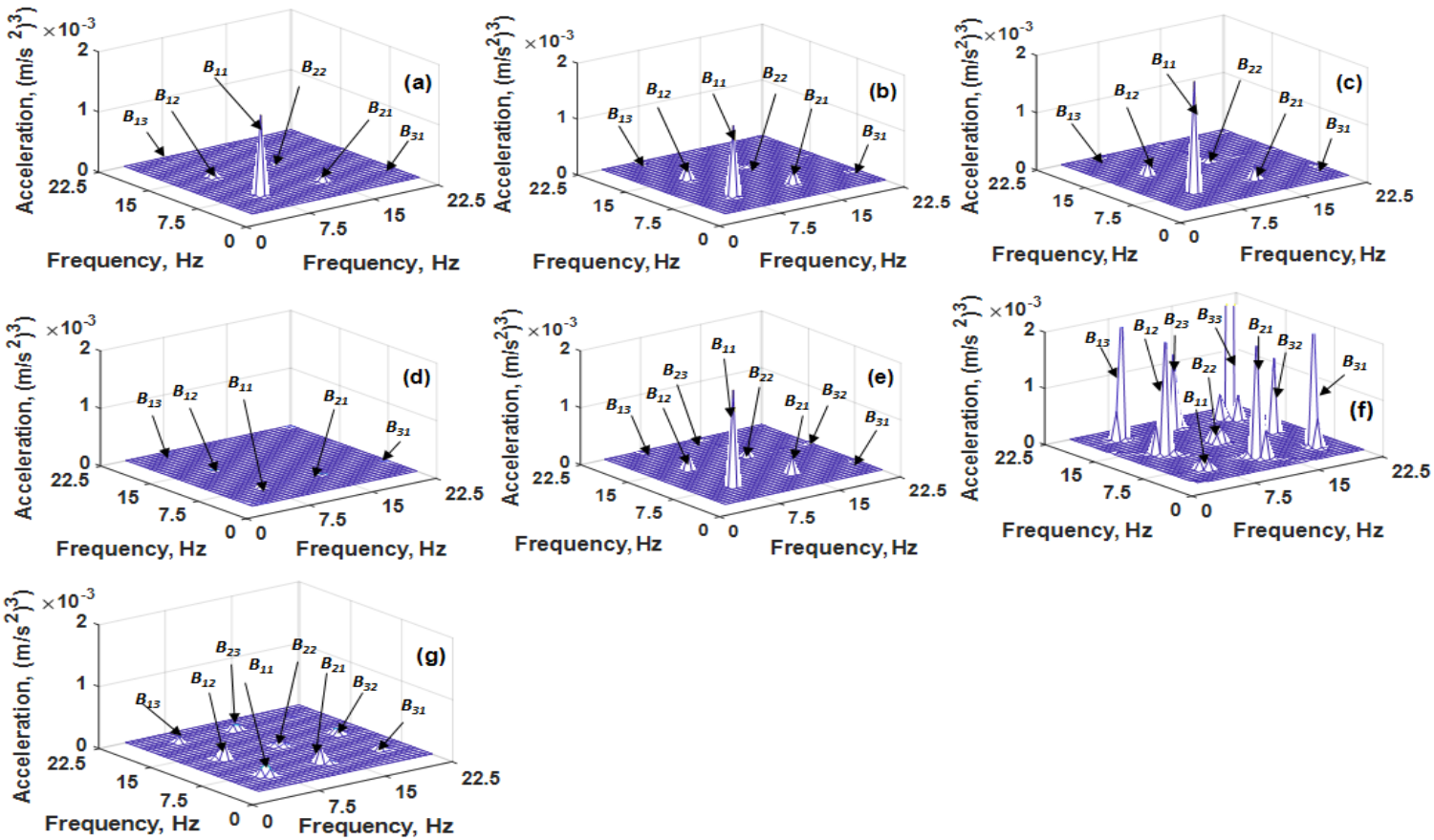

Figure 9. 12 Typical pCCB analysis plots at 450 rpm (7.5 Hz) for (a) RMRU (b) M (c) Unb (d) CBg1 (e) CBg2 (f) RubD1 (g) RubD2.

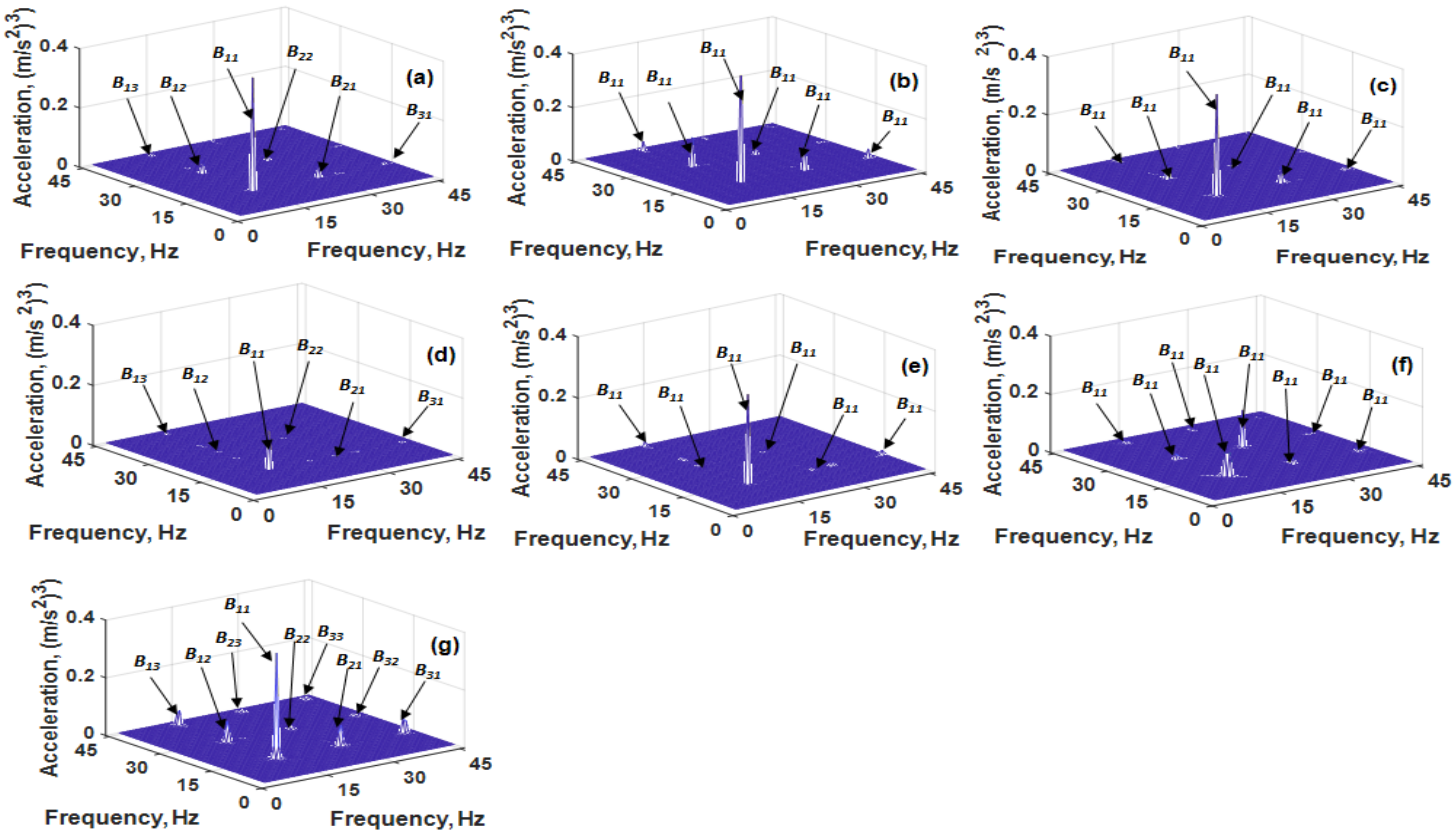

Figure 9. 13 Typical pCCB analysis plots at 900 rpm (7.5 Hz) for (a) RMRU (b) M (c) Unb (d) CBg1 (e) CBg2 (f) RubD1 (g) RubD2.

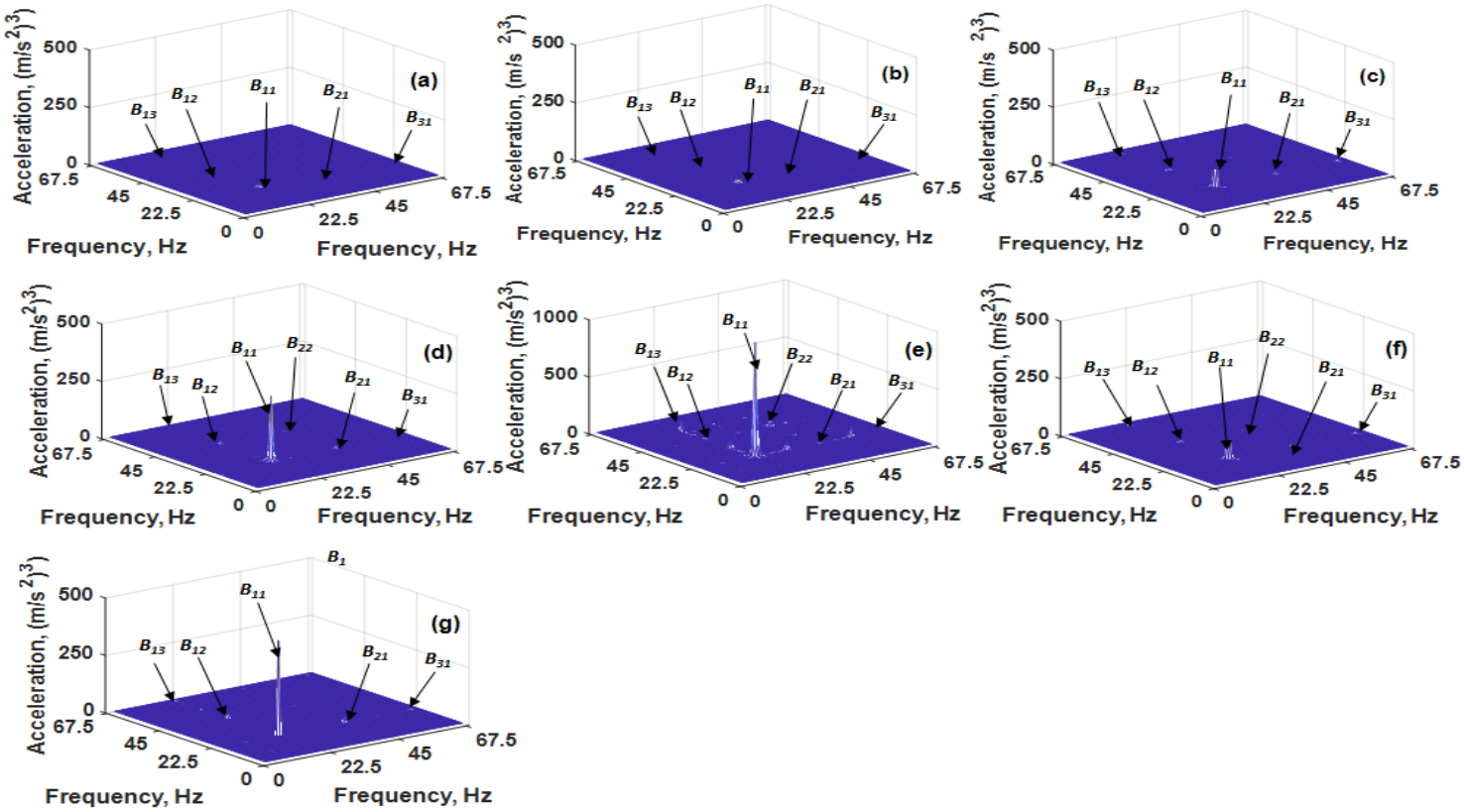

Figure 9. 14 Typical pCCB analysis plots at 1350 rpm (7.5 Hz) for (a) RMRU (b) M (c) Unb (d) CBg1 (e) CBg2 (f) RubD1 (g) RubD2.

9.3.2 Application of novel dFAVF and AT-pCCB fault identification method for SFTR-2

Data matrix was developed for the dFAVF model based on equation (3.41) and that of AT-pCCB based on equation (3.49) and (3.50). The normalisation and PCA-based classificatio of the matrix is shown in Figure 9.15 and Figure 9.16 which are representations of the proposed dFAVF and T-pCCB methods. Figure 9.15 (a) is the PC1vsPC2 classification for dFAVF and Figure 9.15 (b) is the PC1vsPC2vsPC3 classification for dFAVF. Figure 9.16 (a) is the PC1vsPC2 classification of AT-pCCB amplitude components only (AT-ApCCB) and figure 9.16 (b) is the PC1vsPC2 classification of AT-pCCB real and imaginary components (AT-RIpCCB). Figure 9.16 (c) is the PC1vsPC2vsPC3 classification of AT-pCCB amplitude components (AT-ApCCB) and figure 9.16 (d) is the PC1vsPC2vsPC3 classification of AT-pCCB real and imaginary components (AT-RIpCCB).

Figure 9.15 (a) and (b) showed the classification of the rotor and bearing faults using the novel dFAVF multiple speed in a single analysis. Figure 9.15 (a) gives a PCA-based pattern recognition classification using PC1vsPC2. It showed the clustering and separation of conditions. However, the rotor conditions tend to overlap while bearing conditions, especially **Bg1Cg** and **Bg2Cg**, are far from the rotor conditions. **Bg3Cg** and **Bg4Cg** conditions are seen closer to the rotor condition, with **Bg4Cg** overlapping the rotor conditions. Figure 9.15 (b) gives the PCA-based pattern recognition classification using the PC1vsPC2vsPC3.

In Figure 9.15 (a), all conditions retain appearance, but **CBg1** has some spread. Also, **Bg4Cg** appeared in front of the rotor conditions. This observation shows that the **Bg4Cg** case may not have overlapped with the rotor conditions but is further separated in front of them.

Figure 9.16 (a) and (b) shows the PCA-based pattern recognition using PC1vsPC2 and PC1vsPC2vsPC3 respectively in classification for the proposed AT-ApCCB fault identification approach. Figure 9.16 (a) shows the clustering and separation of all conditions. The rotor faults were seen to be well separated except for the overlap between **RMRU, Unb** and **M**, with part of **RubD1**. The bearing conditions are seen

around the left upper part of the plot, with **Bg2Cg** showing some spread, thus having overlap with **Bg1Cg** and **Bg2Cg**, while **Bg4Cg** is positioned ahead in line with other bearing conditions. The CBg1 case showed a split in its observation as some parts of the data are close to other rotor faults while the others are far apart towards the right of the plot. Figure 9.16 (b), a plot of PC1vsPC2vsPC3, a 3D view is obtained, and observation shows the bearing conditions clustering and overlapping themselves around the left part of the plot with **Bg4Cg** case further apart. The rotor conditions are observed in the middle section of the plot. However, **CBg1** has split data, where one is close to other rotor conditions, and the other is further separated towards the far right of the plot.

Figure 9.16 (c) and (d) shows the PCA-based pattern recognition using PC1vsPC2 and PC1vsPC2vsPC3 in classification for the proposed AT-RIpCCB fault identification approach. Figure 9.16 (c), a 2D representation of the PCA-based classification, showed clustering and separation of all conditions. The rotor conditions in the plot are seen around the bottom with **RMRU**, **M, Unb** and **RubD1** overlapping. The **CBg1** and **CBg2** conditions occupied the bottom right of the plot, with some spread from both conditions observed. However, **CBg1** split its data, a part is between the overlapped rotor conditions, and the other is towards the far right of the plot after the **CBg2** condition. This split observed in **CBg1** could result from the machine state during data collection, which is made obvious during the pCCB analysis. On the other hand, the bearing condition is observed at the top left part of the plot. A distinct observation is that the separation of conditions for the AT-RIpCCB is further than that of AT-ApCCB, indicating a clearer machine condition diagnosis in a single analysis.

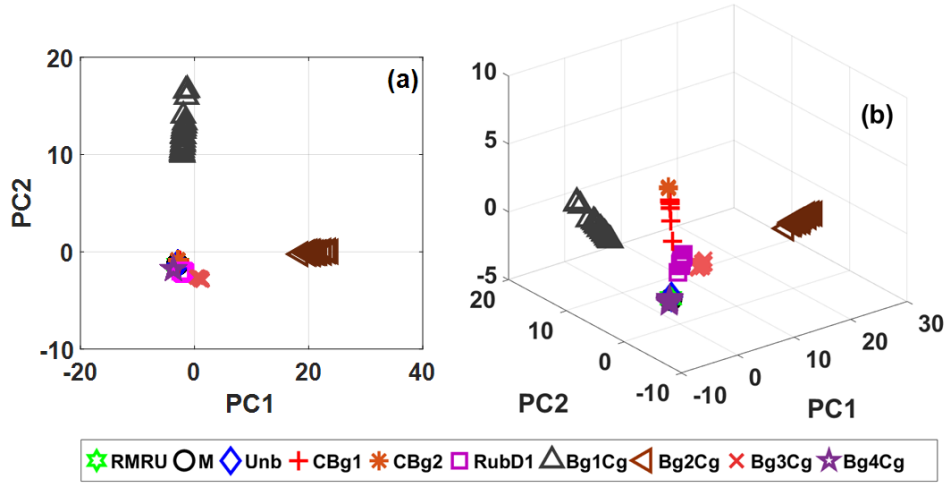

Figure 9. 15 dFAVF classification of SFTR-2 conditions at(a) PC1vsPC2 (b) PC1vsPC2vsPC3.

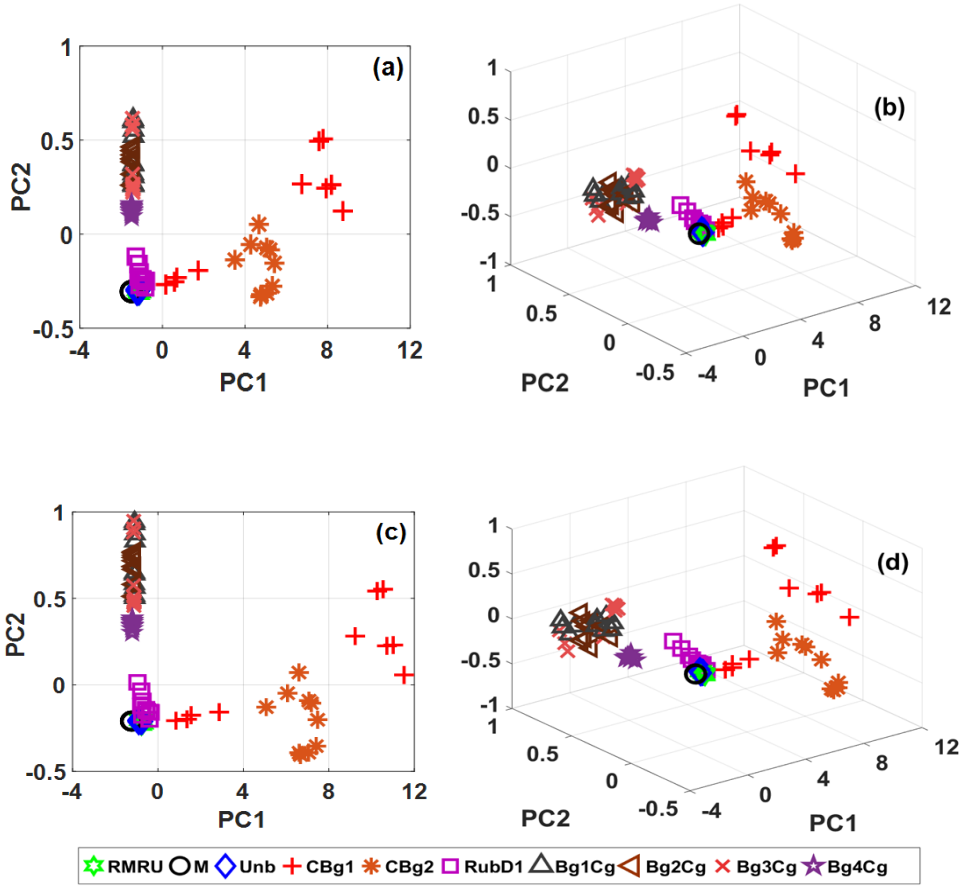

Figure 9. 16 Classification of combined SFTR-2 conditions for multiple speed single analysis with (a) AT-ApCCB (PC1vsPC2) (b) AT-ApCCB (PC1vsPC2vsPC3) (c) AT-RIpCCB (PC1vsPC2) (d) AT-RIpCCB (PC1vsPC2vsPC3).

9.3.3 Observation/ Discussion

The result from the application of the proposed dFAVF and AT-pCCB methods on improved SFTR-2 has been presented in subsection 9.3.2. It could be seen that the dFAVF method had distinct clustering and separation for individual conditions and mainly for the rotor and bearing conditions. This distinct separation of these faults could be because of their frequency range of occurrence, i.e., low (rotor faults) and high (bearing faults) frequency ranges. Furthermore, the observation from the AT-pCCB method, which is observed in two sub-methods, AT-ApCCB and AT-RIpCCB, gave some valuable classification of machine conditions. Observation showed good separation between rotor and bearing conditions and individual clustering of all conditions. A unique feature of this method is that individual rotor and bearing conditions are observed clearly. However, in the dFAVF approach, rotor conditions overlap, except when zoomed in, their clustering is seen. Also, the main difference between the AT-ApCCB and AT-RIpCCB is that the latter showed better separation of individual conditions. However, these are mere observations based on visibility on the PCA plots. The data quantification approach would be useful to determine the certainty and verify the claims of these indications on the plots.

9.4 Combined analysis with extended rotor and bearing faults

A combination of features from the SFTR-1 and SFTR-2 is carried out in this section. The aim was to strengthen the proposed fault identification models and investigate systems where machines with similar configurations enjoy useful fault diagnoses without the need for trending historical data.

9.4.1 Application of novel dFAVF and AT-pCCB fault identification method for combine SFTR-1 & 2

Equation (3.41), (3.49) and (3.50) are representation of the data matrix for computing the proposed dFAVF and AT-pCCB models. Normalisation was carried out afterward. Figure 9.17 presents the classification of PCA-based pattern recognition using the dFAVF method for combining features from SFTR-1 and SFTR-2 at single and multiple speeds. Figure 9.17 (a), a multiple-speed, single analysis for the consolidated rotor and bearing fault using the dFAVF method, gave a distinct separation of the bearing defect from the rotor faults. The rotor conditions are seen to overlap each other close to the

zero-point. The bearing conditions are well separated from each other and the rotor conditions. However, Bg4Cg was observed very close to the rotor conditions. Figure 9.17 (b) shows the 3D representation of the PCA-based pattern recognition approach for combined features from the SFTR-1 and SFTR-2 using the novel dFAVF. The 3D representation is a plot of PC1vsPC2vsPC3. The observation showed a distinct separation of the bearing conditions from the rotor. The rotor faults were seen to overlap each other, and the bearing conditions were separated in various directions from the rotor condition. The **Bg4Cg** case is very close to the rotor condition in Figure 9.17 (a) is observed to be some distance from the rotor condition in the 3D view in Figure 9.17 (b).

Figure 9.18 shows the features from the combined SFTR-1 and SFTR-2 using the proposed novel AT-pCCB fault identification model to classify consolidated rotor and bearing faults in a single analysis. Figure 9.18 (a) is a representation of the2D, PC1vsPC2 plot AT-pCCB amplitude component classification (AT-ApCCB). As can be seen, clustering and separation of the rotor from bearing faults overlap on all bearing conditions and few rotor conditions. Also, figure 9.18 (b) shows the classification from a 3D view with a PC1vPC2vsPC3 plot. Here, the separation between the rotor and bearing condition was conspicuous, with a huge overlap between the bearing conditions and a small separation of the **Bg4Cg** condition. Figure 9.18 (c) showed the same classification as Figure 9.18 (a) but with better separation between conditions. Likewise, Figure 9.18 (d) showed the same classification but better separation of machine conditions than Figure 9.18 (b).

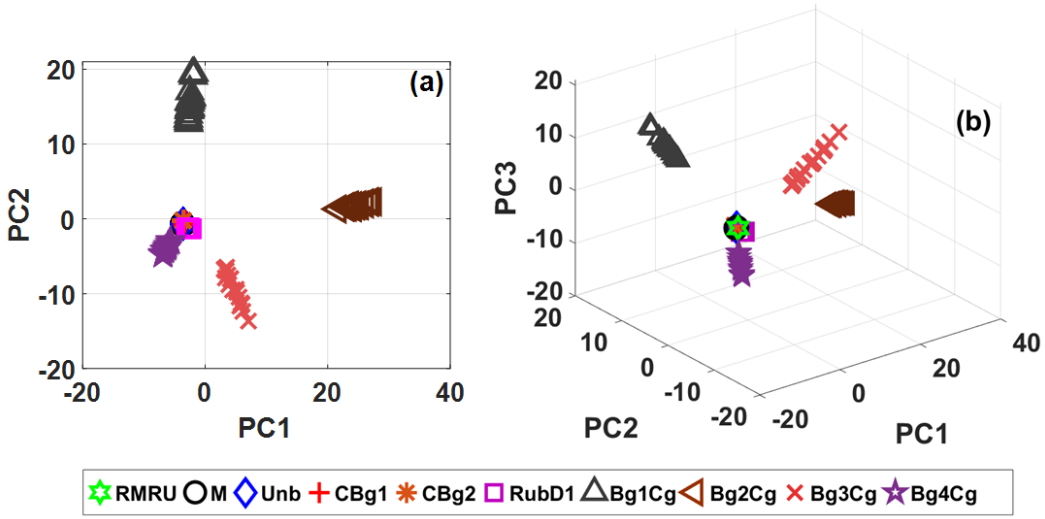

Figure 9. 17 dFAVF classification of combined SFTR-1&2 conditions at(a) PC1vsPC2 (b) PC1vsPC2vsPC3.

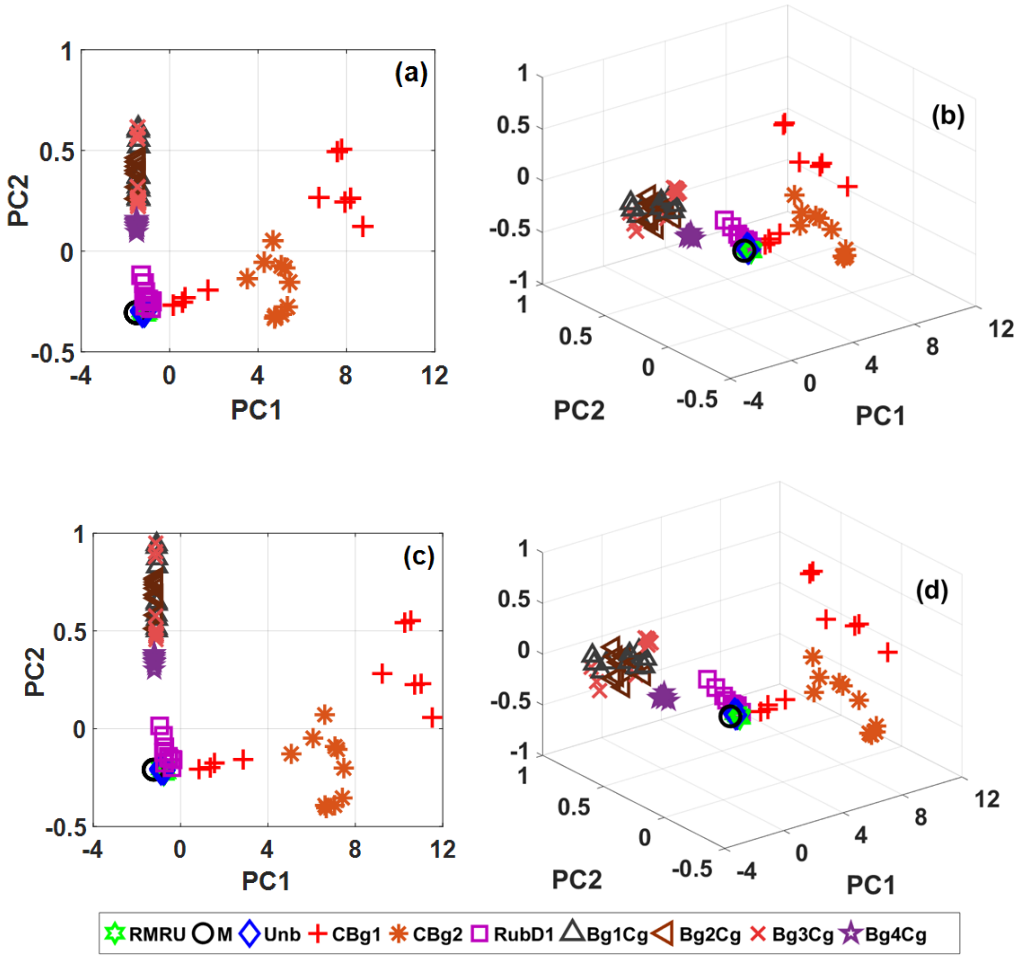

Figure 9. 18 Classification of combined SFTR-1&2 conditions for multiple speed single analysis with (a) AT-ApCCB (PC1vsPC2) (b) AT-ApCCB (PC1vsPC2vsPC3) (c) AT-RIpCCB (PC1vsPC2) (d) AT-RIpCCB (PC1vsPC2vsPC3).

9.4.2 Observation/ Discussion

Continued research into similar machines with different foundation flexibilities has been investigated in this study using data from the improved SFTR-1and SFTR-2 in a single analysis. The data from the SFTR-1 and SFTR-2 were useful in classifying an extensive range of machine faults, i.e., rotor and bearing faults, in a single analysis. The aim is to advance studies that explore understanding rotating machines' behaviour to fault identification and diagnosis, with similar machines installed in different locations having varying foundation flexibilities. Standardisation in recent times means similar machines with the same features are produced and supplied worldwide. Their installation type or foundation setup influences the flexibilities of this machine in terms of their natural frequencies (critical speeds). The development of a fault identification approach that can effectively diagnose machine conditions notwithstanding its foundation will be accepted, especially in industries with similar production plants across the globe. Also, the transference of these fault identification methods to older, similar machines with no baseline data that will be insensitive to diagnosis is investigated. So, by combining parameters from both test rigs, understanding various machine behaviour with respect to fault identification can be investigated.

Overall, the proposed dFAVF method classified the rotor and bearing faults in the combined test rig. The clustering of each condition and the separation between each are distinct. However, the rotor conditions seem to overlap. The AT-pCCB method, i.e., AT-ApCCB and AT-RIpCCB methods, gave each method a distinct classification, with the rotor faults separated from the bearing fault for each. A unique comparison of the dFAVF and AT-pCCB showed that the former gives a more explicit and distinct cluster of the rotor conditions while the latter showed overlap. However, a zoomed view of the dFAVF method showed distinct separation of all rotor conditions except for overlap between misalignment and unbalance.

9.5 Discussion

Investigations have been carried out using the proposed novel dFAVF and AT-pCCB methods for fault identification of signals from the SFTR-1, SFTR-2 and combined SFTR-1 & 2. A useful classification of machine conditions has been achieved overall. The dFAVF method classified a consolidated rotor and bearing faults and showed good clustering of individual conditions and separation for the rotor and bearing conditions. However, there seems to be an overlap in the rotor conditions except for the zoomed view, which showed useful separation for the rotor faults.

The classification using the AT-pCCB method showed good clustering for individual conditions and separated the rotor from bearing conditions. However, this model's separation shows a conspicuous rotor fault with the bearing, unlike in the dFAVF, where the rotors seem to overlap and are close to each other when a single consolidated analysis is done. Understanding of the result was observed from the quantification section of this thesis (section 9.6), which showed the values for the differentiation of baseline RMRU from the faulty conditions. Here, rotor faults are closer to each other, and that of AT-pCCB is separated except for the case of RubD1. However, the bearing cases for dFAVF showed better separation than AT-pCCB. The sensitivity of the diagnostics features is a contributory factor to why the AT-pCCB showed better classification than dFAVF for the rotor faults. Due to its complex conjugate computation, the spectrum analysis used in the dFAVF model only contained amplitude and no phase information. On the other hand, the AT-pCCB model had the bispectrum analysis, where both the amplitude and phase information are present in the computation.

Overall, this observation is seen in the SFTR-1, SFTR-2 and a combination of SFTR-1 & 2. The behaviour of the rotor and bearing faults from this novel approach is said to be from their frequency range, where the rotor-related faults have a low-frequency range, and the bearing faults have a high-frequency range. The usefulness of this study can be extended to include the mid-frequency range faults, i.e., the gear faults.

9.6 A comprehensive comparison between results from SFTR-1 and SFTR-2

The studies in earlier sections provided useful diagnosis approaches with the proposed novel dFAVF and AT-pCCB methods. However, these were from mere observation of the PCA plots. Notwithstanding the result, quantifying the outcome would help support and verify the usefulness of the proposed methods. Therefore, a comparison of the test rigs using results from the proposed fault classification methods is investigated and discussed in subsection 9.6.1.

9.6.1 Data quantification for discrimination of faulty conditions with respect to baseline RMRU for individual SFTR-1 & 2

Figure 9.19 comprehensively compares all proposed methods at the different PCA classification tools with the differentiation of **RMRU** to faulty conditions at multiple speeds for the SFTR1 and SFTR-2. This presents a single overview of the comparison. Comparing the various methods showed variation in the separation with respect to **RMRU** for the proposed methods. In SFTR-1, while misalignment, **CBg1** and **Bg1Cg** tend to have higher separation in the AT-RIpCCB method, dFAVF gave higher separation at **Unb**, **RubD1, Bg2Cg, Bg3Cg**, and **Bg4Cg**. Also, as observed in the PCA plot where AT-RIpCCB showed further separation than AT-ApCCB, there was a consistent increase for all conditions comparing AT-ApCCB to AT-RIpCCB. In SFTR-2, **RubD1, Bg1Cg, Bg2Cg, Bg3Cg** and **Bg4Cg** were higher in dFAVF than in AT-pCCB. However, the separation at **M, Unb, CBg1, and CBg2** were higher in AT-pCCB than in dFAVF. A similar observation was seen in the PC1vsPC2 and PC1vsPC2vsPC3, respectively. However, the values increased in most cases due to incorporating an additional principal component (PC). This classification aims to help the vibration analyst investigate a single analysis as they can select the method that provides a better understanding of fault identification of their investigated machines.

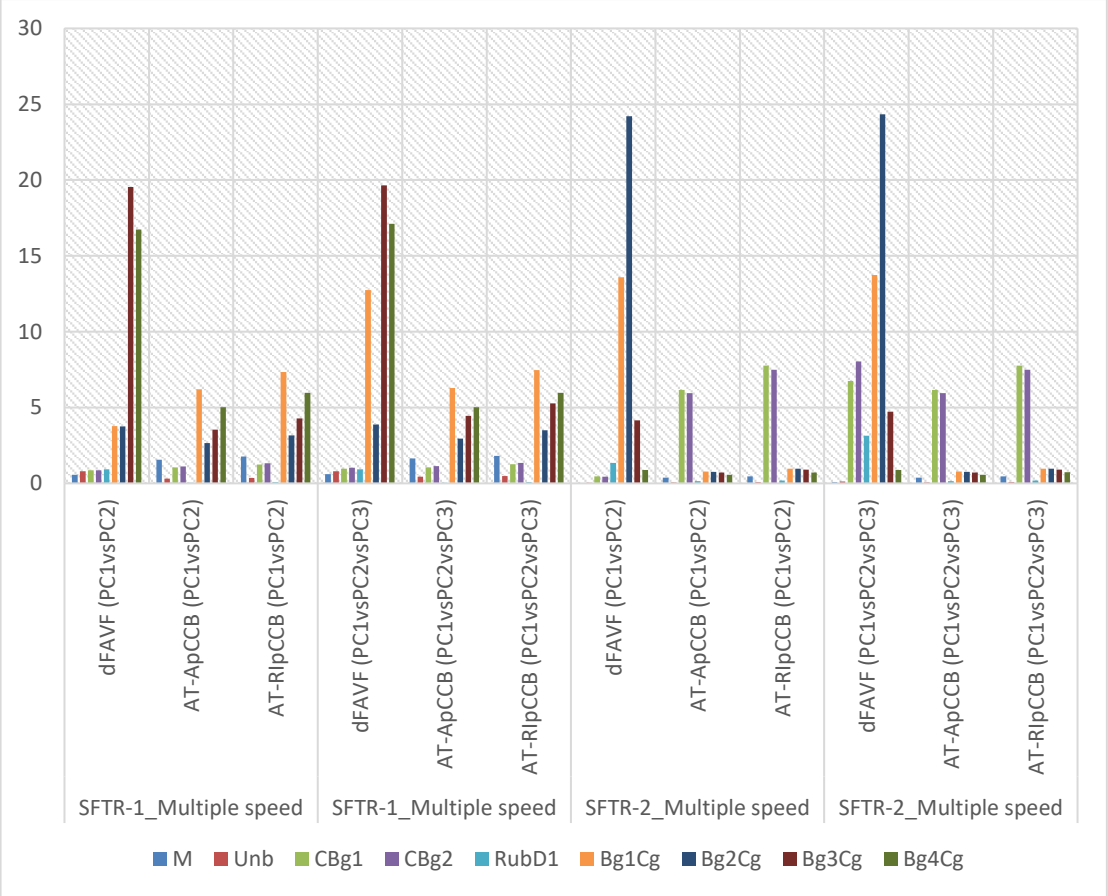

Figure 9. 19 Classification of SFTR-1 conditions multiple speed single analysis.

9.6.2 Data quantification for discrimination of faulty conditions with respect to baseline RMRU for combined SFTR-1 & 2

Figure 9.20 presents a comprehensive bar chart plot for the combined SFTR-1 and SFTR-2 data quantification for the proposed methods at the various PCA classification when **RMRU** was differentiated from the faulty conditions. However, for PC1vsPC2, **M, Unb, Bg1Cg, Bg2Cg, Bg3Cg** and **Bg4Cg** was observed to have a higher separation value at the dFAVF method than in the AT-pCCB method, while **CBg1** and **CBg2** had a higher separation value in AT-pCCB than in dFAVF method. Also observed was the consistent increase in separation value from the AT-ApCCB to the AT-RIpCCB method, which is consistent with observations from the PCA plots. A similar observation was also made in PC1vsPC2vsPC3. However, most conditions had higher separation values for PC1vsPC2vsPC3 compared to PC1vsPC2. Also, observation showed good separation for bearing conditions which are in the high-frequency range, while the rotor showed

reasonable separation, as they are in the low-frequency range. However, as stated earlier, the decision on which method fits the fault diagnosis of a particular machine should be made by the vibration analyst, who understands the machine's behaviour over time of application.

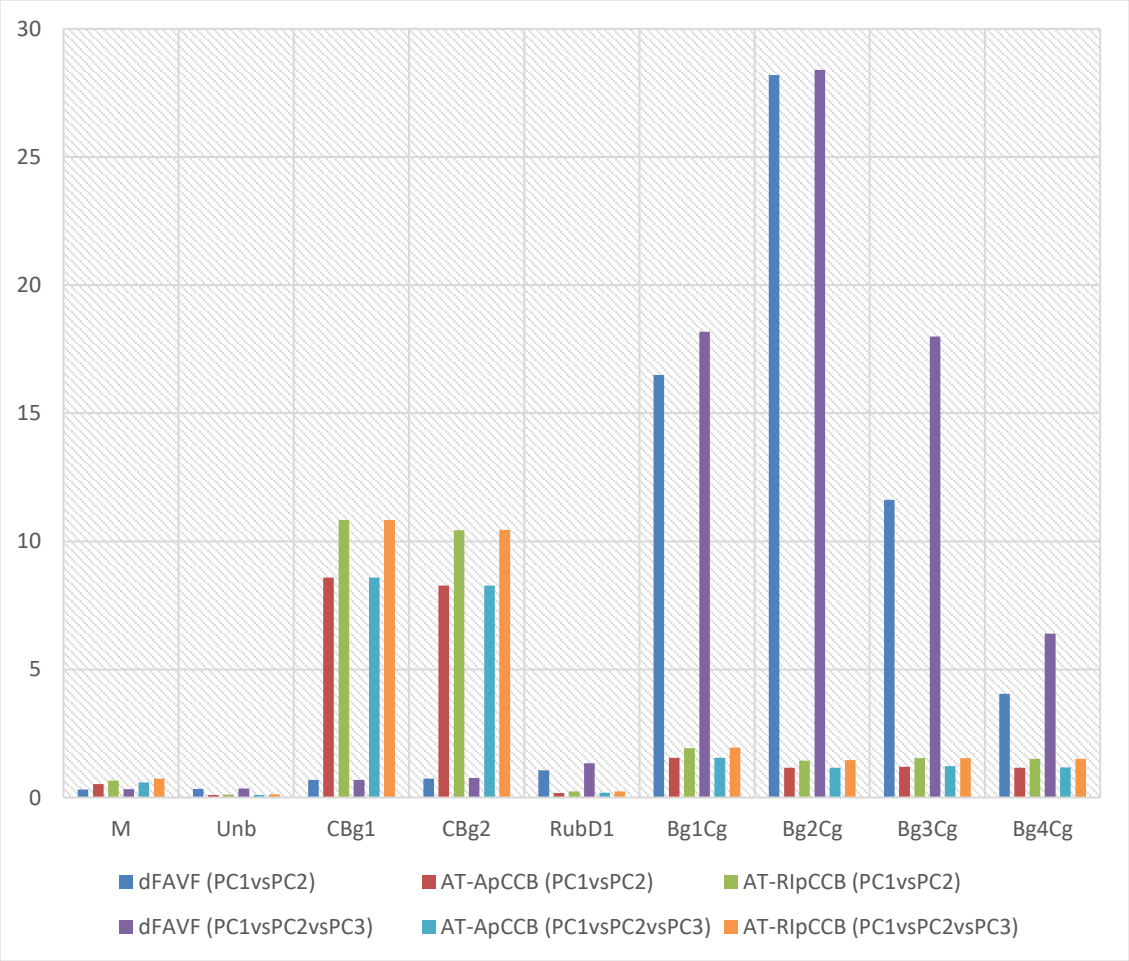

Figure 9. 20 Bar chart representing a differentiation of faulty from RMRU condition.

9.7 Chapter summary

A comprehensive study using the proposed novel dFAVF and AT-pCCB fault identification approaches has been carried out using signals from the SFTR-1 and SFTR-2 with more rotor and bearing faults simulated. Useful fault classification for the consolidated rotor and bearing fault analysis was achieved. Further investigation will strengthen the method and analyse features from multiple foundations with similar machine configurations, combining the two test rig's features for a consolidated rotor and bearing fault classification. The results showed clustering of individual conditions and separation between the rotor and bearing faults. However, the AT-pCCB proved better in classifying the rotor faults as better views of the rotor condition were observed compared to the dFAVF, which had overlapping rotor faults unless it was zoomed. The quantified approach helped verify observation from the PCA-based classification as the separation values were able to show the evidence of the faults and the separation of rotor form bearing, which indicates their frequency range of occurrence. The presence of amplitude and phase information in the pCCB components makes the AT-pCCB model better at classifying rotor faults. Overall, these proposed approaches have proven to classify rotor and bearing fault conditions in a single analysis. However, the knowledge of the machine's dynamic behaviour would determine the best approach to be applied in the fault diagnosis by the vibration analyst.

CHAPTER 10

CONCLUSION AND FUTURE WORK

This chapter present the conclusion of this research study, contribution to knowledge and future work.

10.1 Overall summary

Vibration-based condition monitoring (VCM) for fault identification is popular in the early detection of faults in rotating machines. The importance of rotating machine in the industry cannot be overstated. In recent times industrial machinery tend to be complex in operation due to computerisation and industry 4.0. Asset management holds views that continuous improvement of machine integrity in an industrial environment ensures availability and reliability. Hence, the need to keep improving vibration-based condition monitoring techniques. Critical part of rotating machines such as rotor and bearing encounter faults during their operation. The dynamic behaviours of these faults can be better understood from their frequency range, i.e., rotor-related faults show up in the low-frequency range and bearing faults are seen high-frequency range. Traditional time and spectrum analysis has been useful in diagnoses of the rotor and bearing faults. However, fundamental defect frequencies obtained from the bearing characteristics are useful for bearing fault diagnosis. Envelope analysis provides good monitor for bearing frequency ranges where the defect's repetitive impacts occur and cut out non repetitive impact signal. Several research, have proposed novel fault identification approach of both rotor and bearing faults individually. This research presents a novel consolidated fault identification and detection approach for rotating machines running at different steady state speed. Experimental rig with different foundation flexibilities were employed to generate data with single sensor per bearing pedestal. Initial investigation used data collected by a previous PhD student who is currently in the supervisory team of this research, from a flanged-based flexible test rig (FFTR) which he built. Preliminary investigation used the existing data from the FFTR, collected below the rig's first critical speed. Time domain parameter i.e., root mean square (RMS), crest factor (CF), kurtosis (Ku) and frequency domain parameter i.e., 1x – 5x harmonics of the machine running speed and spectrum energy, all of which are useful condition indicators extracted from the measured vibration data which where obtain when the rig was running at different speed. A baseline residual misalignment residual unbalance (assumed to be the healthy state) and faulty (rotor-related) conditions which include misalignment, shaft bow, mechanical looseness and shaft rub were selected for the FFTR. The time and

frequency domain analysis were first presented to explain the challenge faced in analysing data obtained at different speeds. Once this is done, the selected features with useful condition indicator were employed to carry out analysis. These features where extracted from acceleration signals. Investigation was done at 1200 rpm (20 Hz), 1800 rpm (30 Hz) and 2400 rpm (40 Hz) with useful information at steady state speed for the FFTR. However, the multi-speed analysis which had a combination of the 3 speeds in a single analysis yielded successful results where all conditions separated distinctly. Achieving this result further validated earlier study which proposed the unified multispeed analysis (UMA) as different sets of faults where employed. This study and the UMA were both carried out with vibration acceleration signals for rotor faults only when test rig operated below its first critical speed. Improving this approach became the focus, therefore the velocity signal was considered for analysis. This is in line with recommendation where velocity parameters that are good condition indicators such as CF and RMS are useful especially in detecting rotor-related fault. The time and frequency domain analysis were also presented for the velocity signal obtained by integrating the measured acceleration signal. Waveforms and spectrums indicated similar features as those of acceleration. Similarly, features where extracted from time and frequency domain parameters of the velocity signal. Analysis of these features was done on three steady state speed. The classification of velocity features gave better result than acceleration. Further investigation led to the improvement of acceleration-based time and velocity-based frequency domain analysis. This was done to create a background for classification of an extensive range of rotating machine faults. The improved approach gave a more outstanding classification than both acceleration and velocity individually.

Many industrial machines are built with multiple shaft and multiple bearing operating at multiple speeds over several critical speeds. Understanding of such machine dynamics and characteristics of faults that show up is helpful in early detection of faults. In line with this, current research improved the earlier flanged-based flexible test rig (FFTR) to become spring-based flexible test rig (SFTR). This was achieved by redesigning the bearing pedestal and replacing the flange with springs. The aim is to alter the foundation flexibility so that the test rig can run above and below various

critical speeds. Based on modal analysis the first few natural frequency allowed for the test rig to operate below and above its first critical speed. Vibration signals from the STFR-1 was collected when machine ran at 450 rpm (7.5 Hz) below first critical speed, 900 rpm (15 Hz) and 1350 rpm (22.5 Hz) above first critical speed for baseline residual misalignment residual unbalance (assumed to be the healthy state) and faulty (rotor and bearing defect) conditions which include unbalance, misalignment, and shaft rub, shaft crack and bearing cage defect for the STFR. Investigation was done using acceleration features with useful classification. The acceleration signal for the SFTR-1 was converted to velocity using omega arithmetic method. Validating the improved approach, led to a proposed novel data fusion of acceleration and velocity features (dFAVF) model for identification of a wide range of rotating machine faults (rotor-related and bearing). The dFAVF model gave better separation at the multi-speed analysis. This separation was clearer and further than that of acceleration features classification. The novelty of this work is that rotor and bearing faults was detected and distinguished in a single analysis.

As faults develop on a system, a vibration signal's frequency structure is altered by either change in magnitude or phase of its periodic components. The spectrum density helps to determine these harmonic components of a signal. These components were used in classification of consolidated rotor and bearing faults. However, during computation, phase information is lost due to its combination with the conjugate of the Fourier transform. This limitation is resolved in the higher order spectrum (HOS) analysis which retains both amplitude and phase. Earlier studies proposed the poly-Coherent Composite Bispectrum (pCCB). However, current study considered only the pCCB components in its analysis. In this study, the first few pCCB components from the spring-based flexible test rig (SFTR-1) were used to further identify and classify rotor faults with machine operating both below and above its first critical speed. The outcome showed useful classification of various machine conditions. A further investigation covered the improvement of the pCCB components where a range of pCCB components were investigated to understand their sensitivity in determining overall machine behaviour as well as behaviour of certain rotating machine faults. Results showed that some additional pCCB components tend to give better sensitivity

under crack shaft and shaft rub, which makes them choice parameter in diagnosing these conditions. Since the pCCB is a complex number with real and imaginary parts, further investigation to improve its classification features was achieve by combining the real and imaginary pCCB components features when the machine ran both below and above its first critical speed. Investigation showed better clustering of each condition as compared to amplitude of pCCB components. Since acceleration-based time-domain features such as kurtosis (Ku) and crest factor (CF) help in investigation of impulsive signal which are found in bearing defect, useful results from the pCCB diagnosis ushered the inclusion of bearing features for a simple yet robust diagnosis. Thus, a proposed novel acceleration-based time domain features and poly-coherent composite bispectrum components (AT-pCCB) model for a consolidated rotor and bearing fault diagnosis is presented. Fault classification using the novel AT-pCCB gave clearer separation of rotor and bearing. To strengthen the result in this study, more rotor and bearing faults from similar machines installed with different foundation flexibility that is the improved spring-based flexible test rig 1 (SFTR1) and spring-based test rig 2 (SFTR2) were investigated. On the overall, optimal fault identification was achieved for a consolidated diagnosis of machines' critical part. The separation between the rotor-related and bearing faults may be because of their frequency range. Thorough observations shows that the aims of this research have been achieved.

10.2 Achieved objectives and contributions to knowledge

A description showing how each of the objectives given in chapter one (section 1.4) of this thesis were clearly achieved is presented here.

1. **To carryout data trending of time and frequency (spectrum) domain parameters using an existing data from an earlier built flange-based flexible test rig (FFTR) which ran only below its first critical speed. This will help to determine parameter sensitivity for fault identification.**

Data trending is very important in fault identification and diagnosis. It involves strategic representation of signal trends, extraction of features from signals, representation of these trends, comparison to infer their state in the process. The

data trend showed how various parameters can contribute to indicating the presence of different faults in a signal.

An earlier study extracted some time and frequency domain features in developing models for the proposed unified multispeed analysis (UMA) and multiple speed multiple foundation (MSMF) approaches, yielding a robust fault classification and identification methods. To build on this study, data trending of some of the parameters selected in the studies were carried out in this study to check for their sensitivity in diagnosing machines' fault especially for the consolidated rotor and bearing faults. The selected features included time domain, root mean square (**rms**), crest factor (**CF**), and kurtosis (**Ku**), and frequency domain, **1x,2x,3x,4x,5x** and spectrum energy (**SE**). The result of the data trend on the acceleration-based vibration signals obtained when the test rig operated at 400 rpm (20 Hz) showed the presence of the faults simulated in the test rig due to the sensitivity of the amplitude. However, the individual features used in this trending were considered at the four different bearing location. It was observed that some features showed high magnitude close to the bearing where they were simulated.

Though the results were indication of the sensitivity of the features at individual analysis, this approach will be cumbersome for a vibration analyst as large data would be analysed to identify faults. Thus, these sensitive features were considered for data fusion in the current study. Thus, this study proposed data fusion approach using various sensitive features obtained from the analysis of time and frequency domain parameters in vibration signal.

2. **To improve fault identification using acceleration and velocity features an approach developed from existing unified multispeed analysis (UMA) where only acceleration data from an earlier built flange-based flexible test rig (FFTR) which ran only below its first critical speed was used.**

An improved fault identification using acceleration and velocity features was accomplished. The aim was to improve an earlier unified multispeed analysis (UMA) which considered only acceleration features of rotor-related faults while

the flanged-based flexible test rig (FFTR) operated below its first critical speed. Acceleration signals are very useful in fault diagnosis especially in the identification of bearing defects. On the other hand, velocity signals are useful in detecting rotor faults. However, rotor faults using acceleration data was carried out in the earlier UMA.

Acceleration-based vibration signals from earlier FFTR were collected at a sampling frequency of 10kHz at 400 rpm (20 Hz), 800 rpm (30 Hz) and 1200 rpm (40 Hz) all below the machine's first critical speed which was 50.66 Hz. The machine conditions from the available data included residual misalignment residual unbalance (RMRU), misalignment (M), shaft bow, mechanical looseness, and shaft rub. A preliminary investigation tried to replicate the earlier proposed UMA by classifying the machine conditions by using PCA pattern recognition approach in fault classification where selected principal components (PCs) are plotted against each other. In this study, a plot of PC1vsPC2 was carried out. This classification helped to validate the UMA. Further investigation led to the conversion of acceleration data into velocity. Similar classification was carried out using velocity features. The results showed more separation between each machine condition which indicated better fault identification analysis. Since the aim is to observe a wide range of machine faults, sensitive features from acceleration and velocity data were used in classifying machine conditions. The results showed improved classification when compared with that of only acceleration and velocity features classification of rotor faults. The study proposed the simple data quantification approach for comparing the acceleration features analysis (UMA), velocity features analysis and combined acceleration and velocity features analysis by differentiating the baseline-RMRU from faulty rotor conditions. Comparison across the three scenarios showed the improved acceleration and velocity features analysis gave better separation which is indicated a clearer fault diagnosis for the rotor faults.

3. **To improve the existing FFTR to a spring-based flexible test rig (SFTR) so that it operates below and above its first critical speed. Afterwards, both rotor and bearing faults will be simulated on the SFTR.**

The research improved the existing flange-based flexible test rig (FFTR) to the current spring-based test rig (SFTR). This was to allow machine to run over its first critical speed a representation of most industrial system.

Most industrial rotating machines are complex, having multiple shafts connected to multiple bearings and operates at multiple speed running over the machine critical speeds (natural frequencies). This operation can be observed especially in aircraft and some turbomachines. To investigate such complex system, the FFTR which already has multiple rotor and multiple bearing and a which has a flange-based bearing pedestal was modified to lower its first critical speed to 11.52 Hz using spring bearing pedestals, thus a spring-based flexible test rig was built. On the other hand, the machine conditions simulated in the FFTR were only rotor related, however, the research aims to investigate and extensive range of rotating machines' critical parts faults which includes rotor and bearings. Thus, the simulated faults in the SFTR-1 were rotor-related RMRU, misalignment, unbalance, crack, rub, and bearing cage defects.

4. **To develop a novel fault identification approach for diagnosis of a rotating machines consolidated critical parts (i.e., rotor and bearing) faults in a single analysis.**

The study proposed the novel data fusion of acceleration and velocity features (dFAVF) for rotor and bearing faults classification and identification in. a single analysis. Preliminary investigation improved the UMA approach by classifying acceleration and velocity features for rotor faults diagnosis, where machine data from the FFTR were collected below machines' first critical speed. However, to obtain a robust fault identification approach, both rotor and bearing faults have been simulated using the SFTR-1.

Acceleration-based vibration signals were collected at 10kHz sampling frequency, for rotor faults (RMRU, M, Unb, CBg1, CBg2 and RubD1) and, bearing cage defects (Bg1Cg and Bg2Cg). The signals were collected at 450 rpm (7.5 Hz) below machines' first critical speed, 900 rpm (15 Hz) and 1350 rpm (22.5 Hz) both above machines' first critical speed. Initial investigation used acceleration data for analysis where both time and frequency domain analysis were carried out and the sensitive parameters extracted i.e., time domain, rms, CF and Ku, and frequency domain 1x-5x and SE. PCA pattern recognition approach was employed in data classification where PC1 is plotted against PC2. However, the current classification lend extra credence to the UMA approach as all conditions were classified and separated showing good diagnosis and fault identification. Thereafter, acceleration signal is converted to velocity using the omega arithmetic approach. At this point, the acceleration-based time domain for the bearing defects and velocity-based frequency domain for rotor faults were fused to develop a model for classification. The result showed better clustering and separation for the dFAVF than acceleration analysis which was achieved in. a single analysis. Another observation is that the rotor faults tend to overlap for most of it but separated when zoomed in, and they tend to cluster together at same location in the plot which is further away from the bearing faults. This happened based their frequency range of occurrence. As the rotor faults are low frequency range and bearing faults are high frequency range.

To understand the diagnostic information present in the PCs, the research observed the PCA-based fault classification approach with increased number of principal components (PCs) and compared PC1vsPC2 and PC1vsPC2vsPC3. Observation showed that PC1vsPC2vsPC3 showed better classification than PC1vsPC2. However, a simple data quantification approach for that differentiates the baseline RMRU from faulty conditions for rotor and bearing was carried out while comparing the increased PCs classification, the PC1vsPC2vsPC3 gave higher magnitude than PC1vsPC2 indicating more diagnostic information is present.

5. **To improve an existing poly-coherent composite bispectrum (pCCB) method for rotor related fault identification while analysing the complex number components which combines the real and imaginary part of the pCCB components for fault identification.**

The research improved an existing poly-coherent composite bispectrum (pCCB) fault detection approach, by investigating the pCCB components which can detect rotor faults effectively mainly shaft crack and rub faults. Note that the spectrum analysis loses its phase information due to the complex conjugate of the Fourier transform (FT) computation. However, the pCCB analysis optimises the spectrum analysis where the amplitude and phase information are retained in its computation and signals from multiple sensors are integrated in its analysis.

In this thesis, vibration signals investigated under the pCCB analysis were from the SFTR-1, collected at 3 different speed 450 rpm (7.5 Hz), 900 rpm (15 Hz) and 1350 rpm (22.5 Hz) for rotor faults (RMRU, CBg1, CBg2, RubD1). The pCCB components; B_{11}, B_{12}, B_{13} are extracted for classification just like it was done in earlier study. The classification was PCA-based where plots of PC1vsPC2 was observed. The results reaffirm earlier proposed fault diagnosis using pCCB components. Further investigation led to additional pCCB components in the analysis which included B_{11}, B_{12}, B_{13} and B_{22}. PCA-based pattern recognition approach carried out, showed good clustering and separation of all conditions especially the CBg1, CBg2 and RubD1. This improvement indicates that the information in B_{22} is useful in diagnosing these faults as there is the 2x and 4x components in their spectrum plots. To expand the analysis using pCCB components, a comparison of the amplitude to the real and imaginary (complex number) components of the pCCB were investigated for classifying rotor faults. The parameters extracted where used in PCA-based pattern recognition approach for classification. The outcome showed the real and imaginary pCCB classification gave better separation of the machine conditions than the amplitude of pCCB classification.

Also, comparison of PC1vsPC2 and PC1vsPC2vsPC3 plot was carried out, however, the PCs plot comparison did not indicate much difference. Thus, additional PCs

may not provide useful information in the PCCB classification. A simple data quantification approach that differentiates baseline RMRU from faulty conditions for rotor faults for the pCCB analysis scenarios were carried out and comparison of PC1vsPC2 and PC1vsPC2vsPC3 done. The value reaffirms that the real and imaginary pCCB classification of rotor faults had more separation than the Amplitude of pCCB, however, the difference for the PC plots did give much difference.

6. **To develop a novel fault identification approach using a blend of time domain and pCCB components for a single analysis of extensive range of rotating machine critical part faults.**

The research proposed a novel hybrid feature reduction method using the acceleration-based time domain and pCCB (AT-pCCB) components for rotor and bearing fault classification in. a single analysis. This method comprised of acceleration features from bearing faults and pCCB components from rotor faults for classification. The proposed AT-pCCB is subdivided into the AT-ApCCB and AT-RIpCCB which are the acceleration-based time-domain and amplitude of pCCB and the acceleration-based time-domain with real and imaginary pCCB respectively. Classification showed good separation of individual conditions, however, the rotor faults were seen to cluster together around a location far from the bearing conditions. This again indicates the frequency range of their occurrence where rotor faults occur around the low frequency range and bearing faults around the high frequency range. However, the AT-RIpCCB tends to show better separation for individual classification than the AT-ApCCB. Notwithstanding both sub approaches provided good indication for both rotor and bearing faults in. a single analysis.

A simple data quantification approach differentiates RMRU from faulty conditions for rotor and bearing diagnosis for the AT-ApCCB and AT-RIpCCB models was carried out. The research observed and compared the PCA-based fault classification approach with increased number of principal components (PCs) (PC1vsPC2 and PC1vsPC2vsPC3).

7. **To understand fault identification and dynamic behaviour of similar rotating machines with different foundation flexibility using the methods to be proposed. So that vibration signals from more than one test rig are investigated and analysis observed while combining data from these rigs.**

Industrial rotating machines are sometimes similar in structures, dimensions, and models due to standardisation; but their dynamics behaviour may be different due to installation foundation or/and location. Also, some old machines lack baseline data that could be useful for comparison in fault diagnosis. Understanding the dynamic behaviour of these machines would improve fault diagnosis, such that the fault identification parameters may be insensitive for the different machine. Thus, fault identification approach can be successfully implemented so that data from one machine can support fault identification in another.

The research carried out an enhance fault identification approach by observing the dFAVF and AT-pCCB (AT-ApCCB and AT-RIpCCB) with extensive rotor and bearing faults classification multiple foundation (SFTR-1 and SFTR-2) and multiple speed. Thereafter, combining features for classification of machine conditions, to understand both machine and fault behaviour for similar but different machines using the proposed methods. The research observed and compared the PCA-based fault classification approach with increased number of principal components (PCs) (PC1vsPC2 and PC1vsPC2vsPC3). A simple data quantification approach that differentiates RMRU from faulty conditions for rotor and bearing diagnosis was carried out and the outcome shows the AT-pCCB gave better classification of rotor faults than dFAVF, while the rotor and bearing faults classification supported the low and high frequency range occurrence.

10.3 Future Work and recommendations

This thesis has presented findings in relation to the aims and objectives set out that is the development of consolidated rotor and bearing fault identification approach in rotating machines with a single analysis. However, all the intentions are still yet to be met. These will be considered in future research projects. They include.

1. **Simulate other types of bearing faults for consolidation with rotor faults.**

The study has carried out preliminary consolidated rotor and bearing faults diagnosis in a single analysis, where only one bearing fault (cage defect) have been simulated experimentally at multiple locations. Thus, further work to observe the various bearing failure (inner race, outer race, ball, and cage) in a consolidated fault single analysis should be carried out. This helps to extend fault identification and improve the fault identification approach.

2. **Incorporate 'mid' (gear) frequency range faults into the proposed model that considered only 'low' (rotor) and high (bearing) frequency range faults.**

This study considered the 'low' (rotor related) and 'high' (bearing related) in a single analysis. However, the 'mid' frequency range faults (gear related) would also contribute to improve fault identification and gain better understanding of machine behaviour with respect to the various fault conditions especially for machines with all three critical components.

3. **Use anti-friction (Split bearings) bearing which can simulated the various bearing faults conveniently than the rolling element bearing.**

The rolling element bearings were used to simulate bearing faults. Simulation of fault on this component is very demanding such on the inner race and outer race destroys the component beyond use while only the ball and cage fault simulation is possible, the hardness of the ball containing the lubricated grease makes it difficult to simulate a ball fault. However, the anti-friction bearing is built in such a way that allows each fundamental frequency faults simulation done with precision of depth and thickness without affecting machine operation. Thus, further studies should consider the anti-friction bearing such as the fluid bearing which is popular in many industrial systems.

4. **Apply industrial data to further validate the proposed dFAVF and AT-pCCB which were developed using lab-based data.**

Data from a lab-based test rig has been used by the proposed approaches i.e., dFAVF and AT-pCCB to successfully classified a consolidated rotor and bearing fault in a singles analysis. Extending the approaches to industrial data would help validate and also improve the proposed methods.

5. **Investigate consolidated fault identification and classification using artificial intelligence where data are trained.**

Recent industrialisation and mechanisation demand a quick, robust but simple fault identification approach that will aid prompt maintenance response for effective and efficient production and operation of the machine. The recent artificial intelligence fault classification approach such as ANN, KNN, Kernel and so on would be useful in observing fault classification for a consolidated rotor and bearing fault conditions in a single analysis as the training of data can efficiently produce useful classification information with data being incorporated into the classification model.

6. **Use of finite element analysis to further validate the proposed fault identification method as well as foundation flexibilities investigations.**

Theoretical approach such as finite element analysis (FEA), is a useful tool in validating experimental results. In as much as there are some drawbacks in application of FEA models, it can simulate various machine systems such as foundation flexibilities and, also various rotor and bearing faults which can be classified using the proposed methods.

7. **Using other bearing fault diagnosis approaches. for investigating a consolidated rotor and bearing fault diagnosis in a single analysis.**

This study focused on time domain features (RMS, crest factor and kurtosis) for bearing fault features classification. However, there are several developed methods for bearing faults detection such as shock pulse monitoring, wavelet

transform, permutation entropy, fuzzy entropy etc. Bearing diagnostics features from any of these methods fused with features for rotor diagnosis would provide an alternate consolidated rotor and bearing fault diagnosis in a single analysis.

8. **Apply feature reduction approach to manage huge vibration data collected for analysis.**

In vibration analysis, there is always huge data collected and the analyst may find it cumbersome managing these data for classification. This study proposed a reduced features for classification method (AT-pCCB). However, further studies should be carried out to improve the approach to obtain useful and sensitive features that retains the faults behaviours while those features with less sensitivity can be taken out.

9. **Carry out velocity-based bispectrum analysis and comparing with acceleration for investigating both rotor and bearing fault since it is mostly useful in analyses of non-linear signals.**

This study focused on acceleration-based poly-coherent composite bispectrum (pCCB) analysis with useful fault identification and improvement of diagnosis method. Further work should consider bispectrum analysis using velocity signal as this may give useful parameters for improved fault identification in comparison of acceleration parameters for both rotor and bearing analysis.

10. **Fault simulation would consider two or more faults at a time as against individual faults simulation done in this study, most industrial cases have more than one fault at a time.**

In this study, all faults were simulated individually and independent of each other. However, in industrial scenarios multiple faults exist at a time on the same machine, for example, a machine may have misalignment which would have led to looseness and thus crack in the inner race. Therefore, further work would be to

simulate multiple faults existing simultaneously on the test rig and investigate individual classification of the faults.

APPENDIX A

A1 Acceleration and velocity spectrum amplitudes for observation

The amplitude of the acceleration and velocity spectrum have been presented in Table A1 to A8. Table A1.1 and A1.2 are those for bearing one acceleration and velocity data respectively. Table A1.3 and A1.4 are Bearing 2 acceleration and velocity data respectively. Table A1.5 and A1.6 are Bearing 3 acceleration and velocity data respectively, and Table A1.7 and A1.8 are for Bearing 4 acceleration and velocity data respectively.

Table A. 1 Acceleration spectrum data for all conditions with harmonics and SE for Bg1.

	RMRU	M	S-Bow	M-looseBg3	RubD2
1x	0.1873	0.1309	0.4573	0.1804	0.0867
2x	0.0936	0.0645	0.0698	0.1073	0.0457
3x	0.0401	0.0187	0.3459	0.1258	0.0439
4x	0.0238	0.0129	0.0289	0.0083	0.0137
5x	0.0096	0.0095	0.0378	0.0408	0.0109
SE	0.0186	0.0605	0.1477	0.0305	0.0567

Table A. 2 Velocity spectrum data for all conditions with harmonics and SE for Bg1.

	RMRU	M	S-Bow	M-looseBg3	RubD2
1x	1.491078	1.042012	3.638943	1.435251	0.690281
2x	0.744537	0.513312	0.555541	0.85381	0.363663
3x	0.318928	0.148932	2.752536	1.000748	0.349095
4x	0.18908	0.102413	0.230746	0.06595	0.109366
5x	0.076165	0.075426	0.301005	0.32518	0.087507
SE	1.491078	1.042012	3.638943	1.435251	0.690281

Table A. 3 Acceleration spectrum data for all conditions with harmonics and SE for Bg2.

	RMRU	M	S-Bow	M-looseBg3	RubD2
1x	0.4298	0.3746	0.6299	0.2923	0.2877
2x	0.0556	0.0378	0.0999	0.0155	0.0405
3x	0.0857	0.0237	0.7891	0.0868	0.0809
4x	0.0223	0.0103	0.0329	0.1359	0.0264
5x	0.0199	0.0196	0.0663	0.1295	0.1406
SE	0.0235	0.0763	0.1869	0.0389	0.0716

Table A. 4 Velocity spectrum data for all conditions with harmonics and SE for Bg2.

	RMRU	M	S-Bow	M-looseBg3	RubD2
1x	3.420053	2.980954	5.013072	2.326098	2.289367
2x	0.442244	0.3011	0.794774	0.123209	0.321904
3x	0.681775	0.188546	6.279342	0.691005	0.643949
4x	0.17722	0.081667	0.262373	1.08162	0.210229
5x	0.158992	0.156209	0.52729	1.030913	1.118632
SE	3.420053	2.980954	5.013072	2.326098	2.289367

Table A. 5 Acceleration spectrum data for all conditions with harmonics and SE for Bg3.

	RMRU	M	S-Bow	M-looseBg3	RubD2
1x	*0.3549*	*0.2626*	*0.5681*	*1.6410*	*0.1559*
2x	*0.0467*	*0.0472*	*0.0592*	*0.1467*	*0.0291*
3x	*0.0866*	*0.0339*	*0.4966*	*0.5097*	*0.0328*
4x	*0.0336*	*0.0229*	*0.0268*	*1.1245*	*0.0240*
5x	*0.0157*	*0.0282*	*0.0236*	*1.6057*	*0.0573*
SE	*0.0277*	*0.0879*	*0.1990*	*0.0394*	*0.0822*

Table A. 6 Velocity spectrum data for all conditions with harmonics and SE for Bg3.

	RMRU	M	S-Bow	M-looseBg3	RubD2
1x	2.824068	2.089438	4.520794	13.05905	1.240264
2x	0.37101	0.375655	0.471172	1.167574	0.231669
3x	0.689145	0.270044	3.951796	4.056407	0.260881
4x	0.267653	0.181912	0.213344	8.948533	0.191249
5x	0.125288	0.223996	0.18819	12.7781	0.456042
SE	2.824068	2.089438	4.520794	13.05905	1.240264

Table A. 7 Acceleration spectrum data for all conditions with harmonics and SE for Bg4.

	RMRU	M	S-Bow	M-looseBg3	RubD2
1x	*0.2519*	*0.2158*	*0.3169*	*0.2455*	*0.1351*
2x	*0.0102*	*0.0165*	*0.0222*	*0.0379*	*0.0122*
3x	*0.0746*	*0.0189*	*0.1813*	*0.0611*	*0.0135*
4x	*0.0084*	*0.0138*	*0.0154*	*0.0496*	*0.0110*
5x	*0.0104*	*0.0143*	*0.0124*	*0.0981*	*0.0202*
SE	*0.0186*	*0.0568*	*0.1201*	*0.0248*	*0.0509*

Table A. 8 Velocity spectrum data for all conditions with harmonics and SE for Bg4.

	RMRU	M	S-Bow	M-looseBg3	RubD2
1x	2.00467	1.717048	2.521763	1.953562	1.074987
2x	0.081691	0.131501	0.176724	0.301394	0.097107
3x	0.593367	0.150561	1.44248	0.485839	0.107561
4x	0.066785	0.109642	0.12217	0.395483	0.087572
5x	0.082581	0.113634	0.098685	0.780412	0.160561
SE	2.00467	1.717048	2.521763	1.953562	1.074987

A2 Rolling element bearing characteristic frequencies

Figure 5.2 show a diagram representing the internal structure of a typical ball bearing, the inner race, outer race, balls, and cage are represented clearly. The fundamental frequencies can be calculated based on the geometry of the bearing [56].

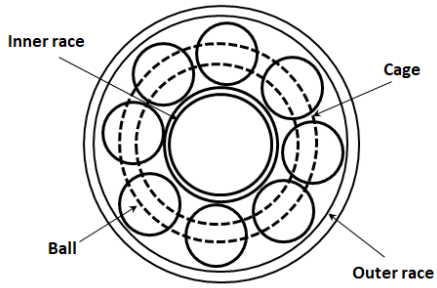

Figure A 1 Schematic of a rolling element bearing.

According to Jyoti [56], rolling bearing consist of the inner race, which is mounted directly on the shaft, the outer race which is connected to the bearing housing or machine pedestal and a number of balls. In diagnosis of the rolling element bearings defects, some frequencies are generated based on the bearing geometry and the relative speed between the inner and outer race [12]. These frequencies are called the fundamental fault frequencies or the bearing characteristics frequencies. Knowledge of the bearing geometry helps to determine the fundamental fault frequencies which are ball pass frequency inner race (BPFI), ball pass frequency outer race (BPFO), fundamental train frequency (FTF) and ball spin frequency (BSF) [56] [12]. They are mathematically represented as:

$$BSF = \frac{d_b}{d_p} f_r \left(1 - \left(\frac{d_b^2}{d_p^2}\right) cos\beta^2\right) Hz \tag{A1}$$

$$BPFI = \frac{n}{2} f_r \left(1 + \frac{d_b}{d_p} cos\beta\right) H \tag{A2}$$

$$BPFO = \frac{n}{2} f_r \left(1 - \frac{d_b}{d_p} cos\beta\right) Hz \tag{A3}$$

$$FTF = \frac{f_r}{2} \left(1 - \frac{d_b}{d_p} cos\beta\right) Hz \tag{A4}$$

Here ball diameter and pitch circle diameter are represented by d_b and d_p respectively. The f_r represents relative speed between the inner race and outer race i.e., shaft speed, and β is the ball contact angle [56].

A3 Engineering drawing for the design of the SFTR bearing pedestal

The modification from the flanged-based flexible test rig (FFTR) to the spring-based flexible test rig (SFTR) was a major objective in this research. The design was carried out using SolidWorks 3D CAD tool for engineering drawing. The outcome of the design is presented in Figure A.2 and A.3. The engineering drawing sheet showing the projections is presented in Figure A.2 while the 3D view of the completed design is presented in Figure A.3. The design was done in such a way to allow the springs to connect the bearing and the shaft to the system, while having the shaft centralised at every of the four-bearing pedestal. This was achieved with some clearance, although it wasn't calculated.

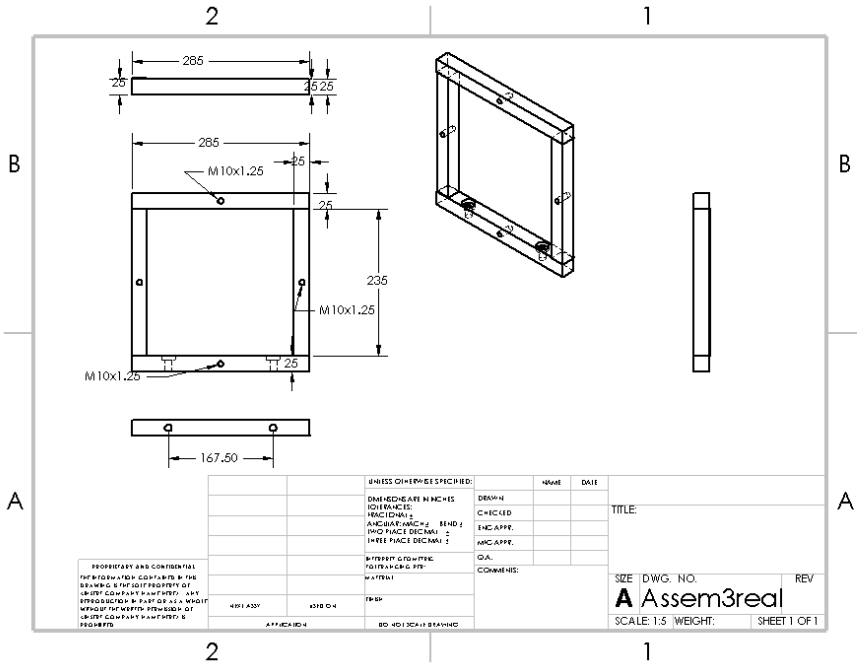

Figure A 2 Engineering drawing showing the projections for the designed SFTR bearing pedestal.

Figure A 3 A 3D engineering drawing showing the designed SFTR bearing pedestal

A4 Matlab codes used in both rotor and bearing analysis

Acceleration/ Velocity time and Frequency domain analysis

```
clc
clear all
%acc_vel_spectra
%Inputs
load Healthy_Res_Mis_Res_Unb_40Hz_Data.txt;
 ch=4;
 f1=40;   %1st harmonic frequencies;
 nh=5; % number of harmonics needed
a= zeros(ch);
aa= 120000;

%Residual Misalignment Residual Unbalance data%
a=Healthy_Res_Mis_Res_Unb_40Hz_Data(1:aa,:);

a=a(:,[1:4]);
fs=10000;
N=2^14;
shift=floor(N/4);

%filter-----------------
[B,A]=butter(4,1/(fs/2),'high');
[h,fe]=freqz(B,A,N,fs);

figure(1000);
clf
plot(fe,abs(h));

for i=1:ch;
    a(:,i)=filtfilt(B,A,a(:,i));
end

dt=1/fs;
t=[0:1:length(a)-1]'*dt;

a= a*9.81*10; %m/s^2

for i=1:ch;
    figure(i)
    clf
    plot(t,a(:,i));
    grid on
    xlabel('Time,  s')
    ylabel('Acceleration, m/s^2')
end

% Time Domain Analysis
pp=zeros(ch,1); %peak to peak
rms=zeros(ch,1); %rms
CF=zeros(ch,1); %crest factor
ku=zeros(ch,1); %kurtosis

for k=1:ch;
   pp(k,1)=max(a(:,k))-min(a(:,k));
```

```
   rms(k,1)=sqrt(mean(a(:,k).^2));
   CF(k,1)=max(a(:,k))/rms(k,1);
   ku(k,1)=kurtosis(a(:,k));
end

% Acceleration Spectrum Analysis
av=floor((length(a)-N)/shift)-1;
df=fs/N;
freq=[0:1:N/2-1]'*df;
S_A=zeros(N/2,ch);

for i=1:ch;
    for k=1:av;
        ks=(k-1)*shift+1; ke=ks+N-1;
        aa=a(ks:ke,i);
        af=fft(aa)/(N/2);
        aff=af(1:N/2,1);
        S_A(:,i)=S_A(:,i)+aff.*conj(aff);
    end
end

S_A=S_A/av;

for i=1:ch;
    S_A(:,i)=sqrt(S_A(:,i));
end

SE = zeros(ch,1);
for i= 1:ch
    SE(i,1)= mean(S_A(i,:)).*df;
end

%Velocity spectra Analysis
S_V=zeros(N/2,ch);

for i=1:ch;
   for k=2:N/2;
        w=(2*pi*freq(k));
        S_V(k,i)=1000*S_A(k,i)/w;  %mm/s
    end
end

% plots only

nn1=floor(1/df);
nn2=floor(240/df);

for i=1:ch;
    figure(i+100)
    clf
    plot(freq(nn1:nn2),S_A(nn1:nn2,i);
    hold
    grid on
    xlabel('Frequency, Hz')
    ylabel('Acceleration, m/s^2')
end

 for i=1:ch;
```

```
    figure(i+200)
    clf
     plot(freq(nn1:nn2),S_V(nn1:nn2,i);
     hold
    grid on
    xlabel('Frequency, Hz')
    ylabel('Velocity, mm/s')
end
```

Bearing Fault Analysis

```
clc
clear all

%Inputs
load Sprg1111_Brg2_Ball_Fault_22_5_Hz_Data.txt;
a =Sprg1111_Brg2_Ball_Fault_22_5_Hz_Data;
clear Sprg1111_Brg2_Ball_Fault_22_5_Hz_Data.txt;
 ch=4;
 f1=8.54;   %1st harmonic frequencies;
fc = 2400;
fs=10000;
a= zeros(ch);
%aaa= 120000;

 a =Sprg1111_Brg2_Ball_Fault_22_5_Hz_Data;

% a=Sprg1111_Brg1_Ball_Fault_22_5_Hz_Data(1:aaa,:);
 %a=a(:,[1:4]);



fs=10000;
N=2^14;
shift=floor(N/4);


%filter-----------------
[B,A]=butter(10,500/(fs/2),'high');

[h,fe]=freqz(B,A,N,fs);
dt=1/fs;
t=[0:1:length(a)-1]'*dt;


df=fs/N;
freq=[0:1:N/2-1]'*df;

a= a*9.81*10; %m/s^2

figure(1000);
clf
plot(freq,abs(h(1:N/2)));%filter plot
grid on

for i=1:ch;
    a(:,i)=filtfilt(B,A,a(:,i));
```

```
end

% Time domain with filter only
figure(1)
for i=1:ch;

    figure(i)
    clf
    plot(t,a(:,i));
    hold
    xlabel('Time.s')
    ylabel('Acceleration, m/s^2')
end

% Time domain analysis
pp=zeros(ch,1); %peak to peak
rms=zeros(ch,1); %rms
CF=zeros(ch,1); %crest factor
ku=zeros(ch,1); %kurtosis

for k=1:ch;
   pp(k,1)=max(a(:,k))- min(a(:,k));
   rms(k,1)=sqrt(mean(a(:,k).^2));
   CF(k,1)=max(a(:,k))/rms(k,1);
   ku(k,1)=kurtosis(a(:,k));
end

av=floor((length(a)-N)/shift)-1;

S_A=zeros(N/2,ch);

for i=1:ch;
    for k=1:av;
        ks=(k-1)*shift+1; ke=ks+N-1;
        x=a(ks:ke,i);
        af=fft(x)/(N/2);
        aff=af(1:N/2,1);
        S_A(:,i)=S_A(:,i)+aff.*conj(aff);
    end
end
S_A=S_A/av;

for i=1:ch;
    S_A(:,i)=sqrt(S_A(:,i));
end

SE = zeros(ch,1);
for i= 1:ch
    SE(i,1)= mean(S_A(i,:)).*df;
end

h1=floor(f1/df)+1;
[v,loc]=max(S_A(h1-2:h1+2,3));
h1=h1-3+loc;

for ih=1:nh;

   h(ih)=ih*h1-(ih-1);
```

```
fh(ih)=freq(h(ih));
S_Ah(ih,:)=S_A(h(ih),:);
end

% plots only

nn1=floor(1/df);
 %nn2=floor(240/df);
nn2=floor(5000/df);

for i=1:ch;

    figure(i+100)
    clf
    plot(freq(nn1:nn2),S_A(nn1:nn2,i));
    hold
    grid on

    xlabel('Frequency, Hz')
    ylabel('Acceleration, m/s^2')
end

%Hilbert (Envelope Analysis)
for i=1:ch
 aa(:,i)=abs(hilbert(a(:,i)));

 aa(:,i)=aa(:,i)-mean(aa(:,i));
end

% Time domain with filter and Envelope

figure(2)
%
for i=1:ch;
    figure(i+200)
    clf
    plot(t,a(:,i));
    hold
    plot(t,aa(:,i),'r');
    grid on
    xlabel('Time.s')
    ylabel('Acceleration, m/s^2')
end



%Acc Spectrum with filter and Envelope

avv=floor((length(aa)-N)/shift)-1;
S_Ae=zeros(N/2,ch);

for i=1:ch;

    for k=1:avv;
        ks=(k-1)*shift+1; ke=ks+N-1;
         x=aa(ks:ke,i);
        af=fft(x)/(N/2);
```

```
        aff=af(1:N/2,1);
        S_Ae(:,i)=S_Ae(:,i)+aff.*conj(aff);
    end
end

S_Ae=S_Ae/avv;
SEe = zeros(ch,1);

for i= 1:ch
    SEe(i,1)= mean(S_Ae(i,:)).*df;
end


 %harmonics;
%1st harmmonics

h1=floor(f1/df)+1;
[v,loc]=max(S_Ae(h1-2:h1+2,3));
h1=h1-3+loc;

for ih=1:nh;

   h(ih)=ih*h1-(ih-1);
fh(ih)=freq(h(ih));
S_Aeh(ih,:)=S_Ae(h(ih),:);
% S_Vh(ih,:)=S_V(h(ih),:);

end

% plots only

nn1=floor(1/df);
 nn2=floor(500/df);
%nn2=floor(100/df);

for i=1:ch;

    figure(i+300)
    clf
    plot(freq(nn1:nn2),S_Ae(nn1:nn2,i));
    hold
    plot(fh,S_Aeh(:,i),'*r');
    grid on

    xlabel('Frequency, Hz')
    ylabel('Acceleration, m/s^2')

end
```

Poly-Coherent Composite Bispectrum

```
clear all;
clc;
load Sprg1111_Brg1_Ball_Fault_7_5_Hz_Data.txt;
Data=Sprg1111_Brg1_Ball_Fault_7_5_Hz_Data;
```

```
clear Sprg1111_Brg1_Ball_Fault_7_5_Hz_Data;
a=Data(1:1400000,1:4);
a(1:1400000,1:4)=10*9.81*(a(1:1400000,1:4));

arraykcl = [];
for cc = 1:20;
    disp 'cc';
aa=a(1+(cc-1)*33300:cc*33300,1:4);

FF=2.79;
FS=10000;
dt=1/FS;
%n=length(ay);
n=length(aa);
T=(0:1:n-1)*dt;
N=2^14;
df=FS/N;
F=(0:1:N/2-1)*df;
n_cf=floor(FF*4/df);
% [Bi,Ai]=butter(4,3/(FS/2),'high');
[Bi,Ai]=butter(10,500/(FS/2),'high'); %for bearing data filter
H=freqz(Bi,Ai,N);

ch1=1;
ch2=2;
ch3=3;
ch4=4;

for i=1:4;
    aa(:,i)=filtfilt(Bi,Ai,aa(:,i));
end

nlap=floor(0.95*N);
nav=floor((n-N)/(N-nlap));
d=N-nlap;

PSD1=zeros(N/2,1);
PSD2=zeros(N/2,1);
PSD3=zeros(N/2,1);
PSD4=zeros(N/2,1);

CSD1=zeros(N/2,1);
CSD2=zeros(N/2,1);
CSD3=zeros(N/2,1);

NN=N/4;
B=zeros(NN,NN);

%FT Calculation
for s=1:nav;

    L1=(s-1)*d+1;
    L2=L1+N-1;

    A1=aa(L1:L2,ch1);
    X1=fft(A1)/(N/2);
    X1=X1(1:N/2);
    Y1=conj(X1);
```

```
    PSD1=PSD1+X1.*Y1;

    A2=aa(L1:L2,ch2);
    X2=fft(A2)/(N/2);
    X2=X2(1:N/2);
    Y2=conj(X2);
    PSD2=PSD2+X2.*Y2;

    A3=aa(L1:L2,ch3);
    X3=fft(A3)/(N/2);
    X3=X3(1:N/2);
    Y3=conj(X3);
    PSD3=PSD3+X3.*Y3;

    A4=aa(L1:L2,ch4);
    X4=fft(A4)/(N/2);
    X4=X4(1:N/2);
    Y4=conj(X4);
    PSD4=PSD4+X4.*Y4;


    CSD1=CSD1+X1.*Y2; % CSD1 plus the PSD of 1st channel multiply by
PSD complex conj of the 2nd channel
    CSD2=CSD2+X2.*Y3; % CSD2 plus the PSD of 2st channel multiply by
PSD complex conj of the 3nd channel
    CSD3=CSD3+X3.*Y4; % CSD3 plus the PSD of 3st channel multiply by
PSD complex conj of the 4nd channel

end

PSD1=(PSD1/nav);
PSD2=(PSD2/nav);
PSD3=(PSD3/nav);
PSD4=(PSD4/nav);

CSD1=(CSD1/nav);
CSD2=(CSD2/nav);
CSD3=(CSD3/nav);

%Coherence Calculation
Coh12=(abs (CSD1).^2./(PSD1.*PSD2));
Coh23=(abs (CSD2).^2./(PSD2.*PSD3));
Coh34=(abs (CSD3).^2./(PSD3.*PSD4));


%Composite Spectrum Calculation
Xpoly=zeros(N/2,1);
Cpoly=zeros(N/2,1);%coherent poly cross power spectral density,
because it contains signals from all 4 bearings

    for s=1:nav;

    L1=(s-1)*d+1;
    L2=L1+N-1;

    A1=aa(L1:L2,ch1);
    X1=fft(A1)/(N/2);
```

```
    X1=X1(1:N/2);
    Y1=conj(X1);

    A2=aa(L1:L2,ch2);
    X2=fft(A2)/(N/2);
    X2=X2(1:N/2);
    Y2=conj(X2);

    A3=aa(L1:L2,ch3);
    X3=fft(A3)/(N/2);
    X3=X3(1:N/2);
    Y3=conj(X3);

    A4=aa(L1:L2,ch4);
    X4=fft(A4)/(N/2);
    X4=X4(1:N/2);
    Y4=conj(X4);


    Xpoly=(X1.*Coh12.*X2.*Coh23.*X3.*Coh34.*X4);

    Xinstant=((Xpoly).^(1/4));

    Yinstant=conj(Xinstant);

    Cpoly=Cpoly+Xpoly;

        %-------------Composite Spectrum Magnitude--------

        h=floor(FF/df)+1;

for i=1:4;
    hh=i*h-(i-1);
    [mag,loc]=max(abs(Xinstant(hh-2:hh+2)));
    harM(i)=mag;
    harL=(hh-3)+loc;
    Fh(i)=F(harL);
end

%-------------------Composite Spectrum Phase Calculation------------
for ia=1:4;
    hha=ia*h-(ia-1);
    [magc,locc]=max(Xinstant(hha-2:hha+2));
    harMc(ia)=magc;
    harLc=(hha-3)+locc;
    Fhc(ia)=F(harLc);
end

F1=harMc(1); FF1(cc,s)=abs(F1);
F2=harMc(2); FF2(cc,s)=abs(F2);
F3=harMc(3); FF3(cc,s)=abs(F3);


PhF1(cc,s)=(atan(imag(F1)/real(F1)))*(180/pi);
PhF2(cc,s)=(atan(imag(F2)/real(F2)))*(180/pi);
PhF3(cc,s)=(atan(imag(F3)/real(F3)))*(180/pi);
```

```
        %-------------Composite Bispectrum-------------------
        for p=1:NN;

            for q=1:NN;

                BB=Xinstant(p)*Xinstant(q)*Yinstant(p+q-1);
                B(p,q)=B(p,q)+BB;

            end
        end

    end

 Cpoly=Cpoly/nav;%when plotting the coherence poly cross power
spectral density, you have to use 4th root of the averaged Cpoly bcos
it contains 4 signals.

 CCpoly=(sqrt(Cpoly).^(1/4));%CCpoly (which is the 4th root of
Cpoly)should be used for the plot, so that there will only be one
power of amplitude.

  B=B/nav;

    %-----------Composite Bispectrum Magnitudes Calculation----------

    for i=1:3;
    for k=1:3;

        hi=i*h-(i-1);
        hk=k*h-(k-1);

        Bo=abs(B(hi-2:hi+2,hk-2:hk+2));
        BH(i,k)=max(Bo(:));
    end
end

BiB1=BH(1,1);
BiB2=BH(1,2);
BiB3=BH(1,3);

%--Composite Bispectrum Phase Calculations---------------------------
----

for ii=1:3;
    for kk=1:3;
        hii=ii*h-(ii-1);
        hkk=kk*h-(kk-1);
        Bpo=(B(hii-2:hii+2,hkk-2:hkk+2));
        BHp(ii,kk)=max(Bpo(:));
    end
end

BiiB1=BHp(1,1);% complex numbers
BiiB2=BHp(1,2);
BiiB3=BHp(1,3);
```

```
PhB11=(atan(imag(BiiB1)/real(BiiB1)))*(180/pi);
PhB12=(atan(imag(BiiB2)/real(BiiB2)))*(180/pi);
PhB13=(atan(imag(BiiB3)/real(BiiB3)))*(180/pi);

PhB22=(atan(imag(BiiB4)/real(BiiB4)))*(180/pi);
PhB23=(atan(imag(BiiB5)/real(BiiB5)))*(180/pi);
PhB33=(atan(imag(BiiB6)/real(BiiB6)))*(180/pi);


kcl(cc,:)=[harM(1) harM(2) BiB1 BiB2];

end

    %-----------------------Filter plot----------------------
    figure(1)
    clf

    plot(F,abs(H(1:N/2)))

     %-----------------------Plotting the Composite Spectrum---------
--------
    figure(2);
    clf
    plot(F,abs(CCpoly));
    grid on
    xlabel('Frequency, Hz');
    ylabel('Amplitude, (m/s^2)');




     %--------------Plotting Composite Bispectrum--------------------
-------
    ns=round(3/df)+1;
    nn=round(FF*4/df);

    figure(3);
    clf

    mesh(F(ns:nn),F(ns:nn),abs(B(ns:nn,ns:nn)));
    grid on
    xlabel('Frequency, Hz');
    ylabel('Frequency, Hz');
    zlabel('Accel, (m/s^2)^3)');
return
```

REFERENCES

[1] Y. Lei, J. Lin, Z. He, and M. J. Zuo, "A review on empirical mode decomposition in fault diagnosis of rotating machinery," *Mech. Syst. Signal Process.*, vol. 35, no. 1–2, pp. 108–126, 2013, doi: 10.1016/j.ymssp.2012.09.015.

[2] J. Limin, Y. Dechen, L. Xiaofeng, Q. Yong, and C. Guoqiang, "Adaptive Control of Rotor-bearing System with Coupling Faults of Pedestal Looseness and Rub-impact," *TELKOMNIKA Indones. J. Electr. Eng.*, vol. 11, no. 2, pp. 926–934, 2013, doi: 10.11591/telkomnika.v11i2.2054.

[3] M. I. Friswell *et al.*, "Dynamics of Rotating Machines," 2010.

[4] L. Tan, S. Cao, Y. Wang, and B. Zhu, "Direct and inverse iterative design method for centrifugal pump impellers," *Proc. Inst. Mech. Eng. Part A J. Power Energy*, vol. 226, no. 6, pp. 764–775, 2012, doi: 10.1177/0957650912451411.

[5] M. Saimurugan and R. Nithesh, "Intelligent fault diagnosis model for rotating machinery based on fusion of sound signals," *Int. J. Progn. Heal. Manag.*, vol. 7, no. 2, pp. 1–10, 2016.

[6] No Name, "Hands on vibration," *acoem*, 2022. https://www.oneprod.com/resources/news/hands-on-vibration/ (accessed Mar. 07, 2022).

[7] G. Maggio, "Flymca's customized and innovative stranding solutions," *Expometals.net*, 2013. https://www.expometals.net/en-gb/news-page-flymca-sl/flymcas-customized-and-innovative-stranding-solutions-id7520 (accessed Mar. 07, 2022).

[8] G. F. Song, Z. J. Yang, C. Ji, and F. P. Wang, "Theoretical – experimental study on a rotor with a residual shaft bow," vol. 63, pp. 50–58, 2013, doi: 10.1016/j.mechmachtheory.2013.01.002.

[9] J. K. Sinha, A. W. Lees, M. I. Friswell, and R. K. Sinha, "The Estimation of foundation Models of flexible machines. Identification in Engineering Systems," in *Proceeding of Third International Conference*, 2002, pp. 300–310.

[10] H. Taplak, S. Erkaya, and I. Uzmay, "Experimental analysis on fault detection for a direct coupled rotor-bearing system," *Meas. J. Int. Meas. Confed.*, vol. 46, no. 1, pp. 336–344, 2013, doi: 10.1016/j.measurement.2012.07.005.

[11] J. K. Sinha, *Vibration Analysis, Instruments, and Signal Processing*, 1st ed. Boca Raton: CRC Press Taylor & Francis Group, 2015.

[12] D. Felten, "Understanding Bearing Vibration Frequencies," *Easa Curr.*, no. September, pp. 1–3, 2003, [Online]. Available: http://electromotores.com/PDF/InfoTecnica/EASA/Understanding Bearing Vibration Frequencies.pdf.

[13] S. Nakhaeinejad, M., Ganeriwala, "Observation of Dynamic Responses of Misalignments," *TechNote, SpectraQuest Inc*, Richmond, Sep. 2009.

[14] A. Wysoclci and B. Feest, "Bearing failure: Causes and cures," *EC M Electr. Constr. Maint.*, vol. 96, no. 2, pp. 52-X6, 1997.

[15] J. K. Sinha and K. Elbhbah, "A future possibility of vibration based condition monitoring of rotating machines," *Mech. Syst. Signal Process.*, vol. 34, no. 1–2, pp. 231–240, 2013, doi: 10.1016/j.ymssp.2012.07.001.

[16] K. Luwei, A. Yunusa-Kaltungo, and J. Sinha, "A simplified rotor-related faults

detection approach based on a combination of time and frequency domain features," *J. Maint. Eng.*, vol. 1, pp. 138–147, 2016.

[17] M. Mohamad-Ali, Y. Soumaya, and L. Aouni, "Diagnosis of rotor bearings using logical analysis of data," *J. Qual. Maint. Eng.*, vol. 17, no. 4, pp. 371–397, Jan. 2011, doi: 10.1108/13552511111180186.

[18] F. Al-badour, M. Sunar, and L. Cheded, "Vibration analysis of rotating machinery using time – frequency analysis and wavelet techniques," *Mech. Syst. Signal Process.*, vol. 25, no. 6, pp. 2083–2101, 2011, doi: 10.1016/j.ymssp.2011.01.017.

[19] K. C. Luwei, "Condition monitoring using vibration analysis to detect rotor related faults in rotating machines," The University of Manchester, 2013.

[20] A. D. Nembhard and J. K. Sinha, "Unified Multi-speed analysis (UMA) for the condition monitoring of aero-engines," *Mech. Syst. Signal Process.*, vol. 64–65, pp. 84–99, 2015, doi: 10.1016/j.ymssp.2015.04.027.

[21] A. Yunusa-Kaltungo, J. K. Sinha, and K. Elbhbah, "An improved data fusion technique for faults diagnosis in rotating machines," *Meas. J. Int. Meas. Confed.*, vol. 58, pp. 27–32, 2014, doi: 10.1016/j.measurement.2014.08.017.

[22] A. D. Nembhard and J. K. Sinha, "Unified Multi-speed analysis (UMA) for the condition monitoring of aero-engines," *Mech. Syst. Signal Process.*, vol. 64–65, pp. 84–99, 2015, doi: 10.1016/j.ymssp.2015.04.027.

[23] A. D. Nembhard, J. K. Sinha, and A. Yunusa-Kaltungo, "Development of a generic rotating machinery fault diagnosis approach insensitive to machine speed and support type," *J. Sound Vib.*, vol. 337, pp. 321–341, 2015, doi: 10.1016/j.jsv.2014.10.033.

[24] K. A. Elbhbah and J. K. Sinha, "A composite vibration spectrum for a machine for vibration based condition monitoring," *Proc. ASME Des. Eng. Tech. Conf.*, vol. 1, no. PARTS A AND B, pp. 123–128, 2012, doi: 10.1115/DETC2012-70052.

[25] A. Yunusa-Kaltungo, J. K. Sinha, and A. D. Nembhard, "A novel fault diagnosis technique for enhancing maintenance and reliability of rotating machines," *Struct. Heal. Monit.*, vol. 14, no. 6, pp. 604–621, 2015, doi: 10.1177/1475921715604388.

[26] A. D. Nembhard, "On-bearing Vibration Response Integration for Condition Monitoring of Rotating Machinery Doctor of Philosophy (PhD)," 2015, [Online]. Available: https://www.research.manchester.ac.uk/portal/en/theses/onbearing-vibration-response-integration-for-condition-monitoring-of-rotating-machinery(f713f156-11f3-4e10-846e-0b9b709f0ff9).html.

[27] A. Yunusa-Kaltungo, "Vibration-based condition monitoring of rotating machines," pp. 1–154, 2015, [Online]. Available: https://tel.archives-ouvertes.fr/tel-01370989.

[28] J. Yan, Y. Hu, and C. Guo, "Rotor unbalance fault diagnosis using DBN based on multi-source heterogeneous information fusion," *Procedia Manuf.*, vol. 35, pp. 1184–1189, 2019, doi: 10.1016/j.promfg.2019.06.075.

[29] M. Altaf *et al.*, "Automatic and Efficient Fault Detection in Rotating Machinery using Sound Signals," *Acoust. Aust.*, vol. 47, no. 2, pp. 125–139, 2019, doi: 10.1007/s40857-019-00153-6.

[30] A. K. Jalan and A. R. Mohanty, “Model based fault diagnosis of a rotor-bearing system for misalignment and unbalance under steady-state condition,” *J. Sound Vib.*, vol. 327, no. 3–5, pp. 604–622, 2009, doi: 10.1016/j.jsv.2009.07.014.

[31] T. D. Shook and R. S. Reddy Gorla, “Finite element analysis and redesign of a compressor hub spinner,” *Finite Elem. Anal. Des.*, vol. 28, no. 1, pp. 19–31, 1997, doi: 10.1016/S0168-874X(97)81960-9.

[32] C. A. Felippa and Carlos A. Felippa, “FEM Modeling: Introduction,” *Introd. to Finite Elem. Methods*, pp. 1–15, 2004, [Online]. Available: http://www.colorado.edu/engineering/cas/courses.d/IFEM.d/IFEM.Ch06.d/IFEM.Ch06.pdf.

[33] V. N. Patel and N. Kushwaha, “Modelling and analysis of a cracked rotor : a review,” *Arch. Appl. Mech.*, vol. 90, no. 6, pp. 1215–1245, 2020, doi: 10.1007/s00419-020-01667-6.

[34] G. F. Song, Z. J. Yang, C. Ji, and F. P. Wang, “Theoretical-experimental study on a rotor with a residual shaft bow,” *Mech. Mach. Theory*, vol. 63, pp. 50–58, 2013, doi: 10.1016/j.mechmachtheory.2013.01.002.

[35] R. Walker, S. Perinpanayagam, and I. K. Jennions, “Rotordynamic faults: Recent advances in diagnosis and prognosis,” *Int. J. Rotating Mach.*, vol. 2013, 2013, doi: 10.1155/2013/856865.

[36] R. Barron, *Engineering Condition Monitoring Practice, Methods and Applications*. New York: Addison Wesley Longman, 1999.

[37] Y. Lei and M. J. Zuo, “Fault diagnosis of rotating machinery using an improved HHT based on EEMD and sensitive IMFs,” *Meas. Sci. Technol.*, vol. 20, no. 12, 2009, doi: 10.1088/0957-0233/20/12/125701.

[38] K. C. Luwei, J. K. Sinha, and A. Yunusa-kaltungo, “A simplified rotor-related faults detection approach based on a combination of time and frequency domain features,” pp. 1–13, 2016.

[39] J. K. Sinha, “Higher Order Spectra for Crack and Misalignment Identification in the Shaft of a Rotating Machine,” *Struct. Heal. Monit.*, vol. 6, no. 4, p. 10, 2007.

[40] S. Wegerich, “Similarity-based modeling of vibration features for fault detection and identification,” *Sens. Rev.*, vol. 25, no. 2, pp. 114–122, 2005, doi: 10.1108/02602280510585691.

[41] S. P. E. Goldman, *Vibration Spectrum Analysis: apractical approach*, 2nd ed. New York: Industrial Press Inc, 1999.

[42] R. Masoni *et al.*, “Supporting Remote Maintenance in Industry 4.0 through Augmented Reality,” *Procedia Manuf.*, vol. 11, no. June, pp. 1296–1302, 2017, doi: 10.1016/j.promfg.2017.07.257.

[43] Z. Li, Y. Wang, and K. S. Wang, “Intelligent predictive maintenance for fault diagnosis and prognosis in machine centers: Industry 4.0 scenario,” *Adv. Manuf.*, vol. 5, no. 4, pp. 377–387, 2017, doi: 10.1007/s40436-017-0203-8.

[44] R. B. Randall, J. Antoni, and S. Chobsaard, “A COMPARISON OF CYCLOSTATIONARY AND ROLLING ELEMENT BEARINGS,” *Int. Conf. Acoust. Speech, Signal Process.*, pp. 3882–3885, 2000.

[45] J. K. Sinha, *Vibration Analysis, Instruments, and Signal Processing*. Boca Raton: CRS press, Taylor and Francis, 2015.

[46] J. K. Sinha, “Condition Monitoring; MEAM MSc Module,” no. June, 2016.

[47] Z. S. Innovations, “Time and Frequency Domain Analysis,” 2015. https://www.zseries.in/mathematics lab/time and frequency domains/#.YiaQ6ujP1PZ (accessed Mar. 07, 2022).
[48] I. Y. Tumer and A. Bajwa, “A survey of aircraft engine monitoring systems,” in *Proceeding of the 35th Joint Propulsion Conference and Exhibit*, 1999, pp. 221–224.
[49] Z. Huo, Y. Zhang, P. Francq, L. Shu, and J. Huang, “Incipient Fault Diagnosis of Roller Bearing Using Optimized Wavelet Transform Based Multi-Speed Vibration Signatures,” *IEEE Access*, vol. 5, pp. 19442–19456, 2017, doi: 10.1109/ACCESS.2017.2661967.
[50] A. D. Nembhard, J. K. Sinha, and A. Yunusa-Kaltungo, “Experimental observations in the shaft orbits of relatively flexible machines with different rotor related faults,” *Meas. J. Int. Meas. Confed.*, vol. 75, pp. 320–337, 2015, doi: 10.1016/j.measurement.2015.08.007.
[51] A. D. Nembhard, J. K. Sinha, and A. Yunusa-Kaltungo, “Development of a generic rotating machinery fault diagnosis approach insensitive to machine speed and support type,” *J. Sound Vib.*, vol. 337, pp. 321–341, 2015, doi: 10.1016/j.jsv.2014.10.033.
[52] L. You, J. Hu, F. Fang, and L. Duan, “Fault diagnosis system of rotating machinery vibration signal,” *Procedia Eng.*, vol. 15, pp. 671–675, 2011, doi: 10.1016/j.proeng.2011.08.125.
[53] M. Loeb, “Spectrum Analysis,” *J. Am. Chem. Soc.*, vol. 20, no. 5, pp. 383–384, 2002, doi: 10.1021/ja02067a010.
[54] J. Courrech and M. Gaudet, “Envelope analysis - the key to rolling-element bearing diagnosis,” *Bruel & Kjaer*, pp. 1–4.
[55] H. Konstantin-Hansen, “Envelope analysis for diagnostics of local faults in rolling element bearings,” *Brüel & Kjær, Denmark*, 2003, [Online]. Available: http://bksv.it/doc/bo0501.pdf.
[56] J. K. Sinha, “Machinery, Vibration and Analysis; MEAM MSc Module,” p. 170, 2015.
[57] B. Geropp, “Envelope Analysis - A Signal Analysis Technique for Early Detection and Isolation of Machine Faults,” *IFAC Proc. Vol.*, vol. 30, no. 18, pp. 977–981, 1997, doi: 10.1016/s1474-6670(17)42527-4.
[58] A. Fernandez, “Demodulation or envelope analysis,” *Power MI*, 2022. https://power-mi.com/content/demodulation-or-envelope-analysis (accessed Mar. 07, 2022).
[59] K. Elbhbah and J. K. Sinha, “BISPECTRUM: A TOOL FOR DISTINGUISHING DIFFERENT FAULTS IN ROTATING MACHINE Keri,” pp. 1–7, 2012.
[60] A. Rivola and P. R. White, “Use of Higher Order Spectra in Condition Monitoring: Simulation and Experiments,” pp. 1317–1328, 1999, doi: 10.1115/detc99/vib-8332.
[61] I. M. Howard, “Higher-order spectral techniques for machine vibration condition monitoring,” *Proc. Inst. Mech. Eng. Part G J. Aerosp. Eng.*, vol. 211, no. 4, pp. 211–218, 1997, doi: 10.1243/0954410971532622.
[62] W. J. Wang, Z. T. Wu, and J. Chen, “Fault identification in rotating machinery using the correlation dimension and bispectra,” *Nonlinear Dyn.*, vol. 25, no. 4,

pp. 383–393, 2001, doi: 10.1023/A:1012985802317.
[63] W. B. Collis, P. R. White, and J. K. Hammond, “Higher-order spectra: The bispectrum and trispectrum,” *Mech. Syst. Signal Process.*, vol. 12, no. 3, pp. 375–394, 1998, doi: 10.1006/mssp.1997.0145.
[64] J. M. Shan and R. Stockton, “Vibration analysis of rotating machinery using a bispectrum,” *J. Sound Vib.*, vol. 200, no. 4, pp. 533–539, 1997, doi: 10.1006/jsvi.1996.0635.
[65] G. Wang, F. Gu, I. Rehab, A. Ball, and L. Li, “A Sparse Modulation Signal Bispectrum Analysis Method for Rolling Element Bearing Diagnosis,” *Math. Probl. Eng.*, vol. 2018, 2018, doi: 10.1155/2018/2954094.
[66] K. Elbhbah, J. K. Sinha, W. Hahn, and G. Tasker, “Application of Composite Spectrum in Steam Turbo-Generator Set,” *Mech. Mach. Sci.*, vol. 23, pp. 411–420, 2015, doi: 10.1007/978-3-319-09918-7.
[67] K. Elbhbah and J. K. Sinha, “FAULT DIAGNOSIS IN ROTATING MACHINE USING COMPOSITE BISPECTRUM,” no. July, p. 2013, 2013.
[68] K. Elbhbah and J. K. Sinha, “Bispectrum for fault diagnosis in rotating machines,” *17th Int. Congr. Sound Vib. 2010, ICSV 2010*, vol. 2, no. September 2014, pp. 1290–1297, 2010, doi: 10.13140/2.1.1546.3684.
[69] A. Yunusa-Kaltungo, J. K. Sinha, and A. D. Nembhard, “Use of composite higher order spectra for faults diagnosis of rotating machines with different foundation flexibilities,” *Meas. J. Int. Meas. Confed.*, vol. 70, pp. 47–61, 2015, doi: 10.1016/j.measurement.2015.03.041.
[70] A. Yunusa-kaltungo, J. K. Sinha, and A. D. Nembhard, “A novel faults diagnosis technique for enhancing maintenance and reliability of rotating machines Akilu Yunusa-Kaltungo, Jyoti K. Sinha*, Adrian D. Nembhard.”
[71] I. Bucher and D. J. Ewins, “Modal analysis and testing of rotating structures,” *Philos. Trans. R. Soc. A Math. Phys. Eng. Sci.*, vol. 359, no. 1778, pp. 61–96, 2001, doi: 10.1098/rsta.2000.0714.
[72] Z. Liguo, W. Yutian, Z. Sheng, and H. Guangpu, “The fault diagnosis of machine based on modal analysis,” *2009 Int. Conf. Meas. Technol. Mechatronics Autom. ICMTMA 2009*, vol. 1, no. 5, pp. 738–741, 2009, doi: 10.1109/ICMTMA.2009.455.
[73] C.-W. Lee and K.-S. Kwon, “Identification of Rotating Asymmetry in Rotating Machines by Using Reverse dFRF,” vol. 215, pp. 1191–1199, 1999, doi: 10.1115/detc99/vib-8267.
[74] E. S. Gutierrez-Wing, “Modal analysis of rotating machinery structures,” *Am. Inst. Aeronaut. Astronaut. Aerosp. Sci. Meet. 14 th, Washington, D. C*, no. September, p. 169, 2003, [Online]. Available: http://www.csa.com/partners/viewrecord.php?requester=gs&collection=TRD&recid=A7618858AH.
[75] X. Chen, J. Yang, X. Sheng, Z. An, and B. Li, “The operation modal analysis of the structure crack fault diagnosis based on pseudo-successive data,” *Vibroengineering Procedia*, vol. 14, pp. 108–114, 2017, doi: 10.21595/vp.2017.19213.
[76] P. Pennacchi, N. Bachschmid, A. Vania, G. A. Zanetta, and L. Gregori, “Use of modal representation for the supporting structure in model-based fault

identification of large rotating machinery: Part 1 - Theoretical remarks," *Mech. Syst. Signal Process.*, vol. 20, no. 3, pp. 662–681, 2006, doi: 10.1016/j.ymssp.2004.11.006.

[77] P. Pennacchi, N. Bachschmid, A. Vania, G. A. Zanetta, and L. Gregori, "Use of modal representation for the supporting structure in model-based fault identification of large rotating machinery: Part 2 - Application to a real machine," *Mech. Syst. Signal Process.*, vol. 20, no. 3, pp. 682–701, 2006, doi: 10.1016/j.ymssp.2004.12.005.

[78] F. Castanedo, "A review of data fusion techniques," *Sci. World J.*, vol. 2013, 2013, doi: 10.1155/2013/704504.

[79] de A. Juan and R. Tauler, "Data Fusion by Multivariate Curve Resolution," *Data Handl. Sci. Technol.*, vol. 31, pp. 205–233, 2019, doi: 10.1016/B978-0-444-63984-4.00008-9.

[80] Q. Lui and H.-P. Wang, "A case study on multisensor data fusion for imbalance diagnosis of rotating machinery," *Artif. Intell. Eng. Des. Anal. Manuf.*, 2001.

[81] K. C. Luwei, "Data combination for a consolidated diagnosis of rotor and bearing faults," no. 6, 2020.

[82] A. D. Nembhard and J. K. Sinha, "Comparison of experimental observations in rotating machines with simple mathematical simulations," *Meas. J. Int. Meas. Confed.*, vol. 89, pp. 120–136, 2016, doi: 10.1016/j.measurement.2016.04.010.

[83] L. L. Jiang, H. K. Yin, X. J. Li, and S. W. Tang, "Fault diagnosis of rotating machinery based on multisensor information fusion using SVM and time-domain features," *Shock Vib.*, vol. 2014, 2014, doi: 10.1155/2014/418178.

[84] M. Saimurugan and R. Ramprasad, "A dual sensor signal fusion approach for detection of faults in rotating machines," *JVC/Journal Vib. Control*, vol. 24, no. 12, pp. 2621–2630, 2018, doi: 10.1177/1077546316689644.

[85] Mathworks, "Find and visualize natural groupings and patterns in data." Mathworks, 2022, [Online]. Available: https://uk.mathworks.com/discovery/cluster-analysis.html.

[86] S. Bhosale, "Limitation of Cluster Analysis," *BA@SIBMB*, 2011.

[87] I. T. Jolliffe, "Principal Component Analysis, Second Edition," *Encycl. Stat. Behav. Sci.*, vol. 30, no. 3, p. 487, 2002, doi: 10.2307/1270093.

[88] C. M. Bishop, *Pattern Recognition and MAchine Learning*, vol. 53, no. 9. New York: Springer, 2006.

[89] A. Yunusa-Kaltungo and J. K. Sinha, "Effective vibration-based condition monitoring (eVCM) of rotating machines," *J. Qual. Maint. Eng.*, vol. 23, no. 3, pp. 279–296, 2017, doi: 10.1108/JQME-08-2016-0036.

[90] N. Baydar, Q. Chen, A. Ball, and U. Kruger, "Detection of incipient tooth defect in helical gears using multivariate statistics," *Mech. Syst. Signal Process.*, vol. 15, no. 2, pp. 303–321, 2001, doi: 10.1006/mssp.2000.1315.

[91] J. Im, "Introduction to PCA (Principal Component Analysis)," 2018, [Online]. Available: https://medium.com/@jamesim2077/introduction-to-pca-principal-component-analysis-c26dffe2a857.

[92] Y. Huang, X. F. Zha, J. Lee, and C. Liu, "Discriminant diffusion maps analysis: A robust manifold learner for dimensionality reduction and its applications in machine condition monitoring and fault diagnosis," *Mech. Syst. Signal Process.*,

vol. 34, no. 1–2, pp. 277–297, 2013, doi: 10.1016/j.ymssp.2012.04.021.
[93] W. Sun, J. Chen, and J. Li, "Decision tree and PCA-based fault diagnosis of rotating machinery," *Mech. Syst. Signal Process.*, vol. 21, no. 3, pp. 1300–1317, 2007, doi: 10.1016/j.ymssp.2006.06.010.
[94] C. Servière and P. Fabry, "Blind source separation of noisy harmonic signals for rotating machine diagnosis," *J. Sound Vib.*, vol. 272, no. 1–2, pp. 317–339, 2004, doi: 10.1016/S0022-460X(03)00774-0.
[95] A. Malhi and R. X. Gao, "PCA-based feature selection scheme for machine defect classification," *IEEE Trans. Instrum. Meas.*, vol. 53, no. 6, pp. 1517–1525, 2004, doi: 10.1109/TIM.2004.834070.
[96] A. Widodo *et al.*, "Fault diagnosis of low speed bearing based on relevance vector machine and support vector machine," *Expert Syst. Appl.*, vol. 36, no. 3 PART 2, pp. 7252–7261, 2009, doi: 10.1016/j.eswa.2008.09.033.
[97] A. D. Nembhard, J. K. Sinha, A. J. Pinkerton, and K. Elbhbah, "Combined vibration and thermal analysis for the condition monitoring of rotating machinery," *Struct. Heal. Monit.*, vol. 13, no. 3, pp. 281–295, 2014, doi: 10.1177/1475921714522843.
[98] W. Victor, *Machinery Vibration "Measurement and Analysis,"* 1st ed. New York: McGraw. Inc, 1991.
[99] F. S. Nowlan and H. F. Heap, "Reliability Centered Maintenance," San Francisco, 1978.
[100] S. Edwards, A. W. Lees, and M. I. Friswell, "Fault diagnosis of rotating machinery," *Shock and Vibration Digest*, vol. 30, no. 1. pp. 4–13, 1998, doi: 10.1177/058310249803000102.
[101] D. Bently and C. Hatch, *Fundamentals of Rotating Machinery Diagnostics (Design and Manufacturing)*, 1st ed. ASME Press (American Society of Mechanical Engineers), 2003.
[102] A. Muszynska, *Rotordynamics*, 1st ed. Boca Raton, 2005.
[103] Yongxiang Zhang and R.B.Randall, "Rolling element bearing fault diagnosis based on the combination of genetic algorithm and fast kurtogram," *Mech. Syst. Signal Process.*, vol. 23, pp. 1506–1517, 2009, doi: https://doi.org/10.1016/j.ymssp.2009.02.003.
[104] R. Misra, K. Shinghal, A. Saxena, and A. Agarwal, "Industrial Motor Bearing Fault Detection Using Vibration Analysis," *Int. Conf. Intell. Comput. Smart Commun.*, vol. In: Singh, pp. 827–839, 2019, doi: https://doi.org/10.1007/978-981-15-0633-8_86.
[105] T. Brotherton, P. Grabill, R. Friend, B. Sotomayer, and J. Berry, "A Testbed for Data Fusion for Engine Diagnostics and Prognostics," *IEEE Xplore. Restrict.*, pp. 3029–3042, 2002.
[106] A. Morhain and D. Mba, "Bearing defect diagnosis and acoustic emission," *Proc. Inst. Mech. Eng. Part J J. Eng. Tribol.*, vol. 217, pp. 257–272, 2003.
[107] J. Fitch, "Maximum Fault Detection in Rotating Equipment using Wear Debris Analysis," *Machinery Lubrication*, 1999.
[108] L. Duan, M. Yao, J. Wang, T. Bai, and L. Zhang, "Segmented infrared image analysis for rotating machinery fault diagnosis," *Infrared Phys. Technol.*, vol. 77, pp. 267–276, 2016, doi: 10.1016/j.infrared.2016.06.011.

[109] A. Page, “Why you Should be Using Vibration Analysis,” *Reliab. Plant*.
[110] Y. Zhu, W. Jiang, X. Kong, Z. Zheng, and H. Hu, “An accurate integral method for vibration signal based on feature information extraction,” *Shock Vib.*, vol. 2015, 2015, doi: 10.1155/2015/962793.
[111] N. Author, “Dynamic Balancing,” 2013, [Online]. Available: https://johnmaherracing.com/2013/01/project-2110-part-4-dynamic-balancing/.
[112] R. B. Walker, R. Vayanat, S. Perinpanayagam, and I. K. Jennions, “Unbalance localization through machine nonlinearities using an artificial neural network approach,” *Mech. Mach. Theory*, vol. 75, pp. 54–66, 2014, doi: 10.1016/j.mechmachtheory.2014.01.006.
[113] G. C. Z. Jun Hong Zhang, Liang Ma, Jie Wei Lin, “Dynamic Analysis of Flexible Rotor-Ball Bearings System with Unbalance-Misalignment-Rubbing Coupling Faults,” *Appl. Mech. Mater.*, vol. Volumes 10, pp. 448–453, 2011.
[114] M. A. Hassan, D. Coats, K. Gouda, Y. J. Shin, and A. Bayoumi, “Analysis of nonlinear vibration-interaction using higher order spectra to diagnose aerospace system faults,” *IEEE Aerosp. Conf. Proc.*, pp. 1–8, 2012, doi: 10.1109/AERO.2012.6187370.
[115] S. N. Ganeriwala, B. Schwarz, and M. H. Richardson, “Using operating deflection shapes to detect unbalance in rotating equipment,” *Conf. Proc. Soc. Exp. Mech. Ser.*, no. May, pp. 11–13, 2009.
[116] H. Xue, H. Wang, P. Chen, K. Li, and L. Song, “Automatic diagnosis method for structural fault of rotating machinery based on distinctive frequency components and support vector machines under varied operating conditions,” *Neurocomputing*, vol. 116, pp. 326–335, 2013, doi: 10.1016/j.neucom.2012.02.048.
[117] W. Jiao, Q. Yuan, and Y. Chang, “Study on the coupled bending-torsional vibration of unbalanced rotor system with external excitations,” *CSAE 2012 - Proceedings, 2012 IEEE Int. Conf. Comput. Sci. Autom. Eng.*, vol. 1, pp. 332–336, 2012, doi: 10.1109/CSAE.2012.6272609.
[118] A. Abdul-Aziz, M. R. Woike, N. C. Oza, B. L. Matthews, and J. D. lekki, “Rotor health monitoring combining spin tests and data-driven anomaly detection methods,” *Struct. Heal. Monit.*, vol. 11, no. 1, pp. 3–12, 2012, doi: 10.1177/1475921710395811.
[119] M. M. Rahman and M. N. Uddin, “Online Unbalanced Rotor Fault Detection of an IM Drive Based on Both Time and Frequency Domain Analyses,” *IEEE Trans. Ind. Appl.*, vol. 53, no. 4, pp. 4087–4096, 2017, doi: 10.1109/TIA.2017.2691736.
[120] K. Xu, S. Li, X. Jiang, Z. An, J. Wang, and T. Yu, “A renewable fusion fault diagnosis network for the variable speed conditions under unbalanced samples,” *Neurocomputing*, vol. 379, pp. 12–29, 2020, doi: 10.1016/j.neucom.2019.08.099.
[121] F. Jia, Y. Lei, N. Lu, and S. Xing, “Deep normalized convolutional neural network for imbalanced fault classification of machinery and its understanding via visualization,” *Mech. Syst. Signal Process.*, vol. 110, pp. 349–367, 2018, doi: 10.1016/j.ymssp.2018.03.025.
[122] Z. He, H. Shao, J. Cheng, X. Zhao, and Y. Yang, “Support tensor machine with

dynamic penalty factors and its application to the fault diagnosis of rotating machinery with unbalanced data," *Mech. Syst. Signal Process.*, vol. 141, p. 106441, 2020, doi: 10.1016/j.ymssp.2019.106441.

[123] T. S. Morais, J. Der Hagopian, V. Steffen, and J. Mahfoud, "Optimization of unbalance distribution in rotating machinery with localized non linearity," *Mech. Mach. Theory*, vol. 72, pp. 60–70, 2014, doi: 10.1016/j.mechmachtheory.2013.09.012.

[124] D. Zhao *et al.*, "Enhanced data-driven fault diagnosis for machines with small and unbalanced data based on variational auto-encoder," *Meas. Sci. Technol.*, vol. 31, no. 3, p. 35004, 2019, doi: 10.1088/1361-6501/ab55f8.

[125] A. Moosavian, H. Ahmadi, B. Sakhaei, and R. Labbafi, "Support vector machine and K-nearest neighbour for unbalanced fault detection," *J. Qual. Maint. Eng.*, vol. 20, no. 1, pp. 65–75, 2014, doi: 10.1108/JQME-04-2012-0016.

[126] F. P. G. Márquez, R. R. de la H. González-Carrato, and J. M. P. P. and N. Zaman, *Maintenance Management Based on Signal Processing*. Janeza Trdine: InTech, 2013.

[127] S. R. Bognatz, "Alignment of critical and Non Critical Machines," *Orbit*, pp. 23–25, 1995.

[128] M. Ely and K. Vietsch, "The Importance of shaft Alignment . Strategies for Ensuring the Uptime of Rotating Equipment.," 2011, [Online]. Available: https://www.piprocessinstrumentation.com/maintenance-safety/article/15555626/the-importance-of-shaft-alignment.

[129] P. N. Saavedra and D. E. Ramírez, "Vibration analysis of rotors for the identification of shaft misalignment part 1: Theoretical analysis," *Proc. Inst. Mech. Eng. Part C J. Mech. Eng. Sci.*, vol. 218, no. 9, pp. 971–985, 2004, doi: 10.1243/0954406041991297.

[130] P. N. Saavedra and D. E. Ramírez, "Vibration analysis of rotors for the identification of shaft misalignment part 2: Experimental validation," *Proc. Inst. Mech. Eng. Part C J. Mech. Eng. Sci.*, vol. 218, no. 9, pp. 987–999, 2004, doi: 10.1243/0954406041991198.

[131] A. E.-S. A. M. Ahmed, "Effect of Misalignment on the Characteristics of Journal Bearings," *J. Eng. Gas Turbines Power*, vol. 130, no. 4, p. 8, 2008, doi: https://doi.org/10.1115/1.2800347.

[132] J. Meagher, X. Wu, and C. Lencioni, "Response of a warped flexible rotor with a fluid bearing," *Int. J. Rotating Mach.*, vol. 2008, 2008, doi: 10.1155/2008/147653.

[133] T. Gaka and M. Tabaszewski, "An application of statistical symptoms in machine condition diagnostics," *Mech. Syst. Signal Process.*, vol. 25, no. 1, pp. 253–265, 2011, doi: 10.1016/j.ymssp.2010.07.006.

[134] X. Shen, J. Jia, and M. Zhao, "Nonlinear analysis of rub-impact rotor-bearing system with initial permanent rotor bow," *Arch. Appl. Mech.*, vol. 78, no. 3, pp. 225–240, 2008, doi: DOI 10.1007/s00419-007-0155-8.

[135] T. Y. Wu, H. C. Hong, and Y. L. Chung, "A looseness identification approach for rotating machinery based on post-processing of ensemble empirical mode decomposition and autoregressive modeling," *JVC/Journal Vib. Control*, vol. 18, no. 6, pp. 796–807, 2012, doi: 10.1177/1077546311411755.

[136] "Mechanical Looseness," *Mech. Brother.*, [Online]. Available: https://mechanicalbrothers.wordpress.com/2011/01/15/kelonggaran-mekanik-mechanical-looseness/.
[137] C. F. Ngolah, E. Morden, and Y. Wang, "Intelligent fault recognition and diagnosis for rotating machines using neural network," vol. 3, no. 4, p. 17, 2011, doi: DOI: 10.4018/jssci.2011100105.
[138] A. W. Lees, "Fault Diagnosis in Rotating Machinery," in *SPIE Proceedings Series*, 2000, pp. 313–319.
[139] F. Shamoradi, N. Mohammadi, and M. H. Kahkesh, "Steam Turbine Rotor Vibration Failures; Causes and Solutions," *Plant O&M*, pp. 62–65, 2013.
[140] Z. K. Peng, F. L. Chu, and P. W. Tse, "Detection of the rubbing-caused impacts for rotor-stator fault diagnosis using reassigned scalogram," *Mech. Syst. Signal Process.*, vol. 19, no. 2, pp. 391–409, 2005, doi: 10.1016/j.ymssp.2003.09.007.
[141] C. M. Ã. Stoisser and S. Audebert, "A comprehensive theoretical , numerical and experimental approach for crack detection in power plant rotating machinery," *Mech. Syst. Signal Process.*, vol. 22, pp. 818–844, 2008, doi: 10.1016/j.ymssp.2007.11.013.
[142] Z. Ren, S. Zhou, E. Chunhui, M. Gong, B. Li, and B. Wen, "Crack fault diagnosis of rotor systems using wavelet transforms," *Comput. Electr. Eng.*, vol. 45, pp. 33–41, 2015, doi: 10.1016/j.compeleceng.2015.04.010.
[143] C. H. Oppenheimer and K. A. Loparo, "Physically based diagnosis and prognosis of cracked rotor shafts," *Proc. Compon. Syst. Diagnostics, Progn. Heal. Manag.*, vol. 4733, p. 11, 2002, doi: https://doi.org/10.1117/12.475502.
[144] B. Eftekharnejad, A. Addali, and D. Mba, "Shaft crack diagnostics in a gearbox," *Appl. Acoust.*, vol. 73, no. 8, pp. 723–733, 2012, doi: 10.1016/j.apacoust.2012.02.004.
[145] A. K. Darpe, "A novel way to detect transverse surface crack in a rotating shaft," vol. 305, pp. 151–171, 2007, doi: 10.1016/j.jsv.2007.03.070.
[146] G. Mani, D. D. Quinn, and M. Kasarda, "Active health monitoring in a rotating cracked shaft using active magnetic bearings as force actuators," *J. Sound Vib.*, vol. 294, pp. 454–465, 2006, doi: 10.1016/j.jsv.2005.11.020.
[147] R. G. Kirk, G. Sabnavis, R. G. Kirk, M. Kasarda, and D. Quinn, "Cracked Shaft Detection and Diagnostics : A Literature Review," *Shock Vib. Dig.*, no. July, p. 11, 2004, doi: 10.1177/0583102404045439.
[148] J. Wauer, "On the Dynamics of Cracked Rotors: A Literature Survey," *ASME Appl. Mecahnics Rev.*, vol. 43, no. 1, pp. 13–17, 1990, doi: https://doi.org/10.1115/1.3119157.
[149] R. T. Babu, S. Srikanth, and A. S. Sekhar, "Hilbert – Huang transform for detection and monitoring of crack in a transient rotor," *Mech. Syst. Signal Process.*, vol. 22, pp. 905–914, 2008, doi: 10.1016/j.ymssp.2007.10.010.
[150] T. C. Tsai and Y. Z. Wang, "VIBRATION ANALYSIS AND DIAGNOSIS OF A CRACKED SHAFT," *J. Vib. Sound*, vol. 192, pp. 607–620, 1996.
[151] C. Kumar and V. Rastogi, "A Brief Review on Dynamics of a Cracked Rotor," vol. 2009, 2009, doi: 10.1155/2009/758108.
[152] Z. Duan, T. Wu, S. Guo, T. Shao, R. Malekian, and Z. Li, "Development and trend of condition monitoring and fault diagnosis of multi-sensors information fusion

for rolling bearings: a review," *Int. J. Adv. Manuf. Technol.*, vol. 96, no. 1–4, pp. 803–819, 2018, doi: 10.1007/s00170-017-1474-8.

[153] SKF, "Bearing failure and their causes," 1994.

[154] P. McFadden and J. Smith, "Vibration monitoring of rolling element bearings by the high-frequency resonance technique—a review," *Tribol. Int.*, 1984, Accessed: Feb. 17, 2017. [Online]. Available: http://www.sciencedirect.com/science/article/pii/0301679X84900768.

[155] "Determining the Cause of Bearing Failures," *Noria Corp.*

[156] R. B. Randall, J. Antoni, and S. Chobsaard, "THE RELATIONSHIP BETWEEN SPECTRAL CORRELATION AND ENVELOPE ANALYSIS IN THE DIAGNOSTICS OF BEARING FAULTS AND OTHER CYCLOSTATIONARY MACHINE SIGNALS," *Mech. Syst. Signal Process.*, vol. 15, pp. 945–962, 2001, doi: 10.1006/mssp.2001.1415.

[157] I. Attoui, B. Oudjani, N. Boutasseta, N. Fergani, and M. Bouakkaz, "Novel predictive features using a wrapper model for rolling bearing fault diagnosis based on vibration signal analysis," *Int. J. Adv. Manuf. Technol.*, pp. 3409–3435, 2020.

[158] M. Kedadouche, M. Thomas, and A. Tahan, "A comparative study between Empirical Wavelet Transforms and Empirical Mode Decomposition Methods: Application to bearing defect diagnosis," *Mech. Syst. Signal Process.*, vol. 81, pp. 88–107, 2016, doi: 10.1016/j.ymssp.2016.02.049.

[159] R. Yan and R. X. Gao, "Multi-scale enveloping spectrogram for vibration analysis in bearing defect diagnosis," *Tribol. Int.*, vol. 42, no. 2, pp. 293–302, 2009, doi: 10.1016/j.triboint.2008.06.013.

[160] Y. T. Sheen, "An envelope analysis based on the resonance modes of the mechanical system for the bearing defect diagnosis," *Meas. J. Int. Meas. Confed.*, vol. 43, no. 7, pp. 912–934, 2010, doi: 10.1016/j.measurement.2010.03.011.

[161] A. M. Al-Ghamd and D. Mba, "A comparative experimental study on the use of acoustic emission and vibration analysis for bearing defect identification and estimation of defect size," *Mech. Syst. Signal Process.*, vol. 20, no. 7, pp. 1537–1571, 2006, doi: 10.1016/j.ymssp.2004.10.013.

[162] Y. T. Sheen, "A complex filter for vibration signal demodulation in bearing defect diagnosis," *J. Sound Vib.*, vol. 276, no. 1–2, pp. 105–119, 2004, doi: 10.1016/j.jsv.2003.08.007.

[163] J. Lee, "A complex filter for vibration signal demodulation in bearing defect diagnosis," *ReliablePlant*, 2003.

[164] P. Gupta and M. K. Pradhan, "Fault detection analysis in rolling element bearing: A review," *Mater. Today Proc.*, vol. 4, no. 2, pp. 2085–2094, 2017, doi: 10.1016/j.matpr.2017.02.054.

[165] R. B. Randall and J. Antoni, "Rolling element bearing diagnostics-A tutorial," *Mech. Syst. Signal Process.*, vol. 25, no. 2, pp. 485–520, 2011, doi: 10.1016/j.ymssp.2010.07.017.

[166] S. Abdusslam, P. Raharjo, F. Gu, and A. Ball, "Bearing defect detection and diagnosis using a time encoded signal processing and pattern recognition method," *J. Phys. Conf. Ser.*, vol. 364, no. 1, 2012, doi: 10.1088/1742-6596/364/1/012036.

[167] R. Yan, R. X. Gao, and C. Wang, “Experimental evaluation of a unified time-scale-frequency technique for bearing defect feature extraction,” *J. Vib. Acoust. Trans. ASME*, vol. 131, no. 4, pp. 0410121–04101210, 2009, doi: 10.1115/1.3147125.
[168] A. Kumar, Y. Zhou, C. P. Gandhi, R. Kumar, and J. Xiang, “Bearing defect size assessment using wavelet transform based Deep Convolutional Neural Network (DCNN),” *Alexandria Eng. J.*, vol. 59, no. 2, pp. 999–1012, 2020, doi: 10.1016/j.aej.2020.03.034.
[169] J. Antoni and R. B. Randall, “The spectral kurtosis: Application to the vibratory surveillance and diagnostics of rotating machines,” *Mech. Syst. Signal Process.*, vol. 20, no. 2, pp. 308–331, 2006, doi: 10.1016/j.ymssp.2004.09.002.
[170] N. Sawalhi, R. B. Randall, and H. Endo, “The enhancement of fault detection and diagnosis in rolling element bearings using minimum entropy deconvolution combined with spectral kurtosis,” *Mech. Syst. Signal Process.*, vol. 21, no. 6, pp. 2616–2633, 2007, doi: 10.1016/j.ymssp.2006.12.002.
[171] N. Sawalhi and R. B. Randall, “Localized fault detection and diagnosis in rolling element bearings : A collection of the state of art processing algorithms,” *15th Aust. Int. Aerosp. Congr.*, no. Hums, 2013.
[172] C. Engineering, “Structural Engineering,” *No name*, 2022.
[173] “Machine Foundation,” *Daily Civil*, 2022.
[174] A. D. Nembhard and J. K. Sinha, “Vibration-Based Condition Monitoring for Rotating Machinery with Different Flexible Supports,” in *Vibration Engineering and Technology of Machinery. Mechanisms and Machine Science*, vol. 23, Springer, Cham, 2014, pp. 119–127.
[175] A. W. Lees and M. I. Friswell, “Where next for condition monitoring of rotating machinery?,” *Adv. Vib. Eng.*, vol. 5, no. 4, pp. 263–277, 2006.
[176] C. W. Lee, “Mechatronics in Rotating Machinery,” *7th IFToMM-Conference Rotor Dyn.*, no. September, pp. 25–28, 2006.
[177] G. Georgoulas and G. Nikolakopoulos, “Bearing fault detection and diagnosis by fusing vibration data,” *IECON Proc. (Industrial Electron. Conf.*, pp. 6955–6960, 2016, doi: 10.1109/IECON.2016.7794118.
[178] S. Singh and N. Kumar, “Combined rotor fault diagnosis in rotating machinery using empirical mode decomposition,” *J. Mech. Sci. Technol.*, vol. 28, no. 12, pp. 4869–4876, 2014, doi: 10.1007/s12206-014-1107-1.
[179] J. Zhang, X. Lu, J. Lin, L. Ma, and J. Wang, “Dynamic Analysis of a Rotor-Bearing-SFD System with the Bearing Inner Race Defect,” *Shock Vib.*, vol. 2017, 2017, doi: 10.1155/2017/2489376.
[180] H. H. El-Mongy and Y. K. Younes, “Vibration analysis of a multi-fault transient rotor passing through sub-critical resonances,” *JVC/Journal Vib. Control*, vol. 24, no. 14, pp. 2986–3009, 2018, doi: 10.1177/1077546317697828.
[181] M. M. Manjurul Islam and J. M. Kim, “Reliable multiple combined fault diagnosis of bearings using heterogeneous feature models and multiclass support vector Machines,” *Reliab. Eng. Syst. Saf.*, vol. 184, no. 7, pp. 55–66, 2019, doi: 10.1016/j.ress.2018.02.012.
[182] G. Del Vescovo, M. Paschero, A. Rizzi, R. Di Salvo, and F. M. Frattale Mascioli, “Multi-fault diagnosis of rolling-element bearings in electric machines,” *19th*

Int. Conf. Electr. Mach. ICEM 2010, 2010, doi: 10.1109/ICELMACH.2010.5608123.

[183] X. Gong, W. Du, A. Georgiadis, and B. Zhao, "Identification of multi-fault in rotor-bearing system using spectral kurtosis and EEMD," *J. Vibroengineering*, vol. 19, no. 7, pp. 5036–5046, 2017, doi: 10.21595/jve.2017.18671.

[184] G. Anderson, "Providing best-value IVHM solutions for aging aircraft," *Jt. FAA/DoD/NASA Conf. Aging Aircr.*, vol. 1, pp. 1–11, 2006.

[185] L. C. Jaw and W. Merrill, "CBM+ Research Environment - Facilitating technology development, experimentation, and maturation," *IEEE Aerosp. Conf. Proc.*, pp. 1–6, 2008, doi: 10.1109/AERO.2008.4526641.

[186] S. Meshal and F. I. Shamsah, "Enhancement of Field Balancing Methods in Rotating Machines," 2017.

[187] D. J. Inman, *Vibration with Control*. 2006.

[188] P. Borghesani, P. Pennacchi, and S. Chatterton, "The relationship between kurtosis- and envelope-based indexes for the diagnostic of rolling element bearings," *Mech. Syst. Signal Process.*, vol. 43, no. 1–2, pp. 25–43, 2014, doi: 10.1016/j.ymssp.2013.10.007.

[189] J. Van Baren, "Which Transducer Should I Use for my Vibration Test?," *Vibration Research*, Dec. 2020.

[190] R. V. Dukkipati, "Introduction to Mechanical Vibrations," *Solving Vib. Anal. Probl. Using MATLAB*, pp. 1–13, 2007, doi: 10.1016/B978-012269440-0/50001-7.

[191] L. Qihe, "Integration of Vibration Acceleration Signal Based on LabVIEW," *J. Phys. Conf. Ser.*, vol. 1345, no. 4, 2019, doi: 10.1088/1742-6596/1345/4/042067.

[192] Bruel & Kjaer, "Measuring Vibration," *Bruel & Kjaer*, 1982.

[193] R. F. M. Marçal, M. Negreiros, A. A. Susin, and J. L. Kovaleski, "Detecting faults in rotating machines," no. December, pp. 24–26, 2000.

[194] K. Elbhbah and J. K. Sinha, "Bispectrum for fault diagnosis in rotating machines," *17th Int. Congr. Sound Vib. 2010, ICSV 2010*, vol. 2, no. July, pp. 1290–1297, 2010, doi: 10.13140/2.1.1546.3684.

[195] A. Yunusa-Kaltungo and K. Elbhbah, "HOS Analysis of Measured Vibration Data on Rotating MAchines with Different Simulated Faults," in *Advance Condition Monitoring of Machinery in Non-Stationary Operations*, G. Dalpiaz, G. D'Elia, R. Rubini, M. Cocconcelli, F. Chaari, R. Zimroz, W. Bartelmus, and M. Haddar, Eds. Springer Berlin Heidelberg, 2014, pp. 81–89.

[196] K. Elbhbah and J. K. Sinha, "Vibration-based condition monitoring of rotating machines using a machine composite spectrum," *J. Sound Vib.*, vol. 332, no. 11, pp. 2831–2845, 2013, doi: 10.1016/j.jsv.2012.12.024.

[197] M. Pirra, E. Gandino, A. Torri, L. Garibaldi, and J. M. MacHorro-López, "PCA algorithm for detection, localisation and evolution of damages in gearbox bearings," *J. Phys. Conf. Ser.*, vol. 305, no. 1, 2011, doi: 10.1088/1742-6596/305/1/012019.

[198] K. C. Luwei, J. K. Sinha, A. Yunusa-Kaltungo, and K. Elbhbah, "Data fusion of acceleration and velocity features (dFAVF) approach for fault diagnosis in rotating machines," in *MATEC Web of Conferences*, 2018, vol. 211, doi:

10.1051/matecconf/201821121005.
[199] J. Brownlee, “How to calculate Principal Component Analysis (PCA) from Scratch in Python,” *Machine Learning Mastery*, 2019.
[200] D. S. Wilks, *Principal Component (EOF) Analysis*, vol. 100. 2011.
[201] Z. Jaadi, “A Step-by-Step Explanation of Principal Component Analysis (PCA),” *Built in*, 2021. https://builtin.com/data-science/step-step-explanation-principal-component-analysis (accessed Apr. 12, 2021).
[202] A. Yunusa-kaltungo and R. Cao, “Towards Developing an Automated Faults,” *Energies*, vol. 13, no. 1394, p. 20, 2020.
[203] K. C. Luwei, J. K. Sinha, and A. Yunusa-kaltungo, “Optimisation of different acceleration and velocity features for fault diagnosis in rotating machines,” in *Proceeding of 2nd International Conference of Maintenance Engineering*, 2017, p. 10.
[204] S. Wang and F. Xiao, “AHU sensor fault diagnosis using principal component analysis method,” *Energy Build.*, vol. 36, no. 2, pp. 147–160, 2004, doi: 10.1016/j.enbuild.2003.10.002.
[205] A. Prieto-Moreno, O. Llanes-Santiago, and E. García-Moreno, “Principal components selection for dimensionality reduction using discriminant information applied to fault diagnosis,” *J. Process Control*, vol. 33, pp. 14–24, 2015, doi: 10.1016/j.jprocont.2015.06.003.
[206] R. Cao and A. Yunusa-Kaltungo, “An automated data fusion-based gear faults classification framework in rotating machines,” *Sensors*, vol. 21, no. 9, 2021, doi: 10.3390/s21092957.
[207] B. Mnassri, E. M. El Adel, and M. Ouladsine, “Reconstruction-based contribution approaches for improved fault diagnosis using principal component analysis,” *J. Process Control*, vol. 33, pp. 60–76, 2015, doi: 10.1016/j.jprocont.2015.06.004.
[208] B. I. 10816-3:2009 British standards Institute, “Mechanical vibration. Evaluation of Machine Vibration by measurement of non-rotating parts industrial machines with norminal power above 15kW and norminal speed between 120rpm and 15000rpm when measured in situ,” BSI: London.
[209] C. Mercer, “Acceleration, velocity and displacement spectra – Omega Arithmetic,” pp. 1–8, 2006.
[210] British standards Institute, “BS ISO 17359:Condition monitoring and diagnostics of machines– General guidelines,” London, 2011.
[211] E. Swanson, C. D. Powell, and S. Weissman, “A practical review of rotating machinery critical speeds and modes,” *Sound Vib.*, vol. 39, no. 5, pp. 10–17, 2005.
[212] S. Tresser, A. Dolev, and I. Bucher, “Dynamic balancing of super-critical rotating structures using slow-speed data via parametric excitation,” *J. Sound Vib.*, vol. 415, pp. 59–77, 2018, doi: 10.1016/j.jsv.2017.11.029.
[213] J. He and Z. Fu, *Modal Analysis*, 1st Editio. Oxford: Butterworth Heinemann, 2010.
[214] K. C. Luwei and A. Yunusa-kaltungo, “Data combination for a consolidated diagnosis of rotor and bearing faults,” no. 6, pp. 388–399, 2020.
[215] K. C. Luwei, A. Yunusa-Kaltungo, and Y. A. Sha’aban, “Integrated fault detection framework for classifying rotating machine faults using frequency domain data

fusion and Artificial Neural Networks," *Machines*, vol. 6, no. 4, 2018, doi: 10.3390/MACHINES6040059.